THE
PHYSICAL REVIEW
A Journal of Experimental and Theoretical Physics Established by E. L. Nichols in 1893
VOL. 55, NO. 2 JANUARY 15, 1939 SECOND SERIES

Artificial Radioactivity Produced by Protons

L. A. DELSASSO, L. N. RIDENOUR,* R. SHERR† AND M. G. WHITE
Palmer Physical Laboratory, Princeton University, Princeton, New Jersey
(Received November 7, 1938)

The artificial radioactivity produced in targets of Cu, Ni, Ag, Cr and Mo by bombardment with four-Mev protons has been studied. In Cu, the (p, n) reaction gives rise to the radioelements Zn^{63} (half-life 38.5 min., upper limit of positron spectrum 1.8 Mev) and Zn^{65}. Two new radioactive isotopes of Cu are found in Ni bombarded with protons; they have tentatively been assigned as follows: Cu^{58}, half-life 81 sec., and Cu^{60}, half-life 7.9 minutes. Both emit positrons. Also produced in Ni are Cu^{61}, both by the (p, n) and the (p, γ) reaction (threshold <1.8 Mev), and Cu^{64}, by the (p, n) reaction (threshold apparently 2.1 Mev). Proton bombardment of Ag results in a radioactive Cd isotope which emits very soft negative electrons which are believed to be conversion electrons of a nuclear gamma-ray. The identification of the responsible Cd isotope and the mode of decay is discussed. The half-life of this radioelement is 6.7 hours; the threshold for the reaction is 2.4 Mev. 40-minute Mn^{51} is formed by proton bombardment of Cr. This radioelement emits positrons. Three unassigned activities produced in Mo have half-lives of 45 min., 2.7 hours, and 36.5 hours; the last emits negative electrons.

I. INTRODUCTION

WE HAVE studied in some detail the radioactive isotopes produced by bombarding targets of Cu, Ni and Ag with protons; the results are reported here, together with some incomplete data regarding the activities produced in targets of Cr, Mo and Mg.

The proton beam used in this work was produced by the Princeton cyclotron, the construction of which has been described elsewhere.[1] The mean energy of the beam was about 4.0 Mev (cf. Section II).

The activities are in all cases given in units of divisions per minute on a Lauritsen electroscope. One division per minute corresponds roughly to 6.6×10^{-3} microcurie, if one understands by a microcurie the amount of an artificial radioelement in which 3.7×10^{4} disintegrations per second occur, and neglects corrections which arise from the differences in energy of the electrons and positrons emitted from the various radioelements. These corrections will be of two sorts: the first concerns the absorbing power of the electroscope window for electrons of different velocities, while the second arises from the difference in specific ionization of fast and of slow electrons. No attempt has here been made to evaluate them. The window of the electroscope used here was a sheet of Al foil of thickness 2.4 mg/cm².

In several cases, a determination of the sign of the particles emitted by a radioelement was made by the usual method of deflection in a magnetic field, employing a thin-walled Geiger counter as detecting device.

Of the four nuclear reactions which are known to be produced by swift protons; namely, (p, γ),

* Now at Randal Morgan Laboratory of Physics, University of Pennsylvania, Philadelphia, Pennsylvania.
† Now at Department of Physics, Harvard University, Cambridge, Massachusetts.
[1] M. C. Henderson and M. G. White, Rev. Sci. Inst. 9, 19 (1938).

(p, n), (p, d), and (p, α), only the first two seem to have occurred in the cases we have studied. This is hardly surprising, in view of the fact that we have been working in the region of moderately high atomic number, where the potential barrier against the emission of charged particles is rather large. The energy conditions in the case of the (p, n) reaction are especially simple and interesting, and have been formulated explicitly by DuBridge and his collaborators.[2]

A (p, n) reaction followed by radioactive positron decay results in a final nucleus which is identical with the target nucleus; the energy evolved in the nuclear changes all has been supplied by the kinetic energy of the incident proton. The energy required is then, at the least (the neutron being emitted with negligible kinetic energy, and the emission of no gamma-rays being assumed), the difference between n^1 and H^1 mass (0.8 Mev) plus the mass of two electrons (1.0 Mev) plus the upper limit of the positron energy spectrum from the radioelement formed. The excitation function for such a reaction should then show an energy threshold somewhere above two Mev. Its position is definitely fixed by the positron energy in cases in which no gamma-radiation is emitted.

The case in which the radioactive nucleus formed by a (p, n) reaction decays by the capture of an extranuclear electron (presumably with the simultaneous emission of a neutrino) is somewhat similar to that mentioned above, except that the threshold energy for the reaction may be considerably smaller. Using the notation of DuBridge, we may represent the mass-energy relations in this case as follows:

$$Z^A+H^1+E_p=(Z+1)^A+n^1+E_n+\gamma_1 \\ =Z^A+\nu+E_\nu+n^1+E_n+\gamma_1+\gamma_2, \quad (1)$$

where E_p is the energy of the bombarding proton, E_n the energy of the emitted neutron, ν represents the neutrino rest mass (probably zero), E_ν is the energy of the neutrino, and γ_1 and γ_2 allow, respectively, for the formation of the nucleus $(Z+1)^A$ in an excited state, and for its decay into an excited state of the nucleus Z^A.

The minimum value of E_p will be that for which $E_n=\gamma_1=\gamma_2=0$. In this event,

$$E_{p0}=n^1-H^1+\nu+E_\nu=0.8+\nu+E_\nu \text{ Mev}. \quad (2)$$

When E_ν becomes larger than about one Mev, the process of positron decay will compete with that of extranuclear electron capture, so that we may expect thresholds for the production of radioelements which decay by the latter process alone to lie between proton energies of one and two Mev. At these energies, the penetration of charged particles into any but the lightest nuclei is likely to be rare, so that one may expect observational thresholds at energies higher than those predicted by energy considerations alone. Also, of course, one cannot say *a priori* that a disintegration in which $\gamma_1=\gamma_2=0$ will have a large enough probability to permit its observation. If, on account of selection rules, the transition from the nucleus $(Z+1)^A$ to the ground state of the nucleus Z^A is a "nonpermitted" one, while a transition to an excited state of the nucleus Z^A is "permitted," one may observe an energy threshold for the reaction higher than that given by Eq. (2) by the amount, γ_2, of excitation energy of the final nucleus.

II. "Excitation Function" Measurements

In several instances in the course of the investigation reported here attempts were made to measure the energy-yield curve for nuclear reactions by the method of stacked foils which, introduced at Berkeley, has become a standard technique for use with a cyclotron. In order to evaluate the results of such a measurement, it is necessary to know the distribution of energy of the particles composing the primary beam and the thickness of the foils used.

The distribution in range of the particles comprising the proton beam was determined by measuring the ion current to a collector housed in the main accelerating chamber vacuum as a function of the superficial mass of interposed sheets of Al foil. The curve so obtained is shown in Fig. 1. The conversion from range in Al to air range and from air range to energy is taken from data given by Livingston and Bethe,[3] as is the computation of the normal straggling.

[2] DuBridge, Barnes, Buck and Strain, Phys. Rev. **53**, 447 (1938).

[3] Livingston and Bethe, Rev. Mod. Phys. **9**, 245 (1927). Cf. pp. 266–85.

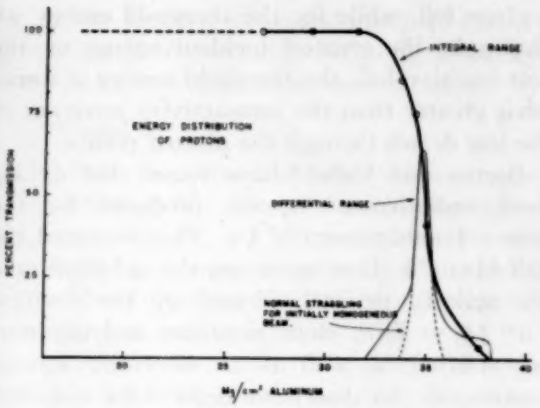

FIG. 1. Range distribution of the proton beam.

It is seen that the energy spread of the beam is a little more than twice that which would be introduced by the straggling of an initially homogeneous beam.

The causes of this broad energy distribution can be divided into two categories: (1) the energy spread inherent in the resonance acceleration method, and (2) irregularities in thickness of the aluminum stopping foils. The latter factor is difficult to evaluate, but visual inspection of the thinnest foils used indicates that a correction to the beam width as measured should be applied. Inhomogeneity of the beam energy due to the cyclotron can arise from the finite size of the ion source, variation of the beam energy with magnetic field setting (see Fig. 1 of reference 2), and broadening of the effective ion source center by magnetic field inhomogeneities. The differential range curve shown in Fig. 1 was obtained by graphical differentiation of the experimental curve, and comparison of it with the curve shown for normal straggling of an initially homogeneous beam suggests that about 75 percent of the particles in the beam are of very nearly the same energy.

Stacked-foil measurements were made in Cu, Ni and Ag; the energy thicknesses of the foils used ranged from 0.1 Mev to 0.2 Mev, depending upon the material of the foil and the energy of the protons incident upon it. The stopping power of the foils was computed from data given by Mano[4] in the case of Ag and Cu; the stopping power for Ni was computed from Mano's formulae to agree with data given by Rosenblum.[5]

Since the actual thicknesses of the rolled foils, as determined by careful weighing, differed somewhat even for foils which were nominally identical, correction for this was made by dividing the activity of any given foil by the superficial mass of the foil, and expressing the corrected activity as divisions/minute per mg/cm². This procedure neglects differences in the self-absorption of the several foils for the electrons each emits, but since the foils were all exceedingly thin and the differences small, the procedure was thought to be justified.

It is clear that the greatest caution must be exercised in interpreting the results of the stacked-foil measurements given here. The initial inhomogeneity of the beam is about 0.25 Mev, and this is rapidly increased by the effect of straggling as the beam passes through the foils; while the thickness of each foil is around 0.15 Mev. This means that, without making any allowance for straggling, the difference in energy between the most energetic proton incident on the front face of a foil and the slowest proton reaching the back face of the same foil is about 400 kev: more than twice as great as the energy thickness of a single foil. During long runs, unavoidable fluctuations in the "tuning" of the cyclotron magnet may introduce still larger variations in the energy distribution of the beam. As already remarked, there is evidence that the beam energy is dependent upon the magnet setting near resonance. Under the circumstances, it did not seem to be necessary to make the customary correction for "recoil" of activated atoms from the rear of one foil to the front of the next. The abscissae of the points actually plotted in the energy-yield curves here given represent the energy in the center of a particular foil of protons which initially had the mean energy of the beam.

One datum, however, can be obtained from the energy-yield curves given here; this is a lower limit for the energy threshold of a particular reaction. Having found the last foil which shows detectable radioactivity, we are fairly safe in saying that the most energetic protons which fell on the first inactive foil were incapable of

[4] Mano, J. de Phys. et Rad. **5**, 628 (1934).

[5] Rosenblum, Ann. de physique **10**, 408 (1928).

producing the reaction in question, within the limits set by the sensitivity of our measuring device. As has been mentioned in the last section, this datum is of particular interest in the case of the (p, n) reaction.

III. Experimental Results

A brief statement of preliminary results has already appeared.[6]

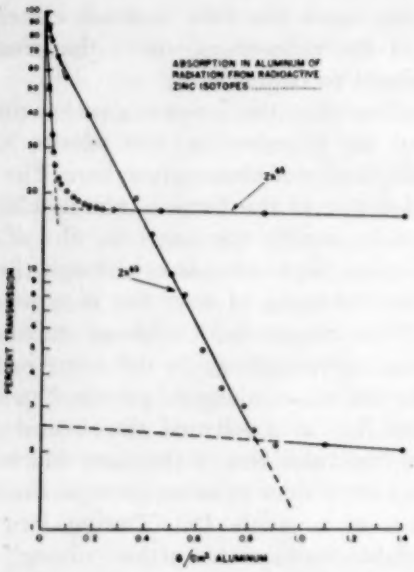

Fig. 2. Absorption curves for the radiation from Zn^{63} and Zn^{65}. The end points are, respectively, 0.82 and 0.20 g/cm², indicating maximum electron energies of 1.77 and 0.55 Mev. Note large intensity of gamma-rays from Zn^{65}.

A. Copper

The production of Zn^{63} by proton bombardment of Cu has already been reported.[6] Its half-life is 38.5 ± 0.8 min. The absorption in Al of the positrons emitted in the decay of Zn^{63} is shown in Fig. 2; their mass range is 0.82 g/cm², leading, by Feather's rule,[7] to an upper energy limit of about 1.8 Mev. The energy threshold to be expected for the reaction Cu^{63} (p, n) Zn^{63} is then 3.6 Mev, by the considerations of Section I. This is in good agreement with the value indicated by the method of stacked foils (see Fig. 3). Since, as mentioned in the preceding section, the points on the energy-yield curves here given represent the mean beam energy in the center of a given foil, while for the threshold energy we shall take the greatest incident energy on the first inactive foil, the threshold energy is somewhat greater than the zero-activity intercept of the line drawn through the plotted points.

Barnes and Valley[8] have found that a long lived radioelement is also produced by the proton bombardment of Cu. They reported the half-life to be about seven months and attributed the activity to Zn^{65}, formed by the reaction Cu^{65} (p, n) Zn^{65}. Both positrons and electrons are emitted, as well as an extremely intense gamma-ray. An absorption curve of the radiation emitted by this radioelement is shown in Fig. 2; the sample of Zn^{65} used for making this curve came from the side of one of the copper dees of the Princeton cyclotron, which had undergone many hours of proton bombardment. The absorption curve shows at least three components. By placing the radioactive sample in a magnetic field it was possible to show that the soft radiation consists largely of charged particles. Fairly intense x-radiation was found to exist in addition to the very intense gamma-ray. Internal conversion of the gamma-ray accounts for the negative electrons observed and the x-rays then arise from the subsequent filling of the K and L shells. Either positron emission or extranuclear

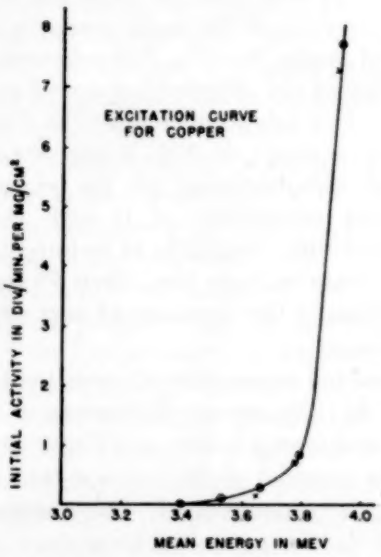

Fig. 3. Energy-yield curve for the reaction Cu^{63} (p, n) Zn^{63}. Crosses and circles represent two different runs. Threshold at 3.6 Mev.

[6] L. N. Ridenour, L. A. Delsasso, M. G. White and R. Sherr, Phys. Rev. **53**, 770 (1938).

[7] Feather, Phys. Rev. **35**, 1559 (1930).

[8] Barnes and Valley, Phys. Rev. **53**, 946 (1938).

electron capture will transform Zn^{65} into Cu^{65}; from the abnormally high ratio of gamma-rays to positrons, both processes seem to occur.

B. Nickel

As has been reported,[6] four different periods are found in the decay of Ni bombarded with protons (see Fig. 4). All have been chemically identified as due to isotopes of Cu. The two longer lived radioelements are readily identifiable as well-known radioactive Cu isotopes.

1. Cu^{64}:—An activity of half-life 12.8 hours, in which both positrons and negative electrons are emitted, is clearly caused by the familiar radioelement Cu^{64}. It can only be formed from Ni by proton bombardment in the reaction Ni^{64} (p, n) Cu^{64}, as the isotope Ni^{63}, from which Cu^{64} could be formed by proton capture, has not been reported to exist as a stable isotope. The energy-yield curve for this radioelement is shown in Fig. 5. The threshold energy for the reaction seems to be between 2.1 and 2.3 Mev, and certainly no higher. This is somewhat puzzling,

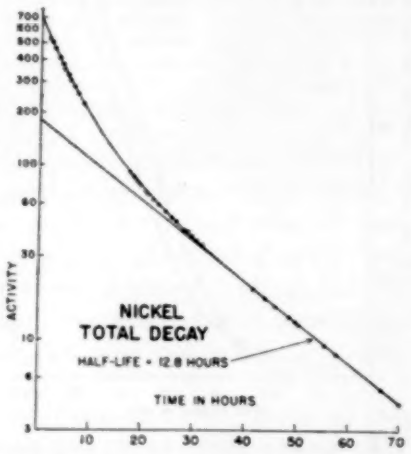

FIG. 4a. Decay curve for Ni bombarded with protons. The long periods—bombardment time 2.5 hours.

as Van Voorhis[9] gives the upper energy limit of the spectrum of the positrons as 0.7 Mev; from the simple considerations already given, one would expect that the energy threshold for this reaction would fall at $1.0+0.8+0.7=2.5$ Mev, at least for those Cu^{64} nuclei which are to emit positrons in their subsequent decay.

We consider the most likely explanation of this result to be the presence in the beam of a small number of high energy protons; protons whose initial energy was 4.2 Mev would reach the foil whose plotted point in Fig. 5 lies at an abscissa of 2.05 Mev with an energy of 2.46 Mev, so that any protons of initial energy higher than 4.2 Mev would contribute to the 12.8-hour activity of that foil. Presence in the bombarded foils of a spurious 13-hour activity caused by

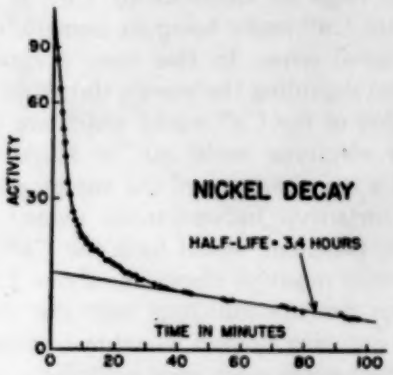

FIG. 4b. Decay curve for Ni bombarded with protons. The short periods—bombardment time 4 minutes.

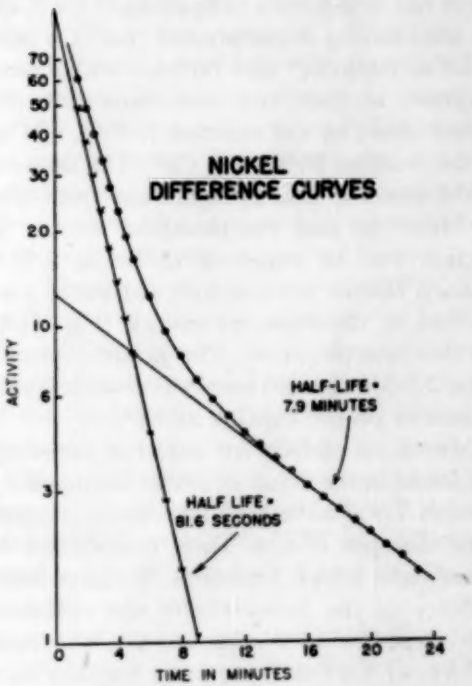

FIG. 4c. Decay curve for Ni bombarded with protons. Difference curves from data of Fig. 4b.

[9] Van Voorhis, Phys. Rev. **50**, 895 (1936).

the presence of a contaminant of unknown nature is considered unlikely.

Because confirmation of this result by other workers has not been made, it is not yet profitable to discuss the possible explanations which could be offered in case the threshold is really too low. Two present themselves at once: (1) Ni^{63} is stable but rare, so that at low energies the Ni^{63} (p, γ) Cu^{64} reaction could take place, and (2) the agreement in half-lives for the emission of positive and negative electrons by Cu^{64} is merely fortuitous, Cu^{64} really being an isomeric nucleus in the usual sense. In this case, a categorical statement regarding the energy threshold for the production of the Cu^{64} nuclei which are to emit negative electrons could not be made on the basis of a measurement of the energy spectrum of the negative beta-particles alone.[2] Below 2.5 Mev, then, one would form the Cu^{64} isomer which emits negative electrons; above 2.5 Mev, both the positron-emitting and the negative electron-emitting isomers would be formed. Both these alternatives seem very unlikely.

2. Cu^{61}:—A nickel target bombarded with protons displays a strong activity of half-life 3.4 hours, in which positrons are emitted. Clearly, this is the well-known radioelement Cu^{61}, chemical tests having demonstrated that it is isotopic with Cu. Both Ni^{60} and Ni^{61} are stable isotopes of nickel, so that this radioelement could be formed either by the reaction Ni^{60} (p, γ) Cu^{61} or by the reaction Ni^{61} (p, n) Cu^{61}. The upper limit of the positron energy spectrum from Cu^{61} is 0.9 Mev,[10] so that the threshold for the (p, n) reaction can be expected to lie at 2.7 Mev. A sharp rise in the energy-yield curve for this reaction at the expected energy (Fig. 5) bears out this interpretation. The production of Cu^{61} below 2.7-Mev proton energy is doubtless entirely because of proton capture in Ni^{60}.

Two short periods for positron emission are also found in the decay of nickel bombarded with protons. These have both been shown chemically to be isotopes of Cu. Their periods are 81 ± 2 seconds and 7.9 ± 0.5 minutes. We have found no evidence of the formation of the radioelement Cu^{62} (half-life 10.0 minutes) by the reaction Ni^{62} (p, n) Cu^{62} or by proton capture in Ni^{61}. Strain and Buck[11] have reported its formation at a proton energy of six Mev, which presumably indicates that the energy threshold for the reaction lies above four Mev and below six Mev.

The short period activities reported here cannot be assigned unambiguously without their discovery in other reactions. They are presumably formed either by proton capture or by the (p, n) reaction, and, neglecting the possibility of nuclear isomerism because none of the known radioactive isotopes of Cu has been found to be isomeric, they may belong to Cu nuclei of mass number 58, 59, or 60. We have suggested[6] the tentative assignment of the 80-second period to Cu^{58} and the 7.9-minute period to Cu^{60}, on the extremely doubtful basis of relating the activity ratio of

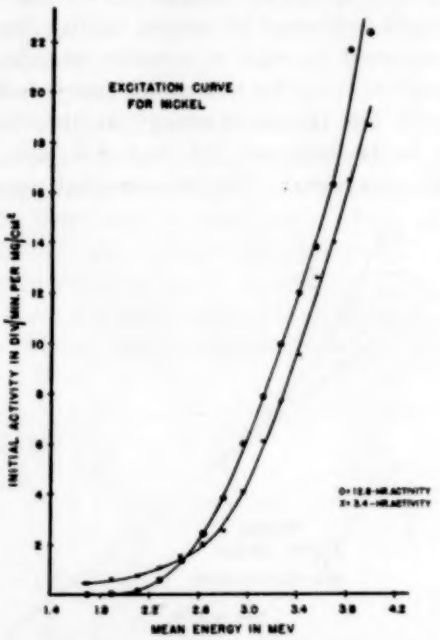

FIG. 5. Energy-yield curves for the long period radioelements produced by proton bombardment of Ni. Crosses —Cu^{61}; circles—Cu^{64}.

the two radioelements to the abundance ratio of Ni^{58} to Ni^{60}.

C. Silver

The strongest activity we have found to be produced by proton bombardment at our energy of four Mev is the 6.7-hour period in Ag. This activity has been shown chemically to be caused by an isotope of Cd, and the radiation which is

[10] L. N. Ridenour and W. J. Henderson, Phys. Rev. **52**, 889 (1937).

[11] Strain and Buck, Phys. Rev. **53**, 943 (1938).

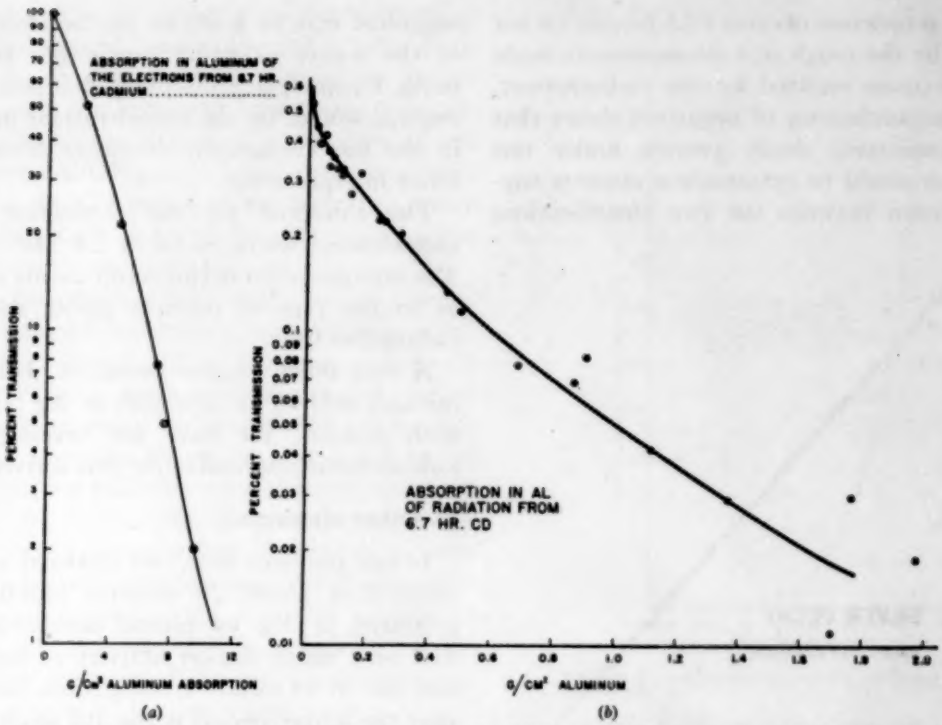

FIG. 6. Absorption in Al of the radiations from the 6.7-hour Cd isotope produced by bombarding Ag with protons. (*a*) Soft component. Mass range of electrons 12 mg/cm², corresponding to an energy of about 90 kev. (*b*) Absorption curve at large absorber thicknesses. While the curve cannot be properly resolved, it is seen to consist of a very weak hard radiation, together with a radiation for which the mass absorption coefficient lies between 2 and 3, corresponding to x-rays of wave-length 0.51 to 0.57A.

emitted is mainly negative electrons of extremely feeble penetrating power. Fig. 6 shows the absorption in Al of this radiation. A weak component of greater penetrating power has a mass absorption in Al which is about that of the *K* radiation of Ag, while there is some indication of a harder radiation still which is of very small intensity.

Now the Cd isotopes which can be formed by proton bombardment of Ag (whose two stable isotopes are Ag^{107} and Ag^{109}) have mass numbers 107, 108, 109 and 110. Indium, to which a radioactive Cd emitting negative disintegration electrons would decay, has stable isotopes of mass numbers 113 and 115. In the absence of any evidence for a chain of disintegrations (see decay curve, Fig. 7), we may assume that the negative electrons emitted are not disintegration electrons, but conversion electrons of a nuclear gamma-ray emitted in some other form of radioactive decay.

Two possibilities may be invoked to explain this case. First, the activity may be caused by the production, by proton capture, of one of the two stable Cd isotopes Cd^{108} or Cd^{110} in a metastable excited state. The subsequent decay of this nucleus to the ground state is accompanied by the emission of a gamma-ray, whose conversion gives rise to the negative electrons observed. The decay of an isomeric Cd^{108} or Cd^{110} by extranuclear electron capture to Ag^{108} or Ag^{110} would be followed by the decay of one of these well-known radioactive Ag isotopes, and since the absorption curve (Fig. 6) shows no evidence of the penetrating electrons associated with these radioelements, we must suppose that gamma-ray decay to the ground state is the only way in which a metastable Cd^{108} or Cd^{110} can be responsible for the activity. A case of this sort has recently been reported.[12]

The second possibility is that the radioactivity is caused by one of the isotopes Cd^{107} or Cd^{109}, produced by the (p, n) reaction. Positron decay

[12] Pontecorvo, Phys. Rev. **54**, 542 (1938).

in a small proportion of cases (< 5 percent) is not ruled out by the rough sign measurements made on the electrons emitted by this radioelement, but the preponderance of negatives shows that the predominating decay process under this assumption would be extranuclear electron capture. Decision between the two identifications suggested may be made by precise identification of the x-rays as being due either to Cd or to Ag. Unambiguous discovery that positrons are emitted would, by the considerations mentioned in the last paragraph, decide in favor of the latter interpretation.

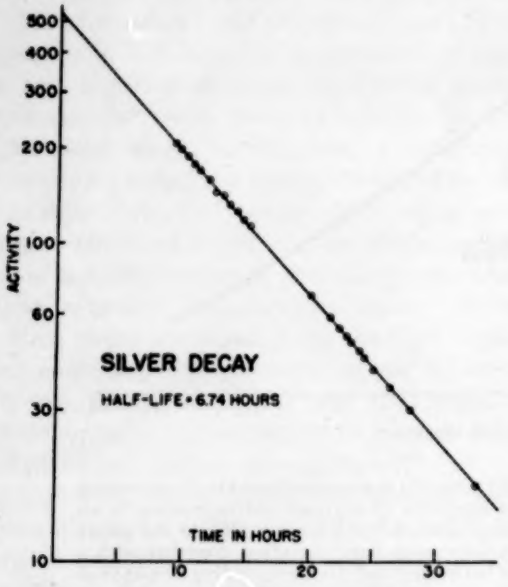

FIG. 7. Decay of radioactive Cd. Bombardment time 3.25 hours.

The threshold for the production of this radioelement seems to be at 2.4 Mev (Fig. 8). The interpretation of this result awaits a decision as to the type of reaction giving rise to the radioactive Cd.

A very much weaker period of about 7 or 8 minutes half-life is produced in Ag bombarded with protons. We have not investigated the radioelement responsible for this activity.

D. Other elements

In our previous note,[6] we reported a positron activity of about 20 minutes half-life to be produced in Mg by proton bombardment, as well as a much weaker activity of some hours half-life. More careful investigations have shown that the longer period is the 107-minute one of F^{18}, caused by oxygen contamination of the target. The shorter period seems also to be caused by a contaminant of unknown nature, since its intensity varies somewhat erratically from one sample of "very pure" Mg to another.

TABLE I. *Summary of the radioactive periods observed.*

TARGET	OBSERVED PERIODS	CHEM.	SIGN OF EMITTED PARTICLES	ASSIGNMENT	μ CURIES PER μAMP.	THRESHOLD Mev	UPPER LIMIT OF β-SPECT. Mev	OTHER REACTIONS	REF.
24 Cr	40 min.	Mn	+	$\left\{\begin{matrix}Cr^{52}(p,\gamma)Mn^{51}\\ Cr^{53}(p,n)Mn^{51}\end{matrix}\right\}$	0.17			$Cr^{52}(d,n)$	3
28 Ni	81 sec.	Cu	+	$Ni^{58}(p,n)Cu^{58}$	1.0				
	7.9 min.	Cu	+	$Ni^{60}(p,n)Cu^{60}$	0.37				
	3.4 hr.	Cu	+	$\left\{\begin{matrix}Ni^{60}(p,\gamma)Cu^{61}\\ Ni^{61}(p,n)Cu^{61}\end{matrix}\right\}$	11.2	1.8 2.7	0.9	$Ni^{58}(\alpha,p)$ $Ni^{60}(d,n)$ $Cu^{63}(n,3n)$	2 1 1
	12.8 hr.	Cu	±	$Ni^{64}(p,n)Cu^{64}$	12.4	2.1	0.7	many	1
29 Cu	38.5 min.		+	$Cu^{63}(p,n)Zn^{63}$	1.6	3.6	1.8	$Ni^{60}(\alpha,n)$ $Zn^{64}(n,2n)$ $Zn^{64}(\gamma,n)$	2 1 1
42 Mo	45 min.		?	?	0.09				
	2.7 hr.		?	?	0.10				
	36.5 hr.		−	?	0.17				
47 Ag	6.7 hr.	Cd	−	see text	33.5	2.4			

[1] M. S. Livingston and H. Bethe, reference 3, pp. 359–360.
[2] L. N. Ridenour and W. J. Henderson, Phys. Rev. **52**, 889 (1937).
[3] J. J. Livingood and G. T. Seaborg, Phys. Rev. **54**, 391 (1938).

It was stated in the earlier note that a chemical separation showed the short period activity to be caused by an isotope of Al; this is not inconsistent with the impurity hypothesis here advanced, as Al was separated in the form of the voluminous $Al(OH)_3$, with which the coprecipitation of a small amount of impurity can easily have taken place. A better half-life value for the short period is about 16 minutes.

Three periods have been identified in the decay of a Mo target bombarded with protons; they are 36.5 ± 5 hours, 2.7 ± 0.4 hours, and 45 ± 5 minutes. The radioelement of longest period emits only negative electrons, while both negatives and positives are emitted by a Mo target soon after bombardment. Presumably either or both of the shorter periods corresponds to the emission of positrons. No identification with known radioelements is proposed for these activities, beyond suggesting that they are isotopes of element 43, because of the potential barrier against the emission of charged particles from a nucleus of such high atomic number.

Two activities have been observed in a target of Cr bombarded with protons; one has a half-life of about 108 minutes for the emission of positrons and is probably to be identified as F^{18} caused by oxygen contamination. The half-life of the other is about 40 minutes; positrons are emitted by this radioelement also, and the result of one chemical separation indicates that it is an isotope of Mn. This confirms the report of this period by DuBridge,[2] who suggested its identification with Mn^{53}. Livingood and Seaborg[13] have recently concluded that this radioelement is best assigned as Mn^{51}. Their half-life value of 46 minutes is doubtless better than that given here, which is quite rough. In addition to the activities already mentioned, there seems to be present a weak period of some days' half-life in Cr bombarded with protons.

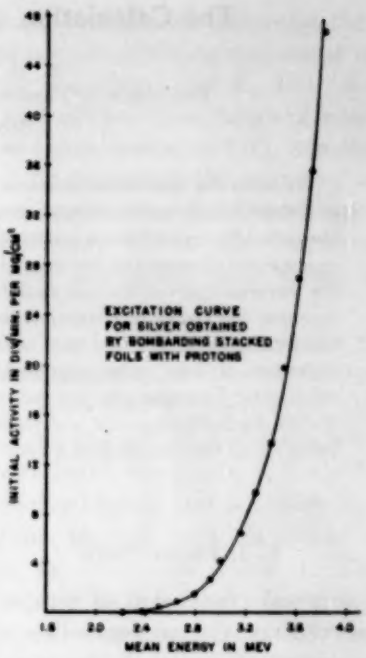

FIG. 8. Energy-yield curve for radioactive Cd.

Table I contains a summary of the radioactive periods reported here, together with some references to other reactions in which are produced known radioelements with which some of them can be identified. A notion of the intensity with which each activity can be produced by four-Mev protons is also given, expressed in terms of microcuries per microampere of ion current on a thick target, corrected to infinite bombarding time.

IV. ACKNOWLEDGMENTS

It is a pleasure to be able to thank Dr. R. C. Newton, of the Department of Chemistry, for suggestions concerning the chemical separations and Mr. John E. Walter for assistance in making the measurements.

[13] J. J. Livingood and G. T. Seaborg, Phys. Rev. **54**, 391 (1938).

The Calculation of Internal Conversion Coefficients

S. M. DANCOFF AND P. MORRISON
Department of Physics, University of California, Berkeley, California

(Received November 21, 1938)

We treat the internal conversion of nuclear γ-rays by methods suited especially to the cases of the artificially radioactive elements. The paper is divided into five parts: Section 1 discusses the radiative transitions in nuclei of middle atomic weights, where one may expect large angular momentum changes and low energy of excitation; in Section 2 we consider the selection rules for the various types of nuclear radiation, and the conditions on their strictness; in Section 3 we examine the choice of potentials for the representation of the multipole fields; Section 4 contains calculations leading to a nonrelativistic formula for the conversion of electric multipole radiation of any order, applicable for $Z<40$ and γ-ray energy $\ll mc^2$; and very simple relativistic formulae are derived, good for high γ-ray energy but restricted to low binding, $Z<30$, for both magnetic and electric multipoles of any order. We summarize the qualitative behavior of the formulae in a conclusion.

1. INTRODUCTION

THE internal conversion of γ-rays was first observed as the superposition of homogeneous groups of emitted electrons on the continuous γ-ray spectrum of certain naturally radioactive elements. The intensities of these lines have been calculated[1] by methods appropriate to these cases: i.e., by using relativistic electron theory necessary for these elements where $Z\sim 80$ and the velocity of the electron in the bound state is large, and for radiation of a few low multipole orders. The integrals involved had to be carried out numerically.

The artificial production of γ-radioactive nuclei of low and middle Z made the extension of the calculations to this range seem desirable. Thus the activity found by Alvarez[2] in Ga^{67} is associated with a line of emitted electrons, presumably conversion electrons of a Zn γ-ray which is emitted after the Ga nucleus captures a K electron to go to Zn^{67}. For the detailed interpretation of such reactions it is helpful to have reliable estimates of the conversion coefficient.

Hebb and Uhlenbeck[3] were led to calculate the internal conversion coefficients for the first five electric multipoles on different grounds. The ideas of von Weizsäcker[4] about nuclear isomers, which ascribe the long lifetime of the metastable nuclear state to a difference of several units of angular momentum between metastable and ground states, and in fact the general ideas of Bohr on nuclear structure, indicated that high multipole orders should frequently be involved in nuclear radiation between states of low excitation. Their calculations were made to ascertain the correction to the estimate of lifetime on the basis of radiative decay alone, when the possibility of decay by electron emission is taken into account.

The formulae of Uhlenbeck and Hebb are completely nonrelativistic, applicable in the range $Z<40$ and for γ-ray energies $\ll mc^2$. We extend the formulae of Uhlenbeck and Hebb to all multipole orders, and obtain simple relativistic results for light nuclei, for magnetic multipoles, and for high multipole order.

2. SELECTION RULES FOR MULTIPOLE RADIATION

The interaction between the electron and the nuclear charge and current we represent as the perturbation on the electron motion by the fields of an oscillating electric or magnetic multipole placed at the nucleus. This treatment is based on a simple argument: the classical multipole fields define normal coordinates for Maxwell's equations by an expansion of the fields in spherical harmonics, and the field of an electric or magnetic 2^L pole when quantized represents a light quantum with angular momentum Lh.[5] Since the

[1] For results and extensive references see H. R. Hulme, N. F. Mott, F. Oppenheimer and H. M. Taylor, Proc. Roy. Soc. **A155**, 315 (1936).
[2] L. W. Alvarez, Phys. Rev. **54**, 486 (1938).
[3] M. H. Hebb and G. E. Uhlenbeck, Physica **5**, 605 (1938).
[4] C. F. v. Weizsäcker, Naturwiss. **24**, 813 (1936).
[5] W. Heitler, Proc. Camb. Phil. Soc. **32**, 112 (1936).

total angular momentum of the system *nucleus* $+\gamma$-*ray* must be conserved, we expect a nuclear transition between states of total angular momentum $\mathbf{J}$ and $\mathbf{J}'$ to emit a quantum represented by a 2^L pole such that $\mathbf{L}=\mathbf{J}-\mathbf{J}'$.

For convenience we summarize the arguments leading to the selection rules for multipole radiation.[6] In the gauge in which

$$\varphi(\mathbf{R})=\int dv\frac{[\rho]_{\text{retarded}}}{|\mathbf{R}-\mathbf{r}|}$$

we can write for the scalar potential at a point distant $\mathbf{R}(R,\Omega)$ from the center of a system of particles with charge e_i and position $\mathbf{r}_i(r_i,\omega_i)$, involved in a transition $\Psi_{J'}\rightarrow\Psi_J$:

$$\varphi(\mathbf{R},t)=\exp\left[\frac{i(E_{J'}-E_J)t}{\hbar}\right]\cdot\int dv\bar{\Psi}_J(\mathbf{r}_i)\times\Psi_{J'}(\mathbf{r}_i)\sum_i e_i\frac{\exp[i\mathbf{k}\cdot(\mathbf{R}-\mathbf{r}_i)]}{|\mathbf{R}-\mathbf{r}_i|}.$$

Suppose that there is no contribution to this integral from any $r_i>\delta$ (δ corresponding to the radius of the nucleus). Then we can make a well-known expansion of the exponential[7] to get

$$\varphi(\mathbf{R},t)=f(R,t)\sum_{\lambda=0}^{\infty}\sum_{m=-\lambda}^{\lambda}C_\lambda f_\lambda(kR)Y_\lambda^m(\Omega)\cdot\sum_{n=0}^{\infty}a_n(k\delta)^{\lambda+2n}\int dv\bar{\Psi}_J\Psi_{J'}\left[\sum_i e_iY_\lambda(\omega_i)\left(\frac{r_i}{\delta}\right)^{2n+\lambda}\right].$$

If $|J-J'|=L$, then in the reduction of $\bar{\Psi}_J\Psi_{J'}$ the lowest spherical harmonic occurring is Y_L, hence the lowest value of λ contributing is $\lambda=L$. Values of λ up to $J+J'$ also contribute, but their contributions are reduced by a factor approximately $(k\delta)^{\lambda-L}$ and this is certainly small for most nuclear γ-rays (for a one-Mev γ-ray, $k\delta<1/15$). This gives a leading term in the scalar potential $\sim Y_L$, just that of a classical electric 2^L pole in this gauge. To find the remaining terms in the scalar potential of such a multipole, we consider all $\lambda>L$ and collect, successively, terms in each power of $k\delta$ that occurs.

Going now to the vector potential, the transformation properties of the current vector enter. The current $\rho\mathbf{v}$ transforms like Y_1. For $|J-J'|=L$, one can now obtain three values of λ corresponding to the lowest power of $(k\delta)$, namely L, $L+1$ and $L-1$. In this gauge the magnetic multipoles have zero scalar potential, and correspond to the single term Y_L in the vector potential. The electric multipoles come from Y_{L+1} and Y_{L-1}.

Like the total angular momentum, the parity of the nuclear states is a constant of the motion; from the reflection properties of the vector potential, we can see that the electric 2^L poles have parity $(-)^L$, the magnetic $(-)^{L+1}$. Thus to a given parity change and ΔJ there corresponds a minimum electric and minimum magnetic multipole as shown in Table I. The higher multipoles, up to $L=J+J'$, permitted by the parity could contribute, but their amplitudes contain the small factor $(k\delta)^{L-L_{\min}}$.

Unless there are some further special symmetries of the nucleus, the lowest multipole allowed will be the most important. We know[8] that the dipole moment of all but the lightest nuclei is reduced by the approximate coincidence of the centers of mass and charge, so that electric dipole and electric quadripole radiation can be comparable, but all other electric multipoles smaller. The fair agreement with experiment[1] in the natural radioactive series supports this. For the magnetic moments, which involve not only the charge and motion, but also the spin properties of the nuclear matter, no analogous reduction of the dipole moment is to be expected. On the other hand, we have the same experiments of Ellis *et al.* to show that, while magnetic dipole and electric quadripole are both allowed

TABLE I. *Minimum allowed multipoles for given parity change and* ΔJ ($L=J-J'$).

Parity Change	Minimum Allowed Multipole: L Even	L Odd
Even	el. 2^L pole mag. 2^{L+1} pole	el. 2^{L+1} pole mag. 2^L pole
Odd	el. 2^{L+1} pole mag. 2^L pole	el. 2^L pole mag. 2^{L+1} pole

[6] Compare, e.g., H. A. Kramers, *Hand- und Jahrbuch der Chemischen Physik*, Vol. I/II, p. 419.

[7] H. Bateman, *Partial Differential Equations*, p. 388.

[8] H. A. Bethe, Rev. Mod. Phys. 9, 222 (1937).

for a transition $\Delta J=1$, even parity change, relatively little magnetic radiation is present.

We shall see that for low energies internal conversion increases very sharply with multipole order. Nevertheless we are still justified in keeping only the lowest multipole, for the reason that while the ratio of the number of electrons ejected to the number of quanta ejected increases with multipole order for long wave-length, the actual *number of electrons ejected falls off*. We have seen that the intensity of γ-rays falls off with multipole order l by a factor $(k\delta)^{2l}$; the number of emitted electrons may be expected to fall off (and we shall see that this is roughly so) by a factor $(k_e\delta)^{2l}$, where k_e is the reciprocal *electron* wave-length. For energies >1 Mev, $k_e\sim k$; for low energies k decreases linearly with energy and k_e as k^1, and both electron and γ-ray wave-lengths increase. Only for energies >20 Mev are $k\delta$, $k_e\delta\sim 1$. For energies lower than this we need consider, for either γ-ray or electron emission, only the lowest multipole order neither forbidden by selection rules nor reduced by any special arguments of symmetry, because here even the electron wave-length is much longer than the nuclear dimensions.

3. Representation of Multipole Fields

In previous work on internal conversion, where only dipole and quadripole fields were required, the "Maxwell" representation was employed; in this representation the electric dipole vector potential is given by

$$\mathbf{A}_1=[0,\ 0,\ (e^{ikr}/kr)]e^{-i\omega t} \qquad +\text{complex conjugate.} \quad (1)$$

The quadripole field is

$$\mathbf{A}_2=[0,\ 0,\ (\partial/\partial z)(e^{ikr}/kr)]e^{-i\omega t} \qquad +\text{complex conjugate.} \quad (2)$$

Higher electric multipole fields are obtained by a corresponding number of differentiations with respect to z. (The scalar potential is obtained in each case from the Lorentz condition.)

These z axis multipoles are, if spherical symmetry otherwise prevails, entirely equivalent to those directed along the x or y axes where successive differentiations are correspondingly along the x or y axes. However, one might erroneously think them also equivalent to multipoles of a "mixed" type, e.g.,

$$\mathbf{A}_2'=[0,\ 0,\ (\partial/\partial x)(e^{ikr}/kr)]e^{-i\omega t} \qquad +\text{complex conjugate,}$$

reasoning from analogy to the case of static multipoles. That this is not so can best be seen from the fact that $\mathbf{A}_2'$ cannot be obtained from $\mathbf{A}_2$ by rotation. In fact, $\mathbf{A}_2'$ is not pure electric quadripole at all, but contains both electric quadripole and magnetic dipole.

Consequently the process of successive differentiation does not yield in any direct way all of the $2l+1$ independent multipoles of the 2^l type which must exist in order that the multipole fields afford a complete set. Moreover, the fields which can be obtained in this way are unsuitable in calculations for general multipole order.[9]

The problem of finding explicit expressions for the general multipole fields has been solved by Heitler,[10] a modification of whose results we use, and by Hansen. Choosing a gauge in which $\operatorname{div}\mathbf{A}'=\varphi'=0$, we obtain expressions for the vector potential of a 2^l electric pole in the following form:[11]

$$\begin{aligned}
A_z' &= e^{-i\omega t}[q_{l-1}{}^m Y_{l-1}{}^m f_{l-1}(kr) \\
&\qquad +q_{l+1}{}^m Y_{l+1}{}^m f_{l+1}(kr)], \\
A_+' &= A_x'+iA_y' = e^{-i\omega t}[Q_{l-1}{}^{m+1} Y_{l-1}{}^{m+1} f_{l-1} \\
&\qquad +Q_{l+1}{}^{m+1} Y_{l+1}{}^{m+1} f_{l+1}], \qquad (3) \\
A_-' &= A_x'-iA_y' = e^{-i\omega t}[P_{l-1}{}^{m-1} Y_{l-1}{}^{m-1} f_{l-1} \\
&\qquad +P_{l+1}{}^{m-1} Y_{l+1}{}^{m-1} f_{l+1}],
\end{aligned}$$

where $\omega=ck$, $Y_l{}^m$ is the spherical harmonic, and

---

[9] One might hope to calculate matrix elements involving $\mathbf{A}_l$ by repeated partial integrations to reduce out the $(l-1)$th order derivative. The integrands are, however, singular at $r\to 0$, so that surface terms occur in each partial integration, rendering the method impracticable.

[10] See reference 5. A similar solution has been given independently by W. W. Hansen, Phys. Rev. **47**, 139 (1935).

[11] In order to make the potentials real, we add to A_z' its complex conjugate and to each of A_+', A_-' the complex conjugate of the other. However probabilities of transitions involving *absorption* of light will depend only on the terms containing $e^{-i\omega t}$ and we will use only these terms throughout, except in the calculation of the rate of radiation.

the coefficients q, Q, P are given by

$$Q_{l+1}{}^{m+1}(l-m+1)^{\frac{1}{2}}=q_{l+1}{}^{m}(l+m+2)^{\frac{1}{2}},$$
$$P_{l+1}{}^{m-1}(l+m+1)^{\frac{1}{2}}=-q_{l+1}{}^{m}(l-m+2)^{\frac{1}{2}},$$
$$Q_{l-1}{}^{m+1}(l+m)^{\frac{1}{2}}=-q_{l-1}{}^{m}(l-m-1)^{\frac{1}{2}},$$
$$P_{l-1}{}^{m-1}(l-m)^{\frac{1}{2}}=q_{l-1}{}^{m}(l+m-1)^{\frac{1}{2}},$$
$$\left(\frac{l+1}{l}\right)^{\frac{1}{2}}\left(\frac{(2l+3)(2l+1)}{(l+1)^2-m^2}\right)^{\frac{1}{2}}q_{l+1}{}^{m}$$
$$=\left(\frac{l}{l+1}\right)^{\frac{1}{2}}\left(\frac{(2l+1)(2l-1)}{l^2-m^2}\right)^{\frac{1}{2}}q_{l-1}{}^{m}=\sigma_l{}^{m}.$$

The constant $\sigma_l{}^{m}$ measures the multipole moment. The radial function $f_l(kr)$ is:

$$f_l(kr)=H_{l+\frac{1}{2}}(kr)/(kr)^{\frac{1}{2}}$$

where $H_{l+\frac{1}{2}}(kr)$ is the Hankel function of the first kind. This gives rise to outgoing waves singular at the origin rather than to standing waves such as Heitler obtained.

The corresponding expressions for a 2^l magnetic multipole are:

$$A_z{}'=e^{-i\omega t}b_l{}^{m}Y_l{}^{m}f_l\cdot m/[l(l+1)]^{\frac{1}{2}},$$
$$A_+{}'=e^{-i\omega t}B_l{}^{m+1}Y_l{}^{m+1}f_l\cdot m/[l(l+1)]^{\frac{1}{2}},$$
$$A_-{}'=e^{-i\omega t}C_l{}^{m-1}Y_l{}^{m-1}f_l\cdot m/[l(l+1)]^{\frac{1}{2}}, \quad (4)$$

$$B_l{}^{m+1}=-1/m[(l-m)(l+m+1)]^{\frac{1}{2}}b_l{}^{m},$$
$$C_l{}^{m-1}=-1/m[(l+m)(l-m+1)]^{\frac{1}{2}}b_l{}^{m}.$$

The rate of radiation is calculated in the usual way and is found to be, for electric multipoles

$$\frac{(\sigma_l{}^{m})^2}{\pi^2\hbar k}\ \text{quanta/sec.} \quad (5)$$

and for magnetic multipoles:

$$\frac{(b_l{}^{m})^2}{\pi^2\hbar k}\ \text{quanta/sec.} \quad (6)$$

The choice of gauge in which div $\mathbf{A}=0$, besides rendering the potentials compact, is particularly suited for use in problems involving interaction of light with matter, where the Hamiltonian (nonrelativistic) is given, neglecting terms in $\mathbf{A}^2$, by

$$H=\frac{1}{2m}\left[\frac{\hbar}{i}\mathbf{grad}-\frac{e}{c}\mathbf{A}\right]^2+e\varphi$$
$$=-\frac{\hbar^2}{2m}\Delta-\frac{e\hbar}{2mic}[\mathbf{grad}\cdot\mathbf{A}+\mathbf{A}\cdot\mathbf{grad}]+e\varphi.$$

Matrix elements of perturbations by the radiation field have the form

$$\int\bar{\Psi}_f\left\{-\frac{e\hbar}{mic}\mathbf{A}\cdot\mathbf{grad}-\frac{e\hbar}{2mic}(\text{div }\mathbf{A})+e\varphi\right\}\Psi_0 dv. \quad (7)$$

If now div $\mathbf{A}$ and φ vanish, the calculation is extremely simplified; the only term remaining is the one in $\mathbf{A}\cdot\mathbf{grad}$.

From this one might conclude that all interaction vanished as the initial velocity approached zero, which disagrees with the results for the conventional gauge. The discrepancy must be looked for in the contribution to the matrix element of the necessarily singular generating function λ of the gauge transformation:

$$\mathbf{A}=\mathbf{A}'+\mathbf{grad}\,\lambda, \quad \varphi=\varphi'-(1/c)(\partial\lambda/\partial t), \quad (8)$$

where $\mathbf{A}$, φ are in the conventional gauge, e.g. (1), (2) and

$$\text{div }\mathbf{A}'=\varphi'=0.$$

Substituting (8) into (7), using charge-current conservation and applying suitable partial integrations, we find that the terms involving λ may be expressed as follows:

$$-\frac{1}{c}\int_V dv(d/dt)(\lambda\bar{\Psi}_f\Psi_0)$$
$$-\frac{e\hbar}{2mic}\int_\Sigma d\boldsymbol{\sigma}\cdot\{\bar{\Psi}_f\Psi_0\,\mathbf{grad}\,\lambda+\lambda\bar{\Psi}_f\,\mathbf{grad}\,\Psi_0$$
$$-\lambda\Psi_0\,\mathbf{grad}\,\bar{\Psi}_f\},$$

where the surface integral is over the bounding surface Σ of the volume V under consideration. The volume integral, integrated from time 0 to t is an oscillating term which does not build up with t and hence does not contribute to the transition probability. If, as is appropriate for the problem of internal conversion, we let our

bounding surface Σ consist of two spheres whose radii approach infinity and zero, respectively, then the integral over the outer surface will vanish because of the regularity of the wave functions and the potentials. We are consequently left with a surface integral over a small sphere surrounding the origin

$$\Lambda=\frac{e\hbar}{mic}\int_{\Sigma(r\to 0)} r^2 d\Omega\left\{\bar{\Psi}_f\psi_0\frac{\partial\lambda}{\partial r}+\lambda\bar{\Psi}_f\frac{\partial\Psi_0}{\partial r}-\lambda\Psi_0\frac{\partial\bar{\Psi}_f}{\partial r}\right\}. \quad (9)$$

To evaluate this, and thus to determine the difference in matrix elements between primed and unprimed gauges, one must know merely the limiting forms for small r of the wave functions and of λ.

Consider now the case of electric multipoles; by comparing (1), (2), etc. with (3), it is easily seen that $\mathbf{A}'$ is more singular than $\mathbf{A}$; hence it follows from (8) that for small r,

$$\mathbf{grad}\,\lambda\sim-\mathbf{A}'.$$

This equation is satisfied by

$$\lambda\sim\frac{\sigma_l^m}{k}\left(\frac{l}{l+1}\right)^{\frac{1}{2}}Y_l^m f_l e^{-i\omega t}$$
$$\sim\frac{\sigma_l^m}{k}\left(\frac{l}{l+1}\right)^{\frac{1}{2}}Y_l^m\left[i(-)^{l+1}\frac{(kr/2)^{-l-\frac{1}{2}}}{(kr)^{\frac{1}{2}}\Gamma(-l+\frac{1}{2})}\right]e^{-i\omega t}. \quad (10)$$

The additive constant is omitted since it does not contribute to (9), which is now completely fixed.

We must still account for the fact that such a difference between gauges exists and must answer the question of which gauge, if either, gives the "right" answer—i.e., that corresponding to the physical problem. We know that any expressions for the potentials of an electrical system in terms of multipoles are approximate, and are valid only outside the region containing the charges and currents. These expressions can therefore be appropriately used only when the effect we wish to calculate (or the predominant part of it) takes place outside this region. If, because of the artificial singularities at the origin introduced in the definition of the multipole potentials, our matrix elements are given a finite contribution from an arbitrarily small region, then we must consider these potentials wrong for our particular problem. If, by a gauge transformation, we are led to another set of potentials for which the integrand of the matrix element is small at the origin, this latter set can be called correct.

In the problem of internal conversion, this condition is satisfied by the unprimed gauge. It is not satisfied by the electric multipoles in the primed gauge; div $\mathbf{A}'$ and φ', while zero throughout space, are integrably infinite at the origin, as can be seen by partially integrating

$$\int_V dv\bar{\Psi}_f\Psi_0\,\mathrm{div}\,\mathbf{A}',$$

where V is a sphere including the origin whose radius is permitted to approach zero.

Nevertheless, the primed gauge still can be advantageously used since the correction necessary to bring it into agreement with the correct gauge is known, namely, (9).

The magnetic multipole potentials in the primed gauge may be used without correction.

4. Calculations

We will calculate the number of electronic transitions per second from the K level to the continuum of an atom of atomic number Z induced by a nuclear 2^l pole with unit rate of radiation. This number, which we call $\alpha_K{}^l$ for electric, and $\beta_K{}^l$ for magnetic multipoles, is defined as the coefficient of internal conversion. Taylor and Mott have shown[12] that it is to be interpreted, in all cases of interest, as the ratio of the number of electrons to the number of quanta leaving the atom, N_e/N_q, and not to $N_e/(N_e+N_q)$ as was originally supposed. In its main effect, the perturbation by the electron serves to induce additional nuclear transitions, not to reduce the number of emitted quanta.

In the first part we limit ourselves to nonrelativistic energies throughout. This gives a range of applicability up to $Z=40$ and γ-ray energies up to 200,000 or 300,000 volts. From these calculations we find an asymptotic expression for high l.

[12] H. M. Taylor and N. F. Mott, Proc. Roy. Soc. **A142**, 215 (1933).

In the second part we derive a formula applicable to low atomic numbers, neglecting the K binding energy with respect to mc^2 and to the γ-ray energy. These formulae are very simple.

A. Nonrelativistic—electric multipoles

The number of transitions per electron per second from a state Ψ_0 in the K shell to a state Ψ_f in the continuum is given by

$$N_e=\frac{1}{\hbar^2}\left|\Lambda-\int d\tau\bar{\Psi}_f\frac{e\hbar}{mic}\mathbf{A}'\cdot\mathbf{grad}\,\Psi_0\right|^2, \quad (11)$$

where Ψ_f is normalized to unit flux through the boundary at infinity. Λ, the surface integral contributed by the gauge transformation, is calculated from (9). Also

$$\Psi_0=(a^3/\pi)^{\frac{1}{2}}e^{-ar},$$

$$\bar{\Psi}_f=Y_l^{-m}\left(\frac{m\pi p}{\hbar}\right)^{\frac{1}{2}}\frac{[\Gamma(l+1+in)\Gamma(l+1-in)]^{\frac{1}{2}}}{\Gamma(l+1)\Gamma(l+\frac{3}{2})}$$

$$\times e^{\pi n/2}(pr/2)^l e^{-ipr}F(l+1+in,\,2l+2,\,2ipr),$$

where $a=Z\alpha(mc/\hbar)$, p is $1/\hbar$ times the momentum of the ejected electron and $n=a/p=Z\alpha/[2\nu-(Z\alpha)^2]^{\frac{1}{2}}$ where ν is the γ-ray energy over mc^2. We require the expression $\mathbf{A}'\cdot\mathbf{grad}\,\Psi_0$, which, using (3), is found to be simply

$$-a\sigma_l^m[l(l+1)]^{\frac{1}{2}}Y_l^m\frac{f_l(kr)}{(kr)}\Psi_0.$$

Both $\mathbf{A}'\cdot\mathbf{grad}$ and λ contain Y_l^m, hence both contribute to transitions to a final state $\Psi_f\sim Y_l^m$.

We make the indicated substitutions and carry out the trivial angular integrations, obtaining

$$N_e=\frac{M^2}{\hbar^2}\left\{[-kr^{l+2}f_{l+1}]_{r=0}+2a(l+1)\int_0^\infty dr f_l r^{l+1}\right.$$

$$\left.\times e^{-\rho r}F(l+1+in,\,2l+2,\,2ipr)\right\}^2,$$

where $\rho=a+ip$ and

$$M=\frac{\sqrt{2}}{\Gamma(-l+\frac{1}{2})}\left(-\frac{2}{k}\right)^l\times M'\ \text{(given below)}.$$

In the radial integral we replace f_l by its most singular term, namely

$$\frac{i(kr/2)^{-l-\frac{1}{2}}(-)^{l+1}}{(kr)^{\frac{1}{2}}\Gamma(-l+\frac{1}{2})}.$$

It can be shown that the contributions of less singular terms are smaller by at least $k^2/(a^2+p^2)\sim v^2/c^2$. With this substitution the radial integral can be carried out in series, and we obtain

$$N_e=\frac{M'^2}{\hbar^2}\left[1-\frac{a}{\rho}\frac{l+1}{l+\frac{1}{2}}\right.$$

$$\left.\times F\left(1,\,l+1+in,\,2l+2,\,\frac{2ip}{\rho}\right)\right]^2, \quad (13)$$

where

$$M'=\frac{e\sigma_l^m}{\pi c}\left(\frac{2a^3\hbar}{m}\right)^{\frac{1}{2}}\frac{p^{l+\frac{1}{2}}}{k^{l+2}}\left(\frac{l}{l+1}\right)^{\frac{1}{2}}$$

$$\times\frac{[\Gamma(l+1+in)\Gamma(l+1-in)]^{\frac{1}{2}}}{\Gamma(l+1)}e^{\pi n/2}.$$

We can express the hypergeometric function F in (13) in terms of two terminating hypergeometric series by using the familiar analytical continuation. If we do so and make use of the formulae:

$$\rho/2ip=(1-in)/2,\quad p^2/k^2=2/\nu(1+n^2),$$

$$\Gamma(l+1+in)\Gamma(l+1-in)$$

$$=\frac{\pi n}{\sinh\pi n}(l^2+n^2)[(l-1)^2+n^2]\cdots(1+n^2)$$

we obtain for the conversion coefficient for two K electrons:[13]

$$\alpha_K{}^l=2N_e\cdot\pi^2\hbar k/(\sigma_l^m)^2,\quad \{v/c\ll 1\}^{14}$$

$$=16\alpha\frac{l}{l+1}[\Gamma(l+\tfrac{1}{2})]^2\left(\frac{2}{\nu}\right)^{l+1}\cdot\frac{n^4}{(1+n^2)^{l-2}}$$

$$\cdot\frac{[(l+1)(1+n^2)^{l-2}e^{-2n\,\mathrm{ctn}^{-1}n}-V_l]^2}{(l^2+n^2)[(l-1)^2+n^2]\cdots(1+n^2)(1-e^{-2\pi n})}, \quad (14)$$

[13] These formulae, up to $l=5$, have been derived by Hebb and Uhlenbeck, reference 3, with whose results we are in agreement. Their parameter η is the reciprocal of our n.

[14] The inequalities in braces give the conditions of applicability of our final formulae.

where

$$V_l=\frac{4^l\prod_{i=1}^{l}(i^2+n^2)}{(1+n^2)^l(2l)!}$$

$$\times\left[in\frac{l+1}{l+in}F\left(1,\ -2l,\ 1-l-in,\ \frac{1-in}{2}\right)-1\right].$$

It satisfies the recursion relation:

$$V_{l+1}=V_l(1+n^2)\frac{l+2}{l+1}+\frac{2^{2l+1}l}{(2l+2)!}\cdot\frac{1}{(1+n^2)}\cdot\prod_{i=1}^{l}(i^2+n^2)$$

so that

$$V_0=0,$$
$$V_1=0,$$
$$V_2=\tfrac{1}{3},$$
$$V_3=4(3+2n^2)/15,\quad \text{etc.}$$

Limit $n\to 0$:

In this limit of low Z, $\mathbf{A}'\cdot\mathbf{grad}\ \Psi_0\to 0$, and only A contributes. We obtain,[15] again for two electrons

$$\alpha_K{}^l=Z^3\alpha^4\frac{l}{l+1}\left(\frac{2}{\nu}\right)^{l+5/2}\quad\begin{matrix}\{v/c\ll 1\},\\ \{Ze^2/\hbar v\ll 1\}.\end{matrix}\qquad(15)$$

The convergence to this limit, however, is not uniform in l.[16]

Asymptotic formula for large l:

This can be most easily arrived at by using the contour integral representation:

$$-\rho\frac{\Gamma(2l+2)}{4^l\Gamma(l+1+in)\Gamma(l+1-in)}\times\int_{-1}^{1}\frac{(1+u)^{l+in}(1-u)^{l-in}}{u+in}du$$

for the hypergeometric function in (13). There is a saddle point on the imaginary axis quite close to the origin:

$$\bar{u}=-\frac{in}{2}+\frac{i}{2}(n^2+2/l)^{\frac{1}{2}}.$$

Carrying out the integration, one obtains a formula closely related to (15), the formula for vanishing Z.

For $l\gg 1$:

$$\alpha_K{}^l=Z^3\alpha^4\frac{l}{l+1}\left(\frac{2}{\nu}\right)^{l+5/2}\left[1-2nl^{\frac{1}{2}}\left\{\frac{(1+n^2+1/2l)-n\mu/2)^l}{(2+l\mu^2)^{\frac{1}{2}}}+O(1/l)\right\}\right]^2,\qquad(16)$$

where $\mu=n+(n^2+2/l)^{\frac{1}{2}}$.

The formula can be further simplified for $n^2l\gg 1$ (i.e., l sufficiently high, not too near threshold). In this case $\mu\to 2n+1/ln$. The principal terms in the bracket cancel and one is left simply with the formula for vanishing Z reduced roughly by a factor l.

$$\alpha_K{}^l=Z^3\alpha^4\frac{l}{l+1}\left(\frac{2}{\nu}\right)^{l+5/2}\cdot O\left(\frac{1}{l}\right)\quad\begin{matrix}\{n^2l\gg 1\},\\ \{v\ll c\}.\end{matrix}\qquad(17)$$

It can be shown that the term $O(1/l)$ will not vanish identically in n.

For $n^2l\ll 1$, (16) goes over into (15), a convergence non-uniform in l.

B. Nonrelativistic magnetic multipoles

In nonrelativistic theory, there is no conversion of magnetic multipole radiation by K electrons, or by any electron with zero orbital angular momentum. The transition from a state with zero to one with l units of orbital angular momentum can be accompanied only by the absorption of a 2^l pole quantum. But since the electron's parity change is $(-)^l$, magnetic radiation is forbidden, since magnetic 2^l pole has parity $(-)^{l+1}$.

Physically this means there are no radial forces on such an electron. The electric field of a magnetic multipole is tangential and the magnetic force is perpendicular to the velocity, i.e., also tangential.

Conversion of magnetic radiation by S electrons thus depends essentially on their spin.

C. Relativistic calculations, neglecting binding

The number of electronic transitions per second from a state 0 in the K shell to a state f in the continuum where the electron is ejected into the

[15] This formula was given by the authors in Phys. Rev. **54**, 149 (1938) where through error it was given as for one K electron.

[16] For increasing l, the tangential component of the magnetic field, and hence the radial Lorentz force, becomes more important.

solid angle $d\Omega$ is given for two electrons in the K shell:

$$N_e d\Omega = \frac{2\pi e^2}{\hbar} d\Omega |H|^2,$$

where $$H = \sum_{\text{spin}} \int dv \bar{\Psi}_f (\boldsymbol{\alpha}\cdot\mathbf{A} + \varphi)\Psi_0,$$

$\boldsymbol{\alpha}$ is the vector whose components are the first three Dirac matrices for $\mathbf{v}/c$, and Ψ_f is normalized to unit energy. The integral is over all space, and the sum over final and initial spin states. If now we make the gauge transformation (8), we obtain

$$H = \sum_{\text{spin}} \left[\int dv \bar{\Psi}_f \mathbf{A}'\cdot\boldsymbol{\alpha}\Psi_0 + \int d\sigma\lambda \bar{\Psi}_f \boldsymbol{\alpha}\cdot\mathbf{n}\Psi_0 \right],$$

where the second term is the analog of (9) in the nonrelativistic case, $\mathbf{n}$ is a unit vector along $\mathbf{r}$, and the surface integral is over a small sphere around the origin. In this approximation, where the influence of the Coulomb field is neglected, we use plane waves for the space-dependent part of Ψ_f. Then the wave functions factor into spin- and space-dependent parts. If we introduce the projection operators,

$$2\tau_0 = 1+\beta,$$

$$2\tau_f = 1 + \frac{\beta mc^2 + \boldsymbol{\alpha}\cdot\mathbf{p}_f c\hbar}{E_f},$$

we can replace the wave functions by $\tau_0\Psi_0$ and $\tau_f\Psi_f$ in H, and the $\sum_{\text{spin}} H\bar{H}$ can be replaced by the sum over both the spin states and the states of positive and negative energy in the well-known way.[17]

We get

$$|H|^2 = \text{Trace}\,[(\mathbf{A}\cdot\boldsymbol{\alpha})\tau_0(\mathbf{A}\cdot\boldsymbol{\alpha})^*\tau_f + (\boldsymbol{\alpha}\cdot\mathbf{N})\tau_0(\mathbf{A}\cdot\boldsymbol{\alpha})^*\tau_f + (\mathbf{A}\cdot\boldsymbol{\alpha})\tau_0(\mathbf{N}\cdot\boldsymbol{\alpha})^*\tau_f + (\boldsymbol{\alpha}\cdot\mathbf{N})\tau_0(\boldsymbol{\alpha}\cdot\mathbf{N})^*\tau_f]$$

with $$\mathbf{A} = C_f \int \mathbf{A}' \exp(i\mathbf{p}\cdot\mathbf{r})dv,$$

$$\mathbf{N} = C_f \int d\sigma\lambda \exp(i\mathbf{p}\cdot\mathbf{r})\mathbf{n},$$

C_f = normalizing constant.

[17] Cf. W. Heitler, *Quantum Theory of Radiation*, p. 150.

Taking the trace and evaluating the space integrals we find the matrix element. Dividing by the rate of radiation, and normalizing, we obtain for the internal conversion coefficient for two K electrons, neglecting binding energy:

$$\alpha_K{}^l = \frac{2Z^3\alpha^4}{\nu^3}\left(\frac{\nu+2}{\nu}\right)^{l-1}\left[\frac{(l+1)\nu^2+4l}{l+1}\right] \quad \{Ze^2/\hbar v \ll 1\}, \quad (18)$$

where $\nu = \gamma$-ray energy in units mc^2.

Magnetic multipoles:

A similar, but simpler, calculation (no gauge term appears) gives for two K electrons:[18]

$$\beta_K{}^l = \frac{2Z^3\alpha^4}{\nu}\left(\frac{\nu+2}{\nu}\right)^{l+1} \quad \{Ze^2/\hbar v \ll 1\}. \quad (19)$$

Limiting cases:

For low-energy γ-rays, $\nu \ll 1$:[18]

$$\alpha_K{}^l = \frac{l}{l+1} Z^3\alpha^4 \left(\frac{2}{\nu}\right)^{l+5/2} \quad \{v/c \ll 1\},$$
$$\beta_K{}^l = Z^3\alpha^4\left(\frac{2}{\nu}\right)^{l+1} \quad \{Ze^2/\hbar v \ll 1\}. \quad (20)$$

For low energy γ-rays and for small binding energy, conversion of magnetic 2^l pole radiation is smaller than that of the electric 2^l pole by a factor

$$\frac{\beta_K{}^l}{\alpha_K{}^l} \to \frac{l+1}{4l}\left(\frac{v}{c}\right)^2.$$

For very high energy γ-rays, $\nu \gg 1$:[19]

$$\alpha_K{}^l = \beta_K{}^l = \frac{2Z^3\alpha^4}{\nu} \quad \{\nu \to \infty\}, \quad \{Ze^2/\hbar v \ll 1\}. \quad (21)$$

In this limit the conversion is independent of multipole type and order, as in the same limit for internal conversion by pair production.[20] Both

[18] This formula may be expected to give a fair estimate for low and middle Z, even though binding is neglected, as magnetic conversion essentially depends on spin. Compare Section 4*B*.

[19] This formula agrees, in the limit of low Z, with the electric dipole formula given by H. Casimir, Physik. Zeits. **32**, 665 (1931). The latter is applicable, for sufficiently large ν, to all Z.

[20] This result is more easily derived by the method suggested in reference 9.

electric and magnetic conversion formulae for negligible binding have the general properties:

(1) For a given l, the conversion increases as ν decreases, the more rapidly the greater l. For $\nu \to \infty$ the conversion for all multipoles approaches a common limit.

(2) For a given ν, conversion increases with l, more and more slowly as $\nu \to \infty$.

L shell:

For conversion from the L shell, (18) and (19) hold provided Z be replaced by $Z-\sigma/2$, where σ is the *energy* screening constant; for the L shell these results are valid for larger values of n than for the K shell.

5. Conclusion

Experiment has established internal conversion, either by detection of the actual electron groups or of the x-rays from the filling of the depleted K levels, in the cases of Rh,[21] Br,[22] Ma,[23] Ag[24] and Au;[25] probably in In[26] and Cd;[27] and, of course, in Zn. In the last, the data are sufficiently complete to assign the conversion tentatively to an electric quadripole radiation.[28] In the others it is not yet possible to classify the radiation. The general features suggested by the von Weizsäcker hypothesis are, however, observed: low energy and long lifetime (metastability) seem to be accompanied by large conversion—pointing to high angular momenta. An interesting check on the picture will be furnished by comparison of lifetime and conversion coefficient, both of which are fixed by multipole order for a given γ-ray energy.

We summarize our results: [Here l is multipole order, $n=Ze^2/h\nu$].

(1) The smaller the γ-ray energy compared to mc^2, the more rapidly conversion increases with multipole order. For large γ-ray energies, the increase with multipole order is much less marked.

(2) The effect of binding is complicated, though in general conversion varies about as Z^3 for given l and energy. For a given value of n, there may be a minimum in the conversion coefficient as l is varied.

(3) For sufficiently large l, and low γ-ray energy the conversion (given by (17)) is of the order of $1/l\times$, the conversion neglecting binding.

(4) The magnetic multipole conversion will be small for low γ-ray energy and $Z<40$.

(5) Quantitative results for γ-ray energies under 0.2 Mev and $Z<40$ will be given by formula (14). For $Z<30$, high energies, and not extremely high multipole order, (18) and (19) give usable estimates. For $Z>50$ numerical calculation is necessary for accurate results.

The authors are pleased to acknowledge the kind and continued assistance of Professor J. R. Oppenheimer.

[21] B. Pontecorvo, Phys. Rev. **54**, 542 (1938).
[22] Philip Abelson, of this laboratory, has detected characteristic bromine x-rays in the activity of Br^{80} (unpublished).
[23] E. Segrè and G. T. Seaborg, Phys. Rev. **54**, 772 (1938).
[24] L. N. Ridenour, L. A. Delsasso, M. G. White and R. Sherr, Phys. Rev. **53**, 770 (1938).
[25] J. R. Richardson, Phys. Rev. **53**, 942 (A) (1938).
[26] We are grateful to Dr. R. Serber for the information that Goldhaber has found electron lines from indium.
[27] J. G. Hoffman and R. F. Bacher, Phys. Rev. **54**, 644 (1938).
[28] L. W. Alvarez, reference 2, p. 497.

Anomalous Scattering of Neutrons by Helium

H. STAUB[1] AND W. E. STEPHENS[2]
W. K. Kellogg Radiation Laboratory, California Institute of Technology, Pasadena, California
(Received November 21, 1938)

The ratio of the cross sections for elastic backward scattering of neutrons in helium and hydrogen has been measured as a function of the neutron energy. This ratio is practically constant between two- and six-Mev neutron energy and has a value of about 1.3. However, at one Mev, the ratio increases to about nine. This anomaly must be caused by resonance scattering occurring from the formation of an unstable compound nucleus He^5. Theoretical considerations show that the level of He^5 involved must be a p level.

INTRODUCTION

THE investigation of the α-particle spectrum of lithium bombarded by deuterons by Williams, Shepherd and Haxby[3] showed that the continuous spectrum caused by the reaction $Li^7+{}_1D^2\rightarrow{}_4Be^8+{}_0n^1\rightarrow 2{}_2He^4+{}_0n^1$ has superimposed on it a homogeneous group of α-particles which was ascribed by these authors to the reaction ${}_3Li^7+{}_1D^2\rightarrow{}_2He^5+{}_2He^4$. From the range of this α-particle group, one concludes that in this case He^5 is left in a state which is unstable against disintegration into an α-particle and a neutron by 0.84 Mev.

We may, therefore, expect that the scattering of neutrons by helium may be strongly anomalous, because of a resonance effect as soon as the energy of the intermediately formed compound nucleus He^5 lies in the neighborhood of this level, which is 0.84 Mev above the level of a separated He^4 and a neutron. The maximum of such an anomalous scattering should occur at a kinetic energy of $(5/4)0.84=1.05$ Mev of the neutron in the laboratory coordinate system.

EXPERIMENTS

The only neutron spectrum having a line at about one Mev arising from the bombardment of light nuclei by deuterons is the one of beryllium, ${}_4Be^9+{}_1D^2\rightarrow{}_0n^1+{}_5B^{10}$. According to the results of Bonner and Brubaker,[4] the neutron spectrum contains (at 0.9 Mev bombarding energy) four lines of about the same intensities at 4.5, 4.0, 2.6 and 1.4 Mev. As these are the maximum energies of the neutrons of each group, the average energy of the neutrons in the group lies appreciably lower. In particular, the line of 1.4 Mev has its maximum intensity around 1.1 Mev. By reducing the bombarding energy to 0.6 Mev, we were able to change the average energy of the neutrons to 1.1 Mev. The high voltage tube used in these experiments has already been described by one of us.[5] The neutrons at right angles to the deuteron beam entered a cloud chamber of 15 cm diameter filled first with ethane and then with helium. By adopting the well-known technique[6] of taking stereoscopic pictures of the cloud chamber, the spectrum of the neutrons was measured once by helium recoils and once by hydrogen recoils. To get the values for the intensities of the lines, one has to correct the number of tracks which are actually observed in the cloud chamber. This correction is due to the fact that the chance of seeing a track with its complete length within the chamber depends on its length and the diameter of the chamber. By dividing the area of the chamber, in which a track of length l, can start and its whole length lie within a chamber of radius r, by the total area of the chamber, we get the correction K,

$$K=(1/\pi)[2\arcsin(1-l^2/4r^2)^{\frac{1}{2}}-l/r(1-l^2/4r^2)^{\frac{1}{2}}]$$

[1] International Exchange Student, now at the Physics Department of Stanford University.
[2] Now a Westinghouse Research Fellow, Westinghouse Research Laboratories, East Pittsburgh, Pennsylvania.
[3] J. H. Williams, W. G. Shepherd and R. O. Haxby, Phys. Rev. **52**, 390 (1937). Confirmed by H. Staub and W. E. Stephens, Phys. Rev. **54**, 236 (1938) and Phys. Rev. **54**, 237 (1938).
[4] T. W. Bonner and G. Brubaker, Phys. Rev. **50**, 308 (1936).
[5] W. E. Stephens and C. C. Lauritsen, Rev. Sci. Inst. **9**, 151 (1938).
[6] T. W. Bonner and G. Brubaker, Phys. Rev. **47**, 910 (1935).

and the true intensity $J_0=J/K$, where J is the actually observed number of tracks.

The ratio of the corrected intensities of two corresponding lines measured with helium and hydrogen recoils, respectively, gives the ratio of the scattering cross sections of helium and hydrogen times an arbitrary constant. As we used in our experiments only the recoils in the forward direction ($\pm 12°$) with respect to the incident neutron beam we obtained only the cross section ratio for the backward scattered neutrons. It can easily be shown that by counting the recoils of helium and hydrogen within the same solid angle in the laboratory system, the corresponding solid angle subtended by the scattered neutrons in the center of gravity system is in both cases the same, as it is independent of the mass of the recoiling particle.

The absolute values of the ratios of the cross sections were determined by measuring this ratio in an ionization chamber for the 2.5-Mev neutrons of the D+D reaction. For this experiment we used a pressure ionization chamber with plane, circular, parallel electrodes connected to a linear amplifier, operating a thyratron and a mechanical counter. If the stopping power of the gas in the ionization chamber is sufficiently high so that the range of a forward recoil atom is much shorter than the depth of the chamber, one gets directly the number of recoils as a function of the energy by counting the number of pulses as a function of their height. This was performed by measuring the number of counts for a given constant number of incident neutrons as a function of the thyratron bias. In this way one gets the integral of the energy distribution curve of the recoils. If the angular distribution of the recoils is isotropic in the center of gravity system the number-energy curve of the recoils is a horizontal straight line dropping to zero at the maximum energy of the recoils. The height of this straight line is a measure of the cross section. For isotropic distribution in the center of gravity system we have in the laboratory system

$$dN_R=2N_0\sigma nd\,\sin\theta\cos\theta d\theta$$

and

$$E_R=\frac{4m}{(m+1)^2}E_0\cos^2\theta,$$

hence

$$dN_R=N_R dE_R=\frac{N_0\sigma nd}{4mE_0/(m+1)^2}dE_R=\text{const}\,dE_R,$$

where N_R is the number of recoils between E_R and E_R+dE_R, N_0 the number of neutrons, n the number of atoms per cc in the ionization chamber, d its depth, E_0 the energy of the neutrons and m the mass of the recoil. By observing the number of recoils N_T as a function of the bias V of the thyratron, we obtain:

$$N_T=\int_V^{V_0}N_R dE_R=-\frac{N_0\sigma nd(V-V_0)}{4mE_0/(m+1)^2},$$

which represents a straight line having its intercept with the abscissa at V_0, the bias corresponding to the maximum energy of the recoils. For protons, the measurements of Dee and Gilbert[7] and Bonner[8] have clearly shown the angular distribution of the recoils to be isotropic. For He, the curve given by Baldinger, Huber and Staub[9] shows that at least for $0<\theta<\pi/4$, the distribution of the recoils is uniform. Also, our results show that the number of recoils plotted against the thyratron bias can be represented by a straight line. Furthermore, even in the case of nonisotropic distribution, still the slope at $V=V_0$ would give the cross section for the backward scattered neutrons.

A very serious distortion of the distribution curve would arise, if the track length of the recoils were much larger than the depth of the chamber. This can be avoided by using a sufficiently high gas pressure. However, this requires a very high collecting voltage in order to collect the ions in a time which is small compared to the time constant of the amplifier. However, we would expect for He and H nonlinear but similar curves whose slope we could compare if the track length of the recoils in both cases were the same. We therefore adjusted the pressures of the helium and the ethane so that the tracks were shorter than the depth of the chamber and had approximately the same track length. However,

[7] P. I. Dee and C. W. Gilbert, Proc. Roy. Soc. **A163**, 265 (1937).
[8] T. W. Bonner, Phys. Rev. **52**, 685 (1937).
[9] E. Baldinger, P. Huber and H. Staub, Helv. Phys. Acta **11**, 245 (1938).

in the case of ethane this procedure would have required too high a collecting voltage. This is because the mobility in ethane is very low at high pressure because of the fact that room temperature is already below the critical temperature of ethane. We therefore used a mixture of ethane and argon. In this way we were able to obtain satisfactorily high stopping power at a reasonable collecting voltage. The recoils of argon have not enough energy to give pulses of appreciable length. In the final experiments we used the following values:

Bombarding voltage	0.6 Mev
Direction of neutrons	90° to ion beam
Depth of chamber	1.0 cm
(1) Helium: Max. energy of recoil	1.67 Mev
Range in air	0.88 cm
Pressure	6.8 atmos.
Stopping power	1.19
Max. track length	0.74 cm
Collecting voltage	2100 volts
(2) Ethane-argon mixture:	
Max. energy of recoil	2.6 Mev
Range in air	11.0 cm
Pressure of ethane	2.3
Pressure of argon	11.2 atmos.
Stopping power	14.42
Max. track length	0.76 cm
Collecting voltage	5700 volts

The three-stage amplifier was of the Wynn-Williams type, with a W. E. 259-B as a first stage tube. The pulses on the thyratron were visually checked by a cathode-ray oscillograph. The characteristic response of the amplifier was found to be linear up to an output potential of 80 volts. The relation between input charge and output voltage was determined by changing the potential of the collecting voltage plate by a given amount ΔV. As the ionization chamber was of the guard ring type, the capacity c between voltage plate and the collector could easily be computed. From this, the induced charge $\Delta q = c\Delta V$ was determined.

The deuterium target consisted of heavy water frozen on a solid copper block which closed a Dewar vessel of thin-walled German silver tubing containing liquid air. Before every run, the target was renewed by opening a stopcock and allowing fresh heavy water vapor to condense. In order to get, during every run, the same number of primary neutrons falling on the ionization chamber, a Lauritsen electroscope was used as a monitor. The target tube had a window of one cm air equivalent aluminum through which the protons of the reaction ${}_1D^2+{}_1D^2 \rightarrow {}_1H^1+{}_1H^3$ were allowed to enter the electroscope. As this reaction has exactly the same excitation function as the one producing neutrons, the total number of neutrons hitting the ionization chamber was always the same for the same deflection of the electroscope. A checking measurement showed that, by inserting absorption foils between the target and the electroscope, the deflection for an equal number of counts of the amplifier at constant bias was independent of the number of foils until an air equivalent of about 14 cm was reached. At this value of the absorption, which is the range of the protons, the deflection dropped suddenly to about 10 percent of its original value, indicating that the deflection of the electroscope is mainly caused by protons and not by x-rays or electrons.

A similar measurement to the one taken with the ionization chamber for the D+D neutrons was performed with the neutrons of the reaction ${}_6C^{12}+{}_1D^2 \rightarrow {}_0n^1+{}_7N^{13}$. The neutrons were observed at an angle of 30° with respect to the ion beam. The neutrons of this reaction are monochromatic[4] with a Q value of -0.28 Mev. So at 30° and 0.83 Mev bombarding energy, the neutrons have an energy of 0.50 Mev. As the ranges of the recoils of He and H are respectively 0.28 and 0.70 cm of air, one can use very low pressure. Actually, the chamber was first filled with 5.5 atmos. of He, and then with 2.8 atmos. of ethane. The collecting voltage in both cases was 1000 v. Unfortunately, the accuracy of these measurements is very poor, because of the fact that the yield of neutrons of this reaction is very small. Furthermore, an appreciable background of neutrons from the reaction D+D was present, which, at the low stopping power in the ionization chamber, does not show a straight line distribution. However, the curves for He and H are similar, and can be compared after adjustment to the same end point.

Results

Figure 1 shows the spectrum of the Be+D neutrons with bombarding energy of 0.6 Mev obtained with hydrogen and helium recoils,

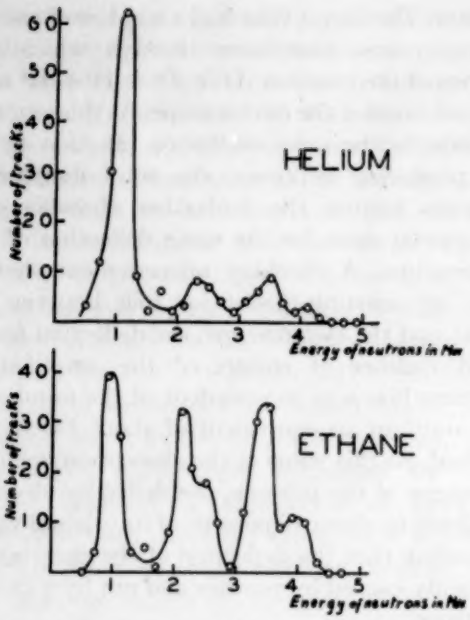

FIG. 1. The spectrum of the neutrons of Be+D at 0.6 Mev bombarding energy measured with helium and hydrogen recoils. The peak on the right side of the line at 2.5 Mev is caused by the neutrons from D+D.

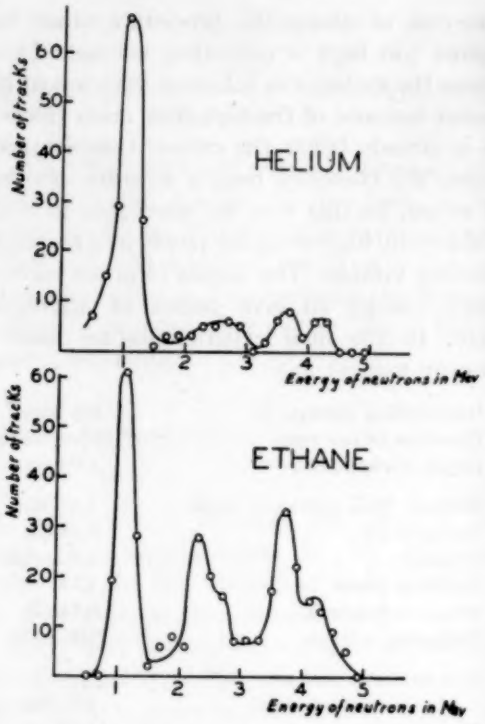

FIG. 2. The spectrum of the neutrons of Be+D at 0.88 Mev bombarding energy measured with helium and hydrogen recoils.

respectively. In the figures, no correction of the intensities for the track length has been applied. In the case of the hydrogen recoils, the chamber was filled with 1.78 atmos. of ethane and water vapor. 1500 pictures gave 278 measurable tracks within $\pm 12°$ to the direction of the incident neutron. From the D−D contamination neutrons, we determined the stopping power of the gas to be 2.96. With this number, the Q values of the four lines are 4.13, 3.54, 2.02 and 0.79 Mev in fairly good agreement with Bonner's[4] values of 4.2, 3.7, 2.2 and 0.9 Mev. It may be pointed out that we did not take any particular precautions to get accurate values of the stopping power. In the case of the helium filled chamber, the pressure was one atmos. helium and water vapor. 7250 pictures yielded 180 tracks. Since, in this case, the D+D contamination did not show up separated from the 2.2-Mev line (because of the small number of tracks in this line) the stopping power was afterward determined by taking a set of pictures with the D+D neutrons. This gives roughly a value of 0.226 for the stopping power using the range energy relation of Blewett and Blewett.[10] The Q values calculated from this number are 4.18, 3.53, 2.29 and 0.80 Mev, in good agreement with the ethane results, except the value 2.29. This seems to be caused by the nonresolved D+D contamination. From the range energy curve of Holloway and Livingston,[11] the stopping power is 0.258 and the Q values are 4.47, 3.69, 2.33 and 0.78 Mev.

A second run was then taken at a bombarding voltage of 0.88 Mev, thus slightly increasing the energy of every neutron group. Fig. 2 shows the results of these measurements. Again for hydrogen recoils the chamber contained 1.93 atmos. ethane with water vapor. Because of the higher bombarding energy, the lines are somewhat wider and the D+D contamination neutrons are not well separated. Therefore, the stopping power was again determined by a run with the D+D neutrons. This gave a stopping power of 3.04. The Q values are: 4.28, 3.74, 2.29 and 0.72 Mev—all being slightly higher than in the previous set.

For the measurements with helium recoils, the chamber was again filled with about one atmos.

[10] A graph of this curve was sent to us by Dr. Bethe.

[11] M. G. Holloway and M. S. Livingston, Phys. Rev. **54**, 18 (1938).

He and water vapor. The calibration by the D+D neutrons gave a stopping power of 0.230, from the range energy curve of Blewett and Blewett[10] and 0.258, from Holloway and Livingston's[11] data. With the curve of Blewett and Blewett, the Q values are 4.09, 3.54, 2.47 and 0.69 Mev, while with the curve of Livingston they are 4.38, 3.70, 2.54 and 0.66 Mev.

The measured intensities J_H and J_{He} of the different lines are given in columns 2 and 4 of Table I. Columns 6 and 7 give the intensities after being corrected for the track length. The corrections (by which the measured value was divided) are listed in columns 3 and 5. The stopping power we used was chosen so that the corrections for corresponding lines in the two different gases are as equal as possible. In the last column the values of J_{He}/J_H times an arbitrary constant, A, are listed. The value of A is, of course, different for the two sets at 0.6 and 0.88 Mev. Accidentally they are almost equal. The errors given are estimated as the sum of the relative mean statistical errors of two corresponding lines.

The results of the H and He measurements with the counter are shown in Fig. 3 where the number of recoils is plotted against their energy for equal numbers of neutrons of 2.6 Mev entering the ionization chamber. As the curves are practically straight lines, the distribution of the scattered neutrons is in both cases isotropic. Thus the ratio of the total scattering cross section is equal to the ratio of the backward scattering cross sections measured in the cloud-chamber experiments. The transformation of the biasing voltage of the thyratron into energy of the recoil was done in the following way. We extrapolated the straight part of the curve to the intercept with the abscissa at V_0. After having subtracted $V_0'=11$ volts, the voltage at which ignition of the thyratron takes place, V_0-V_0' corresponds to the maximum energy of the recoil (i.e., 2.6 Mev for the hydrogen and $(16/25)2.6=1.66$ Mev for the helium recoils). Since the characteristic curve of the amplifier is linear, one obtains in this manner the energy corresponding to one volt on the grid of the thyratron for every one of the two measurements. This result may be checked in the following way: By

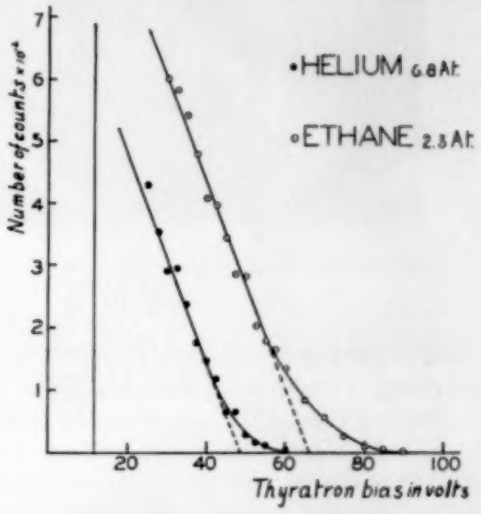

FIG. 3. Number of counts for a given number of incident neutrons as a function of the thyratron bias measured with an ionization chamber filled with ethane and helium, respectively. The vertical line at 11.0 v marks the zero line, i.e., the voltage at which the thyratron breaks down.

inducing a charge of 1.18×10^{-14} coul. on the collecting electrode of the chamber, we obtained a voltage of 56 volts at the output. In the case of helium, the maximum energy of the recoil is 1.67 Mev and the average energy spent per formation of one ion pair is 27.8 ev, so the maximum charge produced by one recoil is

TABLE I. *Measured and corrected intensities J_H and J_{He} of the different lines.*

	Mean Energy	J_H	Track Length Corr. for H	J_{He}	Track Length Corr. for He	J_H Corr.	J_{He} Corr.	$(J_{He}/J_H)A$
0.6 Mev set	1.1	77	0.97	126	0.84	79	149	1.88±0.27
	2.3	93	0.76	24	0.71	122	34	0.28±0.06
	3.6	78	0.51	24	0.56	153	43	0.28±0.06
	4.1	23	0.37	7	0.47	62	15	0.24±0.10
0.88 Mev set	1.3	117	0.93	146	0.89	126	164	1.30±0.16
	2.5	84	0.73	29	0.73	115	40	0.35±0.07
	3.8	92	0.43	19	0.56	214	34	0.16±0.04
	4.3	27	0.27	12	0.47	100	26	0.26±0.09

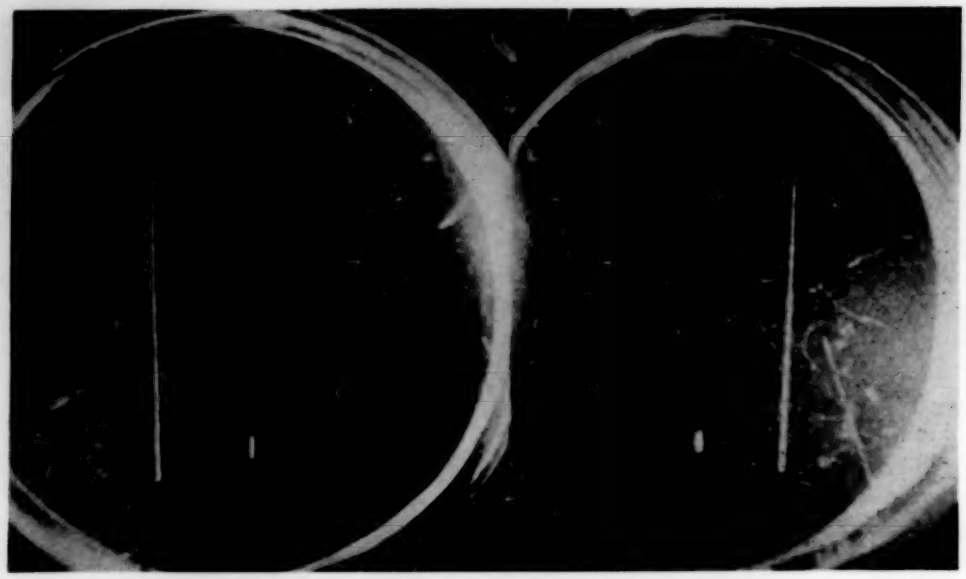

FIG. 4. Two recoils of He and H, respectively, arising from the D+D neutrons in a cloud chamber filled with a mixture of methane and helium.

$(1.67\times10^{6})(1.6\times10^{-19})/27.8=0.96\times10^{-14}$ coul. Of this charge we estimated that, because of the finite collecting time of the ions, about 86 percent reach the collector.[12] From these data we would estimate that the highest pulses should be 38.5 volts. The observed end point lies at $49-11=38$ volts. In the case of the ethane, the sensitivity of the amplifier was unchanged. The maximum charge produced is $(2.6\times10^{6})(1.6\times10^{-19})/25.6=1.63\times10^{-14}$ coul., 66 percent are estimated to reach the collector, so the maximum voltage is estimated to be 51 volts. The observed value is 55 v. Following the procedure described before, one obtains now the ratio of the scattering cross sections by the following formula:

$$\frac{\sigma_{He}}{\sigma_{H}}=\frac{(dN_R/dE_R)_{He}}{(dN_R/dE_R)_{H}}\frac{n_{H}}{n_{He}}\cdot\frac{4m_{He}}{(1+m_{He})^{2}},$$

using for dN/dE_R the slopes of the two straight lines. As the pressure of the ethane was 2.3 atmos. and that of helium 6.8 atmos., the ratio $n_H/n_{He}=2.03$. The slopes of the two lines are 6.33 and 9.10, respectively, so

$$\sigma_{He}/\sigma_{H}=1.41\pm0.18 \text{ at } 2.5 \text{ Mev}.$$

This result was checked roughly by taking cloud-chamber pictures of the recoils arising from the DD neutrons in a chamber filled with a mixture of methane and helium. One of these pictures containing a helium and a proton recoil both in the forward direction is shown in Fig. 4. The few number of tracks measured on these pictures indicate a ratio of σ_{He}/σ_{H} of about 1.5.

In the case of the carbon neutrons, the ratio of the cross section was determined in the same way, but the accuracy is certainly much smaller. The result we obtained indicates that:

$$\sigma_{He}/\sigma_{H}=0.4 \text{ at } 0.5 \text{ Mev}.$$

It cannot be decided whether the angular distribution is isotropic or not, because of the general uncertainty of the observed points.

With the value of 1.41 of the cross-section ratio at 2.5 Mev, we are now able to determine the value of the constant A. Then the ratio of the corrected intensities observed with the cloud

TABLE II. *Values of* σ_{He}/σ_{H}.

Neutron Mean Energy Mev	σ_{He}/σ_{H} Backward	Neutron Mean Energy Mev	σ_{He}/σ_{H} Backward
0.5	0.4±0.2	2.5	1.41±0.18
1.0	9.5±1.4	3.6	1.4 ±0.3
1.2	6.5±0.8	3.8	0.8 ±0.2
2.2	1.4±0.3	4.1	1.2 ±0.5
2.4	1.8±0.4	4.3	1.3 ±0.5

[12] C. E. Wynn-Williams, Proc. Roy. Soc. **131**, 391 (1931).

chamber gives directly σ_{He}/σ_H. The result is given in Table II. ($A=1.41/0.28=5.04$.) A further point at $E=0$ is obtained by using the value $\sigma_{He}/\sigma_H=0.05$ for thermal neutrons given recently by Carroll and Dunning.[13] As here again the angular distribution is certainly isotropic, this value holds also for the backward scattering. Some points at higher energies may be obtained from the measurements of Bonner and Brubaker[4] and Staub and Stephens[14] on the neutron spectrum emitted when boron is bombarded by deuterons. These results are shown in Fig. 5. The measurements of Bonner and Brubaker were done with a methane-filled cloud chamber. The four lines have mean energies of 13.0, 8.8, 5.9 and 4.1 Mev. Only the two low energy lines can be used, since the recoils of the higher energy groups

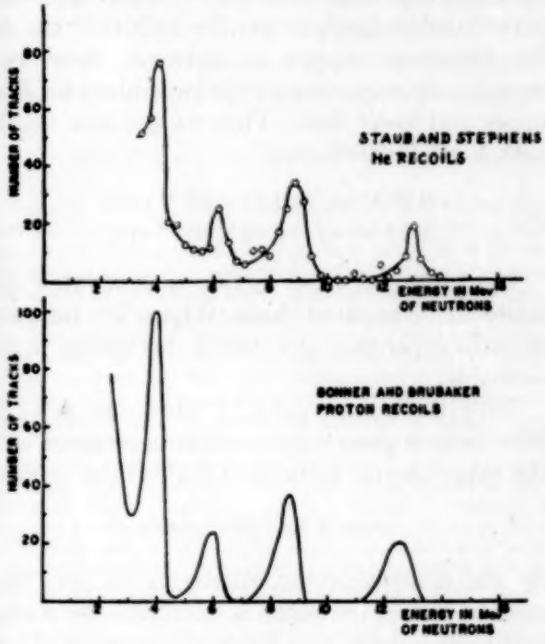

FIG. 5. The neutron spectrum of B+D measured by He and H recoils, respectively.

had to pass through a sheet of mica, thus making the track length correction to be applied very uncertain. The corrected intensities are 1.0 and 3.45 for the 5.9- and 4.1-Mev lines, respectively. In the case of the helium recoils, one obtains from the data of Staub and Stephens the corrected intensities 1.2 and 5.1. If we adjust now the ratio of the intensities at 4.1 Mev to be 1.3, we obtain 1.1 for the ratio of the backward scattering cross section at 5.9 Mev. Fig. 6 shows the results of all the measurements. The shape of the curve between 0.5 and 1 Mev and 1 and 2.4 Mev is, of course, very uncertain because of the lack of measured points.

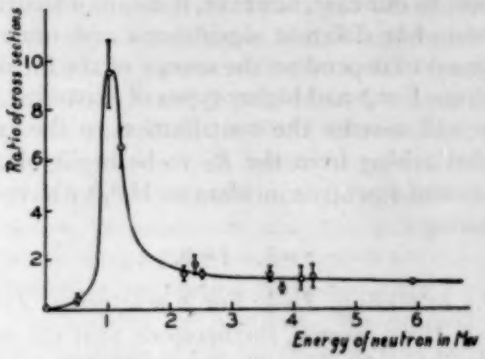

FIG. 6. The ratio of the backward scattering cross section of helium to hydrogen as a function of the energy of the incident neutron. (The energy is measured in the laboratory coordinate system.)

DISCUSSION

The theory of the elastic scattering of neutrons, as influenced by the presence of a resonance level has been given by Bethe and Placzek[15] for heavy nuclei. Although it is doubtful whether as light a nucleus as He^5 can be treated according to this theory, there should remain certain features characteristic for any resonance scattering. Indeed one can assume the cross section for elastic scattering to have the form[15]

$$\sigma=\frac{\pi}{(2s+1)(2i+1)}\sum_J(2J+1)\times\left|2R_J e^{i\delta}+\sum_\gamma\left(\frac{\Gamma_{\gamma J}\lambda_{\gamma J}}{E_A+E_P-E_{\gamma J}+\frac{1}{2}i\gamma_{\gamma J}}\right)\right|^2.$$

The second part within the bars represents the amplitude of the out-going wave caused by resonance scattering. The first part takes care of an additional scattering which can be thought of arising from an effective potential. The main difference between our formula and the one of Bethe and Placzek lies in the phase factor

[13] H. Carroll and J. R. Dunning, Phys. Rev. **54**, 541 (1938).

[14] H. Staub and W. E. Stephens, Phys. Rev. **53**, 212 (1938).

[15] H. A. Bethe and G. Placzek, Phys. Rev. **51**, 450 (1937), (Formula 54).

$e^{i\delta}$. Indeed, while for heavy nuclei one has to assume the wave function to vanish at the surface of the nucleus and thus the phase δ to be zero, one has for a light nucleus to leave this phase undetermined, unless one wants to trust a particular model. Furthermore, the quantity R_J in the case of Bethe and Placzek can be assumed to be a constant, properly called the nuclear radius. In our case, however, it means a length of a somewhat different significance and must be assumed to depend on the energy of the incident neutron. For p and higher types of scattering, we may well assume the contribution to the cross section arising from the R_J to be negligible. In the case of a neutron incident on He^4, we have the following:

$$s=\tfrac{1}{2}, \quad i=0.$$

For s scattering, $J=\frac{1}{2}$. For p scattering, $J_1=\frac{1}{2}$, $J_2=\frac{3}{2}$. If we assume, furthermore, that the spin-orbit interaction is small, we have in the case of p scattering the same resonance energy for both levels and may well assume their width to be the same. Furthermore, as we do not know any other type of disintegration, the partial neutron width is equal to the total width. Thus we get at exact resonance,

$\sigma_s=4\pi(R^2+\lambda_r^2+2R\lambda_r \sin\delta)$ for an s resonance level,

$\sigma_p=4\pi(R^2+3\lambda_r^2)$ for a p resonance level.

One may notice that in the case of a p level, there occurs no phase δ in the expression for σ, as in this case the s potential wave and the p resonance wave do not interfere.

As we observed in our experiments, only the forward scattered recoils within an angle of $\pm 12°$, we have to consider the angular distribution of the recoils. For the s scattering, the distribution in the center of gravity system is isotropic. In the case of p type, it is proportional to $\cos^2\varphi$ per unit solid angle where φ is the angle of the scattered neutron with respect to the direction of incidence. Considering that between the angle θ of the recoil nucleus in the laboratory system and the angle φ there exists the relation $2\theta=-\varphi$, one obtains for the fraction of recoils between θ and $\theta+d\theta$

$N_s(\theta)d\theta=\sin 2\theta d\theta$ for s scattering,

$N_p(\theta)d\theta=3\cos^2 2\theta \sin 2\theta d\theta$ for p scattering.

Integrating these between 0° and 12° gives the numerical factors $a_s=0.0432$ and $a_p=0.1187$. Thus we get now for the partial scattering cross section σ' for recoils between 0° and 12° at exact resonance:

$$\sigma_s'=4\pi\times 0.0432(R^2+\lambda_r^2+2R\lambda_r \sin\delta)$$
$$\sigma_p'=4\pi(0.0432R^2+3\times 0.1187\lambda_r^2).$$

For the numerical evaluation we cannot say anything about the value of δ; thus we are only able to give an upper and lower limit for σ_s'. Furthermore, we have no certain values for R. However, our ratio of cross sections at 2.6 Mev neutron energy, together with the value $\sigma_H=2.1\times 10^{-24}$ cm² for the cross section of hydrogen[16] gives the quite reasonable value for R of 4.8×10^{-13} cm (assuming $\sigma_{He}=4\pi R^2$). On the other hand, with Carroll and Dunning's[13] value $\sigma_{He}=1.5\times 10^{-24}$ cm² at $E=0$, we get $R=3.4\times 10^{-13}$ cm. As the resonance energy is between these two energies, we may consider the two values for R as upper and lower limit. Thus we get now finally with $\lambda_r=5.5\times 10^{-13}$ cm:

$$0.003\leq\sigma_s'\leq 0.58\times 10^{-24} \text{ cm}^2,$$
$$1.42\ \leq\sigma_p'\leq 1.48\times 10^{-24} \text{ cm}^2.$$

The hydrogen cross section at 1.05 Mev can easily be computed from Wigner's[17] formula, since an experimental value at this energy is not available.

With the values $\epsilon_1=0.11$ Mev and $\epsilon_2=2.15$ Mev (which gives σ in excellent agreement with the experimental value at 2.6 Mev) one obtains

$$\sigma_H=3.54\times 10^{-24} \text{ cm}^2.$$

As the neutron-proton scattering at one Mev neutron energy certainly is isotropic, the partial scattering cross section for recoils between 0° and 12° becomes

$$\sigma_H'=0.153\times 10^{-24} \text{ cm}^2.$$

Thus we get, finally, for the ratios of the cross sections:

$0.02\leq L\leq 3.7$ for an s resonance level,

$9.1\ \leq L\leq 9.4$ for a p resonance level.

[16] W. H. Zinn, S. Seeley and V. W. Cohen, Phys. Rev. **53**, 921 (1938).

[17] H. A. Bethe and R. F. Bacher, Rev. Mod. Phys. **8**, 117 (1936).

Our results thus indicate strongly that the anomalous scattering is due to a p resonance level.[18]

The assumption of a weak spin-orbit interaction cannot theoretically be justified. However, figuring out the ratio L under the assumption of strong spin-orbit coupling leads to the result that again L would be much smaller than the observed value (4.8 for $J=\frac{3}{2}$).

It may be pointed out that we would expect that the observed ratio L would be somewhat smaller than the actual because the neutron line has an appreciable width (caused by the penetration in the resonance peak of the cross section). Assuming that the resonance peak has a width of about 0.2 Mev and the neutron line a width of 0.1 Mev (probably less) one estimates that under the most unfavorable conditions the measured ratio L should be about $\frac{2}{3}$ the actual ratio. So we still think our experiment to be in fairly good agreement with the assumption of a p resonance level.

Our result does not say anything, of course, about the existence of a stable He^5 as suggested by Joliot and Zlotowski.[19] As such a stable level would be about 3.6 Mev lower than the one here considered, it would not give an appreciable contribution to the cross section.

It may be of interest to note that the existence of the anomalous n-He scattering cross section described above explains the appearance of a rather strong group of low energy neutrons in the experiments of Baldinger, Huber and Staub[9] on the neutron spectrum of the D+D reaction. While Bonner,[20] using proton recoils, found this group to be about 1/10 of the main peak, Baldinger, Huber and Staub found it to have about the same intensity, using He recoils in an ionization chamber. As the low energy peak occurs at about 1.1 Mev, it is obvious that the anomalous cross section gives too high a value for the number of neutrons. We applied the calculated value of the He cross section to these results and found, considering the angular distribution, that the correct intensity is just 11 percent of the main peak in good agreement with Bonner's result.

In conclusion, we wish to thank Mr. R. Becker, Mr. T. Lauritsen and Mr. J. F. Streib, Jr., for valuable assistance, and Dr. F. Bloch, Dr. L. Schiff and Dr. R. Serber for the discussion of the theoretical aspects of this problem. We gratefully acknowledge the support and advice of Dr. C. C. Lauritsen. One of us (H. Staub) is very much indebted to the "Jubiläumsfond" and the "Stipendienfond der Eidgenössischen Technischen Hochschule," Zürich, Switzerland, for a grant enabling him to carry out this work at Pasadena.

[18] As Dr. Bloch pointed out to us, there is a further support for the conclusion that the resonance scattering is of the p type. The peak in the α-particle curve of Williams, Shepherd and Haxby, reference 3, due to the recoil from He^5 shows an additional width of about 0.15 to 0.25 Mev—this value thus is just the width of the resonance level of He^5 here considered. Indeed if it were an s type scattering, there would be no reason why the width should not be of the order of several Mev. The explanation of Bohr of the occurrence of sharp levels in heavy nuclei cannot be applied here, since we cannot expect the neutron to make many collisions in the compound nucleus before it escapes. The explanation seems to lie in the fact that for a given energy the lifetime of the compound nucleus in a p state is considerably longer than that of an s state. A reasonable measure for their ratio is that of the square of the p and s wave functions of the incident neutron. Since this ratio measures the relative probability of finding the neutron in the compound nucleus, it is given by $(R/3\lambda\!\!\!^{-})^2$ which, in our case, is between 13 and 26 for the two limiting values of R. The very fact that the observed width is of the order of 0.2 Mev indicates that the resonance level is a p state.

[19] F. Joliot and I. Zlotowski, Comptes rendus **206**, 1256 (1938).

[20] T. W. Bonner, Phys. Rev. **53**, 711 (1938).

The Angular Distribution of the Disintegration Products of Light Elements

R. O. Haxby, J. S. Allen and J. H. Williams
University of Minnesota, Minneapolis, Minnesota

(Received November 22, 1938)

The angular distributions of the following reactions:

$$Li^6+H^2\rightarrow 2He^4$$
$$H^2+H^2\rightarrow H^3+H^1$$
$$B^{11}+H^1\rightarrow Be^8+He^4$$
$$B^{11}+H^1\rightarrow 3He^4$$

have been investigated over the range of angles from 45° to 150° and over a range of bombarding voltages between 100 and 200 kv. The Li reaction was found to be spherically symmetrical. The deuteron-deuteron protons were found to have an angular distribution in the center of mass system of coordinates represented by $1+0.7\cos^2\theta$ over a range of bombarding voltages from 106 to 190 kv, with no measurable dependence upon deuteron energy. The third reaction, a resonance process, investigated at 190 kv, gave an angular distribution represented by $1+0.7\cos^2\theta$. The continuous energy distribution alpha-particles with ranges greater than 30 mm from the fourth reaction show an angular distribution which is dependent on the proton energy and indicate an intimate connection between the alternate modes of distintegration.

Introduction

UNTIL recently, the few experiments performed on the angular distributions of particles emitted in artificial disintegrations showed no appreciable deviation from spherical symmetry.[1,2] In 1936, however, Kempton, Browne and Maasdorp[3] made a careful investigation of the deuteron-deuteron reactions:

$$H^2+H^2\rightarrow H^3+H^1, \quad (1)$$

$$H^2+H^2\rightarrow He^3+n^1, \quad (2)$$

detecting both protons and neutrons in separate experiments. They discovered a very marked asymmetry in both cases when the number of particles was determined as a function of the angle with respect to the direction of the incident deuteron beam. When the observations were referred to a system of coordinates moving with the center of mass of the two particles, it was found that the angular distributions were symmetrical about 90° and that the number of particles at 0° was approximately 1.5 times that at 90°. Furthermore, the distributions were found to be insensitive to the energy of the incident deuteron between 100 and 200 kv.

Neuert[4] repeated these experiments, observing the protons from reaction (1) in an annular cloud chamber surrounding the target. His results agreed qualitatively with those of the Cambridge experimenters. He studied also the reactions:

$$Li^6+H^2\rightarrow Li^7+H^1, \quad (3)$$

$$B^{11}+H^1\rightarrow Be^8+He^4, \quad (4)$$

$$B^{11}+H^1\rightarrow 3He^4 \quad (5)$$

and established the existence of asymmetry in (4) and (5).

The importance of these observations is made evident when one notes that the assignments of nuclear resonance levels depends upon accurate experimental determinations of angular distributions of disintegration products of such resonance reactions[5] as (4). Indeed, Oppenheimer and Serber[6] definitely exclude certain possibilities for the resonance state of C^{12} on the basis of Neuert's observations. Anisotropic distributions may result only from the penetration of an incident particle with angular momentum and exact experimental data should allow some assignments of this energy state.

[1] F. Kirchner, Physik. Zeits. **34**, 785 (1933).
[2] J. Giarratana and C. G. Brennecke, Phys. Rev. **49**, 35 (1936).
[3] A. E. Kempton, B. C. Browne and R. Maasdorp, Proc. Roy. Soc. **A157**, 386 (1936).
[4] H. Neuert, Physik. Zeits. **38**, 122, 618 (1937).
[5] J. H. Williams, W. H. Wells, J. T. Tate and E. L. Hill, Phys. Rev. **51**, 439 (1937).
[6] J. R. Oppenheimer and R. Serber, Phys. Rev. **53**, 636 (1938).

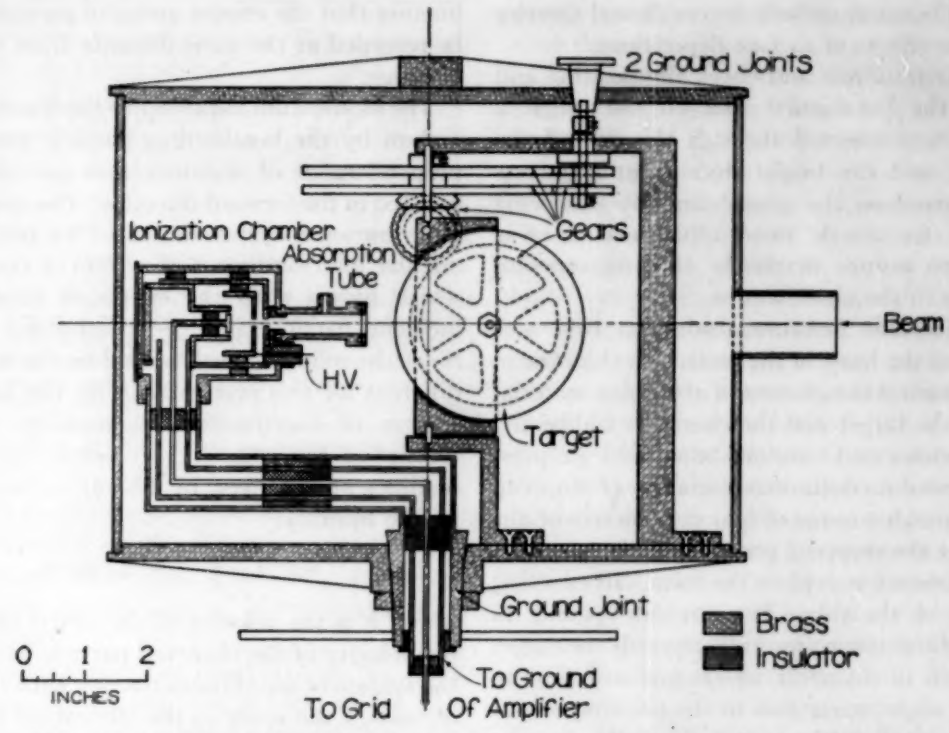

FIG. 1. Cross-sectional view of the angular distribution apparatus. The evacuated enclosure is attached to the ion accelerating tube through the opening marked "Beam" at the right. A vacuum-tight flexible connection is made through the base of the enclosure to the absorption tube.

Such further information as the energy dependence of the angular distribution should contribute much to our theories of disintegration mechanisms. For instance, the nondependence upon energy of the deuteron-deuteron reaction is not understandable from the point of view of the present theory.[7]

In view of the importance of such measurements on reactions involving light nuclei we decided to repeat and possibly extend some of the above observations.

APPARATUS

The angular detecting apparatus is shown in Fig. 1. A ten-inch diameter brass tube which was part of the vacuum system contained the target, air absorption tube and ionization chamber. The target was placed at the geometric center of this enclosure and the ionization chamber could be rotated in such a manner as always to point at this center. This angular motion was accomplished by means of a ground joint accurately centered in the base as shown in Fig. 1. A graduated scale fastened to the bottom of the tapered plug measured the angular position of the chamber with respect to the ion beam entering the side of the evacuated container.

The desirable angular motions of the target were accomplished by gears coupled to two separate ground joints which projected through the top plate. One of these rotated the target about the central axis of the vacuum container and thus varied the angle between the beam and the plane of the target surface. This adjustment was designed to keep the angle of incidence approximately equal to one-half of the angle at which the disintegration particles were observed and consequently reduce to a minimum the effect of any roughness of the target surface. The other tapered plug and set of gears rotated the annular disk target holder about an axis through its center and perpendicular to the plane of the target surface. The purpose of the latter adjustment was to present a fresh target surface

[7] Private correspondence with Professor Oppenheimer.

to the ion beam at periodic intervals and thereby reduce the effects of surface depositions.

In order to adjust and check the position and focus of the bombarded spot on the target a telescope was inserted through the side of the container and the bright fluorescent spot was kept centered on the cross-hairs. By observing the spot for every new adjustment it was possible to reduce markedly the instrumental variations in the observations.

An adjustable pressure absorption tube was fastened to the front of the ionization chamber in order to control the amount of absorbing material between the target and the chamber. Calibrated mica windows and carefully measured air pressures allowed a continuous variation of stopping power through a range of four centimeters of air. To change the stopping power by larger amounts it was necessary to replace the mica foils covering the ends of the tube. The circular opening in the end of the absorption tube towards the target was $\frac{1}{4}$ inch in diameter which was sufficient to allow for slight variations in the position or size of the ion spot on the target. Since the opening near the ionization chamber was $\frac{5}{32}$ inch in diameter, the absorption tube served as a collimator, restricting the angular spread of the observed particles to less than $\pm 5°$. The high voltage apparatus described by Williams, Wells, Tate and Hill[5] was used to accelerate the ions in these experiments. Later modifications such as ion source,[8] voltmeter[9] and current integrator[10] have been described previously.

Experimental Procedure

As the bombarding particle contributes energy to the disintegrating system, the range of the observed particle will depend upon the angle of observation in the laboratory system of coordinates. This change in range with angle is quite marked, particularly in the case of reactions involving light nuclei. In order to eliminate this effect the amount of absorbing material between the target and the ionization chamber was adjusted for every angle of observation in such a manner that the chosen group of particles would be recorded at the same distance from their end of range.

The momentum imparted to the disintegrating system by the bombarding particle results in a preponderance of disintegration particles being emitted in the forward direction. The momentum contribution may be eliminated by plotting the angular distributions in a system of coordinates which moves with the center of mass of the incident particle and the bombarded nucleus. Since the solid angle subtended by the detector is different for this system than for the laboratory system of coordinates, all readings must be multiplied by a factor $g(\theta)$ before the angular readings are changed by $(\theta_r-\theta)$, θ_r being given by the formula:

$$\sin(\theta_r-\theta)=(V/v_r)\sin\theta, \tag{1}$$

where V is the velocity of the center of mass, v_r the velocity of the observed particle measured in the system of coordinates moving with the center of mass, θ the angle in the laboratory system of coordinates between the direction of the observed particle and that of the bombarding beam, and θ_r the corresponding angle in the center of mass system. $g(\theta)$ is given by the formula:

$$g(\theta)=\frac{\sin\theta\, d\theta}{\sin\theta_r\, d\theta_r}=\frac{\sin^2\theta}{\sin^2\theta_r}\cdot\cos(\theta_r-\theta). \tag{2}$$

The quantitative determination of the number of particles was accomplished by a series of comparisons of the numbers emitted at neighboring angles. For example, the ratios of the number emitted per unit solid angle at 75° and 105° to those at 90°, taken as a standard angle, could be obtained without adjusting the angle between the target surface and the incident ion beam. After a sufficient number of separate observations were obtained to insure the validity of the above ratios, the experiments were then extended to another set of angles, e.g. 45°, 60°, 75°, taking 75° as the secondary standard. In this stepwise manner the total angular range available, 45° to 150°, was covered and recorded in terms of the ratio of the number of particles

[8] J. S. Allen, Rev. Sci. Inst. **9**, 160 (1938).
[9] L. R. Hafstad, N. P. Heydenberg and M. A. Tuve, Phys. Rev. **50**, 504 (1936).
[10] J. H. Williams, W. G. Shepherd and R. O. Haxby, Phys. Rev. **52**, 390 (1937).

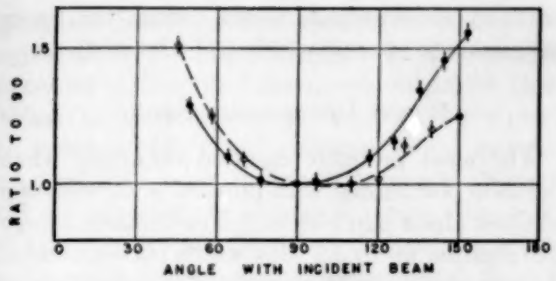

FIG. 2. The angular distribution of protons from the deuteron-deuteron reaction. ($H^2+H^2 \rightarrow H^3+H^1$) at 190 kv. Dashed curve is for the laboratory system, full curve for the center-of-mass system. The ratio of the number of protons per unit solid angle observed at a given angle to the number observed at 90° as the standard is plotted as a function of the angle between the direction of the observed protons and the direction of the incident deuteron beam.

observed per unit solid angle at a given angle to those observed at 90°. These ratios were then transformed from the laboratory system of coordinates to the center of mass system of coordinates.

In order to test the reliability of the above procedure, the angular distribution of the copious, long range alpha-particles from the reaction:

$$Li^6+H^2 \rightarrow 2He^4 \qquad (6)$$

was investigated. The results indicated that the distribution was spherically symmetrical to within the accuracy of the exploratory observations and the internal consistency of the readings indicated that the apparatus was sufficient for the program outlined.

DEUTERIUM

The deuterium target used was NaOD, made by adding D_2O to Na_2O_2 and melting the resultant NaOD onto a nickel plate. This plate was mounted on the brass disk target holder adjacent to some NaOH which served as a fluorescent object in preliminary alignments of the ion beam.

Since the range of the protons from (1) changes rapidly with angle even at a bombarding deuteron energy of 190 kv, readings were taken to insure that all the protons were counted at the various angles. The ionization chamber was made 18 mm deep and the collecting voltage increased to 2000 volts. With these precautions, integral range-numbers curves demonstrated that the stopping power could be adjusted so that all the protons were detected.

The results of the final investigation of the angular distribution is shown in Fig. 2. The open circles show the experimentally determined values of the ratio of the number of protons per unit solid angle observed at a given angle to those observed at 90°. The full circles are the ratios calculated from these by transforming to a system of coordinates moving with the center of mass. It will be seen that the effect of the moving center of mass is very marked, both in the value of the ratio and in the angular coordinates. It may also be noticed that in the center of mass system the curve is symmetrical about 90° to within the statistical variations in the readings. This is obviously necessary, since in this coordinate system the two deuterons are approaching each other with equal velocities.

Following these experiments, the ratios from 90° to 150° were repeated with bombarding deuteron energies of 190 kv and 106 kv. The results of these investigations are plotted in Fig. 3. The full curve is a plot of the expression $1+0.7\cos^2\theta$ where θ is the angle in the center of mass system of coordinates between the observed disintegration protons and the incident deuterons. This curve was chosen by Kempton, Browne and Maasdorp[3] as the mathematical expression which would best fit their results. It may be seen that these results agree with theirs in showing no

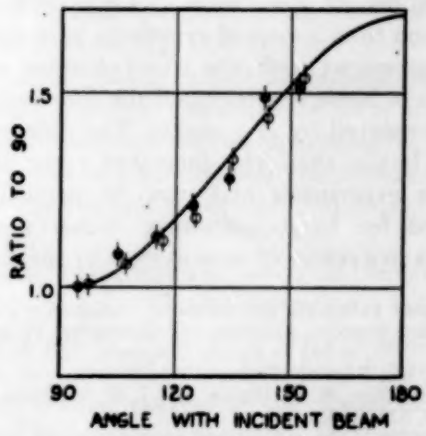

FIG. 3. The angular distribution of protons from the deuteron-deuteron reaction ($H^2+H^2 \rightarrow H^3+H^1$) at incident deuteron energies of 106 kv and 190 kv. The open circles are for 190 kv, the black dots for 106 kv. The full curve is a plot of $1+0.7\cos^2\theta$. All points are in the center-of-mass system.

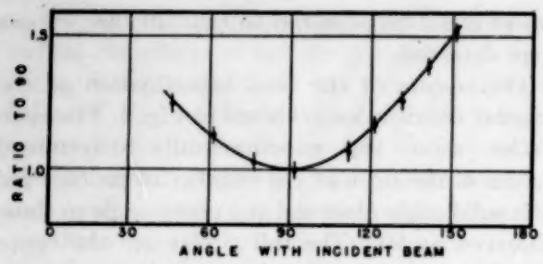

FIG. 4. The angular distribution in the center-of-mass system of the long range alpha-particles from boron under proton bombardment. ($_1H^1+_5B^{11}\rightarrow{}_2He^4+{}_4Be^8$.)

appreciable change in the angular distribution with the energy of the incident deuteron.

BORON HOMOGENEOUS GROUP

The products of bombarding boron with protons are a continuous group of alpha-particles, (3), whose excitation curve is normal and a homogeneous group, (4) of greater range which shows[11] a marked resonance at 160 kv.[12] This latter group was examined separately by interposing the necessary absorbing material between the target and the integral ionization chamber for each angle of observation. The results of these observations at 190 kv, again plotted in terms of the number of alpha-particles per unit solid angle at a given angle relative to those at 90° and transformed to the center of mass system are shown in Fig. 4. Here again, the distribution was found to be symmetrical about 90° and strangely enough, to fit the curve $(1+0.7\cos^2\theta)$. The deviation from spherical symmetry is in qualitative agreement with the cloud-chamber observations of Neuert[13] who found the distribution to be represented by $(1+\cos^2\theta)$. The difference is much larger than the indicated error in the present experiment and may be partially accounted for by transforming Neuert's observations to a center of mass system by the method outlined above which would reduce the latter expression to approximately $(1+0.9\cos^2\theta)$.

BORON CONTINUOUS GROUP

The most probable reaction occurring when boron is bombarded with protons is the emission of three alpha-particles with a continuous energy distribution up to 5.2 Mev which corresponds to a range of 37 mm. The angular distribution of the more energetic particles of this group was examined by reducing the stopping power between the target and the integral ionization chamber so that all particles with ranges greater than approximately 30 mm were recorded. These observations were corrected for the small number, less than twenty percent, of homogeneous long range alpha-particles contributed from reaction (4). The first angular distribution data were taken with a bombarding proton energy of 190 kv. The deviation from spherical symmetry shown in the upper curve of Fig. 5 bears a marked similarity to the results of the homogeneous resonance group from (4). The experiments on the short range continuous group were then repeated at a proton energy of 143 kv, this energy being below the resonance energy, 160 kv, for the competing reaction (4). The resulting angular distribution, shown in the lower curve of Fig. 5, was found to be almost spherically symmetrical to within the errors of the measurements. The rise in this curve at large angles may be caused by adverse statistical fluctuations since comparatively few particles were recorded because of the low yield at this voltage.

These results at 190 kv are very similar to those of Neuert,[4] but again show a smaller

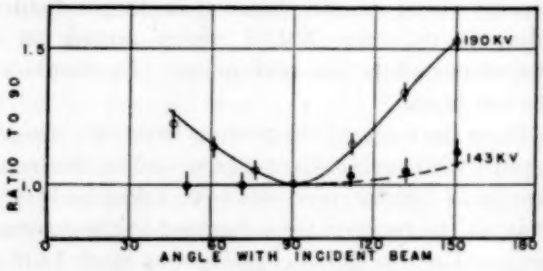

FIG. 5. The angular distribution in the center-of-mass system of alpha-particles with ranges between 30 and 38 mm from boron under bombardment with protons ($_1H^1+_5B^{11}\rightarrow 3_2He^4$) of 190 and 143 kv energy.

[11] Recent values for the resonance voltage are given by Waldman, Waddel, Callihan and Schneider, Phys. Rev. **54**, 543 (1938) as 165 kv and by Bowersox, Bull. Am. Phys. Soc. **13**, 13 (1938) as 172 kv.

[12] J. S. Allen, R. O. Haxby and J. H. Williams, Phys. Rev. **53**, 325 (1938).

[13] Because of the geometrical arrangement of the sensitive portion of the cloud chamber used by Neuert, his observations are a measure of the number of particles per unit solid angle instead of the number in an arbitrary angular range as one might infer from the text of his paper and his manner of correction to express them in the center of mass system of coordinates.

deviation from spherical symmetry. A possible explanation for the difference in the results obtained in the two laboratories might be that Neuert's measurements of ranges of the alpha-particles in his cloud chamber could not be accomplished with sufficient accuracy. Neuert did not consider the change in range with angle of emission as it was less than the probable error in his range measurements. Consequently he did not measure, at all angles, exactly the same group of particles. As there is an increasing number of alpha-particles at the lesser ranges, more particles would be observed at small angles with respect to the proton beam. Consequently the distribution would be observed to be more asymmetrical than is actually the case. Neuert further discovered that as he reduced the absorbing material in the path of the alpha-particles that the angular distribution gradually changed to spherical symmetry. Because of the difficulties of supporting two mica foils in the present apparatus, no attempt was made to investigate the distribution of particles with ranges less than 30 mm.

The surprising difference in the angular distribution of the alpha-particles from (5) when the energy of the bombarding proton was changed from 190 kv to 143 kv led to an investigation to the intermediate energy interval. The observations were restricted to the range of angles between 90° and 150° as it was assumed that the distributions would remain symmetrical about 90°. The distributions obtained are shown in Fig. 6 and it may be seen that there is a gradual

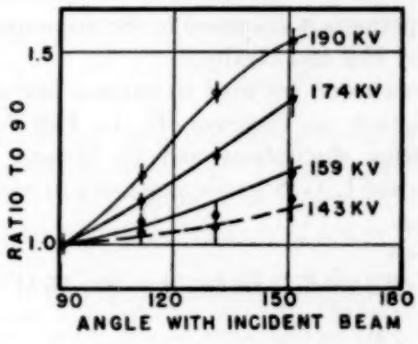

FIG. 6. The angular distribution of alpha-particles with ranges between 30 and 38 mm from boron under bombardment with protons ($_1H^1+_5B^{11}\rightarrow 3_2He^4$) of 143, 159, 174 and 190 kv.

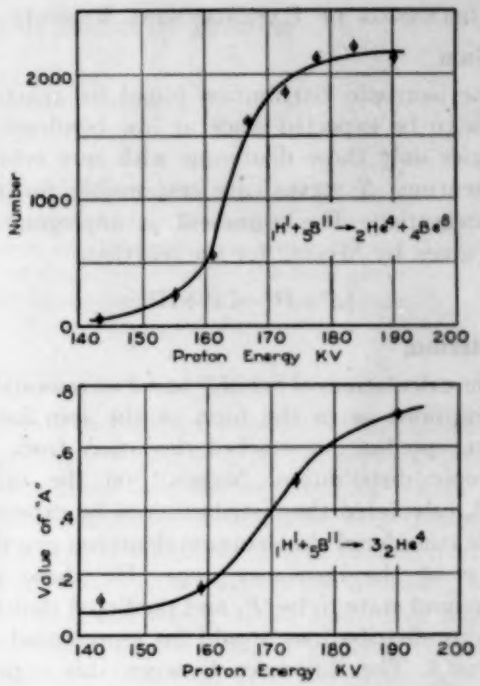

FIG. 7. The upper figure represents the *yield* of alpha-particles with ranges >40 mm from a thick target of boron as a function of the bombarding proton's energy. The lower figure represents the value of the coefficient A in $1+A\cos^2\theta$, the function chosen to represent the anisotropic angular distribution of alpha-particles with ranges >30 mm and <38 mm from a thick target of boron, as a function of the bombarding proton's energy.

change in the anisotropy in this voltage region. This change is *not* caused by the additional number of alpha-particles being contributed at the resonance voltage from reaction (4) since this small number has been subtracted from the total observed. However, there must be some intimate connection between the two competing reactions, for this phenomenon occurs in the voltage region about the resonance voltage, 160 kv, of reaction (4).

In order to clarify this connection the curves of Fig. 6 were fitted by the expression $1+A\cos^2\theta$ and the values of A were determined. These values are plotted as a function of the bombarding proton energy in the lower curve of Fig. 7. The upper curve shows for purposes of comparison the thick target yield curve of homogeneous, long range alpha-particles from (5). It may be seen that there is a marked similarity in the form of these curves.

Discussion of Experimental Results

Lithium

The isotropic distribution found for reaction (6) is to be expected since at low bombarding energies only those deuterons with zero orbital momentum, S waves, are responsible for the disintegration. The argument is analogous to that given by Myers[14] for the reaction,

$$Li^6+H^2\rightarrow Li^7+H^1.$$

Deuterium

The calculations of Schiff,[15] based on reasonable assumptions as to the form of the spin interaction, predict no marked deviation from an isotropic distribution. Myers,[14] on the other hand, calculated the distribution to be expected if one considered the deuteron-deuteron reaction to be of the resonance type. He chose the compound state to be $^3P_1$ and predicted that the angular distributions would be represented by $1+\cos^2\theta$. The difference between this expression and the concordant experimental results, $1+0.7\cos^2\theta$, of the Cambridge group,[3] Neuert's[16] most recent data at 120 kv, and the present experiment is quite real and entirely outside the experimental uncertainty. This disagreement is indicative of an insufficient understanding of the nuclear disintegration process, but unfortunately, the experimental result serves only as a check on any proposed theory and gives no obvious clue to a solution of the problem.

A further significant point in the experimental results is the lack of any appreciable change in the distribution function between 106 and 190 kv. Recently, Neuert[16] found that the anisotropy becomes less marked as the bombarding deuteron energy is decreased to 35 kv, the distribution then being represented by $1+0.2\cos^2\theta$. The slow change of the form of distribution as a function of energy suggests some sort of coupling between two waves having different j values. Since there is no coupling between a P and S wave, the most likely coupling is between a D and S wave. This would probably result in an additional $\cos^4\theta$ term in the distribution function which would be difficult to distinguish if it were small in magnitude.

Boron

The resonance reaction, $B^{11}+H^1\rightarrow Be^8+He^4$, is most amenable to theoretical treatment. Oppenheimer and Serber[6] have discussed the various possibilities on the basis of pertinent selection rules. They conclude that it is not possible to make a definite assignment of the nuclear resonance level of the intermediate nucleus, C^{12}, or the normal state of B^{11}. None of the distributions to be expected from the various combinations of the possible levels agrees with the experimental determination. Myers[14] assigns to C^{12} the excited state $^1D_2$, even and to B^{11} the ground state $^2P_{3/2}$, odd. On the basis of pure Russell-Saunders coupling he predicts the angular distribution $1+3\cos^2\theta$ which is in poor agreement with the present experimental value ($1+0.7\cos^2\theta$) and those of Neuert.[4] The choice of the type of interaction between spin and orbital momenta will influence the theoretical prediction and the experimental results may act as a guide in the selection of a reasonable hypothesis.

No theoretical calculations have been made on the more complex disintegration, $B^{11}+H^1\rightarrow 3He^4$. The striking similarity between the angular distribution of the resonance group and the distribution found for the most energetic alpha-particles in this reaction at high voltages, shown in Figs. 4 and 5, suggests a more intimate connection between reactions (4) and (5) than was previously supposed. Further evidence for this hypothesis is discussed in the accompanying paper by Hill and Haxby.[17]

In conclusion we wish to express our sincere appreciation to Professor E. L. Hill for his stimulating discussions and to Messrs. J. F. Marvin and L. G. Stier for assistance in recording the data.

[14] R. D. Myers, Phys. Rev. **54**, 361 (1938).
[15] L. I. Schiff, Phys. Rev. **51**, 783 (1937).
[16] H. Neuert, Naturwiss. **26**, 429 (1938).
[17] E. L. Hill and R. O. Haxby, Phys. Rev. **55**, 147 (1939).

A Note on the Disintegration of Boron by Protons

E. L. Hill and R. O. Haxby*
University of Minnesota, Minneapolis, Minnesota
(Received November 22, 1938)

The measurements on the angular distribution of the α-particles arising from the bombardment of boron by protons given in the preceding paper are discussed. It is suggested that the particles from the continuous distribution which show an angular distribution have a common origin with the particles in the homogeneous group at 44 mm, and that further, this latter group may not be a truly homogeneous group, but may arise from a peculiarity of the three-particle disintegration.

THE general nature of the theory of the angular distribution of the products arising from nuclear reactions has been discussed by Bethe and Placzek[1] on the basis of the Breit-Wigner[2] resonance theory. If one makes the assumption that but a single resonance level of the intermediate nucleus is involved, and if some assumption about the nature of the angular momentum coupling scheme is made, then it becomes possible to draw some conclusions about the characteristics of the resulting angular distribution. Without such simplifying assumptions, it is necessary to have a detailed theory of the nuclear process in order to make progress.[3]

Unfortunately the evidence is that these simplifications are not likely to be very well satisfied even for the lighter nuclei, where it might be hoped that the "single resonance level" hypothesis would be expected to hold best. Some months ago Oppenheimer and Serber[4] discussed the proton-boron reactions

$$ {}_5B^{11} + {}_1H^1 \rightarrow [{}_6C^{12}] \rightarrow 3\,{}_2He^4 \quad (1) $$

$$ \rightarrow {}_4Be^8 + {}_2He^4 \quad (2) $$

$$ \rightarrow {}_6C^{12} + \gamma. \quad (3) $$

On the basis of the experimental evidence it has been assumed heretofore[4, 5] that reaction (1) arises from the capture of an s proton, and (2) and (3) arise from the capture of a p or even a d proton. The evidence is good[6, 7, 7a] that (2) and (3) arise from a single type of capture process. Oppenheimer and Serber concluded that with this interpretation it would be very difficult to find a type of resonance level of the intermediate nucleus which would satisfy the necessary selection rules, and which would lead to an angular distribution of the α-particles from (2) at all comparable with that observed experimentally. Myers has also discussed reaction (2) from substantially the same point of view and with similar results.[8]

The new information contained in the previous paper now throws considerable doubt on the basis for these calculations. Most important is the observation that at least some of the α-particles in the continuous group attributed to reaction (1) exhibit an angular distribution, and consequently arise from other than s proton capture. On the basis of the evidence it now seems likely that the continuous group consists of at least two kinds of α-particles; (1) a group arising from s proton capture which show no angular distribution, which we designate by α_0, and (2) a group showing an angular distribution which we designate by α_δ. For notational purposes we shall refer to the α-particles in the homogeneous group at 44 mm as α_h.

We cannot be sure as yet that the α_δ- and the α_h-particles have their origins in a common capture process to some definite level of the

* Now at Westinghouse Research Laboratories.
[1] H. Bethe and G. Placzek, Phys. Rev. **51**, 450 (1937).
[2] G. Breit and E. Wigner, Phys. Rev. **49**, 519 (1936).
[3] E. g., as in K. Ochiai, Phys. Rev. **52**, 1221 (1937).
[4] J. R. Oppenheimer and R. Serber, Phys. Rev. **53**, 636 (1938).
[5] J. H. Williams, W. H. Wells, J. T. Tate and E. L. Hill, Phys. Rev. **51**, 434 (1937).
[6] W. Gentner, Zeits. f. Physik **107**, 354 (1937).
[7] B. Waldman, R. C. Waddel, D. Callihan and W. A. Schneider, Phys. Rev. **54**, 543 (1938).
[7a] *Note added in proof:* There is as yet no evidence that the resonance γ-ray from reaction (3) leaves ${}_6C^{12}$ in its normal state.
[8] R. D. Myers, Phys. Rev. **54**, 361 (1938).

intermediate nucleus. The available yield curve data[5] are unfortunately not sufficiently accurate to determine the possible existence of a resonance for the α_θ-particles, although the rapid variation of their observed angular distribution with proton energy in the neighborhood of the resonance (Fig. 6 of the preceding paper) makes it seem quite probable that they are related. This is suggested by the following interpretation of Fig. 7 of the preceding paper. Let $n_0(E)$ and $n_\theta(E, \theta)$ be the numbers of particles measured per unit solid angle in the α_0- and α_θ-groups, respectively, where E is the energy of the incident proton and θ the angle at which the α-particles are being collected. Then the measured angular distribution curves of Fig. 6 (preceding paper) give the function

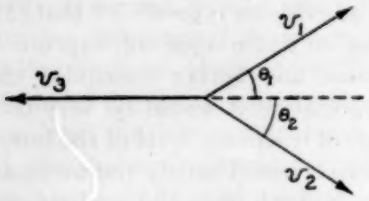

FIG. 1. The three-particle disintegration.

$$F(E, \theta)=\frac{n_0(E)+n_\theta(E, \theta)}{n_0(E)+n_\theta(E, \tfrac{1}{2}\pi)}\sim 1+A(E)\cos^2\theta$$

as a function of θ, for different values of E. If we set

$$n_\theta(E, \theta)=n_\theta(E, \tfrac{1}{2}\pi)+\eta(E, \theta)$$

we get

$$A(E)\cos^2\theta\sim\eta(E, \theta)/[n_0(E)+n_\theta(E, \tfrac{1}{2}\pi)].$$

Over the width of the resonance level the denominator is approximately constant, increasing gradually with E, since $n_0>n_\theta$, so that $A(E)$ follows approximately the form of $\eta(E, \theta)$ as a function of E. If η follows the resonance curve, that is, if the α_θ-particles of the continuous group follow the same resonance process as do the α_h-particles, then $A(E)$ will do likewise. Conversely, the experimental result of Fig. 7 may be interpreted as evidence that the α_θ- and the α_h-particles have a common origin. The test would be more significant if it could be performed with a thin target, in which case $A(E)$ would be expected to follow almost a simple resonance form of curve, but the small numbers of particles from a thin target would undoubtedly make the angular distribution measurements difficult. According to Professor Williams, it may be possible to test this point further by an examination of the yield curves of selected portions of the α-particle distribution with a highly differential counter. Such experiments are being initiated.

One may well question whether the long range α-particle group really is a homogeneous group arising from a definite reaction (2) in which the nucleus ${}_4Be^8$ is left in a stable or quasi-stable state, or whether it is only a portion of a more extended distribution overlapping the continuous group. Professor Williams has also pointed out that the homogeneity of this group may be questioned on the grounds that at proton energies above the resonance energy, the yield curve of the α-particles does not continue to decrease, but flattens out to give a measurable yield (Fig. 3 of reference 5). Recent measurements of Bowersox at the University of Chicago show[9] that at higher proton energies (up to 400 kv) the yield curve of the α_h-particles increases approximately on a Gamow curve. If the observed resonance group is not really a homogeneous group arising from a definite reaction like (2), then it either may be overlapping a true homogeneous group, or may have a somewhat lower energy than such a group, depending on the magnitude[9a] of the binding energy of ${}_4Be^8$.

The possibility that the α_h-particles may be only *apparently* homogeneous is suggested by the following simple consideration. Consider a three-α-particle disintegration pictured in Fig. 1, the center of mass of the system being considered at rest. The equations of momentum and energy give us three relations connecting the five variables v_1, θ_1, v_2, θ_2, v_3. Take v_1 and θ_1 as independent variables and compute the change Δv_3

[9] R. B. Bowersox, Bull. Am. Phys. Soc. **13**, 13 (1938); Phys. Rev. in course of publication.

[9a] *Note added in proof:* According to S. K. Allison, E. R. Graves, L. S. Skaggs and N. M. Smith, Bull. Am. Phys. Soc. **13**, Paper 43 (1938) the binding energy of ${}_4Be^8$ is 0.31 ± 0.06 Mev with respect to two α-particles.

in v_2 due to changes Δv_1 and $\Delta\theta_1$. We find

$$\Delta v_3 = -\frac{\Delta v_1[v_1 - v_2\cos(\theta_1+\theta_2)] + \Delta\theta_1 \cdot v_1 v_2 \sin(\theta_1+\theta_2)}{v_3 + v_2\cos\theta_2}.$$

Now for $\theta_1=\theta_2=0$, $v_1=v_2$, which corresponds to the case for which particle 3 gains the maximum energy, the other two particles going off together, we get

$$\Delta v_3 = 0 \text{ for all } \Delta v_1 \text{ and } \Delta\theta_1.$$

Thus if we measure only the *fast* particles from reactions of nearly this type we shall find a substantially homogeneous group. The small number of particles in the observed α_A-group, and its apparent relation to the continuous group may mean that it has its origin in some such peculiarity of the disintegration phenomenon, and that its existence is not contingent on the possibility of a definite reaction (2).

In order to make this argument complete we should need to know whether there is a reasonably large probability that the three-particle disintegration may occur in this way. This question cannot be discussed with any assurance since we are quite unaware of the factors governing the disintegration from the intermediate state. A rough approach to the problem may be made by a study of the "*a priori* probability distribution" along the lines discussed by Uhlenbeck and Goudsmit.[10] While the form of their distribution curve is incorrect, it does predict that about one percent of the particles would have energies within five percent of the maximum energy. This is of the order of magnitude of that found in the experiment,[8] but because of the uncertainty in the theoretical energy distribution this argument is only illustrative in character.

It may be remarked in passing that the details of the derivation of their formula (13) by Uhlenbeck and Goudsmit seem to be open to some question because of the arbitrary treatment of the coordinates $\mathbf{R}_1$ and $\mathbf{R}_2$. A more detailed analysis yields the distribution function (for equal masses)

$$f(\epsilon) \sim \epsilon^{\frac{1}{2}}(E - \tfrac{3}{2}\epsilon),$$

which is not quite symmetrical. However, the experimental results show clearly that the whole analysis is insufficient, and a more intimate picture of the nuclear process is required.

[10] G. Uhlenbeck and S. Goudsmit, *Zeeman Verhandelingen* (1935), p. 201.

Lastly we note that the angular distribution measurements on the protons from the deuteron-deuteron reaction may be interpreted by the same method as used above for the continuous α-particles from reaction (1). Fig. 3 of the preceding paper shows that the form of the distribution is

$$1 + A\cos^2\theta,$$

where A = const. for E between 106 and 190 kv. The measurements of Neuert[11] show that in the neighborhood of 40 kv the distribution has a much smaller angular dependence than at the higher deuteron energies. As in the boron case this would result if the protons consisted of one group which was angular dependent and another which was not, with the former group showing a broad resonance at low deuteron energies. The data do not appear to be sufficiently detailed to permit any definite check on this hypothesis.

The authors wish to express their thanks to Professors G. Breit and J. Bardeen for various discussions of the boron reactions.

[11] H. Neuert, Naturwiss. **26**, 429 (1938).

The Isotopic Constitution of Uranium and the Half-Lives of the Uranium Isotopes. I†

ALFRED O. NIER*
Research Laboratory of Physics, Harvard University, Cambridge, Massachusetts

(Received November 3, 1938)

A mass spectrographic determination of the relative abundances of the uranium isotopes has been made. The following abundance ratios were found: $U^{238}/U^{235} = 139 \pm 1$ percent; $U^{238}/U^{234} = 17{,}000 \pm 10$ percent. A search was made for other isotopes but none was found. From the above values, together with the results of the alpha-particle counting experiments of Kovarik and Adams, and the assumption that the actinium series is 4.6 percent as active as the uranium, the following decay constants are computed: U_I, 1.520×10^{-10} yr.$^{-1}$; U_{II}, 2.6×10^{-6} yr.$^{-1}$; AcU, 9.72×10^{-10} yr.$^{-1}$. The corresponding half-lives are, respectively, 4.56×10^9 yr., 2.7×10^5 yr. and 7.13×10^8 yr.

IN EVALUATING the decay constants of the three naturally occurring uranium isotopes, $U^{238}(U_I)$, $U^{234}(U_{II})$, and U^{235}(AcU), a knowledge of the relative abundances would be extremely useful. Although two mass-spectrographic studies of uranium have been made, there is no record of any direct determination of the abundances. Aston[1] showed that at least 97 percent of the uranium atoms had the mass 238, while Dempster,[2] who was able to detect U^{235}, estimated that it must have an abundance less than one percent that of U^{238}. U^{234} has not until the present been detected mass-spectrographically. The present paper concerns itself with a mass-spectrographic study from which it is possible to make determinations of the relative abundances of all three isotopes.

Apparatus

A description of the mass spectrometer used in this work has already been given.[3] It may be described briefly as an apparatus in which positive ions are formed by the collision of a controlled beam of low energy electrons with the vapor or the gas of the substance to be investigated. The ions formed by the impact of the electrons are drawn out of the ionizing region, are accelerated and sent around a 180° magnetic analyzer. The analyzed ion current is measured with an electrometer tube amplifier. For the study of relatively nonvolatile substances use is made of a small furnace located inside of the mass-spectrometer tube just above the ionizing region. A compound containing the element to be studied is placed in the furnace which when heated to a suitable temperature volatilizes its contents. Through an opening in the furnace a molecular beam passes into the electron stream where ionization then takes place.

UCl_4 and UBr_4 were found to be satisfactory as sources of ions. A typical mass spectrum is shown in Fig. 1. Three peaks are clearly visible in the figure. The most abundant isotope is, of course, U^{238}, the parent of the uranium-radium family (for obvious reasons, only the lower portion of this peak is shown). The second most abundant isotope is U^{235}. U^{234}, the isotope in radioactive equilibrium with U^{238}, is just visible in the spectrum.

Results

In view of the fact that it was at one time thought[4] that the U_I/AcU ratio might be a function of the age of the mineral in which the uranium is found this ratio was measured for three different samples of widely different geologic age. Table I gives the results obtained. Each of the numbers given is the average of ten determinations of the ratio. The relatively large random variations noted in the table are caused principally by the fact that it was difficult to maintain an absolutely constant stream of vapor from

† Preliminary report, Phys. Rev. **53**, 922 (1938).
* This work was done while the writer was a National Research Fellow at Harvard University. Present address, Department of Physics, University of Minnesota, Minneapolis, Minnesota.
[1] F. W. Aston, Nature **128**, 725 (1931).
[2] A. J. Dempster, Nature **136**, 180 (1935).
[3] A. O. Nier, Phys. Rev. **53**, 282 (1938).
[4] National Research Council Bulletin No. 80, *Age of the Earth* (1931), p. 113.

the furnace. Not only did the pressure in the vapor beam fluctuate randomly, but it also decreased steadily as time progressed. In the case of the uranium from the Swedish Kolm, two compounds, UCl_4 and UBr_4 were tried as sources of ions and gave the same ratio within the experimental errors. As the UBr_4 was found to be more satisfactory as far as steadiness of evaporation was concerned, it alone was used for studying the Wilberforce and Dakeite uranium. Practically all of the readings given correspond to abundances determined for U^+ ions. However, a few determinations (as noted) were made in the UBr^+ and UCl^+ part of the spectrum. The values obtained here are seen to be in good agreement with those found for the U^+ ions when one considers that the UBr^+ and UCl^+ ions are not as plentiful as the U^+, and that, moreover, the resolution of the peaks for these higher mass numbers is not as good as for the lower masses. From this study it seems safe to conclude that within the experimental errors the ratio does not depend upon the compound used nor upon the particular type of ion investigated.

The close agreement between the average values found for the three samples indicates that the ratio does not depend upon the source of the uranium. Allowing for systematic errors such as errors in calibration, discrimination of apparatus against different mass numbers, etc., one can probably safely assume that the best value for the ratio is 138.9 or 139, with a limit of error of one percent.

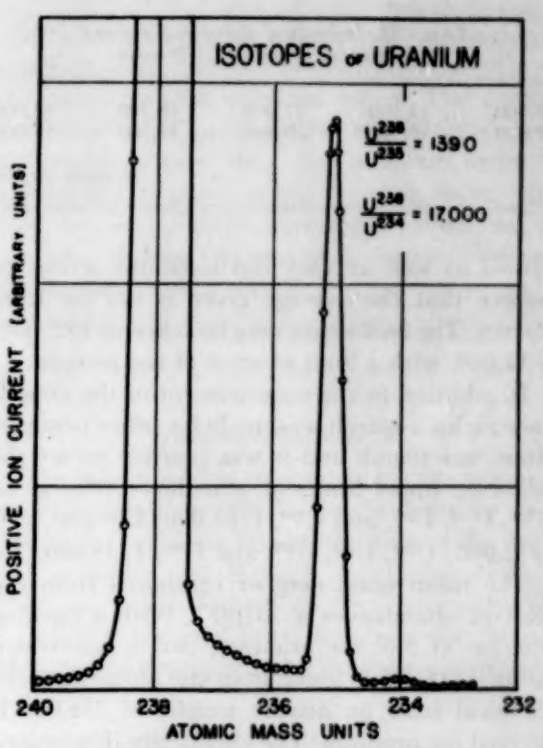

FIG. 1. Mass spectrum showing isotopes of uranium. The experimental points are obtained by plotting positive ion current passing through the exit slit of the analyzer as a function of the energy of the ions while the magnetic field is held constant. As there is a definite relation between the energy and the mass of the ions collected, namely, energy × mass = a constant, the voltage scale can be readily changed to a mass scale, as was done in the figure. The width of the peaks is, of course, caused by the finite width of the slits used and the imperfections in focusing.

TABLE I. U^{238}/U^{235} *ratio in different minerals.*

Source of Uranium	Kolm* (Sweden)		Uraninite† (Wilberforce, Ont.)		Dakeite‡	
Approximate Age	4×10^9 yr.		1.0×10^9 yr.		1×10^9 yr.	
	Ratio	Type of Ion Studied	Ratio	Type of Ion Studied	Ratio	Type of Ion Studied
	139.0	U^+ in UCl_4	140.8	U^+ in UBr_4	139.7	U^+ in UBr_4
	139.4	"	135.3	"	139.7	"
	139.1	"	135.3	"	136.6	"
	139.4	"	142.3	"	138.0	"
	137.5	UCl^+ in UCl_4	137.1	"	137.8	"
	138.0	U^+ in UBr_4	139.4	"	138.2	"
	138.8	"	139.1	"	141.3	UBr^+ in UBr_4
	140.7	UBr^+ in UBr_4	139.7	"		
			139.6	"		
			139.4	"		
			140.3	UBr^+ in UBr_4		
Averages	139.0		138.9		138.8	

* Baxter and Bliss, J. Am. Chem. Soc. **52**, 4848 (1930).
† Baxter and Bliss, J. Am. Chem. Soc. **52**, 4851 (1930).
‡ Larson, Mineralogist, Feb. 1937; American Mineralogist, May 1937; Duke, Mineralogist, March 1938.

The U^{238}/U^{234} ratio was determined only for the uranium found in the Swedish Kolm. Table II gives the results obtained. Each number is the result of one carefully made determination. Because of the extreme rarity of the U^{234} isotope great accuracy in the measurement of this ratio cannot be hoped for. It was not possible to determine the ratio for the U^+ ions formed from the UCl_4 as an unknown rare impurity contributed to the 234 peak. During the time that the UCl_4 was in the tube the apparent U^{238}/U^{234} ratio measured for the U^+ ions increased steadily and appeared to be approaching the values given in the table, indicating the impurity was gradually being eliminated. In view of the fact that the ratios as measured in three different ways

TABLE II. *Individual determinations and average value of the U^{238}/U^{234} ratio.*

18,400	14,500	17,000	18,300	16,000
17,600	16,300	20,800	15,700	13,000
				Average 16,800

agreed as well as they did leads the writer to believe that the average given is not far from correct. The final result may be taken as $U^{238}/U^{234}=17{,}000$, with a limit of error of ten percent.

In addition to the measurement of the abundance ratios a search was made for other isotopes. None was found, and it was possible to set the following upper limits of abundance relative to U^{238}: U^{242}, U^{241}, and U^{240}, 1/65,000; U^{239} and U^{237}, 1/12,000; U^{236}, U^{233}, U^{232}, and U^{231}, 1/35,000.

The mean mass number computed from the relative abundances is 237.977. With a packing fraction of 5.6[5] for uranium, and a conversion factor 1.000275 in going from the physical to the chemical scale an atomic weight of 238.045 is derived for uranium. The chemically determined value is given as 238.07.

The half-life of U_I

Kovarik and Adams[6] found 24,770 alpha-particles given off by a gram of uranium per second, a determination from which they computed a decay constant $=1.532\times10^{-10}$ yr.$^{-1}$ or a half-life $T=4.52\times10^{9}$ yr. for U_I. In view of recent developments, their computations should be modified to include: (1) a change in the electronic charge from 4.77 to 4.80×10^{-10} e.s.u.;[7] (2) a change in the atomic weight of uranium from 238.17 to 238.045; (3) the results of the present investigation that only approximately 139 out of every 140 uranium atoms are those of U_I; (4) the fact that approximately 4.6 out of every 204.6 alpha-particles[8] counted were caused by the decay of U^{235}. If these corrections are made one finds the decay constant of U_I to be 1.520×10^{-10} yr.$^{-1}$, a value which corresponds to a half-life, $T=4.56\times10^{9}$ yr.

The half-life of U_{II}

Two methods have been employed in making determinations of the half-life of U_{II}. The first of these makes use of the Geiger-Nuttall law, an empirical relation between the decay constant of an alpha-raying substance and the range of the particles. From older range determinations[9] a half-life of 10^{8} yr. was computed for U_{II}. More recent determinations[10] lead to values around 10^{6} yr.

The second method employed in measuring $T(U_{II})$ is to separate chemically a known amount of U_{II} and to measure its specific activity. By this method Collie[11] found the half-life to be something over 10^{6} yr. Walling[12] determined a value of 3.4×10^{5} yr., while Gratias,[13] in repeating Collie's experiment, discovered an inaccuracy in the method employed and arrived at the value 1.7×10^{5} yr.

From the present work $T(U_{II})$ may be determined from the formula (1)

$$\lambda(U_I)N(U_I)=\lambda(U_{II})N(U_{II}), \qquad (1)$$

which expresses the fact that U_I and U_{II} are in radioactive equilibrium. Substituting the known quantities given earlier in the paper in the formula one obtains a value $\lambda(U_{II})=2.60\times10^{-6}$ yr.$^{-1}$. The corresponding half-life is 2.7×10^{5} yr. This new and highly direct measurement is thus seen to be in essential agreement with the results obtained from the chemical separation experiments and adds considerable weight to the conclusion of Sizoo and Wytzes[14] that the Geiger-Nuttall relation is not accurate enough for a determination of $T(U_{II})$. The writer's computation is, of course, based upon the tacit assumption that all U^{238} and U^{234} atoms are radioactive.

The half-life of AcU

Several attempts have been made to determine the half-life of actino-uranium. In each case the

[5] A. J. Dempster, Phys. Rev. **53**, 869 (1938).
[6] A. F. Kovarik and N. I. Adams, Phys. Rev. **40**, 718 (1932).
[7] J. W. M. Du Mond and V. L. Bollman, Phys. Rev. **50**, 524 (1936); G. Kellström, Phil. Mag. **23**, 250 (1937); Bond, Proc. Roy. Soc. **A149**, 206 (1937); P. J. Rigden, Nature **141**, 82 (1938); W. V. Houston, Phys. Rev. **52**, 751 (1937); G. B. Banerjea and B. Pattenaik, Nature **141**, 1016 (1938); J. A. Bearden, Phys. Rev. **51**, 378 (1937).
[8] See following paper.
[9] B. Gudden, Zeits. f. Physik **26**, 110 (1924).
[10] G. C. Laurence, Phil. Mag. **5**, 1027 (1928); F. N. D. Kurie, Phys. Rev. **41**, 701 (1932); H. Zeigert, Zeits. f. Physik **46**, 669 (1928); S. Bateson, Can. J. Research **5**, 567 (1931).
[11] C. H. Collie, Proc. Roy. Soc. **A131**, 541 (1931).
[12] E. Walling, Zeits. f. physik. Chemie **10**, 467 (1930).
[13] O. A. Gratias, Phil. Mag. **17**, 491 (1934).
[14] G. J. Sizoo and S. A. Wytzes, Physica **4**, 791 (1937).

method employed made use of the knowledge that the uranium and actinium series end ultimately as isotopes of lead having the masses 206 and 207, respectively. From the isotopic analysis of the lead found in a uranium mineral of known age, the relative activities of the actinium and uranium series at the present time and the decay constant of U_I, it was possible to find the decay constant of AcU. As the result of calculations of this sort, Rutherford[15] arrived at the value $T(\text{AcU}) = 4.2\times10^8$ yr.; Kovarik,[16] 2.7×10^8 yr.; v. Grosse,[17] 4×10^8 yr.; Western and Ruark,[18] 4.45×10^8 yr.; Meyer,[19] 7.0 and 6.3×10^8 yr.

From the relative abundances of the uranium isotopes it is possible to obtain this quantity by a quite independent method requiring only as additional information a knowledge of the decay constant of U_I and the present activity ratio of the actinium and uranium series. The careful investigation of large number of radiogenic lead samples indicates[8] that the actinium series is 4.6 percent as active as the uranium series. This fact is conveniently expressed by means of Eq. (2). Making the necessary substitution one finds $\lambda(\text{AcU}) = 9.72\times10^{-10}$

$$0.046 = \lambda(\text{AcU})N(\text{AcU})/\lambda(U_I)N(U_I), \quad (2)$$

yr.$^{-1}$ or $T(\text{AcU}) = 7.13\times10^8$ yr.

[15] Lord Rutherford, Nature **123**, 313 (1929).
[16] A. F. Kovarik, Phys. Rev. **35**, 1432 (1930).
[17] A. v. Grosse, Phys. Rev. **42**, 565 (1932); J. Phys. Chem. **38**, 487 (1934).
[18] F. Western and A. E. Ruark, Phys. Rev. **44**, 675 (1933); **45**, 628 (1934).
[19] S. Meyer, Wien Ber. IIa, **146**, 175 (1937); **146**, 581 (1937).

ACKNOWLEDGMENTS

The writer wishes to express his appreciation to Professor Kenneth T. Bainbridge who suggested the problem. The prosecution of the work was possible only through the cooperation of Professor G. P. Baxter of the Department of Chemistry, Harvard University, who very kindly prepared and supplied the uranium compounds used.

JANUARY 15, 1939 PHYSICAL REVIEW VOLUME 55

The Isotopic Constitution of Radiogenic Leads and the Measurement of Geological Time. II

ALFRED O. NIER*
Research Laboratory of Physics, Harvard University, Cambridge, Massachusetts

(Received November 3, 1938)

The isotopic constitution of 21 samples of radiogenic lead has been determined with a mass spectrometer and the results have been correlated with mineral analysis data available for the specimens from which the leads were extracted. The common lead contamination in the samples was found, on the whole, to agree closely with that estimated from earlier atomic weight determinations. The AcD/RaG ratios (Pb^{207}/Pb^{206} ratios corrected for common lead contamination) appear to be in better agreement with a value 4.6 percent for the present day ratio of the activity of the actinium series to that of the uranium series than with the directly determined and commonly accepted value 4.0 percent. The results indicate that AcU was not nearly as abundant in the early days of the earth as was at one time believed.

The measurement of geologic age from AcD/RaG ratios is discussed and it is shown that in the event of mineral alteration the ages obtained are more reliable than those found from the Pb/U ratios.

The relatively small amount of Pb^{204} present in samples containing a large amount of thorium indicates that it is extremely unlikely that Pb^{208} decays to Pb^{204}.

IT IS a well-known fact that the natural disintegration of uranium results in the ultimate formation of two stable isotopes of lead, Pb^{206}(RaG) and Pb^{207}(AcD), while the

* This work was done while the writer was a National Research Fellow at Harvard University. Present address, Department of Physics, University of Minnesota, Minneapolis, Minnesota.

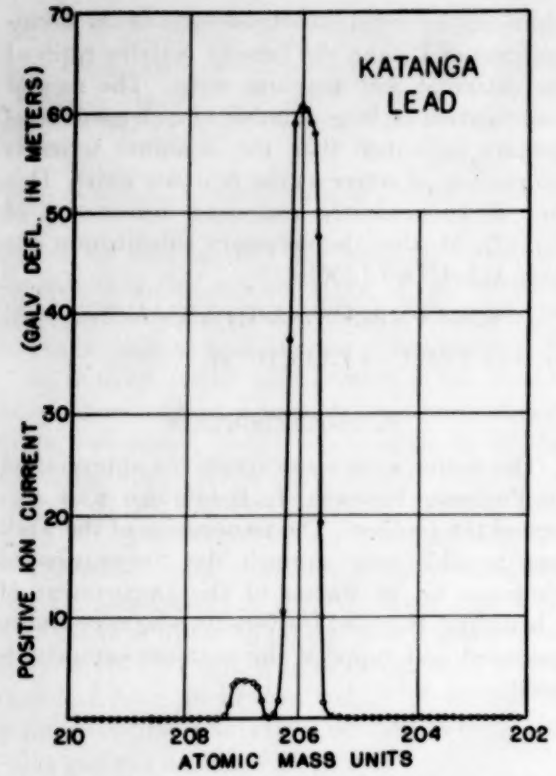

FIG. 1. Mass spectrum showing isotopes of uranium lead. The experimental points are obtained by plotting positive ion current passing through the exit slit of the analyzer as a function of the energy of the ions while the magnetic field is held constant. As there is a definite relation between the energy and the mass of the ions collected, namely, energy $\times$mass = a constant, the voltage scale can be readily changed to a mass scale, as was done in the figure. The width of the peak is, of course, caused by the finite width of the slits used and the imperfections in focusing.

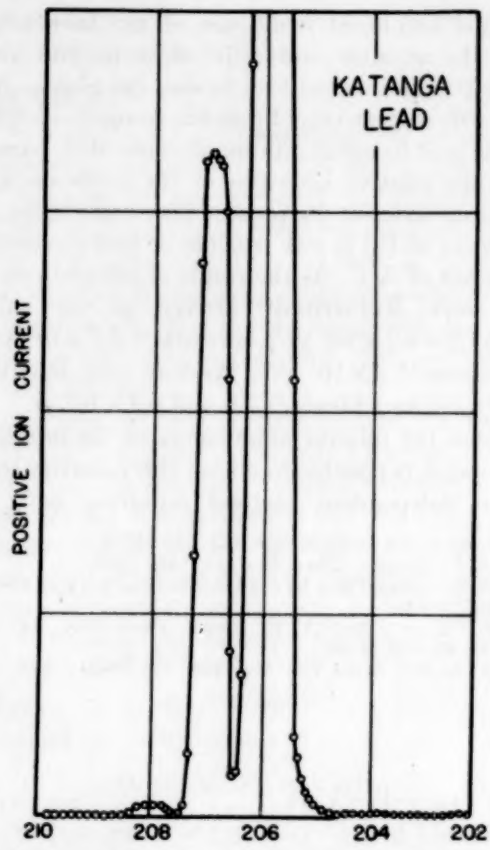

FIG. 2. Figure 1 drawn with an enlarged ordinate scale. The peak at 208 is caused by a trace of ordinary lead impurity.

disintegration of thorium leads to the single isotope Pb^{208}(ThD). Thus it can be seen that from the known decay constants of uranium and thorium, together with the so-called Pb/U and Pb/Th ratios for a radioactive mineral, it is possible to compute the mineral's age, provided one knows the amount of common lead impurity present. As the atomic weight of common lead, 207.21, differs considerably from that of either uranium lead, approximately 206.03, or thorium lead, approximately 207.98, the amount of contamination can usually be found from the atomic weight of the lead in question. An isotopic analysis gives one the same information, and, in addition, in the case of uranium minerals, provides important data on the rate of disintegration of the actinium series—data which, as will be seen, furnishes an important check on the mineral's age as computed from the Pb/U ratio.

In the present work, the relative abundances of the isotopes of a number of radiogenic leads were determined. The results obtained are especially interesting, as most of the samples are the identical ones for which mineral analysis data are available. Moreover, chemical atomic weight determinations have been made on many of the samples.

APPARATUS AND PROCEDURE

The mass spectrometer differed from that described in the previous paper only in that it did not contain the small internal furnace used to volatilize the substance studied. It was the same one as was used in some earlier work.[1] The particular technique developed for the study of

[1] A. O. Nier, Phys. Rev. **52**, 933 (1937).

lead has been described elsewhere.[2] Briefly, it may be stated that lead ions are produced by the bombardment of lead iodide vapor with electrons, that an analysis can be obtained in less than two days, and less than six mg of lead are consumed in the process.

The complete absence of water or grease vapor in the apparatus, together with the extreme purity of the samples, entirely eliminates any difficulties with impurities, especially hydrides.

As the ion currents are measured with an electrometer-tube amplifier, it is possible to obtain accurate relative abundances merely by determining galvanometer deflections. The quantitative measurement of ion currents with electrical instruments is certainly to be preferred to the method generally employed in mass spectrographs in which the magnitude of the ion current is determined from the blackening of photographic plates.

The iodine used in preparing the lead iodide was especially purified, since $Br^{79}I^{127}$ and $Br^{81}I^{127}$ have molecular weights 206 and 208, the same as two of the isotopes of lead.

Results

The isotopes of uranium lead, Pb^{206} and Pb^{207}, are clearly seen in Fig. 1, which is a mass spectrum obtained for a specimen of Katanga pitchblende, sample 6 of Table I. That this particular specimen is remarkably free from ordinary lead contamination may be concluded from Fig. 2, in which the lower portion of Fig. 1 is drawn with a greatly enlarged ordinate scale. It is to be recalled that in common lead, Pb^{208} is more than twice as abundant as any of the other isotopes, Pb^{207}, Pb^{206} and Pb^{204}. As a contrast to Fig. 1 is shown Fig. 3, a spectrum obtained for some St. Joachimsthal pitchblende, sample 1 of Table I. This specimen contains a large proportion of common lead. The spectrum shown in Fig. 4 is for Norwegian thorite, sample 20 of Table I, a specimen containing ThD(Pb^{208}) contaminated by small amounts of common and uranium leads.

In Table I are given, together with other information, the relative abundances of the isotopes in 21 samples of radiogenic lead. The bulk of these leads were extracted from uranium minerals

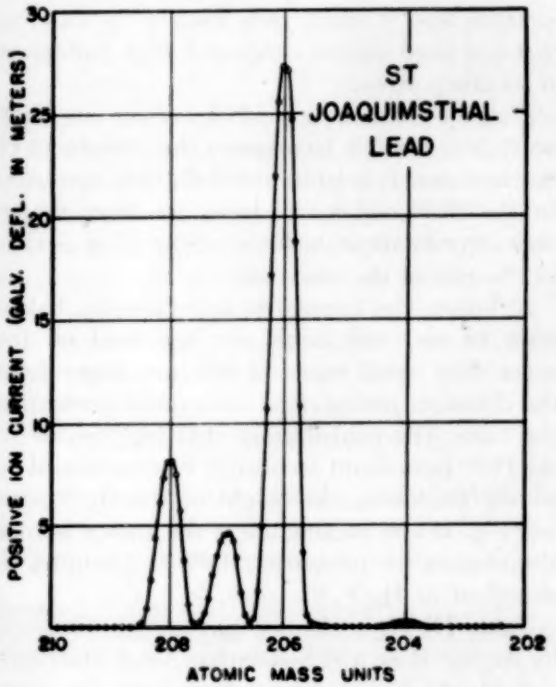

FIG. 3. Mass spectrum for lead extracted from St. Joachimsthal pitchblende. Both common and uranium leads are present here.

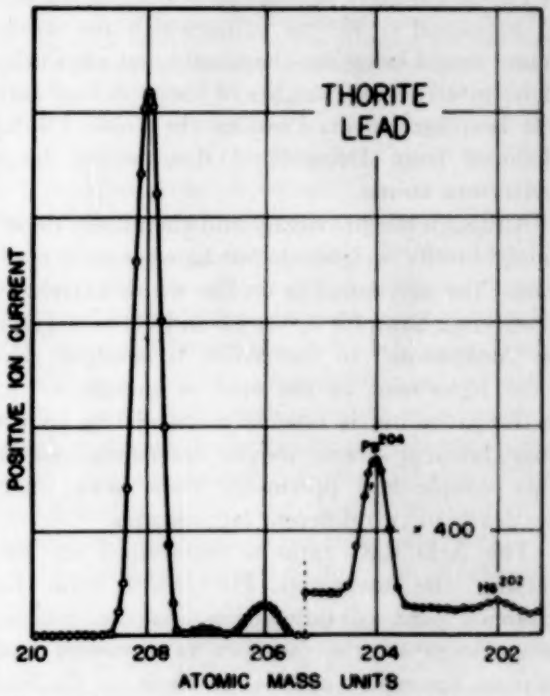

FIG. 4. Mass spectrum for lead extracted from Norwegian thorite. The thorium lead is contaminated by small amounts of common and uranium lead in this case. The ordinate scale in the 204 to 202 region has been increased by a factor of 400.

[2] A. O. Nier, J. Am. Chem. Soc. **60**, 1571 (1938).

containing essentially no thorium. A few, numbers 13, 14, 15, 17 and 18, contained some thorium, while in two only, numbers 16 and 20, did the amount of thorium exceed the uranium.

The isotope abundances (relative to the most abundant isotope in each sample) are all believed to be correct to *within at least one percent* unless otherwise noted. An idea of the ability of the apparatus to reproduce results is gained from an examination of the data for samples 2, 6, 8, 10 and 13, where two separate analyses were made. It should be emphasized that the two analyses in each case were obtained at totally different times and that at least one other sample had been in the apparatus between the two analyses. In several cases, months passed and many samples, including some of common lead, were investigated between the two analyses.

The atomic weights were computed from the abundances by first calculating the mean mass number and converting this by assuming the packing fraction of lead to be +1.55, and the conversion factor in going from the physical to the chemical scale to be 1.000275. The choice of +1.55 as the packing fraction is quite arbitrary. It happened to be the value which the writer found would bring the chemically and physically determined atomic weights of common lead[2] into the best agreement. Possibly the value 2.0–2.3 deduced from Dempster's[3] data would be a better one to use.

Although the physically and chemically determined atomic weights do not agree exactly in all cases, the agreement is on the whole extremely gratifying. Samples 8, 11, 12 and 19 were given as "unknowns" to the writer to analyze. The close agreement in the case of sample 8, the Katanga curite, is especially interesting as the two chemical atomic weight determinations on this sample had previously been made *independently* in two different laboratories.

The AcD/RaG ratio is determined by correcting the measured Pb^{207}/Pb^{206} ratio for common lead contamination. As the relative abundances of the isotopes of common lead depend somewhat upon the source of the lead there is some uncertainty as to how the correction should be made. Fortunately, these variations appear to follow fairly definite rules,[2] and for the samples so far studied the relative abundances fell between rather definite limits. Table II gives the relative abundances for the two extreme samples of common lead so far investigated, numbers 1 and 7 of Table I, reference 2.

In the case of thorium-free radiogenic minerals one should be able to find what type of common lead impurity is present by comparing the Pb^{208}/Pb^{204} ratio with the data of reference 2.

Actually, in 20 of the 21 samples investigated the amount of common lead is so small that one need not take account of the variations in its composition. In a number of samples where the abundance of Pb^{204} was very low no attempt was made to measure the amount of it as the determination would be of no particular value. It is of interest to note that the ability of the apparatus to detect and measure relatively small amounts of Pb^{204} is of considerable value in the study of minerals containing both uranium and thorium. In that case, one may conveniently use Pb^{204} as an accurate measure of the common lead contamination provided, of course, the amount of common lead is small, as is usually the case, so that one need not be concerned with variations in its composition.

Figure 4 gives one a good idea of the ease with which it is possible to measure the abundance of rare isotopes. It is to be noted that the spectrum for the Pb^{204} region and lower has been drawn with an ordinate scale 400 times as great as that for the rest of the spectrum.

Although the apparatus was carefully baked prior to use, and liquid air was used on the traps, very small traces of mercury vapor from the diffusion pumps were sometimes present in the tube. The contribution that Hg^{204} made to the Pb^{204} peak could accurately be determined by merely measuring the height of the Hg^{202} peak (see Fig. 4) and making use of the known isotope abundances for mercury.[1] Hg^{202} is 4.4 times as abundant as Hg^{204}.

Table III gives the isotopic analysis obtained by Aston,[4] Rose and Stranathan,[5] and Mattauch and Hauk[6] for samples taken from the same

[3] A. J. Dempster, Phys. Rev. **53**, 869 (1938).

[4] F. W. Aston, Proc. Roy. Soc. **A140**, 535 (1933).

[5] J. L. Rose and R. K. Stranathan, Phys. Rev. **50**, 792 (1936).

[6] J. Mattauch and V. Hauk, Naturwiss. **25**, 763 (1937).

regions as were some of the writer's. All percentage abundances have been converted to abundances relative to the most abundant isotope for the sake of comparison. In the case of the Great Bear Lake, Morogoro and thorite material, the *identical* samples were used by the several investigators so that the results are strictly comparable. The discrepancies in the table lie considerably outside of the writer's limits of error.

The Relative Activities of the Actinium and Uranium Series

As the intermediate members of the uranium and actinium series are short lived compared with the ages of the minerals with which we are concerned, it is possible to write the following expressions relating the radiogenic lead and uranium isotopes

$$N(\mathrm{Pb}^{206}) = \mathrm{RaG} = N(\mathrm{U_I})(\exp[\lambda(\mathrm{U_I})t]-1), \quad (1)$$

$$N(\mathrm{Pb}^{207}) = \mathrm{AcD} = N(\mathrm{AcU})(\exp[\lambda(\mathrm{AcU})t]-1), \quad (2)$$

$$\frac{N(\mathrm{Pb}^{207})}{N(\mathrm{Pb}^{206})} = \frac{\mathrm{AcD}}{\mathrm{RaG}} = \frac{N(\mathrm{AcU})}{N(\mathrm{U_I})} \frac{\exp[\lambda(\mathrm{AcU})t]-1}{\exp[\lambda(\mathrm{U_I})t]-1}. \quad (3)$$

Eq. (3) predicts the manner in which the Pb^{207}/Pb^{206} ratio (corrected for ordinary lead contamination) in a uranium mineral should depend upon the mineral's age. Conversely, if all the constants in the equation have been properly evaluated it should be possible to determine the age from the Pb^{207}/Pb^{206} ratio.

If one calls the present day ratio of activities of the actinium and uranium series R, one can write

$$R = \lambda(\mathrm{AcU})N(\mathrm{AcU})/\lambda(\mathrm{U_I})N(\mathrm{U_I}). \quad (4)$$

Solving Eq. (4) for $\lambda(AcU)$, substituting the results in Eq. (3) and replacing $N(U_I)/N(AcU)$ by 139 (see previous paper), one has

$$\frac{N(\mathrm{Pb}^{207})}{N(\mathrm{Pb}^{206})} = \frac{\mathrm{AcD}}{\mathrm{RaG}} = 139 \cdot \frac{\exp[139R\lambda(\mathrm{U_I})t]-1}{\exp[\lambda(\mathrm{U_I})t]-1}. \quad (5)$$

In Fig. 5 is plotted Pb^{207}/Pb^{206} *versus* t for various values of R substituted in Eq. (5). The decay constant of U_I is chosen as 1.520×10^{-10} yr^{-1}.* The experimental points shown in the figure are obtained from the data given in Table I. The ages given in column 16 are computed from Eq. (1), with allowance, of course, for the fact that the equation refers to numbers of atoms, while the Pb/U ratios refer to weights of material. The points corresponding to samples 3, 7, 8, 14 and 20 are not plotted. Samples 3 and 7, Katanga yellow specimens, are definitely known to be alteration products of samples 2 and 6, Katanga black specimens, and hence, not reliable for age determinations. Likewise, 8 and 14, Katanga curite and Manitoba uraninite, respectively, were extracted from minerals which had suffered alteration. Sample 20, Norwegian

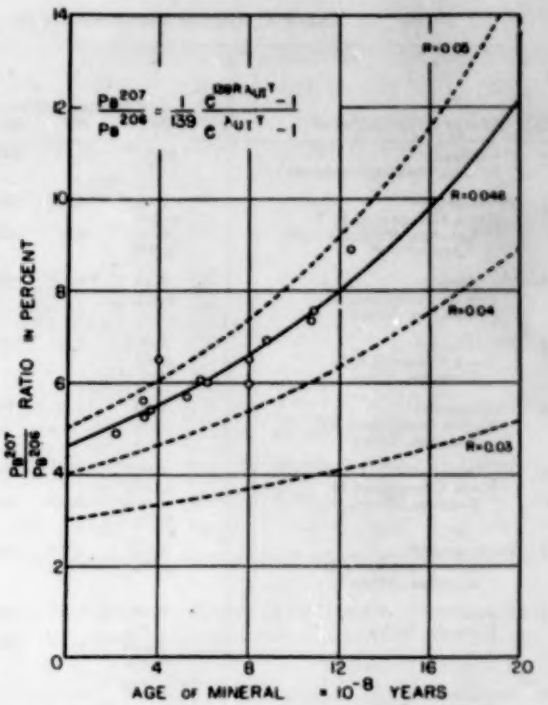

FIG. 5. Pb^{207}/Pb^{206} (corrected for common lead impurities) as a function of the age of the mineral from which the lead was extracted. The curves are plotted according to the formula in the diagram for various assumed values of R (the ratio of activities of the actinium and uranium series). The circles are experimentally determined points.

* In a trial computation λ was taken as 1.524×10^{-10} yr.$^{-1}$, a value depending upon the commonly accepted value, 4.0 percent for the ratio of activities of the actinium and uranium series. When it was found that R should be 4.6 rather than 4.0 percent $\lambda(U_I)$ was changed to 1.520×10^{-10} to take account of the difference. As $\lambda(U_I)$ depends only very slightly upon the value assumed for R it makes very little difference what exact value one assumes for $\lambda(U_I)$ so far as the discussion which follows is concerned.

TABLE I. *Relative abundances of the isotopes in 21 samples of radiogenic lead.*

1	2	3	4	5	6	7	8	9
		Isotope Abundances				Mean Mass	Atomic Weight	
No.	Mineral and Source[a]	208	207	206	204	Number	Physical	Chemical
1.	Pitchblende[7] St. Joachimsthal, Bohemia	32.5	17.75	100	0.884 ±3%	206.536 ±0.005	206.511	206.50[7]
2.	Pitchblende[9] Black Component I Katanga, Belgian Congo, Africa	0.042 ±10%	6.03	100		206.058 ±0.001	206.033	206.00[9]
		0.047 ±20%	6.07	100				
3.	Pitchblende[9] Yellow Component I Katanga, Africa	0.51 ±3%	6.27	100	<0.02	206.068 ±0.001	206.043	205.97[9]
4.	Pitchblende[9] Black Component Ia Katanga, Africa	0.092 ±5%	6.04	100		206.059 ±0.001	206.034	
5.	Pitchblende[9] Yellow Component Ia Katanga, Africa	2.09 ±2%	6.96	100		206.102 ±0.001	206.077	
6.	Pitchblende[10] Black Component II Katanga, Africa	0.077 ±10%	6.08	100		206.060 ±0.001	206.035	206.04[10]
		0.076 ±5%	6.08	100	<0.006			
7.	Pitchblende[10] Yellow Component II Katanga, Africa	0.247 ±3%	6.23	100	0.007 ±20%	206.063 ±0.001	206.038	206.05[10]
8.	Curite[12] Katanga, Africa	0.186 ±3%	6.11	100	<0.02	206.061 ±0.001	206.036	206.027[12] 206.03[13]
		0.180 ±3%	6.13	100				
9.	Pitchblende[14] Beaver Lodge Lake, N. W. T., Canada	0.309	6.31	100	0.0557 ±3%	206.113 ±0.001	206.088	206.08[10]
10.	Pitchblende[15] Great Bear Lake, N. W. T., Canada	(a) 2.51	9.76	100	0.063 ±3%	206.130 ±0.001	206.105	206.06[10]
		(b) 2.54	9.73	100	0.061 ±5%			
11.	Cyrtolite[17] II Bedford, N. Y., U. S. A.	2.22	6.07	100	0.0443 ±2%	206.096 ±0.001	206.071	206.07[12]
12.	Cyrtolite[18] I Bedford, N. Y.	4.29	6.89	100	0.095 ±5%	206.139 ±0.002	206.114	205.92[19]
13.	Uraninite[20] Besner, Ont., Canada	1.082 ±2%	6.73	100		206.082 ±0.001	206.057	206.05[12]
		1.06 ±2%	6.73	100	0.0073 ±10%			
14.	Uraninite[21] Huron Claim, Manitoba, Canada	6.51	16.17	100	0.022 ±20%	206.238 ±0.002	206.215	
15.	Uraninite[22] Wilberforce, Canada	6.16	7.49	100	0.011 ±20%	206.174 ±0.002	206.149	206.195[23]
16.	Thorianite[24] Ceylon, India	100.	3.43	59.0	0.006 ±20%	207.252 ±0.01	207.227	207.21[24]
17.	Uraninite[21] Morogoro, Tanganyika Territory, Africa	0.18 ±10%	5.98	100	0.001 ±20%	206.060 ±0.001	206.035	
18.	Cleveite[25] Auselmyren, Holt Aust-Agder, Norway	1.05	7.55	100	0.0006 ±50%	206.089 ±0.001	206.064	
19.	Cleveite[26] Pied des Monts, Quebec, Canada	1.92 ±2%	7.60	100	0.047 ±5%	206.103 ±0.002	206.078	
20.	Thorite[27] Brevig, Norway	100.	1.22 ±2%	5.53	0.061 ±5%	207.883 ±0.001	207.858	207.90[28]
21.	Kolm[29] Güllhögen, Sweden	(a) 1.91 ±2%	7.29	100	0.050 ±20%	206.102 ±0.002	206.077	206.01[29]
		(b) 2.08 ±2%	7.34	100	0.055 ±5%			
		(c) 2.07 ±2%	7.42	100				

TABLE I (*Continued*).

No.	Mineral and Source	10 AcD/RaG %	11 Mineral Analysis % U	12 % Th	13 % Pb	14 Pb/U	15 RaG/U^{238}	16 Age from RaG/U^{238} in 10^6 yr.	17 ThD/Th	18 Age from ThD/Th in 10^6 yr.	19 Age from AcD/RaG in 10^6 yr.
1.	St. Joachimsthal Pitchblende	4.88	60.24	—	3.22	0.0536	0.0302	227	—	—	140
2.	Katanga Black I Pitchblende	6.00	74.9	—	6.7	0.089	0.0845	616	—	—	610
		6.05									
3.	Katanga Yellow I Pitchblende	6.07	58.5	—	8.4	0.144	0.1358	973	—	—	635
4.	Katanga Black Ia Pitchblende	6.00									610
5.	Katanga Yellow Ia Pitchblende	6.13									655
6.	Katanga Black II Pitchblende	6.05	77.2	—	6.48	0.0839	0.0797	582	—	—	625
7.	Katanga Yellow II Pitchblende	6.13	68.5	—	6.74	0.0983	0.0930	676	—	—	655
8.	Katanga Curite	6.05	65.3	—	9.7	0.1483	0.1405	995	—	—	625
9.	Beaver Lodge Pitchblende	5.62	51.16	—	2.492	0.0488	0.0447	333	—	—	460
10.	Great Bear Lake Pitchblende	8.88	52.32	—	10.51	0.201	0.180	1251	—	—	1420
11.	Bedford Cyrtolite II	5.41	6.73	—	0.351	0.0522	0.0486	361	—	—	375
12.	Bedford Cyrtolite I	5.23	7.29	—	0.374	0.0513	0.0454	341	—	—	300
13.	Besner Uraninite	6.63	67.6	1.57	7.69	0.114	0.1062	765	0.0359	787	825
14.	Huron Claim Uraninite	15.9	54.14	12.37	15.47	0.285	0.232	1570	0.0579	1252	2200
15.	Wilberforce Uraninite	7.33	53.52	10.37	9.26	0.173	0.1532	1077	0.0452	983	1035
16.	Ceylon Thorianite	5.67	11.8	68.9	2.34	0.198	0.0723	531	0.0209	461	485
17.	Morogoro Uraninite	5.96	70.45	0.2	8.30	0.1177	0.1117	803	—	—	595
18.	Norwegian Cleveite	7.54	67.18	2.76	11.19	0.1666	0.1543	1085	0.0385	840	1090
19.	Pied des Monts Cleveite	6.88	49.25	—	6.67	0.1354	0.1233	882	—	—	905
20.	Norwegian Thorite	6.1 ±30%	0.45	30.10	0.35		0.0324	243	0.016	355	—
21.	Swedish Kolm	6.47	0.462	—	0.026	0.056	0.0517	388	—	—	770

* References for this column refer to analyses of minerals appearing in columns 11, 12, and 13.

[7] G. P. Baxter and C. I. Kelley, J. Am. Chem. Soc. **60**, 62 (1938).

[8] G. P. Baxter and C. M. Alter, J. Am. Chem. Soc. **55**, 2785 (1933).

[9] Samples 4 and 5 were fresh extractions from the *same* mineral samples as were samples 2 and 3, respectively.

[10] G. P. Baxter, J. H. Faull, Jr., and F. D. Tuemmler, J. Am. Chem. Soc. **59**, 702 (1937).

[12] G. P. Baxter and C. M. Alter, J. Am. Chem. Soc. **57**, 467 (1935).

[13] O. Honigschmid, unpublished, referred to in reference 12.

[14] G. P. Baxter and M. E. Averill, J. Am. Chem. Soc. **59**, 705 (1937).

[15] J. P. Marble, J. Am. Chem. Soc. **58**, 434 (1936). Sample (a) obtained from J. P. Marble through G. P. Baxter. Sample (b) identical lead as was used by Aston for his isotope analysis and obtained from A. v. Grosse. Both samples were taken from the same original lot. It is interesting to note that in spite of extensive chemical treatment in different laboratories the isotopic analysis for the two samples are in nearly perfect agreement.

[16] J. P. Marble, J. Am. Chem. Soc. **56**, 854 (1934).

[17] O. B. Muench, J. Am. Chem. Soc. **56**, 1536 (1934).

[18] O. B. Muench, Am. J. Sci. **21**, 356 (1931).

[19] G. P. Baxter and C. M. Alter, J. Am. Chem. Soc. **55**, 1445 (1933).

[20] H. V. Ellsworth, Am. Mineral. **16**, 577 (1931).

[21] DeLury and Ellsworth, Am. Mineral. **16**, 569 (1931).

[22] R. C. Wells, appears in *Report of the Committee on the Measurement of Geologic Time*, (1931), No. 7, G. Kirsch and A. C. Lane, Proc. Am. Acad. **66**, 365 (1931).

[23] G. P. Baxter and E. W. Bliss, J. Am. Chem. Soc. **52**, 4851 (1930).

[24] O. Honigschmid, Zeits. f. Electrochem. **25**, 91 (1919).

[25] E. Gleditsch, unpublished.

[26] O. B. Muench, unpublished.

[27] K. Fajans, Zeits. f. Electrochem. **24**, 163 (1918).

[28] R. C. Wells, Appears in *Report of the Committee on the Measurement of Geologic Time*, (1930), No. 6, p. 4. Sample (a) was the identical material used in chemical atomic weight analysis. The material had been converted at one time to $Pb(CH_3)_4$ through a rather complicated chemical process. As used finally by the writer it was in the form of PbI_2. Sample (b) had been through the same chemical treatment as sample (a) had. Sample (c) was a fresh extraction from original mineral.

[29] G. P. Baxter and E. W. Bliss, J. Am. Chem. Soc. **52**, 4848 (1930).

TABLE II. *Isotope abundances in two samples of common lead.*

No.	Mineral and Source	Isotope Abundances 206	207	208	204
1	Galena, Great Bear Lake, Canada	35.3	15.30	15.93	1.000
2	Galena, Joplin, Mo., U. S. A.	40.8	15.88	21.65	1.000

TABLE III. *Comparison of isotope abundances obtained by various investigators.*

Mineral	Investigator	Isotope Abundances 206	207	208	204	AcD/RaG	Mean Mass Number
Pitchblende Great Bear Lake	Aston	100	8.8	2.56		7.72	206.125
	R. & S.	100	9.46	3.15		8.24	206.139
	Nier	100	9.73	2.53	0.062	8.88	206.130
Pitchblende Katanga, Africa	Aston	100	7.18	0.02		7.18	206.067
	R. & S.	100	6.74	0.3		6.67	206.069
	M. & H.	100	5.15			5.15	206.049
	Nier No. 6	100	6.08	0.077	0.006	6.05	206.060
Uraninite Wilberforce, Ont., Canada	Aston	100	9.66	6.75		9.67	206.199
	R. & S.	100	8.32	7.17		8.30	206.196
	Nier	100	7.49	6.16	0.011	7.33	206.174
Uraninite Morogoro, Africa	Aston	100	7.42	0.0		7.42	206.080
	Nier	100	5.98	0.18	0.001	5.96	206.080
Thorite Brevig, Norway	Aston	4.88	1.38	100			207.805
	Nier	5.53	1.22	100	0.061		207.883

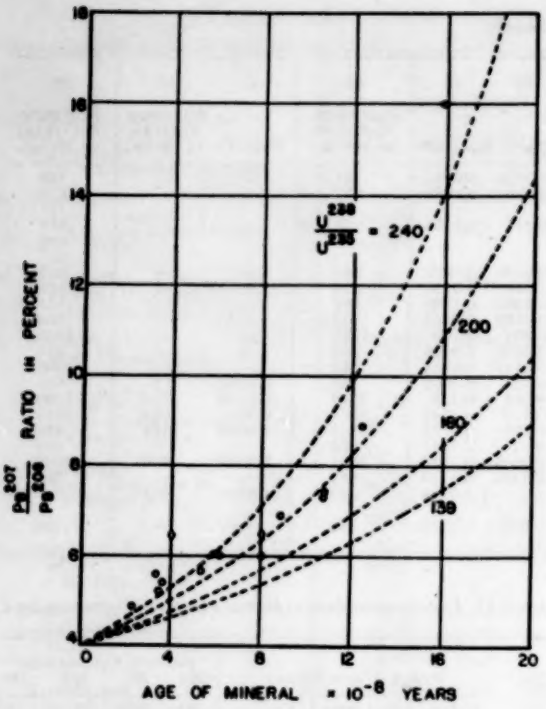

FIG. 6. Pb^{207}/Pb^{206} (corrected for common lead impurities) as a function of the age of the mineral. The curves were plotted for various assumed values for U^{238}/U^{235} on the hypothetical assumption that the actinium series is just 4 percent as active as the uranium. The circles represent the same experimentally obtained points as were plotted in Fig. 5.

thorite, is not included as the accuracy in calculating AcD/RaG was too low. Sample 17, Morogoro uraninite, probably should not have been plotted. Its Pb/U ratio, 0.1177, is much higher than that usually found for the region,[30] and hence indicates that this particular sample has been altered.

The results are seen to be in much better agreement with an assumed $R=4.6\pm0.1$ percent than with the directly determined value 4.0–4.1 percent, as measured by v. Grosse,[31] Gleditsch and Foyn,[32] and Francis and Da Tchang.[33] It is hard to account for the discrepancy. All of the Pb^{207}/Pb^{206} ratios except that for sample 1, the St. Joachimsthal pitchblende, are believed to be correct to about one percent. Because of the large amount of ordinary lead in sample 1, it is difficult to make an accurate correction, and hence, the corrected ratio may be in error by as much as ten percent in this case.

The Pb/U ratios from which the ages of the minerals were calculated certainly could not be in error by an amount large enough to explain the discrepancy, unless the minerals had been altered. If one were to account for the difference in this manner, one would have to assume all of the minerals in question had been altered to about the same extent in the same direction, an extremely artificial hypothesis. Moreover, the alteration would have to be one in which lead rather than uranium had been lost, an occurrence which is just the converse of what is believed usually to happen when uranium minerals suffer alteration.

That the difficulty is caused by an error in the U^{238}/U^{235} ratio seems very unlikely because first of all this ratio was carefully determined and is believed to be correct within a percent, and second, even if this ratio were in error by as much as 10 or 20 percent, it would not explain the large difference in question. At this point one might inquire whether the U^{238}/U^{235} ratio, as measured with a mass spectrometer, is really what enters into the problem; that is to say, could it be possible that not all U^{235} atoms disintegrate, and that the uranium isotope ratio which enters into the equation should thus be greater than 139?. Such a hypothesis does not seem likely, as not only is there no record of the existence of *any* stable isotope of *any* element heavier than bismuth, but moreover, one would have to assume U^{235} to exist in both a stable and an unstable form, an assumption one is reluctant to make on the basis of the evidence presented here. In this connection it seems worth mentioning that even if one admits this possibility and constructs a family of Pb^{207}/Pb^{206} *versus* t curves with U^{238}/U^{235} as a parameter, while R is held fast at 0.04, as was done in Fig. 6, it is not possible to find a curve which fits the experimentally determined points any better than does the chosen curve of Fig. 5. In other words, as far as the isotopic analysis of the leads is concerned there is no reason to believe that the abundance ratio $U^{238}/U^{235}=139$ and the activity

[30] *Age of the Earth*, National Research Council Bull. 80, p. 369.

[31] A. v. Grosse, Phys. Rev. **42**, 565 (1932); J. Phys. Chem. **38**, 487 (1934).

[32] E. Gleditsch and E. Foyn, Comptes rendus **199**, 412 (1934).

[33] M. Francis and T. Da Tchang, Comptes rendus **198**, 733 (1934); Phil. Mag. **20**, 623 (1935).

ratio $R=0.046$ are not the proper quantities to use in the equation.

The writer's Pb^{207}/Pb^{206} *versus* t curve, solid curve in Fig. 5, rises much less rapidly with the age of the mineral than does the relation usually employed and accepted at the present time. The difference is not surprising when one considers that these older computations involve indirectly determined U^{238}/U^{235} ratios lying between 250 and 330,[31, 34–37] numbers in striking disagreement with the writer's directly determined ratio of 139. The curves commonly accepted belong to the family shown in Fig. 6 and rise even steeper than does the steepest curve shown in that figure, the one for $U^{238}/U^{235}=240$. The recent computations of Meyer gave the values 110[38] and 180.[39] These are the only calculated U^{238}/U^{235} ratios falling even near to the writer's value.

In view of the evidence presented in the previous paragraphs, one is forced to conclude that either (1) the relative activities of the actinium and uranium series is higher than has usually been supposed—close to 4.6 percent rather than 4.0 percent, or (2) that some unknown factor or factors not taken into account in the present theories of the disintegration of the actinium and uranium families are causing the disagreement. Should the former and far more likely hypothesis prove to be correct, it will be necessary to modify the decay constants and half-lives commonly accepted for U_I and AcU. The new values will be $\lambda(U_I)=1.520\times10^{-10}$ yr.$^{-1}$, $T(U_I)=4.56\times10^{9}$ yr., and $\lambda(AcU)=9.72\times10^{-10}$ yr.$^{-1}$, $T(AcU)=7.13\times10^{8}$ yr.

TABLE IV. *Variation of the U^{238}/U^{235} ratio with geologic age.*

Number of Years Ago	Ratios Based on Present Work		Ratios Based on Earlier Work	
	$\frac{U^{238}}{U^{235}}$	$\frac{\text{Activity of AcU Series}}{\text{Activity of U Series}}$	$\frac{U^{238}}{U^{235}}$	$\frac{\text{Activity of AcU Series}}{\text{Activity of U Series}}$
0×10^{8}	139.0	0.046	300	0.04
4	100.2	0.065	153	0.079
8	72.2	0.089	79	0.127
12	52.1	0.123	40.3	0.298
16	37.5	0.171	20.8	0.575
20	26.9	0.238	10.6	1.13

[34] Lord Rutherford, Nature **123**, 313 (1929).
[35] A. F. Kovarik, Phys. Rev. **35**, 1432 (1930).
[36] F. Western and A. E. Ruark, Phys. Rev. **44**, 675 (1933); **45**, 628 (1934).
[37] A. Holmes, *Age of the Earth* (Nelson Press, 1937), p. 151.
[38] S. Meyer, Wien. Ber. IIa **146**, 175 (1937).
[39] S. Meyer, Wien. Ber. **146**, 581 (1937).

From these new decay constants one may readily calculate the manner in which the U^{238}/U^{235} ratio has varied throughout geological time. In Table IV are given the results of these calculations together with the corresponding ratios of activities of the actinium and uranium series as computed by Eq. (4). In the second half of the table are tabulated the results for the analogous computations based upon older data. The present day U^{238}/U^{235} ratio is here taken as 300 and the present ratio of activities of the series as 0.04. From a comparison of the data one concludes that in the early days of the earth's history U^{235}(AcU) was not nearly as abundant as was at one time thought, and hence, the heat energy released by its decay did not play nearly so important a part in influencing the earth's thermal history as was at one time believed by some.

The Measurement of Geological Time

The mineral ages as computed from the RaG/U^{238} ratios in the present work are in good agreement with those previously calculated from the Pb/U ratio. In the earlier work the common lead contamination was computed from the atomic weight of the lead and the correction for AcD was made empirically.

In those samples containing both uranium and thorium the isotopic analysis of the lead enables one to make an independent calculation of the mineral's age. This has been done in columns 17 and 18 of Table I. The computations were made by applying an equation analogous to (1) and (2) to the ThD/Th ratio. The recently determined decay constant of thorium,[40] 4.99×10^{-11} yr.$^{-1}$, was employed in the calculations.

TABLE V. *Alteration of 10^{9} yr.-old mineral by loss of 50 percent of uranium t_1 years ago.*

t_1	Approximate Apparent Ages Computed from	
	Pb/U	AcD/RaG
0×10^{8} yr.	2.0×10^{9} yr.	1.00×10^{9} yr.
2	1.8	1.07
4	1.6	1.11
6	1.4	1.15
8	1.2	1.11
10	1.0	1.00

[40] A. F. Kovarik and N. I. Adams, Phys. Rev. **53**, 928 (1938).

Although the uranium and thorium ages are in rough agreement there appear to be some discrepancies. Whether these can be attributed partially to errors in the decay constants and partially to alterations in the minerals or entirely to mineral alterations, one hardly can conclude from the present data. In view of the limited number of minerals investigated the latter hypothesis is to be preferred. The writer does not believe that the differences can be caused by errors in the mineral or isotopic analyses.

An attempt to make age determinations from the AcD/RaG ratio of uranium leads has already been made.[5] The writer believes that the present work demonstrates the practicability of such method provided, of course, the proper decay constant for AcU is employed. The method once well established will, together with the Pb/U analysis of the mineral, give *two completely independent determinations* of age on the same specimen. This fact is especially significant as an alteration of the mineral affects the ages as computed by the two methods in quite different ways. In the case of the alteration of a uranium mineral, uranium rather than lead usually is lost. The age as computed from the Pb/U ratio is thus too high—by an amount depending upon the amount of uranium lost and time at which the loss took place. On the other hand, the age computed from the Pb^{207}/Pb^{206} ratio hardly differs from the true age of the mineral.

This point is perhaps best illustrated by means of an example. Let us consider a uranium mineral 10^9 yr. old which has lost half of its uranium at a time t_1 years ago. Columns 2 and 3 of Table V give the approximate apparent ages of this mineral as computed for various values of t_1 from the present day Pb/U ratio and from the present day AcD/RaG ratio for this mineral. In this case one can clearly see that the AcD/RaG age is far more reliable than that calculated from the Pb/U ratio.

In a similar fashion one may compute the effects of a hypothetical alteration in which lead has been lost. The results shown in Table VI indicate that in this case, too, the age determined from the AcD/RaG ratio is closer to the true age of the mineral than that found from the Pb/U ratio.

TABLE VI. *Alteration of 10^9 yr.-old mineral by loss of 50 percent of accumulated lead t_1 years ago.*

t_1	Approximate Apparent Ages Computed from Pb/U	from AcD/RaG
0×10^8 yr.	5×10^8 yr.	10.0×10^8 yr.
2	6	8.9
4	7	8.5
6	8	8.6
8	9	9.2
10	10	10.0

The calculations indicate the validity of the statement made earlier that the alteration of a mineral affects the ages as computed by the two different methods in different ways. Thus, if one is willing to accept the possibility that the activity of the actinium series is 4.6 percent that of the uranium, as is indicated by Fig. 5, then the close agreement of most of the experimental points in that figure with the solid curve indicates that only a few of the minerals for which data are plotted have suffered serious alteration. In column 19 of Table I are given for comparison the ages as computed from the Pb^{207}/Pb^{206} ratio on the assumption that the solid curve of Fig. 5 properly describes the way in which Pb^{207}/Pb^{206} varies with t.

In discussing alterations of the minerals no mention was made of the possibility that leaching of the intermediate products of the radioactive series might have taken place. Without considering specific examples it would be difficult to predict exactly how such effects might affect the ages as computed by the two methods. In general one might say that a loss of any of the intermediate actinium series products would give a low Pb^{207}/Pb^{206} ratio without appreciably affecting the Pb/U age, while a partial loss of an intermediate product of the uranium series would change both the Pb^{207}/Pb^{206} ratio and the Pb/U ratio, but not in the same amounts. In any event, it appears safe to conclude that with the exception of isolated cases *any* simple alteration will manifest itself in a difference in the ages as computed by the two different methods.

An examination of the figure indicates that only three of the points, those for samples 10, 17 and 21, are in serious disagreement with the curve. The facts concerning sample 17, the

Morogoro uraninite, have been discussed in the third paragraph of the previous section. The discrepancy for samples 10, the Great Bear Lake pitchblende, and 21 can only mean that these samples, too, have suffered alteration of some sort. In the case of sample 21, the Swedish kolm, the discrepancy appears to be particularly serious.

It is of interest to examine the data for samples (3) and (7), the yellow components of the Katanga pitchblende specimens. The Pb^{207}/Pb^{206} ratios indicate the ages must be close to those for the black components while the Pb/U ratios give higher ages, especially in the case of sample (3). The data are thus consistent with the view that the yellow components are alteration products of the corresponding black components and that they have suffered a loss of uranium. This conclusion has been reached quite independently[8] of the present work. The abnormal age obtained for the Katanga curite sample, number 8, from the Pb/U ratio can in all probability be explained by a loss of uranium from the mineral. It is extremely interesting to note that *all* of the Katanga samples have essentially the same AcD/RaG ratio *in spite of* apparent alterations in the minerals.

The data for the uraninite from Manitoba, Canada, sample 14, offer possibilities for speculation. Fortunately, this sample contained very little common lead, as evidenced by the small amount of Pb^{204}, so that one can be reasonably certain that the isotopic analysis is not complicated by the presence of common lead. The uranium and thorium ages for this sample are in definite disagreement, a fact which is not surprising when one considers the alteration processes which this very old mineral has probably suffered.[21, 41] The age as computed from the AcD/RaG ratio is 2.2×10^9 yr., a value greater than the present assumed *age of the earth*. This is especially disturbing, as any alterations by which one might conceivably explain the differences in the ages as computed by the three methods would tend to give a low AcD/RaG ratio. In other words, the true AcD/RaG ratio for the corresponding unaltered mineral would have to be higher than 15.9, and hence, the true age of the mineral would have to be greater than 2.2×10^9 years!

The relatively small amount of Pb^{204} present in the two samples containing the large amount of Th indicates that the opinion advanced by Meyer[38, 42] that Pb^{208} might decay into Pb^{204} is without experimental foundation.

This work was made possible through the very active help and encouragement of Professor G. P. Baxter, Department of Chemistry, Harvard University, who very kindly prepared and furnished most of the lead iodide samples. It is a pleasure to acknowledge the interest taken by Professor Alfred C. Lane, Chairman of the Committee on the Measurement of Geologic Time, through whose efforts a number of the specimens were obtained. Samples 16, 17, 20, and one of the number 10 samples were prepared and supplied by Dr. A. v. Grosse of the University of Chicago.

[41] A. Holmes, *Age of the Earth* (Nelson Press, 1937), p. 167.

[42] S. Meyer, Wien Ber. IIa, **145**, 577 (1936).

The Sensitized Fluorescence of Potassium

ERNST H. KRAUSE
*University of Wisconsin, Madison, Wisconsin**

(Received October 24, 1938)

A mixture of potassium vapor and mercury vapor contained in a tube fashioned after the Cario-Lochte-Holtgreven sodium vapor lamp was radiated by light from a water-cooled mercury arc. The resulting fluorescence radiation contained potassium lines as well as two of the three known K_2 absorption bands and a new band with maximum at 5721A. On exposure of the mixture to light from a hot mercury arc or to light having all wave-lengths shorter than 2800A filtered out, the fluorescence was eliminated. This indicated that the excitation was caused by absorption of 2536A by the mercury. Absorption of the 2536A mercury line raises the mercury atom to the 6^3P_1 state, having an energy of 4.86 volts. The ionization potential of potassium is 4.32 volts; thus in a collision of the second kind, the excited mercury atom has enough energy to ionize the potassium atom. There was no evidence of a potassium emission from an energy state in the continuum equal in energy to the Hg 6^3P_1 or 6^3P_0 states. There were, however, two strong lines in fluorescence which could not be ascribed to the usual K energy levels nor to any probable impurity. To test whether or not ionization of potassium actually takes place, a filament was introduced into the tube to supply electrons. A large increase in intensity of the fluorescence of potassium lines was obtained with the hot filament. It was furthermore found that the intensity increased with filament temperature.

INTRODUCTION

SINCE the original experiment on sensitized fluorescence by Cario and Franck[1] with a mixture of mercury and thallium vapors, several experiments have been performed on the vapors of other elements.[2] In these experiments, a mixture of two kinds of atoms, A and B, was radiated with light of a type which only A could absorb. Some of the A atoms, after absorption of light, underwent collisions of the second kind with B atoms, and raised them to an excited state. Subsequently the B atoms emitted light and returned to the normal state.

In previous experiments on sensitized fluorescence the energy absorbed by the A atoms, usually mercury, was less than the ionization energy of the B atoms. In the present experiment atoms A (mercury) possess, after absorption of light of wave-length 2536A, energy greater than the ionization energy of atoms B (potassium). The 6^3P_1 mercury level has an energy of 4.86 volts, the metastable 6^3P_0 level an energy of 4.66 volts, while the ionization energy of potassium is 4.32 volts. A collision of the second kind with an excited mercury atom in the 6^3P_1 or 6^3P_0 state could therefore result in a normal mercury atom, an ionized potassium atom and an electron with 0.54 or 0.34 volt kinetic energy.

Duffendack and his associates[3-5] have shown that it is possible to produce excited ions by collisions of the second kind with ions of another atom. The present experiment was undertaken to see if the sensitized fluorescence of potassium could be obtained and whether or not it would be possible to form ions by collisions of the second kind between normal atoms of one kind and excited atoms of another kind.

APPARATUS

Although potassium serves the purpose of this experiment very well, it presents a difficult problem from an experimental point of view because of its great activity, especially at higher temperatures. It will turn Pyrex and quartz containers a dark reddish brown at temperatures above 200°C. This raises the problem of keeping clean a window through which to pass the exciting light and also to observe fluorescence.

* Now at the Naval Research Laboratory, Anacostia, D. C.

[1] G. Cario, and J. Franck, Zeits. f. Physik **11**, 161 (1922).

[2] A. C. Mitchell and M. W. Zemansky, *Resonance Radiation and Excited Atoms*, p. 65.

[3] O. S. Duffendack and K. Thomson, Phys. Rev. **43**, 106 (1933).

[4] O. S. Duffendack and J. H. Manley, Phys. Rev. **47**, 56 (1935).

[5] O. S. Duffendack and W. H. Gran, Phys. Rev. **51**, 804 (1937).

The first method tried was a jet arrangement in which the potassium and mercury vapors were fed through two concentric jets onto a liquid-air-cooled surface. The light source and the spectrograph were then focused through separate quartz windows on a point just above the jets. No satisfactory results were obtained by this method.

The final tube which was successful was fashioned after the Cario-Lochte-Holtgreven sodium vapor lamp[6] in which a circulating inert gas was used to prevent the sodium vapor from depositing on the exit window.[7] The tube, as redesigned to be used in the present experiment, is shown in Fig. 1. The circulating gas entered the main tube through the upper side tube, passed through the funnel, through a cylindrical slit and out the lower side tube. A detail of the slit is shown in Fig. 1. A five-cm diameter quartz lens of focal length 8.8 cm for 2536A was waxed to the front of the tube with ordinary sealing wax. It was found necessary to water cool this wax joint with flexible lead pipe. An inlet was provided on the top side of the tube for distilling in potassium. The inlet was sealed off at the constriction after the potassium had been distilled in.

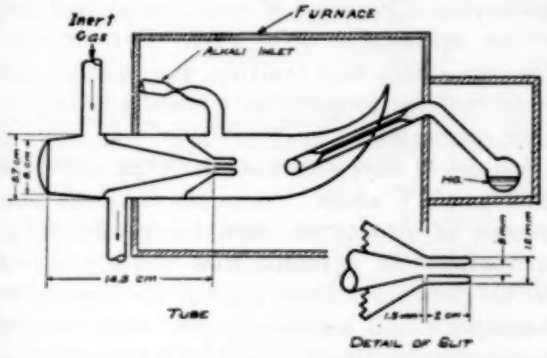

FIG. 1. Diagram of experimental tube.

A bulb containing distilled mercury was connected through a capillary to the side of the main tube. Since the mercury vapor pressure was always less than that of the potassium, a one-half-mm capillary about three cm in length was placed between the mercury bulb and the main tube to keep the potassium from distilling over into the mercury bulb. The capillary was kept at the temperature of the main tube. The tube was so constructed that a furnace could be slipped over it up to the gas exit tube in the front and to include the capillary in back (see Fig. 2). Thus the potassium pressure was determined by the temperature of the tube, while the mercury pressure was determined by the temperature of a furnace which could be slipped over the mercury bulb separately. The temperature in the main furnace was obtained with three chromel-alumel thermocouples.

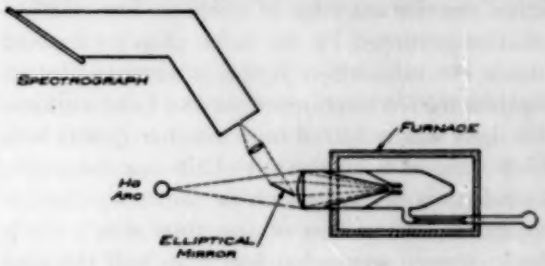

FIG. 2. Arrangement of spectrograph and mercury arc.

For circulating the gas a two-stage mercury vapor pump was used, the smallest jet of which was about one mm in diameter. It was necessary to have a small jet to move the inert gas at pressures of one to three cm. The second stage of the pump was useful when the system was being evacuated. The gas was circulated through a series of two liquid-air traps into the tube. The traps were filled with marbles of about one cm diameter to produce sufficient agitation of the gas so that all parts of it would be brought into contact with a cold surface to remove all traces of mercury. These precautions for the removal of mercury were necessary to prevent absorption of 2536 in the 14.5 cm of gas which the exciting light traversed before reaching the potassium-mercury mixture.

The circulating gas used was 99.5 percent pure neon. A neon pressure of 20 to 25 mm of Hg was found to give the best results, whereas pressures below ten mm were found to be unsatisfactory in that a gradual clouding of the lens took place at the higher potassium pressures.

With the arrangement as described, a continuous run of 100 hours was made with a potassium temperature of 400°C to 450°C with

[6] G. Cario and W. Lochte-Holtgreven, Zeits. f. Physik **42**, 22 (1927).
[7] A. C. Mitchell and M. W. Zemansky, *Resonance Radiation and Excited Atoms*, p. 27.

no perceptible depositing of potassium on the lens. Of the four to five cc of potassium originally distilled into the tube about 10 percent had been swept into the gas exit tube. Despite the fact that the mercury bulb was at room temperature for the greater part of the run, only a small amount of potassium distilled through the capillary.

The optical arrangement is shown in Fig. 2. Light from the mercury arc was focused, by means of the lens on the tube, on a point one mm behind the distant edge of the slit. The emitted radiation returned by the same path to a point outside the tube where it was intercepted by an elliptical mirror aluminized on the front surface. This light was reflected onto another quartz lens which focused it on the slit of the spectrograph. The mirror was cut to such an ellipticity that its projection on the lens of the tube was a circle which covered somewhat less than half the area of the lens.

The light source was a water-cooled, magnetically deflected, quartz mercury arc. Discharge pictures were obtained by connecting a small Tesla coil to a wire surrounding the tube some distance behind the cylindrical slit. Pictures were taken on a spectrograph with *f*4 quartz lenses. Focusing was accomplished with the aid of the red neon glow obtained with the Tesla discharge. The lens distances were calculated for the respective wave-lengths that they were to bring to a focus. By means of the discharge a small red spot was obtained, corresponding to the opening in the tube. This spot could be focused on the slit of the spectrograph and on the mercury arc, thus assuring correct line-up.

Results

In the first runs with potassium in this apparatus, temperatures were used to give potassium pressures of the order of magnitude of those used by Beutler and Josephy for sodium[8] (0.25 mm for Na and 3 mm for Hg). No sensitized fluorescence was obtained for exposures running up to three and four hours.

Sodium was then introduced into the tube to test the system. It was found that sodium fluorescence first appeared at a temperature which corresponded to about five times the pressure recorded by Beutler and Josephy. This difference probably was brought about by the fact that the furnace temperatures as measured in this experiment did not alone determine the sodium pressure or the number of sodium atoms present because sodium atoms were constantly swept away by the flow of neon and the cool neon gas passing through the slit in large quantities very probably cooled the portion of sodium vapor under observation. Further experimentation showed that the optimum sodium pressure was obtained at a temperature of 450°C.

The fluorescence spectra obtained for sodium showed the same sodium lines with the same intensity distribution as found by Beutler and Josephy except that several more lines were observed in the present experiment. These included the 3^2P-3^2D (8196A), the 3^2P-10^2D (4278A), and the 3^2P-11^2S (4292A). Although the intensities of the sodium lines were not measured on a microphotometer, a visual inspection showed that they compared very closely to the intensity distribution as found by Beutler and Josephy under vacuum conditions (i.e., no nitrogen or inert gases present). This indicates that the excitation energy is caused by the 6^3P_1 mercury level having 4.86 volts energy and not to the metastable 6^3P_0 level. Thus it was definitely shown that the tube was suitable and would function properly for a sensitized fluorescence experiment.

A series of runs was made at temperatures of 360°C to 450°C which corresponds to a potassium pressure of two to ten mm for potassium in equilibrium. At a temperature slightly above 360°C, potassium lines started to appear in fluorescence and increased in intensity as the temperature increased. The most intense fluorescence was obtained at the highest temperature. Higher temperatures were not used because several short trials indicated that the potassium loss to the gas-exit tube was rather large. The temperature of the mercury bulb was kept around 150°C. Once the mercury had been kept at this temperature for several hours, enough of it had amalgamated with the potassium in the tube to serve as a continual supply. Thereafter, the mercury bulb could be kept at room temperature.

[8] H. Beutler and B. Josephy, Zeits. f. Physik **53**, 747 (1929).

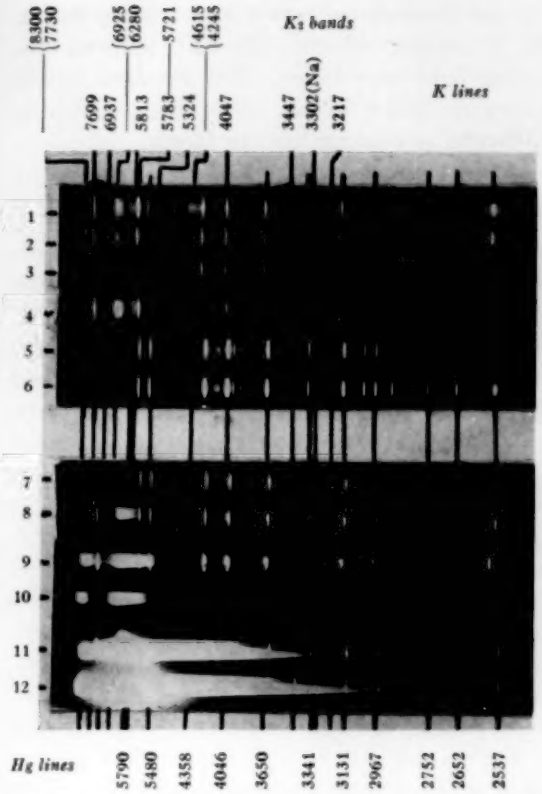

FIG. 3. 1. Sensitized fluorescence of potassium (Exposure 8 hr.). 2. Sensitized fluorescence of potassium (2 hr.). 3. Sensitized fluorescence with all wave-lengths above 2800 filtered out (2 hr.). 4. Discharge through potassium. 5. Mercury arc with same filter as was used in 3. 6. Mercury arc. 7. Sensitized fluorescence of potassium. 8. Sensitized fluorescence with filament at 3.8 amp. 9. Sensitized fluorescence with filament at 4 amp. 10. Filament alone, no exciting radiation. 11. Sensitized fluorescence with filament at 4.5 amp. 12. Sensitized fluorescence with filament at 4.8 amp. Exposures of 7–12 were 30 min.

Typical spectrograms are shown in Fig. 3. The plates used were Eastman 2L which had a medium sensitivity extending to about 9000A. Spectrograms 1 and 4 of Fig. 3 show that bands as well as lines are present in both discharge and fluorescence. In the discharge picture 4 of Fig. 3, all three of the known K_2 absorption bands as well as a new band with maximum at 5721A are observed on the negative. The intensities of these bands and lines relative to each other in discharge and fluorescence are given in Table I.

The intensity of the fluorescence lines in each series decreased with increasing total quantum number. The intensity ratio of lines originating in higher energy states to those originating in lower energy states in a given series is much lower in discharge than it is in fluorescence as can be seen by a comparison of 4 and 1 in Fig. 3.

To prove that the excitation of potassium fluorescence was caused by mercury in the 6^2P state and not by direct absorption of light by potassium vapor, pictures were taken with a hot mercury arc as a source. Direct absorption by potassium vapor would be nearly the same with hot or cold arc source but because of self-reversal of 2536, no sensitized fluorescence would occur for excitation by a hot arc. It was found that for hot arc excitation, no potassium lines appeared, but one K_2 band, that at 6280–6925A, was observed. A further check was made by interposing a Corning filter No. 987AB or No. 987AA in the path of the exciting light. The transmission of the 987AA filter is shown in Nos. 5 and 6, Fig. 3. The short wave transmission limit of No. 987AB was about 2650A which was well below the potassium series limit 2860A. No fluorescence was obtained with either filter in the path of the exciting light as can be seen by comparing spectrograms No. 3 and No. 1. All the lines in No. 3 are scattered light from the Hg arc. It can therefore be concluded that the fluorescence of the potassium lines and the greater part of the fluorescence of the K_2 bands results from the absorption of 2536 by mercury vapor.

The energy diagrams of potassium and mercury are shown in Fig. 4, with the lines obtained by sensitized fluorescence drawn in. These include all the lines shown in the K diagram of Fig. 4 with the exception of the 4^2S-7^2P which is to be discussed later. Higher series lines are very probably present, but are not observed because of their low intensities.

Since the mercury excitation energy was sufficient to ionize the potassium, it was of interest to determine whether or not the potassium lines and bands obtained were a subsequent result of the recombination of potassium ions with electrons. If some source of electrons could be made available for supplying potassium ions with electrons, the intensity of fluorescence should be increased provided potassium ions are present. For this purpose a filament was introduced into the tube to furnish a supply of electrons. The filament was placed horizontally about three mm

behind the slit in the tube (see Fig. 1). It was made of pure tungsten wire about three mm long, silver-soldered onto copper leads which were brought out of the front end of the tube through the wax seal. Runs were then made similar to those without the filament, with the exception that shorter exposures were used. It was assumed that if the effect took place to any extent, fluorescence lines should appear with 30-minute exposures. The results obtained with the filament in the tube are shown in Fig. 3, Nos. 7–12. No. 7 was taken with the filament off and Nos. 8, 9, 11 and 12 with filament currents of 3.8, 4.0, 4.5 and 4.8 amperes, respectively. This corresponded to a filament temperature range estimated to be about 1300°C to 2500°C.

A comparison of Nos. 7 and 8 shows that an exceedingly large increase in the intensity of the principal potassium doublet 4^2P (7699, 7644A) is obtained when the filament is turned on. Furthermore, the intensity of this doublet builds up very rapidly with increasing filament current as can be seen by comparing Nos. 8, 9, 11 and 12. An increase in intensity in the other potassium lines is also noted, but not nearly as great a one. In No. 12, Fig. 3, the higher series potassium lines previously observed and one additional, 4^2S-7^2P (3217, 3218A), can readily be identified. The second member of the principal series of sodium was also observed. To prove that the emitted electrons themselves were not producing excitation, a picture of the filament without the exciting light was taken. This resulted in the continuum shown in No. 10 of Fig. 3 with no evidence of potassium lines or bands.

TABLE I. *Intensities in fluorescence and discharge referred to 7699–7665A as 10.*

Wave-Length	Notation	Intensity in Fluorescence		Intensity in Discharge
		Without Filament	With Filament	
*7699, 7665	$4^2S-4^2P_{3/2,1/2}$	10	200	10
*6965, 6937	$4^2P-4^2D_{3/2,1/2}$	4	Not obs.	1
6939, 6912	$4^2P-6^2S_{1/2,1/2}$			
6560	Unidentified	8	‡	2
6420	Unidentified	Not obs.	‡	5
6000	Unidentified	8	‡	Not obs.
*5896	NaD line	8	‡	6
*5832, 5813	$4^2P-5^2D_{3/2,1/2}$	§	‖	3
5802, 5783	$4^2P-7^2S_{1/2,1/2}$			
*5360, 5343	$4^2P-6^2D_{3/2,1/2}$	Very faint	‡	Not obs.
5340, 5323	$4^2P-8^2S_{1/2,1/2}$			
*4048, 4044	$4^2S-5^2P_{3/2,1/2}$	§	§	2
*3447, 3446	$4^2S-6^2P_{3/2,1/2}$	2	15	Not obs.
*3218, 3217	$4^2S-7^2P_{3/2,1/2}$	Not obs.	2	Not obs.
†8850–7735	$K_2(B'\Sigma-A'\Sigma)$	Not obs.	‡	Very faint
†6925–6280	$K_2(C'\Pi-A'\Sigma)$	8	‡	5
5721	New band, NaK?	20	‡	6
†4613–4243	$K_2(D'\Sigma-A'\Sigma)$	4	Not obs.	Not obs.

* R. Paschen and R. Götze, *Seriengesetze der Linienspektren.*
† W. O. Crane and A. Christy, Phys. Rev. **36**, 421 (1930).
‡ Hidden by W continuum.
§ Hidden by Hg line.
‖ Hidden by Hg line and W continuum.

Discussion

A comparison of the intensity distribution obtained in the sensitized fluorescence of sodium with that obtained by Beutler and Josephy indicates rather definitely that excitation of Na is produced by collision with Hg atoms in the 6^3P_1 rather than the metastable 6^3P_0 state. This shows that even though neon at a pressure as high as 25 mm of Hg was present, it was very ineffective in reducing the excited Hg atoms from the 6^3P_1 to the metastable 6^3P_0 state. When Beutler and Josephy used pressures of eight to ten mm of nitrogen they obtained a very large reduction to the metastable state with a marked change in relative intensity of fluorescence lines. The case of potassium is very similar to that of sodium with the exception that the K pressure was higher. It is to be expected that K atoms would not be especially effective in reducing Hg in the 6^3P_1 state to the 6^3P_0 state because of the large discrepancy between the smallest potassium energy difference and the $6^3P_1-6^3P_0$ energy difference. The number of K_2 molecules was less than one percent of the number of atoms[9] and therefore should produce little effect. It is therefore likely that the excitation of the potassium was caused by 6^3P_1 Hg atoms.

If K ions are formed by collisions of the second kind with excited Hg atoms, their recombination with free electrons should give all of the potassium arc lines. If there are no preferred transitions, the lines originating in the lower energy states should be the most intense since many different transitions would bring K atoms to these levels. Experiment showed that the intensity of potassium lines in fluorescence decreased with increasing quantum number but much less rapidly than the corresponding decrease observed in the discharge spectrum. This indicates that the method of populating energy

[9] F. W. Loomis and R. E. Nusbaum, Phys. Rev. **39**, 89 (1929).

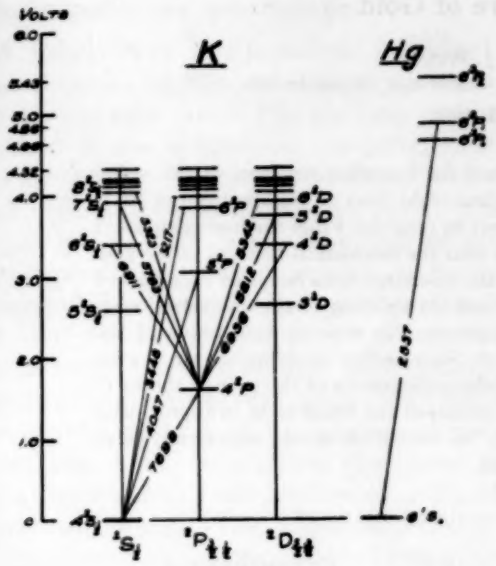

FIG. 4. Energy diagrams of potassium and mercury.

levels in fluorescence was more favorable to the higher energies than the method of populating in discharge.

Further evidence that potassium ions were formed was the very large increase in intensity of the potassium fluorescence when a hot filament was introduced into the fluorescing region. The potential drop across the filament was between 20 and 30 volts. This probably produced an electron current from the center of the filament to the positive filament lead. The field through which the electrons were accelerated was of the order of 75 volts per cm. This, however, did not produce excitation of K atoms as is shown in Fig. 3, No. 10.

The thermionic emission of tungsten in potassium vapor has been studied by Killian.[10] He reports very large electron emission at temperatures as low as 700°C. The emission increases with potassium pressure as well as with filament temperature. It can therefore be expected that in the present experiment, with filament temperatures well over 1300°C and higher potassium pressures, a very large electron emission occurred. If K ions were present, recombination should have been aided. The experiment showed that a hot filament caused a great increase in intensity of all the lines of the principal series of potassium.

No explanation has been found for the two bright lines 6000A and 6560A which appeared in the potassium fluorescence. In the K discharge 6000A was absent, 6560A was very weak and another line at 6420A was observed.

The excitation of the red band 6925–6280A by light from a hot Hg arc but not by light from a cold arc with 2536A filtered out is surprising. The Hg lines in the hot arc are broader and therefore more likely to overlap K_2 absorption bands, but there are no Hg lines which fall within the limits of the band which was excited.

Another unexplained point of interest is the difference in relative intensities of bands in discharge and fluorescence. These are recorded in Table I. The strong band at 5721A may be caused by NaK[11] although this would not seem very likely from the small quantity of Na atoms present as noted by the low intensity of the D line.

The author wishes to express his appreciation to Professor J. G. Winans for suggesting the problem and for furnishing continued counsel throughout its completion and his thanks to Professor E. Wigner for some interesting discussions and advice on this subject.

[10] T. J. Killian, Phys. Rev. **27**, 578 (1926).

[11] R. Ritchl and D. Villars, Naturwiss. **16**, 219 (1928).

Hyperfine Structure of Gold

R. M. ELLIOTT[1] AND J. WULFF
Massachusetts Institute of Technology, Cambridge, Massachusetts

(Received August 4, 1938)

The spectrum of Au I and Au II has been examined for hyperfine structure in the region λ2300–6300A. Splitting has been observed in more than eight lines of the spectrum of Au I, whereas the hyperfine structure of Au II lines could not be resolved. From the four-component structure of the lines λ4437A and λ4607A it is shown that the mechanical moment of the gold nucleus is $(3/2)(h/2\pi)$. The effect of self-reversal in the resonance lines has been investigated and eliminated. The magnetic moment determined from the splitting of the unreversed resonance line λ2428A is found to be 0.195 proton-magneton. No other determination of the magnetic moment is at present possible because of the intermediate coupling shown to exist in the complex electronic configurations of Au I and the inadequacies of the present theory of hyperfine structure. The splitting of the $^2P_{1/2}$ level is estimated and found to be in approximate agreement with that calculated from the $^2S_{1/2}$ level. No indication of any abnormally large $^2P_{1/2}$ separation or of any isotope shift has been found.

INTRODUCTION

SINCE gold is of odd atomic number (79) and atomic weight 197.2, hyperfine structure is to be expected in its spectral lines. Frisch,[2] however, did not find any structure in the resonance line λ2676A with the use of a high resolving power grating. In a report on the spectrum of copper Ritschl[3] noted that the resonance lines of gold were both split into two components and had separations of 0.224 and 0.221 cm^{-1}, respectively. Sibaiya[4] found self-reversal in the above lines and estimated, on the assumption of a nuclear moment of 3/2 for gold, a nuclear magnetic moment of 0.20 nuclear magneton, which is slightly lower than that calculated from Ritschl's data. Preliminary work of the present writers,[5] including intensity measurements, indicated that this value was probably too large.

Although previous work on the atomic weight of gold leads one to believe that an isotope shift should be present, nevertheless, Dempster[6] concludes that if the isotope 199 exists, it is present to an extent of but 0.1 percent or less. One should expect this to be substantiated by a careful examination of the hyperfine structure.

[1] At present with The American Thermos Bottle Co., Norwich, Connecticut.
[2] W. Frisch, Zeits. f. Physik **71**, 92 (1931).
[3] R. Ritschl, Naturwiss. **19**, 690 (1931).
[4] L. Sibaiya, Proc. Indian Acad. Sciences **2**, 313 (1935).
[5] J. Wulff, Phys. Rev. **44**, 512L (1933).
[6] A. J. Dempster, Proc. Am. Phys. Soc. **75**, 8, 755 (1933).

EXPERIMENTAL

Excitation

A modified Schuler tube immersed in a mixture of carbon dioxide and acetone was used for excitation. The demountable design is shown in Fig. 1. The cathode is a spun cylinder of gold, closed at the lower end and fixed in a similar cylinder of aluminum, the latter to prevent the excitation of the copper and zinc of the tube in the event of rupture of the gold cylinder. Spectroscopically pure helium or argon supports the discharge and is continuously circulated through a charcoal trap immersed in liquid air (carbon dioxide and acetone in the case of argon) by a mercury diffusion pump. A 1000-volt generator in series with a stabilizing resistance is used for the power supply. Fig. 2 shows a characteristic curve for the discharge as ordinarily used. This curve is shown for a pressure of approximately two-tenths of a millimeter of mercury. Curves for other pressures do not differ materially from this one except at the point where the discharge changes to an arc. As the pressure decreases this point moves slowly to the left. The potential difference across the tube when arcing is about 130 volts at 0.8 ampere, depending upon the pressure and previous history of the tube. Since arcing is a serious problem in the operation of a tube of this design, the glass shield *G* was inserted to reduce the tendency to arc by lengthening the minimum anode-cathode distance.

Interferometer and spectroscopes

A Fabry-Perot interferometer following the general design of Hansen[7] sufficed for many of the photographs taken. For the long exposures required in the ultraviolet, the interferometer was arranged for evacuation so that the optical path difference could be kept constant.[8] Fused quartz etalons with evaporated films of silver, aluminum-silicon, and aluminum were used. Tolansky[9] has shown that a minor variation in film thickness can cause a severe change in the optical path difference because of the change in phase reversal which may occur with slightly varying film thicknesses. To produce, therefore, as uniform a film as possible, the plates were placed no less than twelve inches away from the evaporating source. The assembled etalons resulting showed no detectable sign of ring motion. The transmission of a single aluminum film used for the far ultraviolet was less than 0.1 percent at 4000A.

In the visible region the interferometer was used with a Zeiss three-prism constant deviation spectrograph with a one-meter focal length camera. In the ultraviolet a Hilger E2 quartz spectrograph was used. Since this is a Littrow-type instrument, the fringes were focused on the slit by means of a 50-cm quartz-fluorite doublet. The variation of focal length of this doublet was not determined, as in the case of the Zeiss instrument, by photographic trial and error method on the fringes themselves, since exposure would then be prohibitively long. Furthermore, a mercury arc was not used since the fringes obtained were too broad. A new method was devised for this work which we believe is not only extremely precise, but in addition, provides a rapid and convenient means of determining the chromatic aberration of any lens. The set-up employed is illustrated in Fig. 3. A mercury arc L was focused by the small lens P on the mirror M_1, thence reflected through the achromat A to the mirror M_2 and back through the achromat to the slit S of the spectrograph. The mirror M_1 is a piece of quartz $8\times2\times1$ millimeters on which one-mil wire had been wound and aluminum evaporated. When the wire was removed it left a series of fine intersecting rulings which formed an ideal object on which to focus. This mirror was placed as close as possible to the slit with its long edge parallel to the jaws. The mirror M_2 was a three-inch flat of good quality. A series of exposures (30 seconds) were made with the spectrograph and the achromat moved between successive ones. It is obvious from the diagram that M_1 and S are conjugate points only when both lie at the focal point of the achromat. A

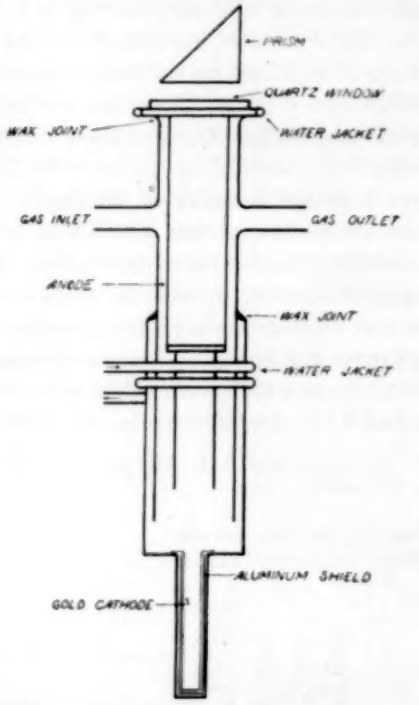

FIG. 1. Hollow cathode discharge tube.

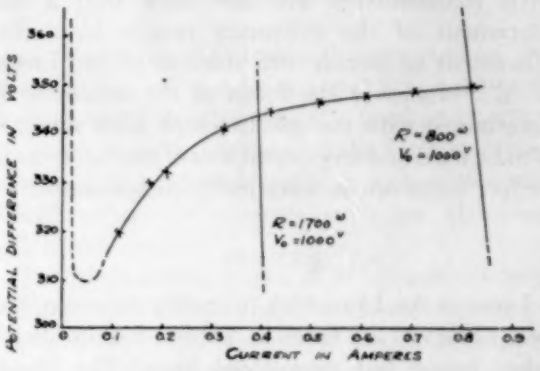

FIG. 2. Tube characteristic curve.

[7] G. Hansen, Naturwiss. **15**, 163 (1927); or Von Bayer, Physik. Zeits. **9**, 831 (1908).
[8] Details of the construction are to be published shortly.
[9] S. Tolansky, J. Sci. Inst. **13**, 8 (261).

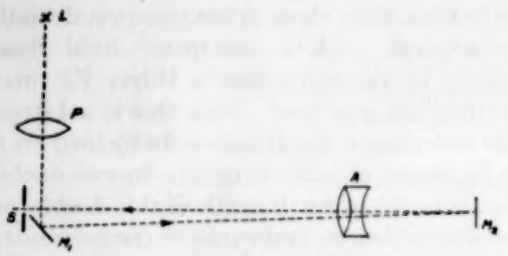

FIG. 3. Optical arrangement for focal length determination.

little consideration will also show that a displacement of the achromat results in a displacement of double the amount of the image of M_1. Moreover the focus of the achromat is determined with the spectrograph with which it is to be used and any deviations of the latter from perfect focus are automatically compensated.

RESULTS

Lines of Au I in which hyperfine structure has been observed are listed in Table I together with other broad but unresolved lines. The classifications and configurations are those of McLennan and McLay.[10] The classifications of Symons and Daley[11] are also given for the lines which they investigated in a study of the Zeeman effect. The latter classifications assume strict *LS* coupling.

In the following lines of Au I no splitting has been observed:

2701 $(5d^9{}_{5/2}\,6s^2{}_0)\ 1_{5/2}-(5d^9{}_{5/2}\,6s_{1/2}\,6p_{1/2})\ 3^0{}_{5/2}$
2848 $(5d^9{}_{5/2}\,6s^2{}_0)\ 1_{5/2}-(5d^9{}_{5/2}\,6s_{1/2}\,6p_{1/2})\ 2^0{}_{7/2}$
3123 $(5d^9{}_{5/2}\,6s^2{}_0)\ 1_{5/2}-(6p)\ {}^2P^0{}_{3/2}$
3308 $(5d^9{}_{5/2}\,6s^2{}_0)\ 2_{3/2}-(5d^9\,6s\,6p)\ 8^0{}_{5/2}$
3795 $(6p)\ {}^2P^0{}_{3/2}-(7d)\ {}^2D_{5/2}$
3898 $(5d^9{}_{5/2}\,6s_{1/2}\,6p_{1/2})\ 1^0{}_{5/2}$
$-(5d^9{}_{5/2}\,6s_{1/2}\,7s_{1/2})\ 3_{7/2}$
3927 $(5d^9{}_{5/2}\,6s_{1/2}\,6p_{1/2})\ 6^0{}_{3/2}$
$-(5d^9{}_{5/2}\,6s_{1/2}\,6d_{1/2})\ 7_{9/2}$
3915 $(5d^9{}_{5/2}\,6s_{1/2}\,6p_{1/2})\ 6^0{}_{7/2}$
$-(5d^9{}_{5/2}\,6s_{1/2}\,6d)\ 8_{5/2}$
4040 $(5d^9{}_{3/2}-6s^2{}_0)\ 2_{3/2}-(5d^9{}_{5/2}\,6s_{1/2}\,6p_{1/2})\ 3^0{}_{5/2}$
4065 $(6p)\ {}^2P^0{}_{1/2}-(6d)\ {}^2D_{3/2}$
6278 $(5d^9{}_{3/2}\,6s^2{}_0)\ 2_{3/2}-(6p)\ {}^2P^0{}_{1/2}$.

Four lines of Au II classified by McLennan and McLay[12] were investigated and no splitting was observed:

4053 $(6s)\ {}^3P_{3/2}-(6p)\ {}^3D_{3/2}$
3803 $(6s)\ {}^3P_{3/2}-(6p)\ {}^3D_{5/2}$
3123 $(6s)\ {}^3P_{3/2}-(6p)\ {}^3D_{5/2}$
2914 $(6s)\ {}^3F_{7/2}-(6p)\ {}^3D_{5/2}$.

The latter notation is that of McLennan and McLay; according to these authors, the lower terms involved in these lines, while not unambiguously assigned, probably belong to a system based on the d^9s ion of Au III. Two additional lines of Au II in which no splitting was observed are λ3874A and λ3581A. These are not listed by McLennan and McLay but are given by Symons and Daley.[11]

Figure 4 shows a series of microphotometer curves of the resonance line λ2676A as observed under different conditions of excitation. The reversal is quite evident in two curves, (a) and (b), but there is no indication of its presence in the bottom curve, (c). Inasmuch as measurements of the photographs which were taken with currents of 0.30 and 0.17 ampere agree to two percent, we

[10] J. C. McLennan and A. B. McLay, Proc. Roy. Soc. **A136**, 35 (1931).
[11] A. S. M. Symons and J. Daley, Proc. Phys. Soc., Lon. **41**, 431 (1929).
[12] J. C. McLennan and A. B. McLay, Trans. Roy. Soc. Can. **22**, 103 (1928).

TABLE I. *Lines of* Au I *in which hyperfine structure has been observed.*

WAVE-LENGTH	CLASSIFICATION McLENNAN AND McLAY	CLASSIFICATION SYMONS AND DALEY	INTENSITY AND SEPARATION
2428	$(6s)\ {}^2S_{1/2}-(6p)\ {}^2P^0{}_{3/2}$		(10) 0 (6) 0.214 cm^{-1}
2641	$(5d^9{}_{5/2}\,6s^2{}_0)\ 1_{5/2}-(5d^9{}_{5/2}\,6s_{1/2}\,6p_{1/2})\ 4^0{}_{7/2}$		(10) 0 (3) 0.10 Not completely resolved
2676	$(6s)\ {}^2S_{1/2}-(6p)\ {}^2P^0{}_{3/2}$		(10) 0 (6) 0.218 cm^{-1}
2748	$(5d^9{}_{5/2}\,6s^2{}_0)\ 1_{5/2}-(5d^9{}_{5/2}\,6s_{1/2}\,6p_{1/2})\ 2^0{}_{5/2}$		Broad but not resolved
3029	$(5d^9{}_{5/2}\,6s^2{}_0)\ 1_{5/2}-(5d^9{}_{5/2}\,6s_{1/2}\,6p_{1/2})\ 1^0{}_{5/2}$	$6s''\ {}^3D_{3/2}-a$	(4) 0 (10) 0.11 Not completely resolved
4437	$(5d^9{}_{5/2}\,6s_{1/2}\,6p_{1/2})\ 3^0{}_{5/2}-(5d^9{}_{5/2}\,6s_{1/2}\,7s_{1/2})\ 4_{5/2}$	$6p''\ {}^4F_{5/2}-6d''\ {}^4D_{5/2}$	(2) 0 (6) 0.066 (7) 0.161 (10) 0.285 cm^{-1}
4607	$(5d^9{}_{5/2}\,6s_{1/2}\,6p_{1/2})\ 4^0{}_{7/2}-(5d^9{}_{5/2}\,6s_{1/2}\,7s_{1/2})\ 4_{5/2}$	$6p''\ {}^4P_{3/2}-6d''\ {}^4D_{5/2}$	(2) 0 (6) 0.065 (8) 0.147 (10) 0.244 cm^{-1}
4792	$(6p)\ {}^3P^0{}_{2/2}-(6d)\ {}^3D_{3/2}$	$6p\ {}^3P_{3/2}-6d\ {}^3D_{3/2}$	Width less than 0.05 cm^{-1}
4811	$(6p)\ {}^3P^0{}_{3/2}-6d\ {}^3D_{3/2}$	$6p\ {}^3P_{3/2}-6d\ {}^3D_{3/2}$	Width less than 0.04 cm^{-1}
5065	$(5d^9{}_{5/2}\,6s^2{}_0)\ 2_{3/2}-(6p)\ {}^2P^0{}_{3/2}$	$6s''\ {}^3D_{3/2}-6p\ {}^3P_{3/2}$	Width less than 0.05 cm^{-1}
5147	$(5d^9{}_{5/2}\,6s_{1/2}\,6p_{1/2})\ 7^0{}_{9/2}-(5d^9{}_{5/2}\,6s_{1/2}\,7s_{1/2})\ 5_{7/2}$	$6p''\ {}^3P_{3/2}-6d''\ {}^4D_{3/2}$	(8) 0 (10) +0.088 cm^{-1}
5262	$(5d^9\,6s\,6p)\ 8^0{}_{5/2}-(5d^9{}_{5/2}\,6s_{1/2}\,7s_{1/2})\ 5_{5/2}$	$6p''\ {}^3D_{3/2}-6d''\ {}^4D_{3/2}$	(10) 0 (7) 0.114 (6) 0.176 cm^{-1}
5837	$(6p)\ {}^3P^0{}_{1/2}-(7s)\ {}^3S_{1/2}$		Width less than 0.4 cm^{-1}

feel sure that reversal is absent at these low currents. The small currents required to obtain the resonance lines free from reversal, together with the fact that the fused quartz etalons begin to absorb at about λ2500A, necessitated exposures of over sixteen hours, even with the most sensitive photographic plates. The accuracy of measurements may be judged from the fact that four separate measurements of the line λ2676A agree to less than two percent. The typical "flag" pattern of the line λ4437A is quite evident from the microphotometer curve of Fig. 5.

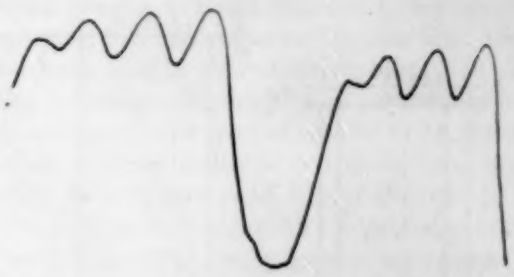

FIG. 5. Photometer curve (retouched) λ4437A, Mag. 30×, separator 1.04 cm.

DISCUSSION AND CONCLUSIONS

The observations on the resonance lines λ2676A and λ2428A permit a determination of the splitting of the $^2S_{1/2}$ and $^2P_{1/2}$ states. The term diagrams are shown in Fig. 6. The theory of Goudsmit shows that the ratio of the splitting in the $^2S_{1/2}$ and $^2P_{3/2}$ states should be over a hundred to one, so that the splitting of the line λ2428A should give directly the separation of the $^2S_{1/2}$ level. The separation of the $^2P_{1/2}$ level can then be determined from the $^2S_{1/2}$ separation and the measurement on λ2676A. The value found is 0.006 cm^{-1}. From the $^2S_{1/2}$ separation the theoretical separation in the absence of perturbation for the $^2P_{1/2}$ level may be calculated. This value is 0.011 cm^{-1}. These values may be considered as in essential agreement when one remembers that the experimental value is determined from the difference of two large quantities. There is no indication, however, of an abnormally large $^2P_{1/2}$ separation. This conclusion is supported by the observations on the lines λ5837A and λ4065A, both of which involve the $^2P_{1/2}$ level and neither of which is split. Because of the high resolving power of the interferometer in this region one would expect to observe such an abnormal splitting if present.

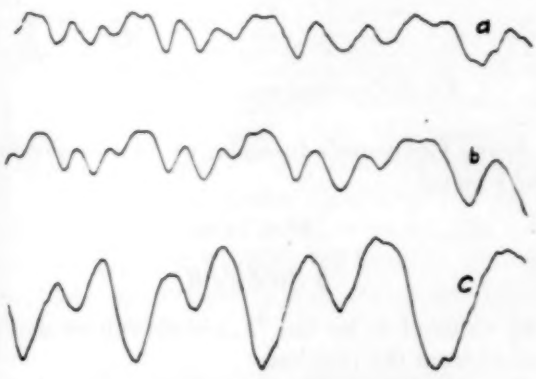

FIG. 4. Photometer traces (retouched) of λ2676A – Mag. 30×. (*a*) Current 0.9 amp.; separator 1.04 cm. (*b*) Current 0.8 amp.; separator 1.04 cm. (*c*) Current 0.17 amp.; separator 1.00 cm.

The evidence for a spin of 3/2 lies in the lines λ4437A and λ4607A. These lines involve the same upper level $(5d^9{}_{5/2}\,6s_{1/2}\,7s_{1/2})\,4_{5/2}$ according to both McLennan and McLay and Symons and Daley. The major portion of the splitting occurring in the two lines originates in the common level involving two *s* electrons.

If the nuclear spin is 3/2 the interval factor calculated from the observed four components in λ4437A, assuming no splitting of the lower level, is 0.032. If the nuclear spin is 5/2, we should have six components, the spacing between the last three being 0.048 cm^{-1} and 0.024 cm^{-1}. Certainly, two components with this spacing could not have escaped notice with the resolving power available at this wave-length. The failure to observe six components and the fact that the interval rule is obeyed more closely for the value 3/2 than 5/2 is indicative of a spin of 3/2.

The assumption that the upper level of λ4437A is not split can be justified. Most important is that no splitting is observed in the case of the lines λ2701A and λ4040A which should involve this level according to McLennan and McLay. The interval factor for this level $(5d^9{}_{5/2}\,6s_{1/2}6p_{1/2})\,3^0{}_{5/2}$ calculated on the basis of pure *LS* coupling and using the splitting factor of 0.107 for the 6*s* electron determined from the resonance line is only 0.001; on the basis of *j–j* coupling it is either 0.021 or 0.015, depending upon the *j* value of the ion formed by removing

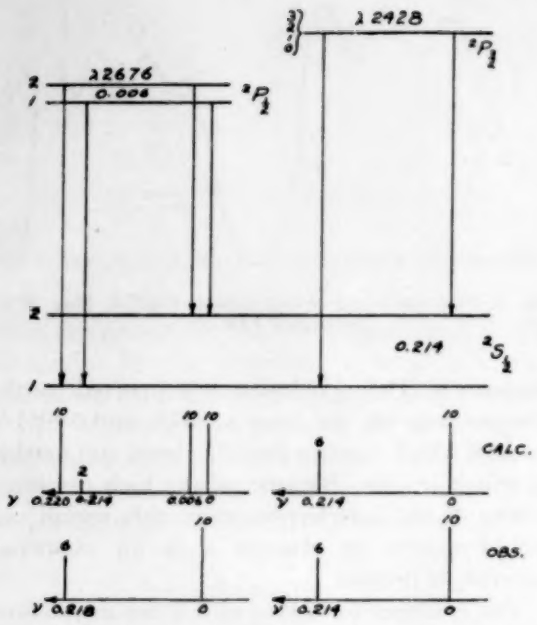

FIG. 6. Energy level diagrams for the resonance lines of Au.

the *s* electron. Experimental evidence discussed below indicates that the coupling in the complex electronic configuration is probably intermediate, so that the interval factor for the $3^0_{5/2}$ level should be small. The fact that the line λ4437A does follow the interval rule closely is further proof that the lower level is not split.

From the observations on λ4607A the splitting of the lower level $4^0_{3/2}$ can be estimated. Since the pattern is not completely resolved the graphical method of Fisher and Goudsmit[13] may be used. The graph for the line λ4607A is shown in Fig. 7. The short vertical dashes represent the observed positions of components and the best fit is obtained for a percentage ratio of +22. This corresponds to an interval factor of 0.008 cm^{-1} for the $4^0_{3/2}$ level.

From the splitting factor for the 6*s* electron calculated from the resonance line, the theoretical factor on the assumption of pure *LS* coupling for the $4^0_{3/2}$ level is 0.026 cm^{-1}, according to the work of Goudsmit and Bacher.[14] For pure *jj* coupling it is −0.021. From this we conclude that the coupling must be intermediate, a conclusion in accord with the point of view of McLennan and McLay.

The splitting factor of the 7*s* electron in the $4_{5/2}$ configuration of both λ4607A and λ4437A cannot be obtained from measurements on these lines since this type of configuration (three electrons of which two are *s* electrons) has not as yet been treated theoretically for any type of coupling.

The two lines λ5147A and λ5260A, both of which show splitting, again involve a common upper level to which McLennan and McLay assign a configuration containing two *s* electrons. The patterns in this case, however, are incompletely resolved and it is not possible to determine the splitting of the lower levels involved. An approximate value of the *A* factor for the $5_{3/2}$ state may, however, be calculated from the splitting of λ5262A if one assumes that the lower level is not split. This value is 0.035 cm^{-1}.

Because of the exceedingly small value of the magnetic moment of gold, certain lines corresponding to those which prove so valuable in the hyperfine structure analysis of copper[15] show no splitting in the case of gold.

From the observed value of 3/2 for the spin of the gold nucleus and the splitting of the resonance line λ2428A, the magnetic moment of gold may be deduced.

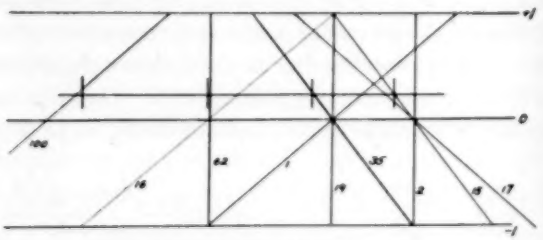

FIG. 7. Graphical analysis for λ4607A.

Using Goudsmit's formula, we first determine the *g* factor:

$$g=\frac{1838\ 3n_e^3a}{8\ R\alpha^2Z_iZ_0^2K}.$$

The value of n_e for the $^2S_{1/2}$ state can be determined from the relation

$$T=RZ_0^2/n_e^2.$$

[13] R. A. Fisher and S. Goudsmit, Phys. Rev. **37**, 1057 (1931).
[14] S. Goudsmit and R. F. Bacher, Phys. Rev. **34**, 1501 (1929).
[15] R. Ritschl, Zeits. f. Physik **79**, 1 (1932).

The term value of the $^2S_{1/2}$ state is given as 74461 cm^{-1} by McLennan and McLay. This corresponds to a value of n_* of 1.21. The value of Z_0 is unity for Au I, and the value of a is 0.214/2 or 0.107 cm^{-1}. The relativity correction K can be calculated from the results of Racah.[16] For $Z_i=79$, $j=\frac{1}{2}$, the value is 2.19. The value for g thus determined is 0.130, which for a spin of 3/2 results in a nuclear moment of 0.195 proton magnetons.

Because of the intermediate coupling present in the complex electronic configurations, no determination of the magnetic moment can at present be made from the splitting observed in the levels corresponding to these configurations.

The 7*s* electron of the $^2S_{1/2}$ state of λ5837A must possess a small interval factor since no splitting has been observed in this line. This is not surprising in view of the rapidity with which the a factor decreases with increasing total quantum number. In the case of Tl II, the ratio of the a factor for the 6*s* and 7*s* electrons is over eight to one; and in Bi I, over thirteen to one. The ratio in the case of Au I is probably at least five to one—how much greater we cannot say.

In conclusion, the present work shows that the nuclear spin of gold is 3/2 and the magnetic moment 0.195 proton-magneton within an experimental error of two percent, disregarding inadequacies in the theory. No indications of an abnormally large $^2P_{1/2}$ separation or of an isotope shift have been found. Electron configurations of McLennan and McLay have been confirmed for several states.

[16] G. Racah, Nuovo Cimento **8**, 178 (1931); and Zeits. f. Physik **71**, 431 (1931).

JANUARY 15, 1939 PHYSICAL REVIEW VOLUME 55

The Fine Structure of the Line λ4686 of Ionized Helium

DJEN-YUEN CHU
California Institute of Technology, Pasadena, California
(Received December 1, 1938)

The fine structure of the line λ4686 of ionized helium emitted from a discharge tube with hollow cathode cooled by liquid air was measured with a Fabry-Perot interferometer. The formula for the pattern obtained with this instrument expressed in Fourier series was applied in the analysis. Of the eight components predicted by theory, four were definitely observed, while the remaining weak ones were inferred from the pattern to be present. Relative intensities and positions of the eight components were found to be in general agreement with theory. The separation between the two strongest components was 0.0095±0.0024 IA or 0.4529 ±0.0109 cm^{-1}. The Rydberg constant for helium was calculated to be 109,722.430±0.030.

ALTHOUGH the fine structure of the lines of ionized helium is of equal interest with that of hydrogen and deuterium, there has been relatively little study made of it. This paper is the report of the use of a Fabry-Perot interferometer, instead of the customary diffraction grating, for this purpose. The difficulty, of course, lies in the overlapping of the orders, but by using a variety of plate separations, the errors caused by this can be minimized.

EXPERIMENTAL ARRANGEMENT

The light came from a hollow cathode glow, excited by direct current. The cathode, made of a copper cylinder 3.4 cm in diameter and eight cm in length, formed the bottom of the discharge tube. Its inside was aluminized by evaporation in order to avoid the emission of ionized copper lines, one of which has a wave-length 4682 so close to the line 4686 that it could not be separated by the prism. The cathode was immersed in liquid air whose level was kept a little lower than the junction where the tapering top of the cathode was sealed to the glass tube. The anode was an aluminum ring just above the cathode and was of such a size that it would not intercept the light from the cathode to the window of the tube. The distance between the anode and

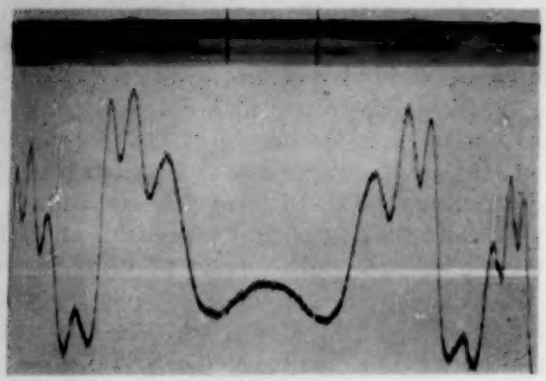

FIG. 1. A sample plate and microphotometer tracing. The upper strip of the plate represents λ4713 of He, the middle strip λ4686, and the bottom strip λ4663 of Al and a portion of the reflected image of 4686.

the cathode was made as small as possible to reduce the space in which the spectrum of neutral helium appeared. The length of the tube, about 36 cm, and the diameter of its top, about 10 cm, were so designed that the solid angle subtended at the collimeter slit by the lens which closed the top of the tube was nearly equal to that subtended by the collimator lens. The diameter of the cathode was such that the image on the slit was sufficiently large to secure fairly uniform illumination.

The discharge was produced at a pressure around 0.3 mm. The helium was kept purified during the exposure by circulation through charcoal traps immersed in liquid air.

The spectrograph consisted of a half-prism silvered on the back and a two-meter camera. The ratio of the focal length of the camera lens to that of the collimator lens was about 5.5 so that the slit image on the plate was wide enough to lessen the effect of photographic grain. Between the collimator and the prism was interposed a Fabry-Perot interferometer with plates 11 cm in diameter separated by three Invar posts held in a brass ring. Intensity marks on each plate were made with essentially the same arrangement as that used by Houston and Hsieh.[1]

In order to detect any shift of fringes that might have occurred during exposure the following method was devised. Two short exposures of about one or two minutes were made on a second plate, one just before and the other immediately after the main exposure which was about 50 minutes. The two pictures lay side by side on the same plate and any shift of fringes during the exposure was easily observed. Plates on which a shift could be definitely detected were rejected.

[1] W. V. Houston and Y. M. Hsieh, Phys. Rev. **45**, 263 (1934).

METHOD OF MEASUREMENT

For each plate to be measured, a microphotometric tracing was taken of the line 4686. (A sample of the line and its tracing is shown in Fig. 1, where four components are readily seen.) The ordinates and abscissae of the tracing were measured on a comparator and used in conjunction with tracings from the intensity marks to obtain a curve of intensity as a function of the square of the distance from the center of the pattern. Corrections were then applied for the deviations from uniform slit illumination and an average of one, two or three orders on each side of the center was taken. This average curve was

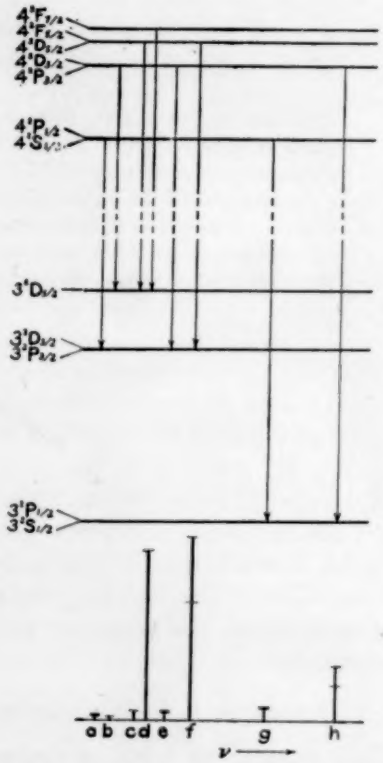

FIG. 2. Energy level diagram for He 4686.

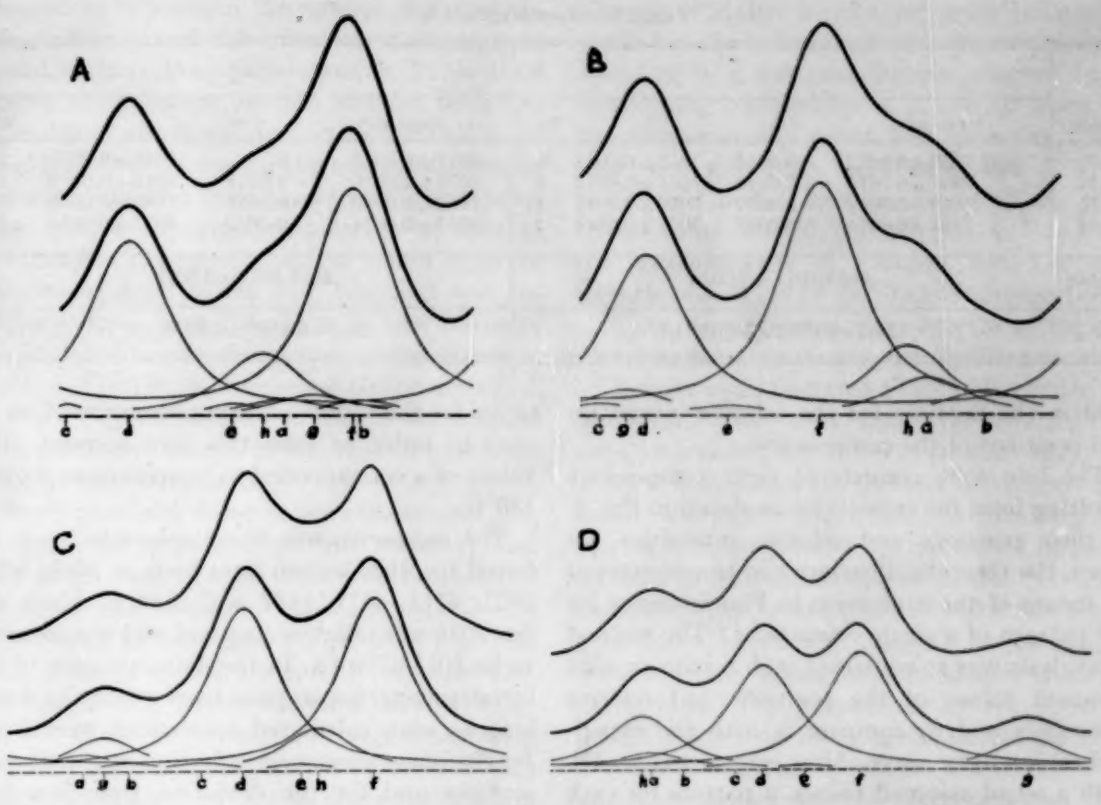

FIG. 3. In each of the drawings the upper heavy curve is the experimental curve, the lower heavy curve is the theoretical one obtained by summing the light curves representing the eight components *a*, *b*, *c*, *d*, *e*, *f*, *g*, *h*. Of the component curves only a part of the whole period is shown, except those of the two strongest components *d*, *f*. *A*. For plate 118 of which $s = 5.9814$ mm; *B*. For plate 124 of which $s = 3.9794$ mm; *C*. For plate 126 of which $s = 2.9878$ mm; and *D*. For plate 134 of which $s = 1.9780$ mm.

TABLE I. *Relative intensities and positions. In the second column are given the interferometer separations; in the third, the pressures both at the start and at the end of exposure; in the fourth, the current. I denotes intensity, that of component f being taken as 1.00. The theoretical intensities* are also given in the second row from the bottom. The theoretical positions calculated by using 1/137.0 for the fine structure constant** are given in the last row, all referred to f. P denotes the position. When no value is given, it means that the position is assumed to have the theoretical value.*

Plate	s mm	p mm Hg	c ma		a	b	c	d	e	f	g	h
118	5.9814	0.33–0.29	140	I	0.07	0.06	0.05	0.77	0.05	1.00	0.09	0.27
				P	—	—	—	−0.4528	—	0	0.7593	1.4907
124	3.9794	0.31–0.28	145	I	0.15	0.10	0.05	0.70	0.04	1.00	0.11	0.30
				P	—	—	—	−0.4555	—	0	0.7486	1.4868
126	2.9878	0.33–0.30	145	I	0.10	0.05	0.05	0.94	0.04	1.00	0.20	0.25
				P	—	—	—	−0.4393	—	0	0.7671	1.4854
134	1.9780	0.23–0.18	130	I	0.15	0.08	0.05	0.89	0.04	1.00	0.25	0.45
				P	—	—	—	−0.4529	—	0	0.8005	1.5167
	Theoretical I				0.026	0.010	0.046	0.924	0.041	1.00	0.062	0.299
	Theoretical P, cm^{-1}				−0.9744	−0.8210	−0.5774	−0.4556	−0.2436	0	0.7577	1.4885

* A. Sommerfeld and A. Unsöld, Zeits. f. Physik **36**, 259 (1926); **38**, 237 (1926); M. Saha and A. C. Banerji, Zeits. f. Physik **68**, 704 (1931).
** R. T. Birge, Phys. Rev. **48**, 918 (1935); R. Ladenburg, Ann. d. Physik **28**, 458 (1937).

TABLE II. *Wave-lengths*, IA.

	λ_f				λ_d			
PLATE	FROM MAX.	COR.	λ	WT.	FROM MAX.	COR.	λ	WT.
118	4685.7030±0.0013	−0.0015	.7015±0.0013	4	.8011±0.0011	0	.8011±0.0011	3
124	.7001±0.0013	+0.0012	.7015±0.0013	3	.8031±0.0010	−0.0015	.8016±0.0010	3
126	.7048±0.0017	−0.0029	.7019±0.0017	2	.7962±0.0020	0.0018	.7980±0.0020	1
134	.7052±0.0016	−0.0028	.7024±0.0016	2	.8013±0.0014	0.0012	.8025±0.0014	2
Mean	4685.7017±0.0014				4685.8012±0.0020			
$\Delta\lambda_{fd}$	$\Delta\lambda_{fd}=0.0995\pm0.0024$ IA				$\Delta\nu_{fd}=0.4529\pm0.0109$ cm^{-1}			

used in the analysis for the relative intensities and positions of the components.

The line 4686 consists of eight components resulting from the transitions as shown in Fig. 2. If their positions and relative intensities are given, the theoretical pattern can be constructed by means of the expression in Fourier series for the pattern of a single component.[2] The method of analysis was to construct such a pattern with assumed values of the positions and relative intensities and to compare it with the experimental intensity curve. After several trials, each with a set of assumed values, a pattern for each plate was finally obtained which fitted the experimental curve best. It was in this way that the intensities I and positions P given in Table I were obtained. Fig. 3(A–D) shows both the experimental and theoretical curves as well as the component curves for four different plates (s represents the interferometer separation).

In the Fourier series used the parameters α and r, which gave the broadening caused by Doppler effect and reflecting power of the silver surfaces of interferometer plates, respectively, were determined from another single line. This was because the structure of the line 4686 was so complex that it would be extremely tedious if besides the relative intensities and positions we had to change α and r in trying to get a theoretical pattern to fit the experimental one. The reflecting powers, r, obtained in this way were in the neighborhood of 0.61, since the source was not very intense and a thicker silver could not be used. Under these circumstances the contribution of the interferometer to the shape of the line cannot be ignored and the Fourier series for the individual components need to be used in order to take this into account. The values of α corresponded to temperatures around 180°K.

The measurements of wave-lengths were referred to other helium lines such as 5048, 5016, 4922, 4713, 4471, 4437 and 4388 of which the line 5016 was taken as standard and was assumed to be 5015.6750 IA. In the determination of the interferometer separations from which the wave-lengths were calculated corrections were made for the phase change on reflection at the silvered surfaces and for the deviation from standard conditions of the temperature and pressure under which the exposure was taken.

RESULTS

Four plates of different interferometer separations were measured. Because of the overlapping not all of the eight components could be observed. On plate 134 four components d, f, g, h were manifestly present, while on the other plates only three components could be definitely resolved. The existence of the four weak components a, b, c, e could be inferred only by the fact that the theoretical patterns deviated too much from the experimental curves when they were assumed absent. Of these four, c and e were the weakest and were always assumed to have the

TABLE III. *Computation of* R_{He}. $(\mu-1)10^7=2789.9$.

λ_{air}	$(\mu-1)\lambda$	r	R_{He}
4685.7017	1.3072	21335.5686	109722.423±0.032
4685.8012	1.3072	21335.1157	109722.437±0.047
		Mean	109722.430±0.040

[2] W. V. Houston, Phys. Rev. **51**, 446 (1937).

theoretical intensities throughout the analysis. The intensities of the other components were found to have the values given in Table I. Of course these values are not unique, since the intensity of one component was so related to its neighbors that increasing the one must decrease the other in order to fit the experimental curve. For example, the component *a* was very close to the component *g* (next order) on plate 126, to the component *h* on plates 124, 134, and was between *g*, *h* on plate 118. Thus its true intensity might be different from the values given in Table I. For the two strongest components *f*, *d*, however, the intensities could be ascertained with certainty, except in the case of plate 124 where *d* was too close to *g*.

As to positions, those of the components *a*, *b*, *c*, *e* could not be determined with certainty, and they were assumed to have the theoretical values in the analysis. The components *g*, *h* were found to have separations from *f* greater than those predicted by theory on plate 134, but appear not to be displaced on the other plates. The two strongest components were found to have a separation in agreement with theory, except in the case of plate 126 where *d* was too close to *f*. This was probably caused by experimental error, for the positions of maxima corresponding to this component were uncertain on the microphotometric tracing.

Table II gives the wave-lengths of the two strongest components *d*, *f*. They were first calculated from the maxima on the intensity curves. The errors were estimated from the uncertainties of the positions of these maxima. Then the corrections due to the displacement of the maxima by neighboring components were accurately determined and given in the columns "Cor." The weights were taken from the number of maxima from which the wave-lengths were calculated. The uncertainties in the mean values of wave-lengths are estimated values rather than the mean deviations which, 0.0003 for λ_f and 0.0008 for λ_d, are too small to be taken as representing the precision.

The wave-length of the component *g* could be calculated from only two plates. It was

$\lambda_g = 4685.5330 \pm 0.0030$ from plate 126,

and $\lambda_g = 4685.5266 \pm 0.0050$ from plate 134.

The uncertainties in this are great because on plate 126 the position of the maximum corresponding to *g* was considerably affected by its neighboring components *a*, *b*, and on plate 134 the maximum was broad and uncertain. However, the separation between *g* and *f*, which is 0.1719 IA, does not deviate from the theoretical value, 0.1665 IA as much as it does in the measurements of Paschen and Leo who found it to be 0.154 IA and 0.152 IA, respectively.

From the calculated wave-lengths of the two strongest components *d*, *f*, the Rydberg constant for helium was calculated (Table III) under the assumption that $\alpha = 1/137.0$. In reducing the wave-lengths in IA to those in vacuum, the index of refraction μ from the formula of Meggers and Peters[3] was used in order that the calculated R_{He} may be comparable with R_H calculated by using the same value of the index of refraction.[4] If we use the latest value of the index of refraction which gives $(\mu-1)\lambda = 1.3175$,[5] R_{He} will be 109722.189 ± 0.030, which is considerably smaller than the above value. The uncertainty of the mean in Table III is not the mean deviation but the mean of the individual uncertainties calculated from the uncertainties of the wave-lengths. The uncertainty here as well as elsewhere in this paper can be regarded as an estimated limit of error. The corresponding probable error would be perhaps about one-fourth of this.

Conclusions

The results of this work show that the positions of the components generally agree with the theory, in particular those of the two strongest components. The separation between these has an average value of 0.0995 IA, which is smaller than the values of 0.106, 0.1023 and 0.104 obtained by Paschen,[6] Kunze[7] and Leo,[8] respectively. It is also a little smaller than 0.1001 which is the calculated value when $\alpha = 1/137.0$. Since only one of the plates showed an appreciable

[3] W. F. Meggers and C. G. Peters, Nat. Bur. Stand. Bull. **14**, 697 (1918).
[4] W. V. Houston, Phys. Rev. **30**, 612 (1927).
[5] D. Bender, Phys. Rev. **54**, 179 (1938).
[6] F. Paschen, Ann. d. Physik **50**, 901 (1916). His later value obtained from the microphotometer curve, 0.098 (see F. Paschen, Ann. d. Physik **82**, 689 (1927)) is close to, but a little smaller than, our value.
[7] P. Kunze, Ann. d. Physik **79**, 610 (1926).
[8] W. Leo, Ann. d. Physik **81**, 757 (1926).

deviation from the value 0.1001, it must be concluded that there is no evidence for a departure from the theory which can be expressed as a change in scale of the whole pattern. Departures which produce a displacement of components which are of small intensity in this line are not, however, excluded.

The relative intensities are different for different plates and not in precise agreement with the theoretically calculated values, yet the deviations are not more than can be attributed to uncertainties in the conditions of excitations and to photometric errors. The too high intensities of the components g, a, b suggest the hypothesis that the $4p$ state is more populous than the others because of the absorption of radiation $1s-4p$. On the other hand, component h does not seem to be sufficiently strong for this to be correct. The unusually high intensities of components g, h on plate 134 are perhaps associated with the low pressure in the same way in which corresponding variations of relative intensity with pressure are observed in hydrogen.[9] That the intensity of f is always greater than that of d is in agreement with Paschen's measurement rather than with that of Leo, who found them equal, and is also in agreement with theory.

The wave-lengths of the two strongest components are smaller than the values obtained by Paschen, Leo and Houston. It is believed, however, that the present measurement is more accurate than the previous ones not only because of the accuracy which is usually attained by the interferometer, but also because of the careful consideration being taken in the correction for displacement of maxima by neighboring components.

The author wishes to express his deepest gratitude to Professor W. V. Houston for his suggestion of the problem, constant direction and helpful guidance throughout the course of the work. The author also wishes to thank Professor I. S. Bowen for his valuable suggestions.

[9] C. D. Shane and F. H. Spedding, Phys. Rev. **47**, 36 (1935).

The Infra-Red Spectrum and Molecular Constants of Carbon Monoxide

S. E. WHITCOMB AND R. T. LAGEMANN
Mendenhall Laboratory of Physics, Ohio State University, Columbus, Ohio

(Received November 28, 1938)

The fundamental and first overtone bands of carbon monoxide have been measured under high resolution and the lines in the positive and negative branches in both bands have been fitted to formulae of the form

$$\nu = a + bm + cm^2 + dm^3.$$

The molecular constants ν_0, I_0, B and C as defined by Colby depend directly on the constants a, b, c, d and have been determined from these measurements. Their values are

$$\nu_0 = 2168.48 \text{ cm}^{-1}, \quad I_0 = 1.429 \times 10^{-39} \text{ g cm}^2, \quad B = 1.38 \times 10^{-6}, \quad C = 6.202.$$

The constants used in electronic work, as defined by Jevons, have also been computed and are in close agreement with previous results.

THE vibration-rotation spectrum of carbon monoxide was originally investigated in this laboratory by Lowry,[1] who was able to obtain only the doublet structure of the fundamental band. More recently, however, the spectrum of CO has been remeasured by Snow and Rideal[2] who were able to resolve partially, at least, both the fundamental and harmonic bands. It has now been found possible to completely resolve this band system into its fine structure and to measure the frequency positions of the lines in both the fundamental and the harmonic. For these measurements a prism-grating spectrometer of a conventional design with a two-meter collimating mirror was available. Echelette gratings of 3600 and 4800 lines to the inch ruled by Wood were used in the first order. The carbon monoxide gas was prepared by passing formic acid vapor over phosphoric pentoxide and then passing the resulting carbon monoxide gas through a liquid-air trap. Glass cells fitted with polished rocksalt windows were used to contain the gas during the investigation. In the case of the fundamental the cell was seven cm long and for the harmonic the cell was 19 cm in length. They were filled to atmospheric pressure for measurement on both bands. In the region of the fundamental the slit widths were equivalent to 0.7 cm^{-1} and galvanometer deflection readings were taken every 0.6 cm^{-1}. In the region of the harmonic the slit widths were equivalent to

[1] E. F. Lowry, J. Opt. Soc. Am. **8**, 647 (1924).
[2] C. P. Snow and E. K. Rideal, Proc. Roy. Soc. **A125**, 462 (1929).

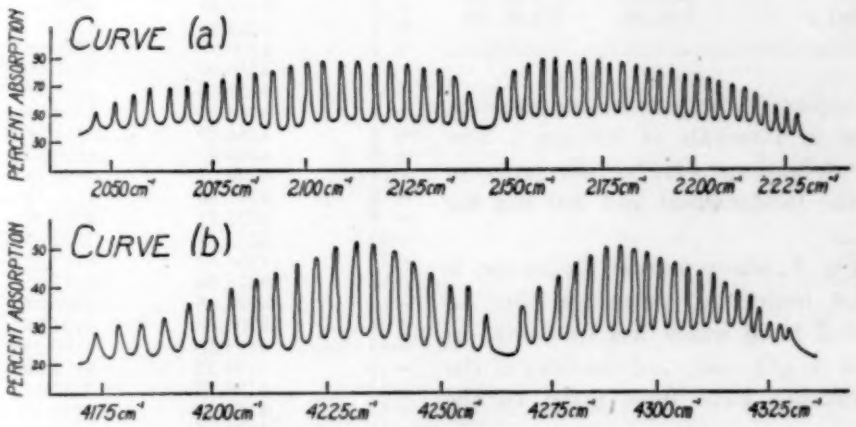

FIG. 1. Absorption plotted against frequency. Curve (a) fundamental band with center at 4.66μ. Curve (b) harmonic band with center at 2.34μ.

TABLE I. *The fundamental band.*

m	OBSERVED ν	COMPUTED ν	DIFFERENCE
+25	2228.16	2227.91	+0.25
+24	2225.31	2225.15	+ .16
+23	2222.33	2222.32	+ .01
+22	2219.48	2219.45	+ .03
+21	2216.45	2216.52	− .07
+20	2213.63	2213.54	+ .09
+19	2210.60	2210.52	+ .08
+18	2207.39	2207.44	− .05
+17	2204.19	2204.31	− .12
+16	2201.06	2201.15	− .09
+15	2197.66	2197.92	− .26
+14	2194.33	2194.67	− .34
+13	2191.15	2191.37	− .22
+12	2187.80	2188.01	− .21
+11	2184.36	2184.61	− .25
+10	2181.30	2181.17	+ .13
+ 9	2177.59	2177.68	− .09
+ 8	2174.17	2174.16	+ .01
+ 7	2170.67	2170.59	+ .08
+ 6	2166.88	2166.98	− .10
+ 5	2163.40	2163.32	+ .08
+ 4	2159.65	2159.63	+ .02
+ 3	2155.78	2155.90	− .12
+ 2	2152.07	2152.14	− .07
+ 1	2148.30	2148.32	− .02
− 1	2140.57	2140.60	− .03
− 2	2136.69	2136.68	+ .01
− 3	2132.86	2132.72	+ .14
− 4	2128.81	2128.73	+ .08
− 5	2124.66	2124.69	− .03
− 6	2120.66	2120.64	+ .02
− 7	2116.54	2116.55	− .01
− 8	2112.55	2112.42	+ .13
− 9	2108.30	2108.26	+ .04
−10	2103.99	2104.07	− .08
−11	2099.82	2099.85	− .03
−12	2095.63	2095.59	+ .04
−13	2091.28	2091.31	− .03
−14	2087.08	2086.99	+ .09
−15	2082.48	2082.66	− .18
−16	2078.32	2078.29	+ .03
−17	2073.90	2073.88	+ .02
−18	2069.50	2069.46	+ .04
−19	2065.07	2065.02	+ .05
−20	2060.70	2060.54	+ .16
−21	2056.46	2056.04	+ .42
−22	2051.80	2051.51	+ .29
−23	2047.26	2046.96	+ .30

1.2 cm^{-1} and values of the percent transmission were obtained at intervals of 0.9 cm^{-1}. The galvanometer deflections were of the order of 100 mm for the fundamental and 200 mm for the harmonic.

Curve (a) Fig. 1, where percent absorption is plotted against frequency, shows the lines of the fundamental band which has its center at 4.66μ. There is no Q branch and the lines of the P and R branches have been fitted to the formula

$$\nu' = 2144.48 \pm 3.865m - 0.01860m^2 \mp 0.0001m^3, \quad (1)$$

where m is the ordinal number of the line counted outward from the center. In Table I are given the observed frequencies of the lines in cm^{-1}, the frequencies as calculated from Eq. (1), and the differences between the observed and calculated values.

The harmonic band, with its center at 2.34μ, is shown in curve (b), Fig. 1. Here again it has been possible to fit the lines in both branches to a formula

$$\nu'' = 4264.96 \pm 3.862m - 0.0353m^2 \mp 0.00004m^3, \quad (2)$$

where m is the ordinal number of the line counted outward from the center. Table II gives the observed frequencies of the lines, the frequencies calculated from Eq. (2), and the

TABLE II. *The harmonic band.*

m	OBSERVED ν	COMPUTED ν	DIFFERENCE
+21	4330.10	4330.12	−0.02
+20	4327.86	4327.76	+ .10
+19	4325.69	4325.33	+ .36
+18	4322.99	4322.81	+ .18
+17	4320.28	4320.21	+ .07
+16	4317.57	4317.55	+ .02
+15	4314.81	4314.81	.00
+14	4311.96	4312.00	− .04
+13	4309.14	4309.11	+ .03
+12	4306.34	4306.15	+ .19
+11	4303.17	4303.12	+ .05
+10	4300.07	4300.01	+ .06
+ 9	4297.06	4296.83	+ .23
+ 8	4293.88	4293.58	+ .30
+ 7	4290.64	4290.25	+ .39
+ 6	4286.96	4286.85	+ .11
+ 5	4283.76	4283.38	+ .38
+ 4	4280.12	4279.85	+ .27
+ 3	4276.41	4276.23	+ 18
+ 2	4272.54	4272.54	.00
+ 1	4268.96	4268.78	+ .18
− 1	4260.95	4261.06	− .11
− 2	4256.90	4257.10	− .20
− 3	4252.86	4253.05	− .19
− 4	4248.93	4248.95	− .02
− 5	4244.79	4244.78	+ .01
− 6	4240.22	4240.53	− .31
− 7	4236.07	4236.21	− .14
− 8	4231.80	4231.82	− .02
− 9	4227.21	4227.37	− .16
−10	4222.68	4222.85	− .17
−11	4218.32	4218.26	+ .06
−12	4213.66	4213.61	+ .05
−13	4209.05	4208.87	+ .18
−14	4204.09	4204.08	+ .01
−15	4199.58	4199.23	+ .35
−16	4194.32	4194.29	+ .03
−17	4189.20	4189.31	− .11
−18	4184.28	4184.23	+ .05
−19	4179.14	4179.11	+ .03
−20	4173.92	4173.92	.00

differences between the observed and calculated values.

Since the last two constants in each of the Eqs. (1) and (2) are not known very accurately, the first two numerical constants in each case have been used to determine the molecular constants ν_0, I_0, r_0, B and C as defined by Colby.[3] The numerical values of these constants are

$\nu_0 = 2168.48\ \text{cm}^{-1}$, $I_0 = 1.429 \times 10^{-39}\ \text{g cm}^2$,
$B = 1.38 \times 10^{-6}$, $C = 6.202$.
$r_0 = 1.124 \times 10^{-8}\ \text{cm}$,

For convenience the molecular constants as defined by Jevons[4] have also been computed and are given below.

$\omega_e = 2168.48\ \text{cm}^{-1}$, $B_e = 1.9543$,
$x_e = 5.534 \times 10^{-3}$, $B_0 = 1.9453$,
$x_e\omega_e = 12.00\ \text{cm}^{-1}$, $B_1 = 1.9232$,
$I_0 = 1.425 \times 10^{-39}\ \text{g cm}^2$, $B_2 = 1.9134$,
$r_0 = 1.122 \times 10^{-8}\ \text{cm}$, $D_e = -6.349 \times 10^{-6}\ \text{cm}^{-1}$.

The values of I_0 and ν_0 as here determined are seen to be in good agreement within the approximation used in the two definitions of the constants. As would be expected, the values of B_e decrease with increasing vibrational quantum number. In Table III a comparison is made with the previously determined values of the moment of inertia and the internuclear distance. The value of I_0 as here determined is seen to be less than previous values from infra-red work, but is in very close agreement with electronic band results. This new value is probably more nearly correct because of the excellent resolution obtained and because of the more precise energy formula used.

TABLE III. *Comparison of the values of the moment of inertia and the internuclear distance here determined with values previously obtained.*

	I_0(g cm^2)	r_0(cm)
Average* of classical doublet separation	1.48×10^{-39}	1.15×10^{-8}
Asundi** from electronic bands	1.38×10^{-39}	1.104×10^{-8}
Gerö, Herzberg and Schmid† from electronic bands	1.438×10^{-39}	1.128×10^{-8}
Snow and Rideal‡ from fundamental fine structure	1.50×10^{-39}	1.15×10^{-8}
Present determination from fine structure of both bands	1.429×10^{-39}	1.124×10^{-8}

* E. F. Lowry, reference 1; W. Burmeister, Verh. d. D. Phys. Ges. **15**, 589 (1913); C. Schaefer and B. Phillips, Zeits. f. Physik **36**, 399 (1926).
** R. K. Asundi, Proc. Roy. Soc. **A124**, 277 (1929).
† L. Gerö, G. Herzberg and R. Schmid, Phys. Rev. **52**, 467 (1937).
‡ C. P. Snow and E. K. Rideal, Proc. Roy. Soc. **A125**, 462 (1929).

In conclusion we wish to acknowledge a grant from the National Research Council which aided in securing the gratings used and to express our appreciation to Dr. H. H. Nielsen for valuable help in both the experimental work and the analysis.

[3] W. F. Colby, Phys. Rev. **34**, 53 (1929).
[4] W. Jevons, *Report on Band Spectra of Diatomic Molecules* (University Press, Cambridge), p. 39.

Continuous Spectra of H_2 and D_2

HUBERT M. JAMES, *Purdue University, Lafayette, Indiana*

AND

ALBERT SPRAGUE COOLIDGE, *Harvard University, Cambridge, Massachusetts*

(Received November 14, 1938)

A complete theoretical calculation has been made of the continuous spectra of H_2 and D_2 arising from transitions from the lower vibrational levels of the $1s\sigma 2s\sigma\,^3\Sigma_g$ state to the unstable $1s\sigma 2p\sigma\,^3\Sigma_u$ state. Use of the Franck-Condon approximation has been avoided by a direct computation of the electric moment of the electronic transition, as a function of nuclear separation; this quantity is found to decrease rapidly with increasing nuclear separation. Spectra are computed for transitions from each of the vibrational levels separately, and absolute mean lives are determined for the various levels. Relative probabilities of excitation from the ground state of the molecule by electron impact are estimated, and the intensity in the spectrum due to excitation by electron impact is computed for a range of energies of the electrons. The Franck-Condon approximation is found to be more satisfactory than was indicated by a previous investigation. There is sharp disagreement of the results with the observations of Smith. This apparently arises from errors in Smith's intensity standard, and emphasizes the need for a more satisfactory intensity standard in the ultraviolet. Agreement with the results of Finkelnberg and Weizel is obtained, but its significance is weakened by uncertainties in the experimental conditions.

INTRODUCTION

IN A recent paper[1] on the Franck-Condon principle we have given a detailed analysis of the problem of calculating the energy distribution in the continuous spectrum of H_2 produced by transitions from the stable $1s\sigma 2s\sigma\,^3\Sigma_g$ to the repulsive $1s\sigma 2p\sigma\,^3\Sigma_u$ state. We there presented a tentative solution based on the Franck-Condon principle, interpreted as the assumption that the electric moment of the electronic transition ($D_{ee'}(r)$ as defined by Eq. (6I)) is practically independent of the nuclear separation r over the range involved. Our results showed marked disagreement with the experimental results of Smith[2] and of Finkelnberg and Weizel,[3] and we were led to conclude that the Franck-Condon assumption is not permissible in this case, but that $D_{ee'}(r)$ must decrease strongly with increasing r.

By use of the potential curves and electronic wave functions which we have since obtained for the states involved,[4] we have been able to carry out a complete theoretical treatment of this continuous spectrum as it would be produced under certain idealized conditions. The principal improvement in the present computations arises from use of computed values of $D_{ee'}(r)$ instead of the Franck-Condon assumption; an additional but less essential improvement arises from our more precise location of the potential curve of the repulsive state. We here present the results of computations on both H_2 and D_2, together with a further discussion of the Franck-Condon assumption and the other approximations usual in computations of intensities of continuous spectra.

ELECTRIC MOMENT OF THE ELECTRONIC TRANSITION

In computing the spectral distribution of energy the first quantity to be calculated is (repeating Eq. (6I))

$$D_{ee'}(r)=\left|\int\cdots\int d\tau_1 d\tau_2 \mathbf{D}(\tau_1,\tau_2,\varphi,\theta)\times F_e(r;\tau_1,\tau_2)F_{e'}(r;\tau_1,\tau_2)\right|.$$

Here F_e and F_e' are the electronic wave functions; in our usual notation

$$F_e=\sum_{mnjkp} C_{mnjkp}[mnjkp];$$

$$F_{e'}=\sum_{m'n'j'k'p'} C'_{m'n'j'k'p'}[m'n'j'k'p'],$$

[1] A. S. Coolidge, H. M. James and R. D. Present, J. Chem. Phys. **4**, 193 (1936). We use the notation of this paper, and refer to it as I in references to figures and equations.

[2] N. D. Smith, Phys. Rev. **49**, 345 (1936).

[3] W. Finkelnberg and W. Weizel, Zeits. f. Physik **68**, 577 (1931).

[4] A. S. Coolidge and H. M. James, J. Chem. Phys. **6**, 730 (1938).

$$[mnjkp]=\frac{1}{2\pi}\{e^{-\delta_1\lambda_1-\delta_2\lambda_2}\lambda_1^m\lambda_2^n\mu_1^j\mu_2^k - e^{-\delta_2\lambda_1-\delta_1\lambda_2}\lambda_1^n\lambda_2^m\mu_1^k\mu_2^j\}\rho^p.$$

The vector **D** is the variable part of the electric moment, but because of the $\sum$ symmetry of both states we need consider only the component along the nuclear axis, which in elliptical coordinates becomes $-er/2(\lambda_1\mu_1+\lambda_2\mu_2)$. We have, then,

$$D_{ee'}(r)=er/2\left|\sum_{mnjkp}\sum_{m'n'j'k'p'}C_{mnjkp}C'_{m'n'j'k'p'} \times\int\cdots\int d\tau_1 d\tau_2[mnjkp](\lambda_1\mu_1+\lambda_2\mu_2)[m'n'j'k'p']\right|.$$

From the special form of the functions, it is readily seen that

$$[mnjkp](\lambda_1\mu_1+\lambda_2\mu_2) =[m+1, n, j+1, k, p]+[m, n+1, j, k+1, p].$$

All the integrals needed for the computation are accordingly of the familiar[5] type

$$\int\cdots\int d\tau_1 d\tau_2[mnjkp][m'n'j'k'p'].$$

Using the wave functions of reference 4, we thus obtain the following values for $D_{ee'}(r)$, expressed in units of electronic charge times Bohr radius:

$r=$	1.3	1.5	1.7	1.87	2.0	2.1	2.3	2.5	2.7	2.9
$D_{ee'}(r)=$	1.719	1.503	1.289	1.128	1.012	0.975	0.845	0.742	0.673	0.611.

This quantity, determined by the electronic wave functions, is the same for H_2 and D_2, to the approximation of separated nuclear and electronic motions which we employ.

As an indication of the reliability of these calculations, we may note that when smooth curves are drawn through the first five and the last five points, respectively, and extrapolated, they fail to join by about 0.025. The two sets of points were computed entirely independently, with different series, and the errors of each set of wave functions are at their maximum in the region of joining (as shown by the corresponding energy values). Further, some of the errors are doubtless of opposite character here, since in the one case the exponential parameter is known to be too small, and in the other too large. The errors in the several computations are thus not likely to be larger than the discrepancy at the point of joining—that is, a very few percent.

[5] H. M. James and A. S. Coolidge, J. Chem. Phys. **1**, 825 (1933).

Potential Curves and Vibrational Wave Functions

As the potential curve for the $^3\Sigma_g$ state we have used an empirical curve of the form suggested by Hylleraas.[6] This is the curve 9 of a previous paper[7] in which we have discussed the problem of determining potential curves from empirical data on vibrational and rotational levels; a summary of its properties will be found there. (This work was carried out before we became aware of the magnitude of the errors in the Hylleraas energy formula, with the aid of which the curve had been constructed.) As the potential curve of the repulsive $^3\Sigma_u$ state we have used the computed curve of reference 4, corrected for convergence, but without the completely negligible correction for the finite mass of the nuclei.

Vibrational wave functions for the $^3\Sigma_g$ state were obtained with the aid of the Massachusetts Institute of Technology differential analyzer, as described in I;[8] the computations for H_2 and D_2 differed only by a change in gear ratios corresponding to the change of the effective mass of the vibrator. As a check on the results we had available analytical wave functions for a Pöschl-Teller curve closely approximating curve 8 of reference 7. The locations of the nodes and maxima of the mechanical and analytic wave functions, and the relative magnitudes of the maxima, were found to agree to within the limit of error in the machine operation. This showed that the machine was giving reliable results and that we could ignore the effects of small errors in the potential curve (such as were later found to exist in curve 9).

[6] E. A. Hylleraas, Zeits. f. Physik **96**, 643 (1935).

[7] A. S. Coolidge, H. M. James and E. L. Vernon, Phys. Rev. **54**, 726 (1938).

[8] We may note that in I we found, by use of a very accurate potential curve, a value of 0.170 ev for the zero-point vibrational energy in H_2, while the separations of all energy levels came out in essential agreement with observation. The value 0.170 ev is definitely too high; in the present work we find instead 0.162 ev. We do not understand the origin of this error in the previous work, but believe it can have had no effect on the other computations.

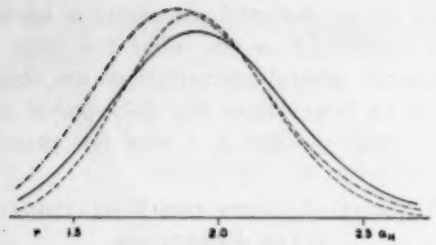

FIG. 1. Wave functions for $V=0$ of H_2 (——) and D_2 (- - - -), comparably normalized. Also product of H_2 function multiplied by $D_{ee'}(r)$ (-·-·-).

As the final stage in the computation of the integral (Cf. Eq. (9I))

$$D_{ev;\ e'E'}=\int dr R_{ev}(r)R_{e'E'}(r)D_{ee'}(r),$$

we determined the vibrational functions for the repulsive curve, $R_{e'E'}$, and simultaneously evaluated the integrals of their products with $R_{ev}(r)D_{ee'}(r)$, introduced into the differential analyzer as the function S of Fig. 3I. The technique of this work was the same as that of our previous paper, and requires no further discussion.

In Fig. 1 we show for comparison the vibrational functions of H_2 and D_2, for $v=0$,[9] and also the former function multiplied by $D_{ee'}(r)$.

[9] The other wave functions for H_2 are, within the accuracy of plotting, the same as those portrayed in Fig. 4I. For comparable normalization, these curves should be divided, not multiplied, by the factors given on page 202 I.

MEAN LIFE OF $^3\Sigma_g$ LEVELS

Relative spectral intensity distributions for transitions from each low vibrational level of the $^3\Sigma_g$ state are given immediately by Eq. (9I), and are shown in Fig. 2 for H_2 and in Fig. 3 for D_2. Within each figure the spectra are given for the same population in the several upper levels, but there is no special relation between the vertical scales in the figures for H_2 and for D_2. (Cf. Figs. 8I, 9I.)

Knowledge of the electric moment now permits a calculation of absolute intensities and of the mean life of a molecule in each vibrational level of the $^3\Sigma_g$ state. We have for the energy radiated per second within a wave-length region $d\lambda$, caused by transitions from the vth vibrational level[10]

$$A_\lambda(v)d\lambda=[8(2\pi)^4c^2(2\mu)^{\frac{1}{2}}/3(E')^{\frac{1}{2}}\lambda^6]D^2_{ev;\ e'E'}d\lambda.$$

The value of $A_\lambda(v)$ is independent of the rotational quantum number K except for a slight dependence of $D_{ev;\ e'E'}$ on K, which we neglect in accordance with the discussion in I. The probability of the transitions responsible for this radiation is per second and per unit range in wave-length, $\lambda A/hc$, and the integral of this over

[10] Eq. (8I), corrected by a factor of 2. This correction applied also to Eq. (7I).

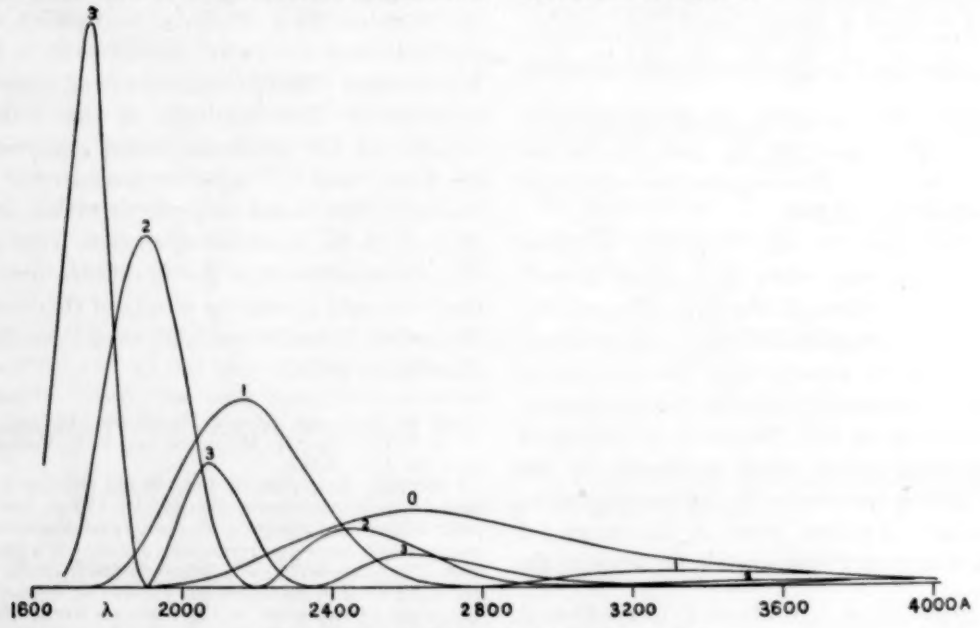

FIG. 2. I_λ for first four vibrational levels of H_2.

all possible wave-lengths is the reciprocal of the mean life of the vibrational state, τ_v:

$$1/\tau_v=[128\pi^4 c(2\mu)^{\frac{1}{2}}/3h]$$
$$\times\int_0^\infty d\lambda[D_{ev;\,e'E'}(\lambda)]^2/\lambda^5(E'(\lambda))^{\frac{1}{2}}.$$

By graphical integration (for convenience λ^2 was used as the variable of integration) we obtain the mean lifetimes given in Table I.

TABLE I. *Mean lifetimes of molecules in various vibrational states.*

v	H_2	D_2
0	1.19×10^{-8} sec.	1.19×10^{-8} sec.
1	1.10×10^{-8}	1.12×10^{-8}
2	1.01×10^{-8}	1.05×10^{-8}
3	0.97×10^{-8}	1.02×10^{-8}
4		1.00×10^{-8}

APPROXIMATE METHODS

The calculations of our previous paper involved the approximation of replacing the true electric moment of the electronic transition, $D_{ee'}(r)$, by a constant (the Franck-Condon approximation) or a linear function of r. In addition, we considered the effects of various other simplifications, and found empirically that very good results could be obtained by method R (the reflection method of Condon[11] and of Winans and Stueckelberg[12]) in which the vibrational wave functions of the repulsive state are replaced by appropriately normalized δ functions at their classical turning points. We are now able to check these approximations against the complete calculation.

To determine the effect of the variation of $D_{ee'}(r)$ it will not be sufficient simply to compare the intensity distributions of the present with those of the previous paper, since the latter were computed with different potential curves, estimated to be upper and lower limits to the real potential curve, and indeed bearing this relation to our final curve wherever the differences are appreciable. For H_2, with $v=0$, we have estimated by several methods of interpolation the result of a F-C computation with the repulsive potential used in the present work. The result varies little with the method of interpolation, and the uncertainty in it is negligible for our purposes. Fig. 4 shows this F-C intensity distribution compared with that given by the complete computation; the F-C approximation produces a shift of the maximum I_λ toward short waves, by about 120A, together with some narrowing of the band.

Figure 4 also shows the errors introduced by use of method R, as compared to a calculation involving use of the exact form of the vibrational wave functions in the repulsive state. Whether or not one takes account of the factor $D_{ee'}(r)$, the agreement of the two methods is surprisingly good. It is clear that the full calculation may be regarded as a refinement upon method R which is unwarranted in any calculation subject to the

[11] E. U. Condon, Phys. Rev. **32**, 858 (1928).
[12] J. G. Winans and E. C. G. Stueckelberg, Proc. Nat. Acad. Sci. **14**, 867 (1928).

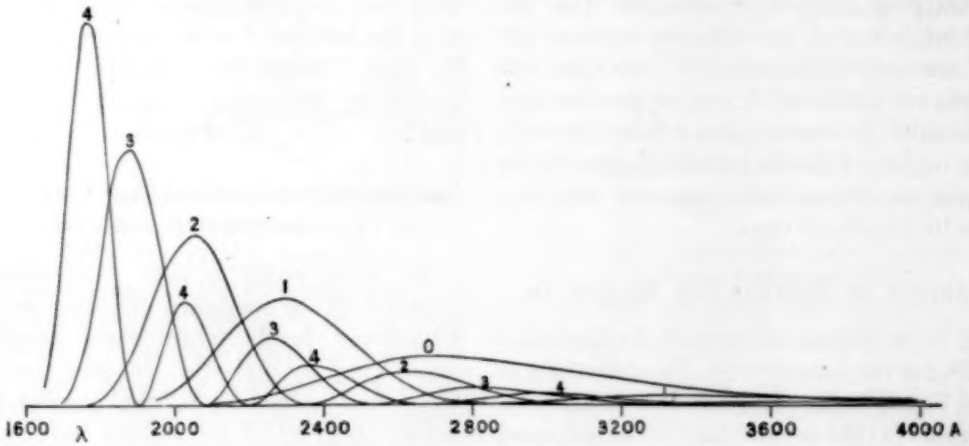

FIG. 3. I_λ for first five vibrational levels of D_2.

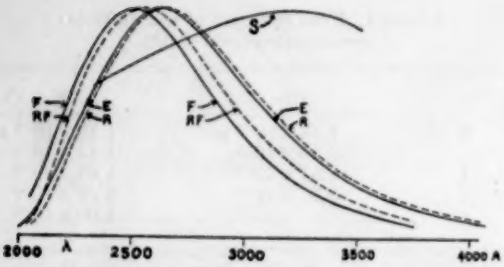

FIG. 4. I_λ for $v=0$ of H_2, by approximate methods. *E*, exact calculation. *F*, Franck-Condon method; *R*, reflection method including variable electric moment; *RF*, same ignoring electric moment; *S*, Smith's results.

much larger errors introduced by the Franck-Condon approximation.

In the case of D_2 the situation is similar. We have not made the full calculation involving only the F-C approximation, but we can estimate the error caused by neglect of $D_{ee'}(r)$ by using method *R* both with and without this factor. The resulting curves are shown in Fig. 5, together with that given by the complete theoretical treatment. As was to be expected, the error introduced by the F-C approximation is rather less than with H_2, the range of r important in the radiation process being the smaller range of the vibrational function of the stable state. (Cf. Fig. 1.)

Application of the ideas of method *R* to the consideration of the spectra caused by transitions from each of the higher vibrational levels shows at once that the intensity maxima corresponding to the loops of the vibrational functions become sharper as the loops becomes narrower, with increasing v. The F-C approximation thus produces smaller errors in the computed locations of the intensity maxima as v increases, but the ratios of intensities at the different maxima will become seriously distorted. For example, for $v=3$ in H_2 the values of $D_{ee'}(r)$ at the first and last maxima of the wave function have the ratio 1.78 to 1; neglect of this factor will exaggerate the short wave maximum with respect to the long wave one by a factor of three.

Comparison of Results for H_2 and D_2

It may be of interest to compare the spectra of H_2 and D_2 for the case of $v=0$. The difference, as shown in Fig. 6, is the resultant of several effects arising from: (a) the smaller breadth of the upper wave functions for D_2 (there being no essential displacement of the maximum), (b) the change in form of the lower vibrational function, (c) the difference in the energies of the upper states. The success of method *R*, which does not involve the lower wave functions, in treating both systems shows that the effect of (b) is very small. Application of this method also shows the effect of (c) to be small. The difference in the spectra thus arises principally from the difference in form of the discrete vibrational functions. The

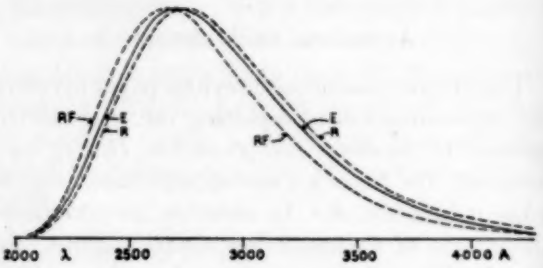

FIG. 5. I_λ for $v=0$ of D_2, by three methods explained under Fig. 4.

effect of this factor can be analyzed into two parts, of which the more obvious is a direct dependence of the breadth of the radiation band on the breadth of the vibrational function. This breadth of the function is inversely proportional to the fourth root of the effective mass of the molecular vibrator. This effect is completely masked, however, by the distortion caused by the λ^{-6} factor in I_λ, which strongly raises the curve on the short wave side. The difference in the spectra may be interpreted as caused principally by the fact that the lighter H nuclei are able to penetrate into the nonclassical region more readily than the heavier D nuclei, so that in the case of H_2 there is a greater probability that electron transitions will occur when the nuclei are far apart.

Dependence of Intensity on Velocity of the Exciting Electrons

We have made a new calculation of the intensity of the combined radiation from several vibrational levels when their population is maintained by inelastic collisions between electrons and molecules in the ground state. As before (Eq. (11I)) we assume that the rate of production of molecules in each vibrational state

is a linear function of the excess of the energy of the electrons over the minimum excitation energy, and that the constants of proportionality for the various levels are in turn proportional to the squares of the overlap integrals of the pertinent vibrational functions with that of the lowest level of the ground state. These constants of proportionality are given in Table II. They are expressed in arbitrary units for each molecule. It will be noted that with D_2 there is a more pronounced tendency than in the case of H_2 for transitions to occur principally to those upper levels which have inner turning-points nearly coincident with the potential minimum of the ground state, in accordance with the usual crude form of the Franck-Condon argument (see Fig. 11). This is to be expected from the more concentrated form of the wave functions.

For a given electronic energy E, the population of each vibrational level of the $^3\Sigma_g$ state should be proportional to the excitation probability as above calculated, multiplied by the mean life of that level. (The latter factor, which we find to vary by about 20 percent over the range of v considered, was treated as constant in I). From the relative populations thus deduced for each value of the electronic energy, and the radiation intensities for unit population, as given in Figs. 2

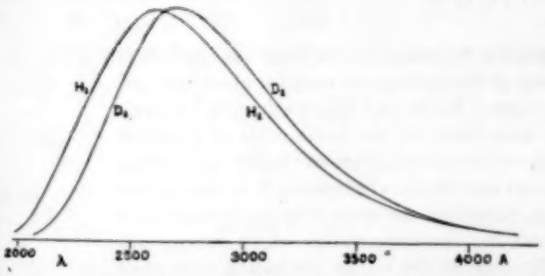

FIG. 6. I_λ for $v=0$ of H_2 and of D_2, for same population of excited state.

and 3, we have obtained the relations between intensity, wave-length and electron energy shown in Figs. 7 and 8. (Cf. Fig. 11I.) In these figures the solid lines are contours on the surface giving I_λ as it depends on E and λ, and show the exciting voltage necessary to produce radiation of a given I_λ at each wave-length. In order to make closer contact with experiment we have also indicated in Fig. 7 the exciting voltages needed to produce a given illumination of the plate of a typical quartz spectrograph, as it depends on λ. The values of I_λ required for constant illumination increase rapidly with decreasing λ because of the increasing spreading of the spectrum caused by variations in the refractive index of the prism and the focal length of the lens.

COMPARISONS WITH EXPERIMENT

On the basis of a comparison of the results of computations using the F-C approximation and the available experimental results, as detailed in I, we were led to conclude that inclusion in the computation of the factor $D_{v'}(r)$ would produce a large shift in the intensity maxima toward the red. The calculations presented in this paper show only a fraction of the expected shift, and it is clear that the F-C approximation is not as bad as we were led to believe.

On the other hand, there remains a very unsatisfactory discordance of the theoretical and experimental results. The results of Smith, supposed to give I_λ for radiation entirely from the state $v=0$ of H_2, are indicated in Fig. 4. It is difficult to believe that the difference between Smith's curve and ours is due entirely to the departure of Smith's carbon arc standard from the assumed black body behavior, but a careful analysis of the situation, along the lines of I, leaves us with no other interpretation to suggest. We wish to emphasize the urgent need for an improved intensity standard in this spectral region and for a repetition of Smith's work when this standard becomes available.

The results of Finkelnberg and Weizel are shown as crosses on Fig. 7. It will be observed that only one of them falls farther than 0.06 ev from a line of constant illumination which passes through the extreme points. If, therefore, the points which they give (obtained by visual estimate) correspond to equal blackening of their

TABLE II. *Excitation constants of molecules in various vibrational states.*

v	H_2	D_2
0	1.00	1.00
1	1.13	1.82
2	0.97	2.12
3	0.62	1.89
4		1.49

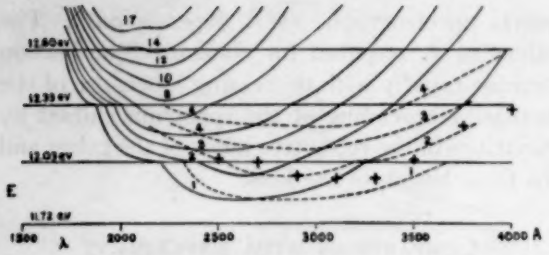

FIG. 7. Relations between I_λ, λ, and energy of exciting electrons E, for H_2. Lines of constant I_λ(——). Lines of constant illumination of plate in quartz spectrograph (- - - -). Data of Finkelnberg and Weizel (+ +). Intensities n arbitrary units.

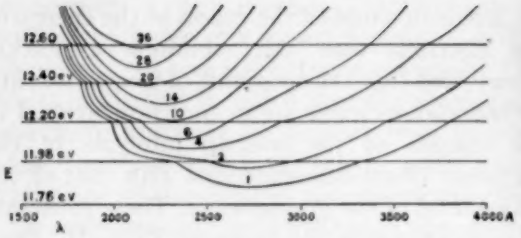

FIG. 8. Lines of constant I_λ for D_2. For explanation see Fig. 7.

plate, and this in turn corresponds to equal exposure, we may say that our calculations agree with their results to within the experimental error, estimated as 0.05 ev. Unfortunately there is no adequate reason to suppose that the assumed conditions are even approximately fulfilled. It seems more than ever desirable to obtain accurately controlled experimental results of this type also.

In conclusion, we wish to thank the Electrical Engineering Department of the Massachusetts Institute of Technology for the use of the differential analyzer. Also, one of us (H. M. J.) wishes to acknowledge gratefully a grant from the Society of Sigma Xi, which materially aided in the progress of this work.

JANUARY 15, 1939 PHYSICAL REVIEW VOLUME 55

Capture of Neutrons by Atoms in a Crystal*

WILLIS E. LAMB, JR.
Columbia University, New York, New York

(Received November 21, 1938)

The precise determination of the properties of nuclear resonance levels from the capture of slow neutrons is made difficult by the fact that most of the substances used for absorbers and detectors are in the solid state, so that the calculations of Bethe and Placzek for the influence of the Doppler effect are inapplicable, since these were based on the assumption of a perfect gas. In this paper, their calculations are generalized to include the effect of the lattice binding. Under the assumption that the crystal may be treated as a Debye continuum, it is shown that for sufficiently weak lattice binding, the absorption curve has the same form as it would in a gas, not at the temperature T of the crystal, however, but at a temperature which corresponds to the average energy per vibrational degree of freedom of the lattice (including zero-point energy). In cases of somewhat stronger lattice binding, the line form is found to be more complicated, and may even have a fine structure. Plots are given of the absorption line in several typical cases. An approximate formula for the cross section for self-indication is also derived.

ACCORDING to the theory of the compound nucleus proposed by Bohr and by Breit and Wigner,[1] the cross section for the capture of a slow neutron with an energy near to a resonance level of a nucleus at rest in free space is given by an equation of the form

$$\sigma=\frac{\Gamma^2}{4}\frac{\sigma_0}{(E-E_0-R)^2+\frac{1}{4}\Gamma^2}, \qquad (1)$$

where σ_0, the cross section at resonance, varies inversely with v, the velocity of the neutron in the rest system, E is the kinetic energy of the neutron, and E_0 is the energy that the neutron

* Publication assisted by the Ernest Kempton Adams Fund for Physical Research of Columbia University.

[1] N. Bohr, Nature **137**, 344 (1936); G. Breit and E. Wigner, Phys. Rev. **49**, 519 (1936).

would have at resonance if the atom were infinitely heavy so that the compound nucleus would take up no recoil energy. For atoms of finite mass, the recoil energy $R=(m/M)E$ must be included in the energy denominator.[2] (We assume that the mass M of the atom is much greater than the mass m of the neutron, and neglect terms of higher order in m/M.) Γ is the total half-value width of the resonance level, and is proportional to the rate of decay of the compound nucleus; in most cases this corresponds to the process of emission of a high energy gamma-ray.

Actually, of course, it never happens that one has to do with a free atom at rest. This somewhat complicates the determination of the properties of the resonance level from slow neutron data. The atoms in a gas may be treated as free, but at finite temperatures, there is a Maxwellian distribution of velocities, and Eq. (1) must be modified, as has been done by Bethe and Placzek[3, 4] for this case. It is here necessary to change the resonance energy denominator according to the relative velocity of the neutron and atom, and to average over the Maxwellian distribution of velocities of the gas atoms. The proportionality of the cross section to $1/v$ is thereby unaltered, as this factor arises just from the normalization of the incident neutron wave function to unit flux required by the definition of a cross section. The result of the averaging gives

$$\sigma=\sigma_0\psi(\xi, x), \tag{2}$$

where

$$x=(E-E_0-R)/\tfrac{1}{2}\Gamma, \quad \xi=\Gamma/\Delta \tag{3}$$

and

$$\Delta=2(RT)^{\frac{1}{2}} \tag{4}$$

is the "Doppler" width of the level.[5] The function

$$\psi(\xi, x)=\frac{\xi}{2\pi^{\frac{1}{2}}}\int_{-\infty}^{\infty}dy\frac{e^{-\frac{1}{4}\xi^2(x-y)^2}}{1+y^2} \tag{5}$$

becomes simple in the following limiting cases:

(a) $\quad x\gg 1/\xi^2, \quad \psi\to 1/(1+x^2),$

i.e., far enough from resonance, the line has its normal form.

(b) $\quad \xi\gg 1, \quad \psi\to 1/(1+x^2),$

i.e., when the natural breadth is much larger than the Doppler breadth, the line is again normal.

(c) $\quad \xi\ll 1, \quad x\ll 1/\xi^2, \quad \psi\to\tfrac{1}{2}\pi^{\frac{1}{2}}\xi e^{-\frac{1}{4}\xi^2x^2},$

i.e., when the natural width is small compared to the Doppler width, the absorption line has an effective width strongly dependent on the temperature.

The total activation induced in a thin detector by a beam of neutrons distributed smoothly in energy is proportional to the area under the absorption curve

$$\int dE\sigma_0\psi(\xi, x)=\tfrac{1}{2}\pi\Gamma\sigma_0, \tag{6}$$

independently of the temperature of the gas. Another quantity of experimental interest is σ_s, the cross section for self-indication[6]

$$\sigma_s=\int\sigma^2dE\Big/\int\sigma dE=\tfrac{1}{2}\sigma_0\psi(\xi\sqrt{2}, 0)$$

$$=(\tfrac{1}{2}\pi)^{\frac{1}{2}}\xi e^{\frac{1}{4}\xi^2}[1-\Phi(\xi/\sqrt{2})], \tag{7}$$

where Φ is the Gaussian error function.

The above results are valid, however, only for free atoms. Most of the experiments, of course, have been performed with solid absorbers and detectors in which the atoms are bound in a crystal lattice of some sort with a characteristic Debye temperature of the order of room temperature, and if the chemical binding is of importance, as we shall see is the case, it is clearly not permitted to apply the free atom theory of the Doppler broadening, as was done by Bethe,[4] to such cases as silver at ordinary temperatures.

We shall want, therefore, to calculate the shape of the absorption line for an atom which is bound in a crystal lattice. We do not expect that the chemical binding will cause any difference in

[2] As it is usually written, the capture cross section refers to the coordinate system in which the compound nucleus is at rest, so that no energy of recoil appears in the denominator of Eq. (1).

[3] H. Bethe and G. Placzek, Phys. Rev. **51**, 462 (1937).

[4] H. Bethe, Rev. Mod. Phys. **9**, 140 (1937).

[5] We will measure temperatures in energy units, taking the Boltzmann constant to be unity. The results quoted here were derived on the assumption that the Doppler width of the level is much less than the energy E_0 at resonance of the neutron. This condition is satisfied in all cases of practical interest, and we shall have occasion to assume it in our calculations also.

[6] See reference 4, Eq. (520).

the $1/v$ variation of the capture cross section. This has been shown analytically for the case of capture by bound protons,[7] but the result is much more generally valid, following in every case just from the normalization of the neutron wave function. The calculation will be made without detailed assumptions about the crystal model, but in using the final result, for simplicity, we will treat the crystal as a Debye continuum, and hence the results will not admit of an exact application to experimental cases. Nevertheless, the general features of the dependence of the absorption line on the characteristics of the lattice and on the temperature may be expected to be fairly independent of the detailed model. For just as in the theory of specific heat, there are several limiting cases in which the results may not depend on the model of the lattice assumed, so that any fairly smooth interpolation should approximate the rigorous result fairly closely. For example, let us consider a crystal lattice at the temperature absolute zero. If the lattice binding is sufficiently strong (as defined below), the absorption line will be normal in form, but centered about $E=E_0$, while for very weak binding, as for instance might be the case with a different substance containing the atom in question, the absorption line will again be normal in form, but centered about an energy $E=E_0+R$. Since in practice, this shift R is often of the order of Γ, the half-width of the absorption line, this change in the curve can be experimentally important, even though the recoil energy is numerically quite small. It might thus be possible to detect the effect of the chemical binding, especially at low temperatures, by use of different crystals, containing in common an element with a slow neutron resonance capture level, but in which the remaining elements do not appreciably capture or scatter slow neutrons of the resonance energy.

In the intermediate cases, the shape of the absorption line is in general much more complicated. However, in the case of weak binding, as defined below, it will be possible to treat the bound atoms as if they were in a gas, not however with a temperature T, but at a larger temperature corresponding to the average energy per vibrational degree of freedom (including zero-point energy) of the crystal.

We must now ask for the probability $W(\{\beta_s\};\{\alpha_s\})$ for the capture of a neutron of momentum $\mathbf{p}$ by a definite lattice atom L of nuclear type A to form a nucleus B with emission of a gamma-ray of wave vector $\mathbf{k}$ when the crystal undergoes a transition from a state $\{\alpha_s\}$ to a state $\{\beta_s\}$. Here the set of numbers denoted by $\{\alpha_s\}$ gives the numbers α_s of quanta (phonons) in the various modes s of oscillation in the lattice. We must consider that the final state is reached through an intermediate state in which there is neither neutron nor gamma-ray, but a compound nucleus[8] C with the lattice in a state $\{n_s\}$. The usual dispersion theory gives, apart from a trivial constant factor,

$$W(\{\beta_s\};\{\alpha_s\}) = \left|\sum_{n_s}\frac{(B\beta_s\mathbf{k}|H'|Cn_s)(Cn_s|H'|A\alpha_s\mathbf{p})}{E_0-E+E(n_s)-E(\alpha_s)+(i/2)\Gamma(n_s)}\right|^2, \quad (8)$$

where $\Gamma(n_s)$ is the total half-value width of the intermediate state (C, n_s).[9] Because of the short range of nuclear forces and hence the independence of the motion in the crystal of the center of gravity and the internal degrees of freedom of the nucleus, the matrix elements of the perturbation H' which appear in the numerator of (8) can be factored into

$$\begin{aligned}(Cn_s|H'|A\alpha_s\mathbf{p}) &= (n_s|\exp(i\mathbf{p}\cdot\mathbf{x}_L/\hbar)|\alpha_s)M_{\text{comp}},\\ (B\beta_s|H'|Cn_s) &= (\beta_s|\exp(-i\mathbf{k}\cdot\mathbf{x}_L/\hbar)|n_s)M_{\text{rad}}(\mathbf{k}),\end{aligned} \quad (9)$$

where $M_{\text{rad}}(k)$ and M_{comp} are the matrix elements for radiation and compound nucleus formation, respectively, for a free nucleus, and, for example,

$$(n_s|\exp(i\mathbf{p}\cdot\mathbf{x}_L/\hbar)|\alpha_s)$$

is the matrix element for transfer of a momentum

[7] W. E. Lamb, Jr., Phys. Rev. **51**, 187 (1937).

[8] We will ignore throughout the circumstance that the compound nucleus C is heavier than the atom A. This neglect is certainly valid if $m\ll M$, as is the case in practice, and may be seen to subject our results to a limitation on the effective width of the level analogous to that met by Bethe and Placzek (reference 5) for free atoms. As there, this limitation is of no importance experimentally.

[9] The curly brackets denoting a set of numbers will be dropped when it will not cause confusion.

$\mathbf{p}$ to the crystal through the Lth atom with excitation of the lattice from a state $\{\alpha_s\}$ to a state $\{n_s\}$. In practice, the lattice is in thermal equilibrium, therefore not in a definite state $\{\alpha_s\}$, and further, because of the high energy of the gamma-ray, the experiments will give only the total probability of capture, i.e., not

$$W(\{\beta_s\};\ \{\alpha_s\})$$

but
$$W(E)=\sum_{\beta_s}\sum_{\alpha_s} g(\{\alpha_s\})W(\{\beta_s\};\{\alpha_s\}), \quad (10)$$

where the sum over the initial states of the lattice is weighted according to the Boltzmann factor $g(\{\alpha_s\})$ for each state when the temperature of the lattice is T. Because of over-all conservation of energy, the magnitude of the wave vector $\mathbf{k}$ in (8) is a function of the final state of the lattice $\{\beta_s\}$. In all cases of importance, however, one may neglect a variation of $\mathbf{k}$ of the order of the zero-point energy of oscillation in the lattice, and perform the sum over the final states of the lattice by use of the completeness relations, finding

$$W(E)=|M_{\text{rad}}|^2|M_{\text{comp}}|^2\sum_{\alpha_s} g(\alpha_s) \times\sum_{n_s}\frac{|(n_s|\exp(i\mathbf{p}\cdot\mathbf{x}_L/\hbar)|\alpha_s)|^2}{[E-E_0-\sum_s(n_s-\alpha_s)\hbar\omega_s]^2+\frac{1}{4}(\Gamma(n_s))^2}, \quad (11)$$

where the energy of the lattice has been expressed in terms of the frequencies ω_s of the lattice oscillations. Thus one sees that the probability of gamma-ray emission is proportional just to the probability of formation of a compound nucleus C irrespective of the state of the lattice, and this despite the fact that very often a gamma-ray may be emitted in a time short compared to the periods of oscillation of the lattice, giving the atom a recoil energy of the order of a hundred volts. Eq. (11) will be much less complicated if one may neglect the dependence of $\Gamma(n_s)$ on the state $\{n_s\}$ of the lattice. This will be so except in the case, unimportant for our purposes, that the main contribution to Γ comes from the emission of slow neutrons, i.e., in case of a large elastic scattering cross section instead of a large capture cross section. If one were also to neglect the energy given to the lattice, the expression (11), from which we will now drop the factor $|M_{\text{comp}}M_{\text{rad}}|^2$, by use once more of the completeness relation would reduce just to

$$1/[(E-E_0)^2+\tfrac{1}{4}\Gamma^2],$$

since
$$\sum_{\alpha_s} g(\{\alpha_s\})=1.$$

We now turn to an evaluation of the matrix elements in Eq. (11). In terms of the wave functions[9]

$$\psi_{n_s}(\mathbf{x}_1,\cdots,\mathbf{x}_N)$$

of the crystal, which is assumed to be periodic in a large volume containing N atoms whose positions are denoted by $\mathbf{x}_1,\cdots,\mathbf{x}_N$, this matrix element is

$$(\{n_s\}|\exp(i\mathbf{p}\cdot\mathbf{x}_L/\hbar)|\{\alpha_s\}) =\int\cdots\int d\mathbf{x}_1 d\mathbf{x}_2\cdots d\mathbf{x}_N\psi_{n_s}^*(\mathbf{x}_1\mathbf{x}_2\cdots\mathbf{x}_N) \times\exp(i\mathbf{p}\cdot\mathbf{x}_L/\hbar)\psi_{\alpha_s}(\mathbf{x}_1\cdots\mathbf{x}_N). \quad (12)$$

We introduce normal coordinates for the crystal in the usual form:[10]

$$\mathbf{x}_G=\mathbf{x}_G^0+\mathbf{u}_G$$
$$\mathbf{u}_G=\frac{1}{N^{\frac{1}{2}}}\sum_{\mathbf{q}}\sum_j \mathbf{e}_{\mathbf{q}j}(A_{\mathbf{q}j}\exp(i\mathbf{q}\cdot\mathbf{x}_G^0/\hbar)+\text{conj.}), \quad (13)$$

where $\mathbf{x}_G^0$ is the equilibrium position of the Gth atom, $\mathbf{u}_G$ its displacement from equilibrium, $\mathbf{e}_{\mathbf{q}j}$ is the unit polarization vector for the wave characterized by the propagation vector $\mathbf{q}$ and polarization j. The spectrum of eigenvibrations is determined by the periodic boundary conditions, and it is cut off at an upper frequency limit such that the number of degrees of freedom agrees with the number $3N$ belonging to the N atoms in the fundamental volume of the lattice. The single index s will often be used to denote the pair of indices $(\mathbf{q}, j)$. In terms of the quantities

$$Q_s=A_s+A_s^*$$
$$P_s=M\dot{Q}_s=iM\omega_s(A_s-A_s^*), \quad (14)$$

where ω_s is the frequency belonging to the sth normal mode, the Hamiltonian of the crystal

[10] See for instance, A. Sommerfeld and H. Bethe, *Handbuch der Physik*, vol. 24/2, second edition (1933), p. 500.

takes the form appropriate for a system of linear harmonic oscillators with coordinates Q_s and momenta P_s

$$H=\sum_s H_s,$$
$$H_s=\tfrac{1}{2}M\omega_s^2Q_s^2+P_s^2/2M. \tag{15}$$

The eigenvalues of this Hamiltonian are

$$E_s=(n_s+\tfrac{1}{2})\hbar\omega_s; \quad n_s=0, 1, 2, \cdots$$

and the wave functions normalized in terms of

$$\xi_s=Q_s(h/2M\omega_s)^{-\frac{1}{2}}$$

are $\psi_{n_s}(Q_s)=(2\pi)^{-\frac{1}{4}}(n_s!)^{-\frac{1}{2}}e^{-\frac{1}{4}\xi_s^2}h_{n_s}(\xi_s)$,

where $h_{n_s}(\xi_s)$ is the n_sth Hermite polynomial. If, for convenience, we take the rest position of the capturing atom $\mathbf{x}_L^0=0$, as may be done without loss of generality, the matrix element (12) with the help of Eq. (13) takes the form

$$\Pi_s\int_{-\infty}^{\infty}d\xi_s\psi_{n_s}(\xi_s)\exp(i\mathbf{p}\cdot\mathbf{e}\xi_s/(2M\hbar\omega_sN)^{\frac{1}{2}})\psi_{\alpha_s}(\xi_s), \tag{16}$$

where the product is to be extended over all the normal modes. Integrals of the form

$$K(n_s, \alpha_s; q_s)=\int_{-\infty}^{\infty}d\xi\psi_{n_s}e^{iq_s\xi}\psi_{\alpha_s}(\xi_s)$$

are readily evaluated[11] by use of the generating formula for the Hermite polynomials. In our case,

$$q_s^2=\frac{(\mathbf{p}\cdot\mathbf{e}_s)^2}{2M\hbar\omega_sN}$$

and is arbitrarily small if we take the fundamental volume of the crystal large enough, so that only terms to the first order in q_s^2 need be kept in $K(n_s, \alpha_s; q_s)$, as will be seen more clearly below. Then there are three possibilities:

$$|K(\alpha_s, \alpha_s; q_s)|^2=(1-2\alpha_sq_s^2)e^{-q_s^2}, \tag{17a}$$
$$|K(\alpha_s+1, \alpha_s; q_s)|^2=(\alpha_s+1)q_s^2e^{-q_s^2}, \tag{17b}$$
$$|K(\alpha_s-1, \alpha_s; q_s)|^2=\alpha_sq_s^2e^{-q_s^2}, \tag{17c}$$

as all the other K's are of higher order. The q_s^2 will enter the final result only linearly in sums like

$$\sum_s q_s^2=R/\theta,$$

where θ is the Debye temperature of the substance. Any sums of the form $\sum_s q_s^4$, etc. would vanish as the transition to the continuum is made, which provides a justification for neglect of the higher powers of the q_s^2 in Eqs. (17).

Consider now the expression

$$W(\alpha_s)=\sum_{n_s}\frac{\Pi_s|K(n_s, \alpha_s; q_s)|^2}{[E-E_0-\sum_s(n_s-\alpha_s)\hbar\omega_s]^2+\frac{1}{4}\Gamma^2}. \tag{18}$$

This is made difficult to evaluate only by the presence in the denominator of the term $\sum_s(n_s-\alpha_s)\hbar\omega_s$. This suggests that it will be convenient to group together the terms in the expression for which this quantity has the same value. One may accomplish this most easily by the introduction of a delta-function, writing (18) as

$$\int_{-\infty}^{\infty}d\rho\,\delta(\rho-\sum_s(n_s-\alpha_s)\hbar\omega_s)\times\sum_{n_s}\frac{\Pi_s|K(\ )|^2}{(E-E_0-\rho)^2+\frac{1}{4}\Gamma^2}, \tag{19}$$

where for the delta-function, use is made of the usual representation

$$\delta(x)=\frac{1}{2\pi}\int_{-\infty}^{\infty}d\mu e^{i\mu x}. \tag{20}$$

Thus one finds

$$W(\alpha_s)=\frac{1}{2\pi}\int_{-\infty}^{\infty}d\rho\int_{-\infty}^{\infty}d\mu\frac{e^{i\mu\rho}}{(E-E_0-\rho)^2+\frac{1}{4}\Gamma^2}\times\sum_{n_s}\prod_s\{|K(n_s, \alpha_s; q_s)|^2\times\exp(-i\mu(n_s-\alpha_s)\hbar\omega_s)\}. \tag{21}$$

From Eqs. (17), one finds

$$I_s=\sum_{n_s}|K(n_s, \alpha_s; q_s)|^2\exp-i\mu(n_s-\alpha_s)\hbar\omega_s$$
$$=e^{-q_s^2}\{1+q_s^2[-2\alpha_s+(\alpha_s+1)e^{-i\mu\hbar\omega_s}+\alpha_se^{i\mu\hbar\omega_s}]\}. \tag{22}$$

[11] F. Bloch and A. Nordsieck, Phys. Rev. **52**, 54 (1937).

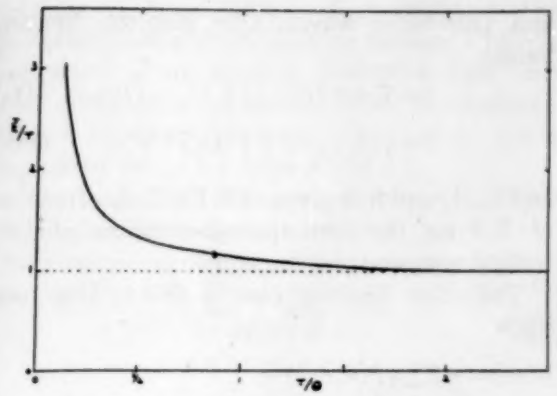

FIG. 1. Plot of the ratio of "effective temperature" and real temperature of a crystal as a function of the real temperature measured in units of the Debye temperature of the substance.

At this point it is most convenient to carry out the average over the values of the initial quantum numbers α_s, since now each α_s appears at most linearly. The result of the averaging is that each α_s above is replaced by its average value $\bar{\alpha}_s$ at thermal equilibrium, where

$$\bar{\alpha}_s=\frac{1}{e^{\hbar\omega_s/kT}-1}. \tag{23}$$

The product over the various oscillators s is then of the form

$$\prod_s(1+\lambda_s q_s^2)=1+\sum_s\lambda_s q_s^2 + \sum\sum_{s<r}\lambda_s\lambda_r q_s^2 q_r^2+\cdots \tag{24}$$

and if one remembers the smallness of the q_s^2, the series may be summed to give exp $(\sum_s\lambda_s q_s^2)$, so that

$$I=\prod_s I_s=\exp\sum_s q_s^2\{(\bar{\alpha}_s+1)e^{-i\mu\hbar\omega_s} + \bar{\alpha}_s e^{i\mu\hbar\omega_s}-2\bar{\alpha}_s\}. \tag{25}$$

Thus one has

$$W(E)=\frac{1}{2\pi}\int_{-\infty}^{\infty}d\rho\int_{-\infty}^{\infty}d\mu\frac{e^{i\mu\rho+g(\mu)}}{(E-E_0-\rho)^2+\frac{1}{4}\Gamma^2}. \tag{26}$$

where the function $g(\mu)$ is given by

$$g(\mu)=\sum_s q_s^2\{(\bar{\alpha}_s+1)e^{-i\mu\hbar\omega_s} + \bar{\alpha}_s e^{i\mu\hbar\omega_s}-1-2\bar{\alpha}_s\}. \tag{27}$$

The integral over ρ in (26) may be done at once by residue formation, and one has the generally valid final result

$$W(E)=2/\Gamma\ \text{Real}\int_0^{\infty}d\mu \times\exp\left[i\mu(E-E_0+i\Gamma/2)+g(\mu)\right]. \tag{28}$$

Naturally, it would be most difficult to evaluate $W(E)$ exactly. One may however easily obtain simple expressions which are valid in the various limiting cases. The function $g(\mu)$ is the cause of the complication, and it is possible to evaluate the integral (28) analytically only in cases where the values of μ given by $\mu\theta\sim1$ do not play a dominant role. For $\mu\theta\ll1$, one may expand in powers of μ and obtain

$$g(\mu)=-i\mu\sum_s q_s^2\hbar\omega_s - \mu^2\sum_s q_s^2(\bar{\alpha}_s+\tfrac{1}{2})(\hbar\omega_s)^2+\cdots. \tag{29}$$

The sums may be evaluated under the assumption of an isotropic crystal, i.e., the velocity of a wave is assumed to be independent of its direction of propagation, although not necessarily of its polarization; and one finds

$$g(\mu)=-i\mu R-\mu^2 R\bar{\epsilon}, \tag{30}$$

where R is again the recoil energy and $\bar{\epsilon}$ the average energy per vibrational degree of freedom of the crystal (including zero point energy). If the condition

$$\tfrac{1}{2}\Gamma+(R\bar{\epsilon})^{\frac{1}{2}}\gg\theta \quad (\text{"weak binding"}) \tag{31}$$

is met, only small values of μ in $g(\mu)$ in the integral (28) need be considered, and one finds

$$W(E)=\frac{2}{\Gamma}\int_0^{\infty}d\mu\cos\mu(E-E_0-R) \times\exp\left(-\tfrac{1}{2}\Gamma\mu-\mu^2R\bar{\epsilon}\right) =\frac{4}{\Gamma^2}\int_0^{\infty}dy\cos yx\exp\left(-y-y^2/\xi^2\right) \equiv(4/\Gamma^2)\psi(\xi,x), \tag{32}$$

where $\psi(\xi,x)$,[12] x, and ξ are as defined by Eqs.

[12] Equation (32) gives Reiche's form of the ψ-function. See Born, *Optik* (1933), p. 482.

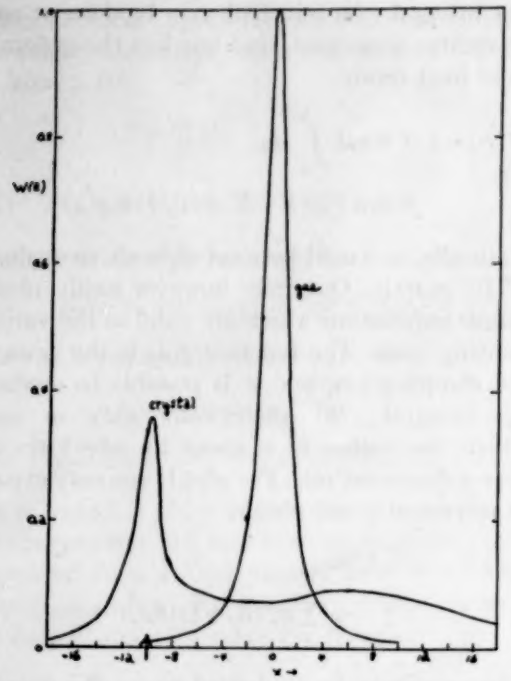

FIG. 2. Plot of the neutron resonance absorption curve in cold solid silver for an assumed value of Γ equal to $\theta/4$. The curve one would obtain with free atoms is shown for comparison. The abscissa measures the distance from resonance in units of $\frac{1}{2}\Gamma$. If the lattice binding were very strong, the curve for the crystal would have the same form for the gas, except that it would be centered about the point shown by the arrow.

(5) and (3), but now with an effective Doppler width

$$\Delta=2(R\bar{\epsilon})^{\frac{1}{2}}, \tag{33}$$

which involves $\bar{\epsilon}$ instead of T. Thus we see that provided only the condition $\Delta+\Gamma\gg 2\theta$ is met, the atoms in a crystal at a temperature T give the same absorption line as they would in a gas at a temperature $\bar{\epsilon}$ equal to the average energy per vibrational degree of freedom of the crystal. This quantity is well known from the theory of specific heats

$$\bar{\epsilon}=\tfrac{1}{3}(\bar{\epsilon}_l+2\bar{\epsilon}_t), \tag{34}$$

where

$$\bar{\epsilon}_j(T)=3\left(\frac{T}{\theta}\right)^3 T\int_0^{\theta_j/T} dt\, t^3\left(\frac{1}{e^t-1}+\tfrac{1}{2}\right), \tag{34j}$$

where the indices l and t refer to the longitudinal and transverse waves. One has the limiting values

$$\bar{\epsilon}=T+\theta\cdot O(\theta/T) \qquad T\gg\theta \tag{34a}$$

$$\bar{\epsilon}=\tfrac{1}{3}(\theta_l+2\theta_t)+T\cdot O(T^3/\theta^3). \tag{34b}$$

In Fig. 1, a plot is given of $\bar{\epsilon}(T)/T$ as a function of T/θ for the case that the various characteristic temperatures are equal.

The other limiting case is $\mu\theta\gg 1$. Here one finds

$$g(\infty)=-2\sum_s q_s^2(\bar{a}_s+\tfrac{1}{2})= -\tfrac{1}{3}[G(T/\theta_l)+2G(T/\theta_t)], \tag{35}$$

where

$$G(x)=\frac{2R}{T}x^3\int_0^{1/x} dt\, t\left(\frac{1}{e^t-1}+\tfrac{1}{2}\right) \tag{36}$$

with

$$G(x)=xR/T \quad x\ll 1, \tag{36a}$$

$$G(x)=\frac{2R}{T}x^2 \quad x\gg 1. \tag{36b}$$

For special ranges of values of $E-E_0$, one may obtain a good approximation to $W(E)$ by splitting the range of integration in Eq. (28) at $\mu\theta=1$, and in each range, using the appropriate expansion for $g(\mu)$. One finds in this way that for very strong binding of the atoms in the crystal ($\theta\to\infty$),

$$W(E)=\frac{1}{(E-E_0)^2+\frac{1}{4}\Gamma^2}, \tag{37}$$

i.e., the normal absorption line centered about $E=E_0$.

In general, however, a certain amount of numerical integration is required to find the shape of the line. To illustrate the possibility of using the general Eqs. (28) and (27) except in the two limiting cases of Eqs. (31) and (37), we give plots of a $2\frac{1}{2}$-volt resonance energy absorption line in a substance at a temperature much lower than the Debye temperature of $\theta=210°$K (Case of cold silver if one abstracts from the difference between θ_l and θ_t), for several assumed values of Γ. In each case, the curve for free atoms at the same temperature is also shown. One sees that for these cases of inter-

mediate binding, there is a rudimentary fine structure in the probability of capture which is suggestive of the neutron absorption *lines* that one would obtain from an atom harmonically bound, say in a molecule with energy levels separated by θ. (See Figs. 2 and 3.)

The area under the general absorption curve (28) may be evaluated immediately, again under the assumption of footnote (4), and one finds

$$\int_0^\infty dE W(E) = \frac{2}{\Gamma} \tag{38}$$

which, of course, agrees with the result for free atoms. The expression for the cross section for self-indication, which involves the integral of the square of $W(E)$ is more complicated, but may be reduced to

$$\sigma_s = \Gamma \int_0^\infty d\mu \exp\left[-\Gamma\mu + g(\mu) + g(-\mu)\right]. \tag{39}$$

In the case $\Gamma + \Delta \gg \theta$, this integral may again be evaluated by expanding $g(\mu)$ for small μ, and the cross section for self-indication has the value corresponding to that for a gas at an effective temperature $\tilde{\epsilon}$ instead of T. In the general case of arbitrary Γ, Δ and θ, however, one may derive an approximate formula by splitting the range of integration at $\mu\theta = 1$,

$$\sigma_s = (\tfrac{1}{2}\pi)^{\frac{1}{2}} \xi e^{\frac{1}{2}\xi^2} \left[\Phi\left(\frac{\xi}{\sqrt{2}} + \frac{\Delta}{\sqrt{2}\theta}\right) - \Phi\left(\frac{\xi}{\sqrt{2}}\right)\right] + \exp\left[2g(\infty) - \Gamma/\theta\right], \tag{40}$$

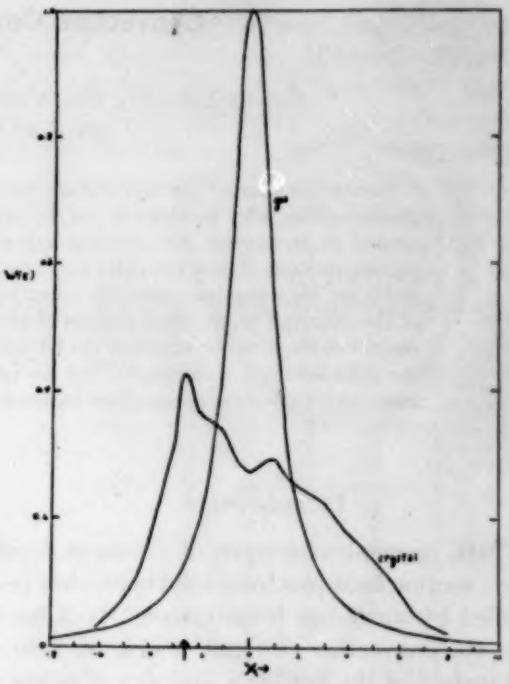

FIG. 3. Same as Fig. 2 except that the assumed value of Γ is now equal to θ. For values of $\Gamma \gtrsim 4\theta$, one is already in the domain of applicability of Eq. (32). The precise value of Γ for silver is not well known experimentally.

which may be used provided the result does not depend too much on the precise value of θ.

This research was largely carried out during the summer session at Stanford University, and I wish to thank Professor F. Bloch for his generous advice and hospitality. I am also greatly indebted to Professor G. Placzek and to Dr. A. Nordsieck for many valuable discussions and suggestions.

Convection Currents in Arcs in Air

C. G. SUITS
Research Laboratory, General Electric Company, Schenectady, New York
(Received December 5, 1938)

Convection currents in and around arcs in air have been studied by Kenty's method of photographing solid particles in the gas stream. By the use of BN powder the air velocities around an arc column with vertical axis are measured throughout the entire region of convection currents. These velocities vary from 130 cm sec.$^{-1}$ at the arc axis to zero at a distance of 2.5 cm. By integrating over the velocity curve, the total heat flow is found to be 75 percent of the electrical input. That portion of the heat flow included in the luminous arc core is 7 percent of the total. By equating the buoyancy force and the viscous force at the arc boundary, the gas viscosity η is measured. The gas temperature corresponding to η is 7000°K, in agreement with known arc temperature measurements.

INTRODUCTION

THE general character of conduction-convection heat loss from solid bodies has been studied by numerous investigators.[1] It is found that the convection currents, which are zero at the surface of the hot body and at a distance of several centimeters, rise to a maximum at a distance of several millimeters from the surface. The full drop in temperature takes place in this region of a few centimeters, with the steepest temperature gradients being directly at the surface of the hot body.

In order to ascertain the similarities between heat loss from solid bodies and from high pressure arcs we have studied experimentally the convection currents within and around arcs in air by a method similar to that used by Kenty with the Hg arc.[2] Kenty introduced CaO and MgO powder into the arc column mechanically and observed the rate of rise of this material as incandescent particles and ionized vapor. In this way he measured the maximum velocity in the axis of the arc, finding values around 50 cm sec.$^{-1}$, increasing for increasing vapor density.

[1] (a) L. Lorenz, Wied. Ann. **13**, 582 (1881); (b) W. Nusselt, Gesundh.-Ing. **38**, 477 (1915); (c) I. Langmuir, Phys. Rev. **34**, 401 (1912); (d) C. W. Rice, J. Inst. Elec. Eng. **42**, 1288 (1923); (e) E. Griffiths and A. H. Davis, Report 9, Food Invest. Bd., H. M. Stationery Off., London (1922); (f) E. Schmidt, Zeits. f. Gesamte Kalt-Ind. **35**, 213 (1928); (g) W. Nusselt and W. Jurges, Zeits. V.D.I. **72**, 597 (1928); (h) E. Schmidt and W. Beckmann, Tech. Mech. & Thermo. **1**, 341, 391 (1930); (i) R. H. Heilman, Trans. Am. Soc. Mech. Eng. **51**, 287 (1929).

[2] C. Kenty, J. App. Phys. **9**, 53 (1938).

EXPERIMENTAL METHODS

In applying Kenty's method to arcs in air, three methods have been found which yield particles satisfactory for photographing: (1) With cored carbons it was found that a sharp tapping of the electrodes knocks out luminous particles which travel upward on the convection currents; (2) carbon dust blown into the arc can be photographed not only in the arc core but also at distances up to five mm from the arc boundary; (3) boron nitride in the form of a very light white powder can be photographed by reflected light at distances as great as one cm from the boundary of the luminous core.

An error will be made in the measurement of these convection currents if the particles which are introduced are so large that they have an appreciable rate of fall in air at the temperature of the convection currents. This error can be estimated from Stokes' law by observing the rate of fall in quiet air at room temperatures. In this way we find that at room temperatures the carbon dust falls freely at a velocity v of 50 cm sec.$^{-1}$ while the boron nitride falls at a rate estimated to be one cm sec.$^{-1}$ The boron nitride is so fine that it will follow the slight convection currents in a still room to an extent which makes the free fall measurement difficult. By Stokes' law,

$$v = 2ga^2\Delta d/9\eta,$$

where g is the customary quantity, a is the radius of the particles, Δd is the difference in density between the gas and the body, and η is the vis-

cosity. For BN the rate of fall correction will evidently be negligible for 100 cm sec.$^{-1}$ convection currents; on the basis of the measured fall rates, the particle radii a are calculated to be

$$a_{BN}=0.6\times10^{-3}\text{ cm},\quad a_C=4.3\times10^{-3}\text{ cm}.$$

The particle diameter in the case of the BN is such that for 1 : 1 magnification it is near the resolving power of the photographic film. The observed traces on the film are larger than indicated by the calculated radii, probably because of halation.

It evidently will be safe to interpret the photographically observed particle velocity as the convection current velocity in the case of the C particles only in the high temperature regions of the arc core, where by virtue of the temperature increase of viscosity the fall rate decreases. Thus for η, calculated from Hassé and Cook,[3] the fall rate for the carbon dust is 17 cm sec.$^{-1}$ at 1000°K and 5 cm sec.$^{-1}$ at 6000°K. Kenty did not observe the fall rate of the particles used in his experiments, but from the evidence that they vaporized and from the fact that his measurements were made on the axis of the arc column an error from this cause does not seem probable.

The photographic method used was similar to that employed in the sound velocity experiments,[4] except that a rotating drum film holder replaced the rotating mirror and stationary film.

The principal observations on the convection velocities in arcs in air are given by Table I and Fig. 1.

Throughout this set of measurements of arc convection currents the following constants apply: Arc current $i\cong$four amp.; arc length $l\cong$three cm; electrodes, National (Projector) cored carbons; for $I=10$ amp. cm^{-2} the arc diameter $D=0.7$ cm. A slit in the optical system restricts the observation to a segment, one mm in width, parallel to the arc axis. An examination of Table I shows that the velocities measured by particles from the electrodes[5] are smaller than by the other two methods and show a large polarity effect. From the measurements with C and BN powder it is believed that the velocity measurements based on these core particles are unreliable. The particles are obviously large and probably have an appreciable free-fall correction. If the size of the particles depends upon the electrode temperature, the large polarity effect would be explained, since the anode crater is much hotter than the cathode. When a particle is released from the upper electrode, it falls for a few millimeters and then reverses its direction and rises rapidly. Although the method of electrode particles is of doubtful merit for quantitative work, it lends itself very well indeed to the demonstration of the existence of the velocity currents in the arc gas.

TABLE I. *Particle velocity in and near arc.*

Case 1—Carbon particles from anode* and cathode**						
Position of anode	Top	B'm	B'm			
Distance from arc axis (cm)	0	0	0			
Velocity (cm sec.$^{-1}$)	75**	35*	80**			
Case 2—Carbon dust blown into arc						
Anode	Top	Top	B'm	B'm		
Dist. (cm)	0	0.5	0	0.7		
Velocity (cm sec.$^{-1}$)	120	112	130	110		
Case 3—Boron nitride blown into arc						
Anode	B'm	B'm	B'm	B'm	B'm	B'm
Dist. (cm)	0	0.5	0.7	1.2	1.4	2.5
Velocity (cm sec.$^{-1}$)	130	70	50	41	34	0.0

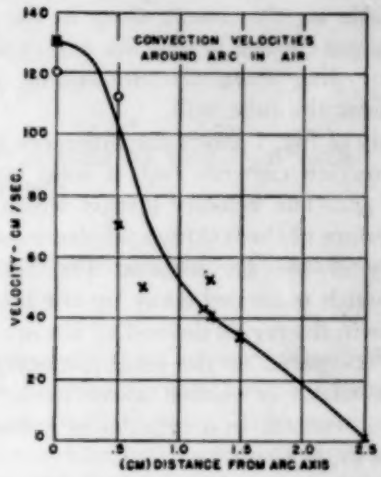

FIG. 1. Convection velocities around arc in air.

DISCUSSION

The measurements with C and BN dust are in good agreement and show velocities which

[3] H. R. Hassé and W. R. Cook, Proc. Roy. Soc. **A125**, 196 (1929).

[4] C. G. Suits, Physics **6**, 315 (1935).

[5] J. A. Van Lund, who took many of the measurements in this paper, devised this method.

vary between 130 cm sec.$^{-1}$ in the arc core and 34 cm sec.$^{-1}$ at a distance of 1.5 cm from the arc axis. The air currents appear to be practically undisturbed at 2.5 cm, which may be taken as the point of zero velocity. The velocities on the arc axis are about two to three times as large as observed by Kenty for the Hg arc at the same pressure, although the lower density of air would lead to a velocity one-seventh as large for our case, according to Elenbaas' theory.[6] The essential difference in the geometry must be held accountable for this result, since in the Hg arc the rising gas column in the tube axis experiences a viscous drag from the descending velocity stream near the tube wall.

A study of Fig. 1 shows the difference between the convection currents near a solid body and near an arc. The velocity stream which is zero at the surface of the solid has a finite value at the boundary of the arc column. The amount of energy which is carried away by the movement of the gas in the region defined by the arc column is small compared to the total arc energy. The heat Δh, which is carried away by a laminar convection current in a cylinder of radius r and thickness dr, is given by

$$\Delta h = 2\pi r dr v C_p \Delta T \rho, \tag{1}$$

where v is the uniform velocity, C_p is the specific heat (in cal. g^{-1}), ΔT is the temperature above ambient, and ρ is the gas density. If T is large, and for a monatomic gas, the product $\Delta T\rho$ is constant and Δh does not depend upon the temperature. For a dissociating gas, ρ experiences a pure temperature effect and an effect due to thermal dissociation; in general, in a nonreactive gaseous mixture of i components the density ρ at the temperature T is given by:

$$\rho(T) = \frac{T_0}{T}\sum\frac{\rho_i p_i}{p_i} = \frac{\rho_0 T_0}{T}\sum\frac{M_i p_i}{p_i},$$

where p_i is the partial pressure and M_i is the molecular weight of the i the component; ρ_0 is the density of atomic hydrogen at the temperature T_0. The quantity

$$\sum M_i p_i / p_i = \bar{M},$$

where $\bar{M}$ is the weighted mean molecular weight. Also

$$C_p = C_{p_1}/\bar{M}$$

where C_{p_1} is the heat capacity in cal. per gram molecule. Hence

$$\Delta T C_p \rho = \Delta T \frac{C_{p_1}}{\bar{M}} \frac{\rho_0 T_0 \bar{M}}{T} \fallingdotseq C_{p_1}\rho_0 T_0$$

if $\Delta T \fallingdotseq T$. The quantity $\Delta T C_p \rho$ is thus constant to the extent to which the heat capacity per gram molecule is constant. This is not precisely true,[7] but in the following calculation we neglect the error. The convection heat Δh can therefore be simplified to

$$\Delta h = 2\pi r dr v a,$$

where $a = 0.124$ cal. cm^{-3} for air. To obtain the heat energy h_c in the arc core, we can integrate

$$h_c = 2\pi \int_0^{0.36} r v(r) dr \tag{2}$$

numerically to obtain

$$h_c = 6.8 \text{ calories.}$$

The total calories in the arc are 96, so that the core portion represents about 7 percent of the total. If we integrate between 0–2.5 cm to get the total convection heat flow h for the $v-r$ curve of Fig. 1, we find $h = 71.5$ calories or 75 percent of the total input. This agreement is satisfactory in view of the heat loss along the electrodes and some radiation loss.

The convection currents arise from a buoyancy force F_b on the heated air of the form

$$F_b = \pi r^2 g h \Delta\rho, \tag{3}$$

where πr^2 is the area of a cylindrical section of height h, $\Delta\rho$ is the gas density difference due to temperature; and are restrained by a viscous force F_v of the form

$$F_v = 2\pi r h \eta dv/dr, \tag{4}$$

where η is the viscosity and dv/dr the velocity gradient at the surface of the cylinder of radius r. The flat top to the $v-r$ curve of Fig. 1 is no

[6] W. Elenbaas, Physica **3**, 484 (1936).

[7] See C_p for O_2 and N_2 in Table I, "Determination of Arc Temperature from Sound Velocity Measurements, II." H. Poritsky and C. G. Suits, Physics **6**, 190 (1935).

doubt caused by the increase of η at the high core temperature. We can equate (3) and (4) at the arc boundary,[5] where $r=0.36$, $dv/dr=130$, and solve for η with the result that

$$\eta=0.0018 \text{ poises.}$$

By Hassé and Cook[4] the temperature of air corresponding to a viscosity of 0.0018 is 7000°K. This concept, therefore, leads to reasonable values of extrapolated viscosity in the correct range of measured arc temperatures, or, conversely, can be viewed as a direct measure of viscosity at high temperature, showing agreement with the extrapolated data of Hassé and Cook. It should be noted that both $\Delta\rho$ and η depend upon temperature. However, when T is large, the dependence of $\Delta\rho$ upon T is negligible in the present instance.

[5] The arc "boundary" as a measurable is discussed in detail in a paper now in preparation.

JANUARY 15, 1939 PHYSICAL REVIEW VOLUME 55

The Probability of Ionization of Mercury Atoms by Collision with Low Velocity Electrons[1]

MAURICE E. BELL*
George Eastman Laboratory of Physics, Massachusetts Institute of Technology, Cambridge, Massachusetts
(Received September 27, 1938)

INTRODUCTION

THE study which is briefly reported here was undertaken late in 1934 and completed in May 1937, with the principal object in mind of establishing beyond any doubt the true form of the ionization probability curve of mercury vapor in the immediate neighborhood of the ionization potential. The two schools of thought are well typified by the experimental results of E. O. Lawrence[2] on the one hand, and of P. T. Smith[3] on the other. Lawrence has maintained that the ionization function rises rapidly with increasing electron energy at the ionization potential and then falls, after which an "ultra-ionization" potential is reached giving rise to another rapid increase in ionization probability followed by another decrease, and so on. The opinion typical of the opposing group is well represented by a quotation from Smith's paper which follows: "The curve indicates that the ionization does not rise sharply at the ionization potential, the rapid rise occurring almost a volt above this potential. Curves obtained with a poor velocity distribution did, however, show a more rapid rise at 10.40 volts." The results here reported are in excellent agreement with Lawrence's experimental findings, although complete agreement with his theoretical deductions is not implied. As will be illustrated below, an apparent ionization was found below the ionization potential of mercury which cast some doubt over the detailed validity of the work, since it was not certain whether this apparent ionization was caused by some impurity, the mercury molecule, or photoelectric emission from the ion collector. Since it was within the range of possibility that this unknown mechanism was also responsible for the maximum and minimum in the ionization curve, it was considered necessary to repeat the work with a more elaborate tube. This work has served as a forerunner of the much more extensive study made by W. B. Nottingham and reported in the paper following this one.

EXPERIMENTAL APPARATUS

After experimenting with a tube design very similar in principle to that used by Lawrence, except that all metal parts were made of tantalum and no wax joints were used, this was abandoned because of the small intensity of electrons

[1] A complete report of this research is on file in the library of the Massachusetts Institute of Technology.
* On the Research Staff of the Westinghouse Electric and Manufacturing Company, East Pittsburgh, Pennsylvania.
[2] E. O. Lawrence, Phys. Rev. **28**, 947 (1926).
[3] P. T. Smith, Phys. Rev. **37**, 808 (1931).

delivered to the ionization chamber. The final tube used evolved after considerable experimentation from a suggestion made by Dr. P. T. Smith that good resolution might be obtained by sending the electrons around an analyzer with a very low velocity after which they could be accelerated into the ion chamber. A diagram of the apparatus is shown in Fig. 1. The indirectly heated cathode of the kind used in the type '77 radio tube was supported concentric with respect to the small cylinder at *C* which was an integral part of the electron analyzer *a*. With a 1.5-volt applied potential between the cathode and the analyzer, the magnetic field was adjusted so that the maximum number of electrons were bent in a circle one centimeter in radius and emitted through the 0.4-mm exit slit. In theory it should have been possible to determine the electron energy from the magnetic field and the dimensions of the ion chamber, but this did not work out in practice probably on account of the disturbing effects of contact potentials and the magnetic field produced by the cathode heating current even though the heater was nearly "noninductive." The voltage scale was established by the retarding potential method. The effect of the magnetic field on the retarded electrons and also reflection effects were neglected. It was assumed that there was no contact difference in potential between the inside and the outside of the ion chamber.

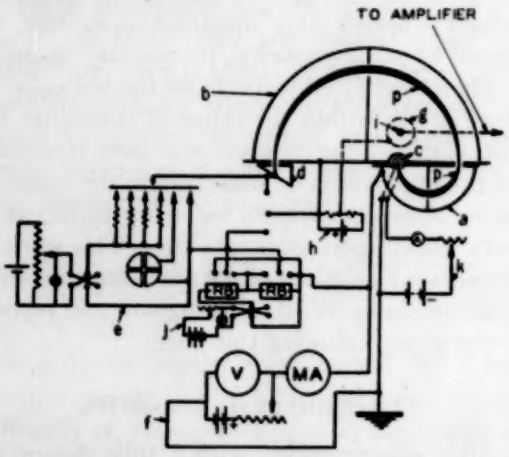

FIG. 1. Diagram of the apparatus. *a*—analyzer; *b*—ion chamber; *c*—cathode; *d*—electron collector; *e*—electron measuring system; *f*—potential source for analyzer; *g*—ion grid; *h*—bias for ion grid; *i*—ion collector; *j*—potential for ion chamber; *k*—cathode supply; *RB*—Leeds & Northrup resistance boxes; *p*—electron path.

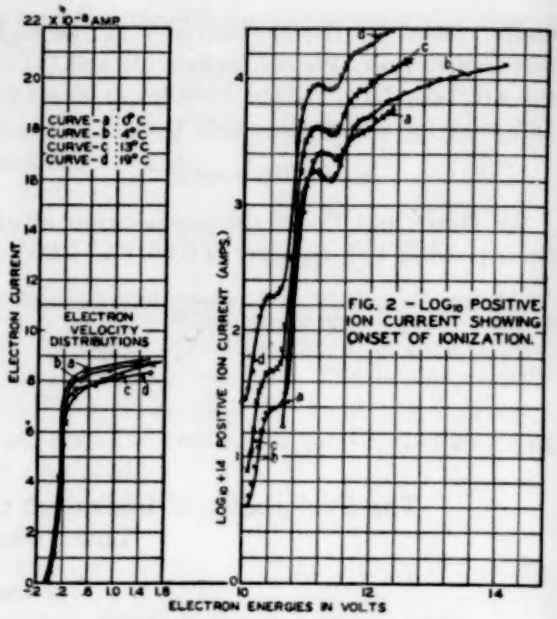
22 X 10⁻⁸ AMP
CURVE - a : 0° C
CURVE - b : 4° C
CURVE - c : 13° C
CURVE - d : 19° C
ELECTRON VELOCITY DISTRIBUTIONS
ELECTRON CURRENT
LOG₁₀ +14 POSITIVE ION CURRENT (AMPS)
FIG. 2 - LOG₁₀ POSITIVE ION CURRENT SHOWING ONSET OF IONIZATION.
ELECTRON ENERGIES IN VOLTS

FIG. 2. Plots of the electron velocity distribution and of the positive ion current to show the onset of ionization.

SURVEY OF RESULTS

The results obtained are well illustrated by the curves of Fig. 2 which show the logarithm of the current measured at the collector *i* as a function of the electron energy as computed by the retarding potential method. These plots bring into prominence the fact that current was observed when the electron energy was less than the ionization potential of 10.38 volts. Subsequently, Nottingham's results showed clearly that this current was caused by the emission of photoelectrons from the ion collector and not caused by the ionization of the mercury molecule or the effects of some unknown impurity. These curves indicate perfectly satisfactory agreement with Lawrence's work since they show all of the essential structural details found in his curves. The chief aim of this research was thus accomplished, and although it opened up a new problem and showed more clearly that additional work should be done to establish the results in terms of the usual standard conditions, it was impossible for the author to continue the work to its logical conclusion. Since this has been done in the very extensive study made by Professor Nottingham, the present research, which was the forerunner of that work, is being reported as briefly as possible.

Ionization and Excitation in Mercury Vapor Produced by Electron Bombardment

W. B. NOTTINGHAM
George Eastman Research Laboratory of Physics, Massachusetts Institute of Technology, Cambridge, Massachusetts
(Received September 27, 1938)

The experimental determination of ionization and excitation in mercury vapor has been accomplished with an apparatus which permitted the evaluation of the electron energy from an accurately known magnetic field and the dimensions of the ion chamber. As a test of the apparatus the value of e/m for the electron was measured and found to be 1.758×10^7 e.m.u. A brief discussion of secondary emission and related effects is given. The ionization probability function is shown to have two important maxima, the first being at 10.8 volts and the second at 32 volts. The detailed structure between 10.4 volts and 16 volts indicates the composite character of the ionization function while the general smooth trend of the curve above 16 volts suggests that the process is relatively free from complication for high energy electrons. The study of photoelectric currents produced yielded new data on the electronic excitation function of the $2^3P_1^0$, $3^3P_1^0$, and $4^3P_1^0$ levels of the mercury atom showing that these have maxima in their probability functions at 5.6, 8.9, and 9.6 volts.

INTRODUCTION

MANY experimenters have undertaken the problem of determining the probability of ionization of mercury vapor as a function of the electron energy.[1–7] These investigators do not agree with each other except in the most superficial way since the experimental techniques differed and in no case were the methods used above criticism. The results here reported are not an exception to this rule although every effort was made to improve the experimental methods so as to be as free from criticism as possible. As the preceding paper shows, Bell obtained a confirmation of Lawrence's work but did not determine the actual yield of ions quantitatively nor did he ascertain the relative yield using an energy scale independent of uncertainties of contact potential differences. A critical examination of his experimental methods indicated the steps which should be followed in order to overcome his difficulties. The present study is thought to be the logical outgrowth of Bell's preliminary experiments.

[1] K. T. Compton and C. C. Van Voorhis, Phys. Rev. **26** 436 (1925).
[2] E. O. Lawrence, Phys. Rev. **28**, 947 (1926).
[3] A. L. Hughes and C. M. Van Atta, Phys. Rev. **36**, 214 (1930).
[4] W. M. Nielson, Phys. Rev. **37**, 87 (1931). R. D. Potter, J. Elisha Mitchell Sci. Soc. **44**, 31 (1928).
[5] P. T. Smith, Phys. Rev. **37**, 808 (1931).
[6] C. R. Haupt, Phys. Rev. **38**, 282 (1931).
[7] M. E. Bell, Thesis at Massachusetts Institute of Technology, 1937 and Phys. Rev. **55**, 201 (1939).

DESIGN AND CONSTRUCTION OF EXPERIMENTAL TUBE

General

The essential parts of the apparatus are illustrated by Fig. 1 in which a top view is shown as 1a. The cathode assembly lay in the semicircular channel formed in the face plate of the ion chamber. The electrons from the filament F were accelerated into the analyzer at slit S_1 and those of the desired energy followed circular paths to the exit slit S_2 after which they were accelerated into the ion chamber at S_3 with an increase in the mean energy by a factor of five. The radius of the electron path increased just enough for the main beam to pass out through the exit slit S_4 and into the "electron cage" EC. In the central part of the ion chamber the positive ion collector P was surrounded by two grids G_1 and G_2. The ion collector P also served as the emitter of photoelectrons when the grid potentials were arranged to exclude positive ions. The four units of this system are seen to be (1) the cathode assembly, (2) the analyzer, (3) the ion chamber with its grids and ion collector inside, and (4) the electron cage. These parts were supported mechanically by attaching the cathode assembly to the analyzer by two strong insulating members constructed as shown in Fig. 2a. The parts were all assembled by spot welding[8] tungsten to tantalum or tantalum to tantalum since no other materials were used in

[8] T. S. Gray and W. B. Nottingham, Rev. Sci. Inst. **8**, 65 (1937).

the construction. In all cases the wires were prepared for welding so carefully that practically no adjustments were needed after the welding was completed. This was necessary in order to eliminate changes in alignment during the period of severe heat treatment given to outgas the metal parts. The electron cage and its guard were mounted on the ion chamber after which the analyzer was firmly attached to the ion chamber by three insulating links. The face plates of the analyzer and the ion chamber were made from a single sheet of very flat 10-mil tantalum by sawing them exactly to size on the milling machine. The slits were also sawed with high precision so that they were in perfect alignment when the outside edges of the plates were exactly true with each other. Three heavy tantalum wires welded together to form a supporting yoke were welded to the ion chamber and the entire assembly was supported on one of the tungsten leads at the top of the tube. The tube blank with its fifteen lead-in wires was first prepared and given a twelve-hour bake under high vacuum at a temperature of 500°C in order to anneal the glass and test the seals. After this, the envelope was cracked off a few inches below the top and the assembled system mounted on a single supporting wire while the remaining electrical connections were made using 5-mil tantalum wire except for filament leads which were two 10-mil leads in parallel. A one-lead support was necessary since a glass tube of this kind undergoes a considerable deformation upon being evacuated. Eight leads were brought in through a "cluster seal" which is a circular array of wires, while the other leads came in on one triple, one double, and two single lead presses. The photographs of Fig. 3 serve to supplement this brief description of the general constructional details.

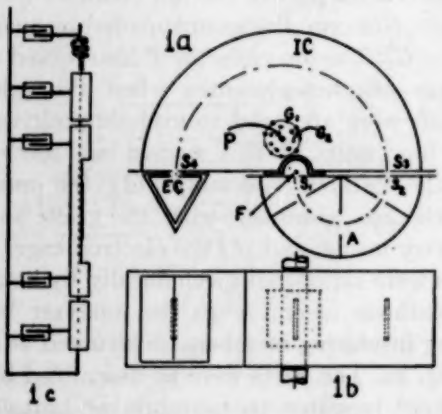

FIG. 1. Diagram of experimental tube. (a) Top view showing cathode F; analyzer A; ion chamber IC; outer and inner grids G_1 and G_2; ion collector P; and electron cage EC. (b) Front view showing location of cathode assembly and slits. (c) Side view of cathode assembly only.

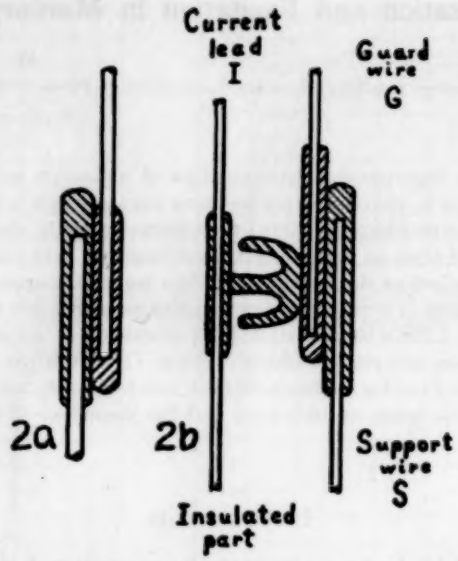

FIG. 2. Construction of insulators. (a) Insulators for mechanical support of heavy structures. (b) Insulators for extremely high insulation of the collectors.

Electron paths inside ion chamber

To a first approximation the equipotential surface halfway between the analyzer exit slit and the entrance slit of the ion chamber, was a plane parallel to the planes of the analyzer and ion chamber face plates. On each side of the median plane the equipotentials penetrated through the slits symmetrically and therefore since the electrons entered this system of equipotentials at a lower velocity than they left, the electron beam was less divergent than it would have been without this lens effect. The electrons as they entered the ion chamber formed a beam nearly homogeneous in energy and directed nearly perpendicular to the face plate of the ion chamber. When no internal field existed within the ion chamber, the electrons traveled in circles with radii proportional to the velocity. For a given magnetic field, the ion chamber voltage V_i with respect to the cathode as read on a voltmeter was adjusted to that value for which the

maximum number of electrons passed around the ion chamber and out the exit slit into the electron cage. This condition obtained when the electron densities at the two edges of the exit slit were the same. When the electron current to *EC* was a maximum one or two percent of the whole beam current fell on the "high energy" side of the exit slit and was collected on the inside of the ion chamber and some thirty to forty percent of the beam fell on the "low energy" side of the slit. If the voltage V_i was decreased slightly the current measured at *EC* decreased in spite of the additional electrons coming in on the "high energy" side of the slit because so many more electrons were intercepted on the "low energy" side of the slit. Thus by varying V_i over a small range the electron beam was made to sweep across the exit slit. If the entrance slit to the ion chamber were of infinitesimal width and all of the electrons projected into it perpendicular to the face-plate, then the diameters of all electron trajectories would lie in the plane of the face-plate and the distance from the entrance slit to the intersection of the trajectory with the face-plate would be directly proportional to the velocity. It would be a simple matter to determine the distribution in electron energy in the beam from the measurement of the current to *EC* as a function of the potential V_i, if these conditions were satisfied. Since the main part of the beam was more or less concentrated into a small part of the total slit width and entered the ion chamber very nearly perpendicular to the face-plate, the energy distribution in the beam was analyzed according to this scheme although it was not entirely free from objection.

In general, the gas pressure was so low that very few electrons were scattered from the beam and yet in order to make sure that the currents measured at *P* were due either to the arrival ions or the emission of photoelectrons, it was necessary to maintain this collector negative with respect to the filament. The large negative potential on *P* relative to the ion chamber repelled the electron beam as indicated by a change in the current measured at *EC*. By using this current as the indicator the outer grid G_1 could be made very slightly positive and the electron trajectories could be brought back to the original location, as was observed when no differences in potential were applied to the elements within the ion chamber. The ratio of the collector potential to the outer grid potential (both relative to the ion chamber) for a "neutral field" along the path of the electron beam, was 250 to one. Since this ratio was independent of the electron energy it is thought that the neutralization of the ion collector field was very nearly perfect all along the electron path in the ion chamber.

Preparation of mercury

Experience has shown that it is impossible to obtain accurate reproducibility of surface conditions over long periods of time if the experimental tube is not sealed off from the vacuum system. In order to supply the tube with a clean source of mercury vapor, a side tube containing a mercury "pellet" was attached to the main tube. This was constructed so that a "pigtail" connected to the pellet could be broken with a sliding glass hammer by turning the entire tube upside down after which, upon returning the tube to its normal position, the mercury ran out of the

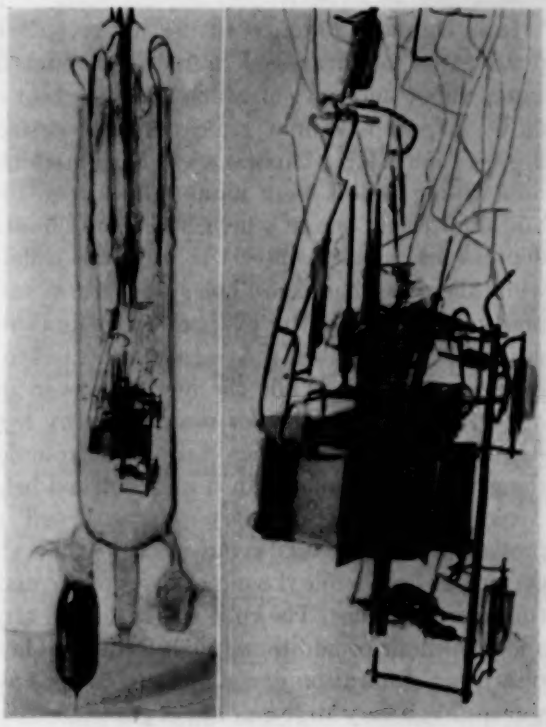

FIG. 3. Photograph of tube before attaching mercury side-arm.

opening to form a pool in the bottom of the side tube. Freshly distilled mercury was put into a still attached to a vacuum system in such a way that the mercury could be distilled out of the first still into a second one which previous to the distillation was baked for many hours at 500°C. After transferring some of the mercury from the first still to the second by slow distillation, the first one was sealed off and about two cubic centimeters of this mercury were distilled into the "pellet" which had also been thoroughly baked. During the final baking of the main tube the side tube containing the unbroken "pellet" was maintained at a temperature of about 300°C while the rest of the tube was baked at 450° to 500°C. This method of preparing the mercury was so effective that no appreciable changes were observed in the surface condition of the filament after releasing the mercury in the main tube. If a very small fraction of a monolayer of contaminating gas had formed on the filament after the release of the mercury it would have been easy to detect it.

Barium-aluminum getter

It is common practice to use a "getter" to remove the last traces of active gases such as water vapor and oxygen which even the best of diffusion pumps cannot remove to the desired degree. Eight "King Laboratories" barium-aluminum 10-mg pellets were mounted between two tantalum rings, one of which had small circular depressions punched into it to hold the pellets, while the other had small holes punched in such positions that the getter evaporated freely in the desired direction when the rings were heated to a high temperature. While the metal parts in the main tube were heated for some hours by high frequency currents a series coil also surrounded the getter ring to maintain it at a dull red heat. After the seal-off capillary was softened in preparation for the final removal of the tube, the getter was fired while the metal parts of the main tube were kept hot. The tube was sealed off after about an hour of additional high frequency heat treatment. Ionization gauge measurements have shown that a very large amount of gas is liberated when the seal-off capillary is first heated but if this is done with sufficient thoroughness no appreciable gas is given off during the actual seal-off operation.

There was some question as to the effect that getter might have in a mercury tube of this kind. Within a very short time after the release of the mercury, the getter deposit changed its appearance by taking on a brighter luster showing that a noticeable amount of mercury had condensed there. The mercury in the reservoir remained just as free from any visible contamination after it was released as before. When it was necessary to condense out the mercury to obtain additional high vacuum data which had not been obtained before the mercury "pellet" was broken, liquid air was put on the mercury side tube. This resulted in a rapid reduction in mercury pressure, as indicated both by electron scattering and by the number of ions per unit number of electrons. The residual pressure of mercury remained constant for a period of about thirty-six hours, during which measurements were made. After that time a dry-ice bath was placed on the getter side-arm and the mercury pressure soon dropped to such a low value that no mercury ions could be detected. These results are interpreted to indicate that the vapor pressure of mercury at 25°C is reduced to 0.02 percent of its normal value when covered by a film of getter.

Electrical Circuits

Filament heating circuit

The filament heating circuit was a modification of one used for the study of thermionic emission[9] and is shown schematically by Fig. 4. The 500-volt generator driven by a synchronous motor furnished power to the thyratron inverter circuit which was controlled by a 200-cycle oscillator connected to the FG-67 grids through two power amplifiers with independent gain control so as to maintain the heating period at exactly one-half cycle. A switch S_1 provided an alternative method of heating the filament from a battery for standardization. With the filament current set at the desired value, the resistance R_5 was adjusted to give a suitable current through the auxilliary filament F_2. The light from this filament fell on the FJ-114 photo-tube and the current was measured by balancing out the IR

[9] W. B. Nottingham, Phys. Rev. **49**, 78 (1936).

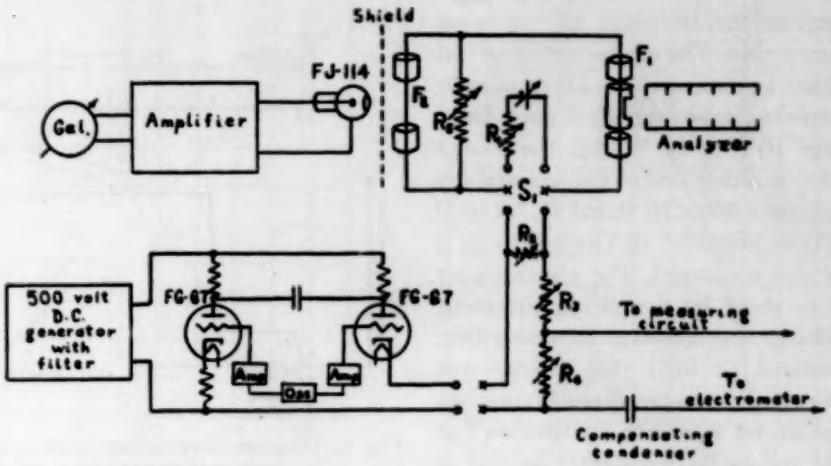

FIG. 4. Diagram of filament heating circuit and "photoelectric ammeter."

drop produced by the flow of current through a high resistance, as indicated by the FP-54 vacuum tube electrometer working in the DuBridge-Brown amplifier circuit.[10] Since it was desirable to make a large number of readings which had to be treated as "simultaneous," it was necessary to hold the filament heating conditions extremely constant and this could be done with the "photoelectric ammeter" shown.

Measuring circuits

The circuit arrangement for the application of potentials to the various elements of the tube and the measurement of currents is shown in Fig. 5. The relatvie potentials of the various elements are shown diagrammatically in Fig. 6. Before entering into the details of the main circuit mention must be made of the "compensating" condenser. Electron emission from the filament to the analyzer was cut off each heating half-cycle because the IR drop produced in resistance R_3 by the heating current made the filament 10 to 40 volts positive with respect to the analyzer depending on the value of R_3. A small capacity coupling existed between the filament heating leads and the input lead to the Compton electrometer used for measuring the small ion and photoelectric currents. By adjusting R_4 to a suitable value and applying the e.m.f. obtained there to the compensating condenser, the effect of the above-mentioned capacity coupling could be exactly neutralized.

The potentials V_1 on the focusing cylinder, V_a on the analyzer, and V_i on the ion chamber were all measured relative to the cathode with a special Leeds & Northrup type K-1 potentiometer arranged so that voltages from zero to 16.1 volts could be measured directly. For voltages higher than this the drop across a 15,000-ohm resistance in series with a 135,000-ohm resistance permitted an accurate measure of the voltage up to 160 volts. This applied particularly to the voltage V_i. Large values of the ion collector voltage V_p' (the superscript indicates that this is relative to the ion chamber instead of the filament) were determined by first setting the required voltage on V_i with the potential divider and then adjusting the battery on V_p' until the difference in potential between the ion collector P and the filament was zero. This is a necessary procedure unless more than one voltage divider is used since for accurate results the divider must be left connected to the circuit or else another 150,000-ohm resistance substituted in its place. With these methods of measurement and adequate voltage sources, all potentials were maintained and known to an accuracy of better than 0.1 percent.

The currents to the analyzer and the ion chamber were measured on carefully calibrated galvanometers and the currents to the ion collector P and the electron collector EC were measured with a small quadrant (needle radius

[10] L. A. DuBridge and H. Brown, Rev. Sci. Inst. 4, 532 (1933).

0.25 cm) Compton electrometer of our own design and construction. The electrometer served as a null indicator to measure the IR drop over resistors for currents larger than 10^{-12} amp. Over the current range 10^{-12} to 10^{-15} amp. the charge was accumulated on either one of two condensers the sizes of which were 400×10^{-12} and 11.7×10^{-12} farad and the time required to charge up to a known voltage was measured. The electrometer was used here to show by a null measurement that all of the charge was stored in the condenser. The e.m.f. required to hold this charge was measured on the potentiometer. Since in all cases the currents measured were not continuous but were a series of pulses lasting 0.0025 second, a capacity shunt across each resistance was necessary in order to eliminate fluctuations in potential of the collecting electrode. The resistances were made by evaporating platinum on the inside wall of evacuated "Pyrex" bulbs. The large condenser mentioned above was quartz-insulated and the small one was built into the electrometer and required no insulator other than that used to support the insulated quadrants. The high insulation switches were made of brass parts insulated by sulphur with contacts gold to gold.

Control of mercury condensation temperature

A six-junction copper-constantan thermopile was constructed with thin wall glass insulators surrounding each junction. A band was made of thin sheet copper to which six tubes made of the same material were soldered to hold the "mercury pool" junctions. This band of copper was fastened around the mercury side tube at the bottom so as to "equalize" the temperature and maintain good thermal contact between the thermal elements and the glass wall at the

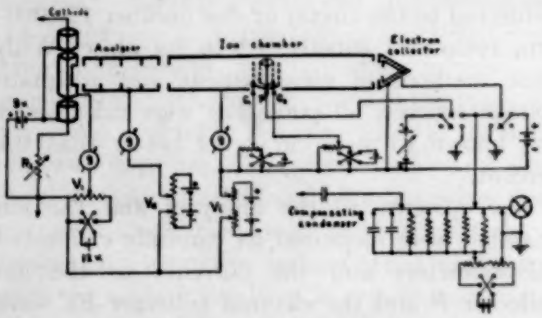

FIG. 5. Diagram of the measuring circuit.

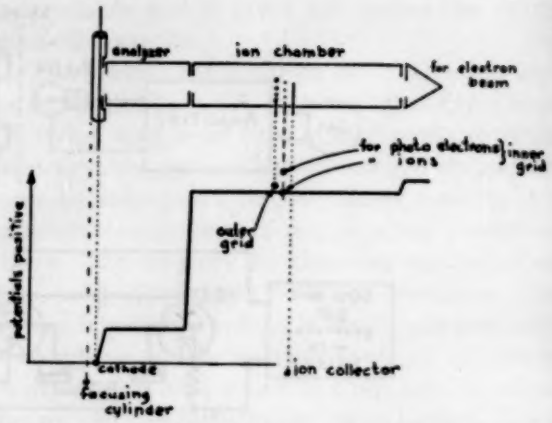

FIG. 6. Diagram showing the relative potentials of the various elements within the tube.

mercury pool. A large spherical vacuum flask served as the temperature bath. Much of the work was done with this flask filled with crushed ice and distilled water but for the temperature range between 0°C and 25°C a more complicated control was needed. For this range a copper heat transfer coil was placed in the bottom of the water filled flask and water of the desired temperature was circulated through the coil. An air jet kept the water bath thoroughly stirred at all times. Manual adjustment of the circulating water temperature was satisfactory and an indication of the thermal e.m.f. was observed continuously with the required accuracy on an L. & N. student potentiometer. The temperature in the ion chamber was estimated by assuming that clean tantalum has the same emissivity at low temperatures as tungsten and by calculating the temperature from the power radiated. The Jones-Langmuir[11] tables were used.

EXPERIMENTAL INVESTIGATION OF THE ELECTRON BEAM

Test of apparatus by determination of electron's e/m

With the filament temperature constant and sufficiently low so that space charge effects could be neglected, the potentials V_a of the analyzer, V_i of the ion chamber, and V_1 of the focusing cylinder, were determined as a function of the magnetic field current by observing the condition

[11] H. A. Jones and I. Langmuir, Gen. Elec. Rev. **30**, 310, 354, 408 (1927).

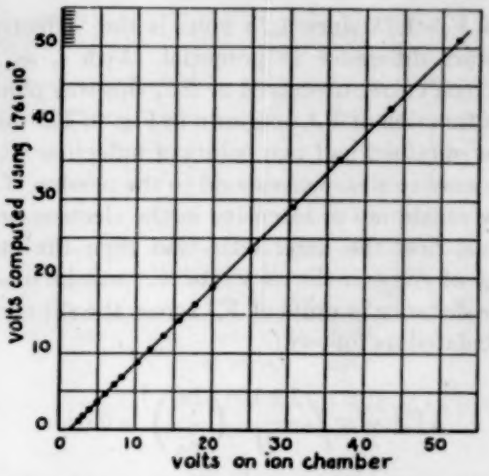

FIG. 7. Linear relation between potential V_i applied to ion chamber and computed electron energy V_m. Least squares determination of e_m/m gave 1.758×10^7 e.m.u. from these data.

for the maximum current to the electron collector EC. If we assume that on the average the electrons entering the ion chamber through the entrance slit and leaving it at the exit slit follow paths with a radius equal to half of the distance between the entrance and exit slits, then the average electron energy inside of the ion chamber can be calculated from Eqs. (1) and (2).

$$V_m=\frac{e_m}{m}\frac{H^2r^2}{2\times10^8}, \tag{1}$$

$$H=\frac{16\pi ni}{50\times5^{\frac{1}{2}}R}. \tag{2}$$

Equation (2) gives the strength of the magnetic field in gauss at the center of a pair of Helmholtz coils constructed with the separation between coils equal to the coil radius R. The total number of turns is n and the current i is in amperes. In Eq. (1), (e_m/m) is the charge to mass ratio in electromagnetic c.g.s. units, r the radius of the path of an electron moving in a plane the normal of which is parallel to the magnetic field when the kinetic energy of the electron is V_m expressed in electron volts. These equations combined with the appropriate constants yield the relations

$$V_m=7.29i^2 \quad \text{and} \quad i=(0.1372V_m)^{\frac{1}{2}}. \tag{3}$$

The value of $(e_m/m)=1.761\times10^7$, which is the spectroscopic value as given by Birge, was used.

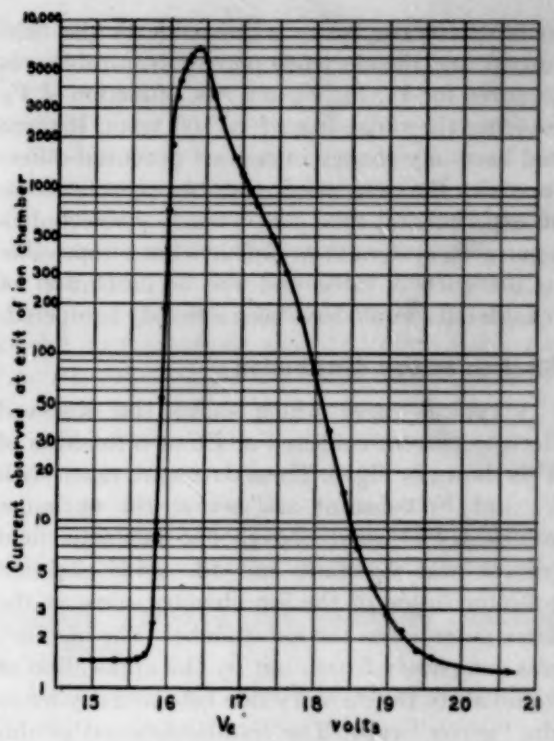

FIG. 8. Electron current collected at EC as a function of V_c.

The fact that the apparatus worked according to expectations is illustrated in Fig. 7 by the straight line relationship between the applied potential V_i required to give a maximum current to the electron collector EC and the computed electron energy V_m. The intercept of this straight line on the V_i axis gave the "effective" contact difference in potential between the inside of the ion chamber and the filament which was 1.28 volts. With 0.995 cm as the radius of the analyzer, a corresponding straight line was obtained for the relation between the analyzer potential V_a and the computed electron energy V_{am}. The experimental points were represented accurately by the equation $V_a=1.29+V_{am}=1.29+0.1955V_m$. The "effective" contact difference in potential between the inside of the analyzer and the filament was thus found to agree with that of the ion chamber to within 0.01 volt, which was even better than might have been expected. The potential V_1, by which the focusing cylinder was maintained negative with respect to the filament, was very nearly a linear function of V_m. In order

to facilitate the ready adjustment of the field current and the electrode potentials, a table was prepared for V_1, V_a, V_i, and i as a function of V_m covering the range from 5 to 100 volts. If there had been any change in contact potential difference with the time as is invariably experienced in an experimental tube continuously connected to a pumping system, it would have been impossible to use such a table and the accumulation of reliable data would have been seriously hampered.

Electron energy distribution

A typical curve which shows the observed electron current collected at EC as a function of V_i is shown in Fig. 8. These data were taken with V_a and V_1 constant and set at the optimum values as discussed above. The magnetic field current was constant and the grids and ion collector inside of the ion chamber were at the same potential as the ion chamber. The mercury was completely frozen out by the application of liquid air to the mercury side tube and dry-ice to the "getter" tube. The results obtained in this way agreed in detail with those obtained before the mercury was admitted to the tube. A logarithmic scale has been used so that one curve can present all of the data since these extend over a range of nearly 10^4 in current. In order to analyze these data we define an electron energy $V_e = V_i - 1.28$ since 1.28 volts is the "effective" contact difference in potential. With i_e as the electron current received at EC, this was plotted as a function of $V_e^{\frac{1}{2}}$, as shown in Fig. 9. The curve thus obtained had two points of inflection which it is easy to show correspond to the passing of the true maximum of intensity in the electron beam across first the inner edge and then the outer edge of the exit slit as V_i (or V_e) was increased. The distance in units of $V_e^{\frac{1}{2}}$ across the slit can be calculated as follows:

$$\Delta V_e^{\frac{1}{2}} = w \Big/ \frac{2\times 10^4}{H}\left(\frac{2m}{e_m}\right)^{\frac{1}{2}} = 0.038i, \qquad (4)$$

where w is the width of the exit slit in cm, H is the magnetic field, and i the current in amperes required to produce the field. In every case the observed distance between inflections agreed with Eq. (4). As V_e was increased the electron beam swept across the inner edge of the exit slit adding a small increment of current to i_e with each small change in V_e. The slope of this curve therefore measured the distribution in electron density across the electron beam and subject to the limitations discussed above it gave the energy distribution in the beam. This simple method of determining the beam distribution applies for that range of $V_e^{\frac{1}{2}}$ which is $\Delta V_e^{\frac{1}{2}}$ wide, as given by

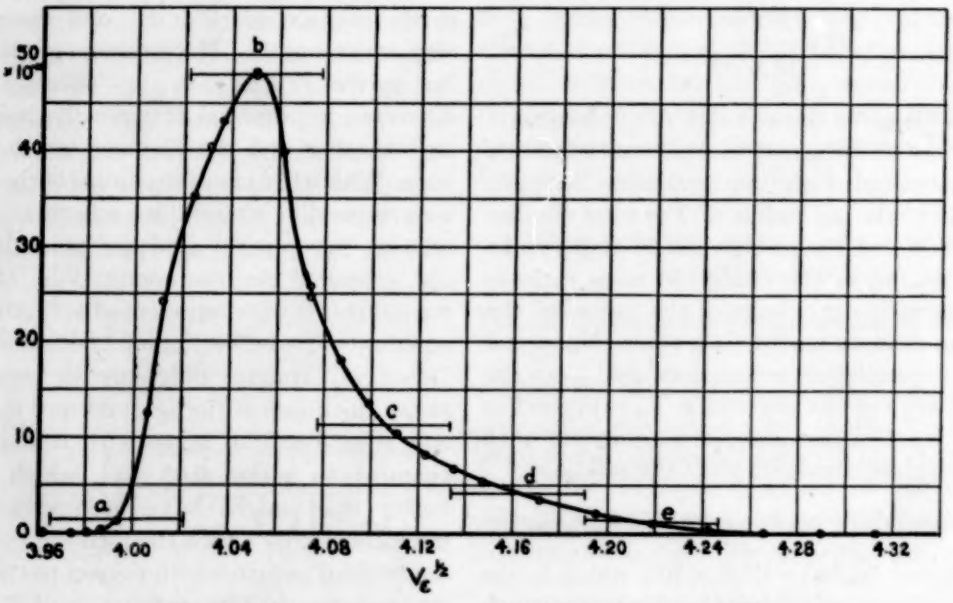

FIG. 9. Electron current collected at EC as a function of $V_e^{\frac{1}{2}}$.

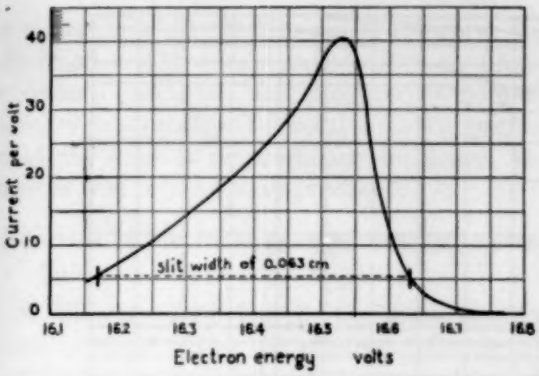

FIG. 10. Electron energy distribution subject to certain approximations.

Eq. (4), beginning at that point on the curve where the slope is appreciably different from zero. For larger values of $V_e^{\frac{1}{2}}$ than the limit of this range the slope of the curve is the difference in the ordinates of the distribution function at the two edges of the exit slit. After correcting $V_e^{\frac{1}{2}}$ by the amount $\frac{1}{2}(\Delta V_e^{\frac{1}{2}})$, the slope obtained was divided by this corrected $V_e^{\frac{1}{2}}$ and plotted against the electron energy as shown in Fig. 10. This correction is very minor but is needed to bring about a more exact correspondence to the energy distribution as related to the center of the slit instead of the inside edge.

Since it was impossible to trace the exact electron orbits from the filament through the analyzer and the ion chamber, the curve of Fig. 10 cannot be said to be a perfectly accurate representation of the energy distribution of the electrons. For reasons given above it is thought that the true energy distribution is at least as good as that shown. According to this curve nearly half of all of the electrons in the beam lie within a band only 0.15 volt wide at about 16.5 volts. If the resolving power of this apparatus is defined by this ratio, which is practically 0.01, equally careful experiments done at selected voltages from 10 to 100 volts showed that the resolving power remained very nearly constant throughout.

Determination of electron current inside ion chamber

The curve shown in Fig. 9 also served the very important function of permitting an accurate determination of the total electron current *inside* of the ion chamber. The straight lines designated "*a*," "*b*," "*c*," etc., divide the important range of observation into five segments each one slit width in extent. The intersection of the center of each of these segments with the experimental curve is a measure of the integral of all of the current in the electron beam within this range. The simple sum of these five readings which for this case was 66×10^{-10} amp., gave the total current inside of the ion chamber. Since the total current to the ion chamber including that received on the outside was 116×10^{-10} amp., the fraction delivered to the inside was 57 percent. As a function of V_m, this fraction varied from 54 percent at 10 volts to 78 percent at 100 volts. A smooth curve passed through all of the points obtained and was used in the calculation of the ionization efficiency, since for this, the number of ionic charges per unit number of electrons is needed.

Electron scattering and secondary emission effects

A characteristic feature of all of the curves giving the electron current *EC* as a function of

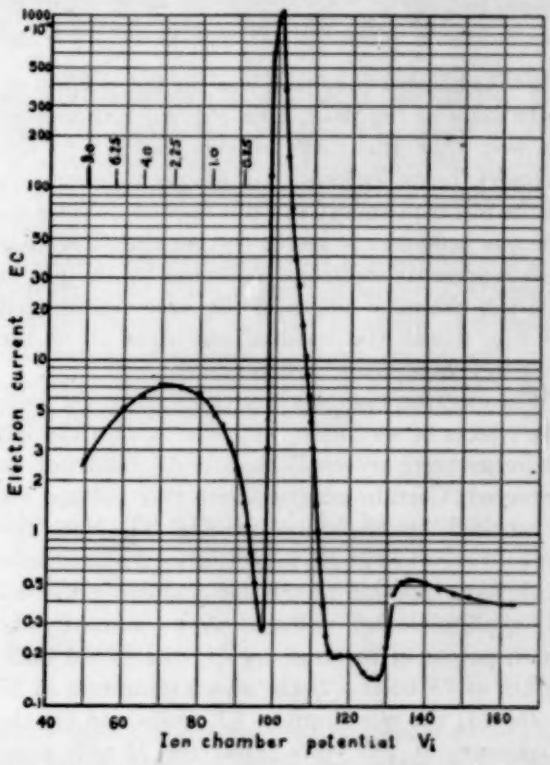

FIG. 11. Electrons collected at *EC* as a function of V_i showing electron scattering and secondary emission effects. Auxiliary scale for secondary electron energies.

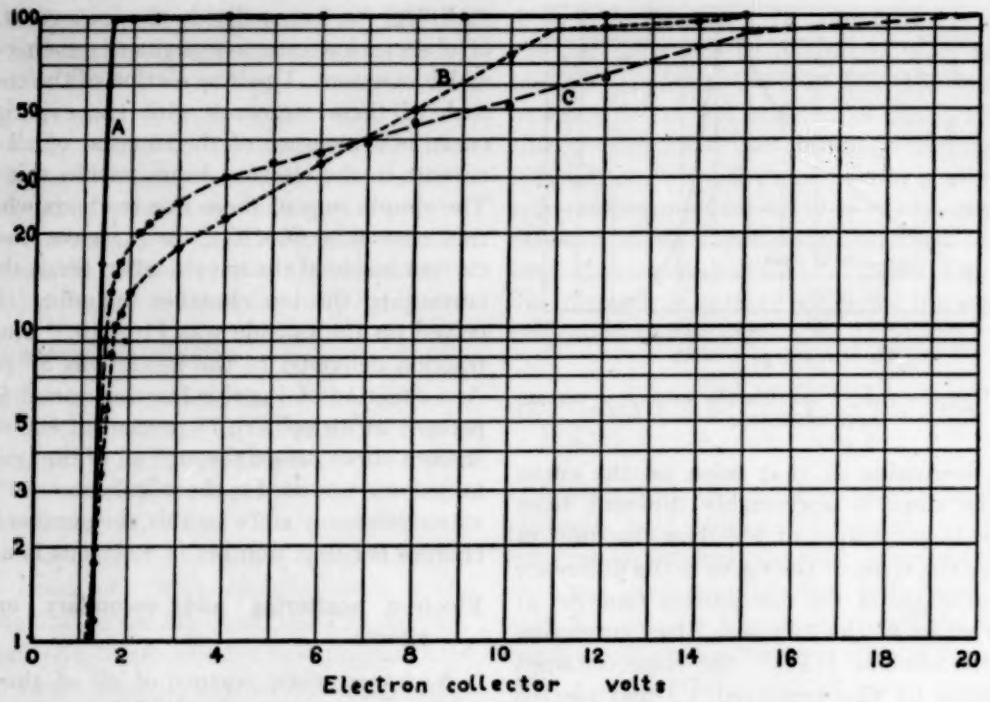

FIG. 12. Electrons collected at *EC* as a function of its potential relative to the cathode. Hg at liquid air temperature, getter at room temperature. Scattering mostly from residual mercury vapor. Scale of ordinates of each curve adjusted to 100 at maximum.

the ion chamber potential was the flat portion on both sides of the peak. (See Fig. 8.) Experiment showed that the ratio of this current to the primary beam current was nearly independent of the electron energy but did depend directly on the gas pressure. It seems certain therefore that this represents electrons scattered by the gas in the ion chamber which in the case represented in Fig. 8 was the residual gas after all of the mercury vapor had been removed.

For electron energies less than about 50 volts the effects of secondary emission within the ion chamber were so small that they could not be detected. Certain effects above this voltage are illustrated by the curve of Fig. 11. Here the current received at *EC* is plotted on a logarithmic scale as a function of the ion chamber potential V_i while all other voltages were constant. The main points of interest are (1) the broad maximum at 75 volts, (2) the sharp minimum at 97 volts, (3) the minimum at 126 volts and (4) the maximum at 135 volts. First the 75 volt maximum must have been due to the fact that a considerable number of the secondary electrons produced by the primary beam had an initial energy of two to three volts as indicated on the auxilliary scale and that these followed circular trajectories from their point of origin into the exit slit. As the beam energy increased the initial secondary electron energy which would permit its path to pass through the exit slit decreased and, since the yield to the exit slit decreased so sharply, one may interpret the 97 volt minimum as an indication that there are relatively few very low energy secondary electrons produced here. The minimum at 126 volts occurred when the main beam of electrons was projected into the right-angled corner formed at the intersection of the curved back of the ion chamber with the flat face plate. On this side of the slit very few secondary electrons found their way into the exit slit and when the beam impinged at the corner even these were absorbed more efficiently and left only the electrons scattered by the gas to give the current observed. The ratio of this current to that at the peak of the curve when compared with that of Fig. 8 illustrates the fact that the gas scattering was nearly independent

of the electron energy. The rise in the curve to a maximum at 135 volts is an indication that more secondary electrons are produced when the primary beam strikes the metal surface at grazing incidence than at perpendicular incidence. The same is true of the x-rays produced.

Collection of electrons against retarding potentials

As illustrated by Fig. 8, the main electron beam as measured at the electron collector *EC* had "wings" on both sides of the peak as a result of the scattering of the electrons by the gas molecules. By applying retarding potentials between the electron collector and the ion chamber an approximate indication of the electron energy distribution of these scattered electrons was obtained. A number of studies were made of electron energy distributions with various settings of the magnetic field and ion chamber potential. Typical of these are the three curves shown in Fig. 12 for which the magnetic field was set to permit 10.84-volt electrons to pass through the ion chamber when a V_i of 12.11 volts was applied. Curve *A* shows the current received by *EC* as a function of its potential relative to the filament when V_i was 12.11 and thus allowed the main beam to go into *EC*. It is of interest to note that no decrease in the current received was observed until the collector was less than two volts positive to the filament or until more than a ten-volt retarding potential existed between *EC* and the ion chamber. Between one and two volts the fall in current was very rapid and detailed analysis showed that this occurred about 0.3 volt sooner than it should purely from the energy standpoint. Three factors contributing to bring about this cut-off were (1) the effect of the magnetic field producing curved orbits for the slowed down electrons, (2) the bending of the electron trajectories due to the distorted electric field in the neighborhood of the slits, and (3) the possible reflection effect[9] for slow electrons.

Curves *B* and *C* were taken with values of V_i of 11.0 and 15.0 volts, respectively, and show that the energy distribution of the scattered electrons was almost Maxwellian in that it was represented by a straight line on a semi-logarithmic plot. Breaks come in these curves at 11.0 and 15.0 volts, as they should, indicating that there was no contact potential difference between the inside of the electron collector and the inside of the ion chamber.

Ionization Efficiency

Formulae for conversion of observed results to standard units

For electron energies greater than 29 volts, it is necessary to distinguish between the *efficiency* of ionization and the *probability* of ionization. The latter is defined in terms of the number of ions of a particular kind such as singly, doubly, or triply ionized atoms which are produced per electron per centimeter path while the *efficiency* of ionization is defined in terms of the total number of units of ionic charge produced per electron per centimeter path. Where ionization in mercury vapor is produced only by single collisions, there is no difference between the efficiency and the probability of ionization below 29 electron volts, but above this each doubly ionized atom contributes two charges to the efficiency function, and so on. The present study has determined only the efficiency of ionization as a function of the electron energy but this can be converted to the ionization probability by using the curves published by Bleakney[12] for the relative proportions of ions of different charges as a function of the energy of the bombarding electrons.

An electron current i_- sent through the ionization chamber along a path of length L through mercury vapor of density n atoms per cubic centimeter, produced a current i_+ of ions observed at the ion collector *P* (of Fig. 1a) which is given by the following formula.

$$i_+ = \alpha i_-(1-\epsilon^{-\epsilon_i n L}). \tag{5}$$

Here α is the fraction of the total number of ions produced which found their way to the collector *P* and ϵ_i the ionization "cross section." This is related to the ionization efficiency E_i by the following:

$$E_i = n_0 \epsilon_i, \tag{6}$$

where $n_0 = 3.56 \times 10^{16}$ which is taken[13] to be the number of atoms per cubic centimeter in an ideal

[12] W. Bleakney, Phys. Rev. **35**, 139 (1930).
[13] R. T. Birge, Rev. Mod. Phys. **1**, 1 (1929).

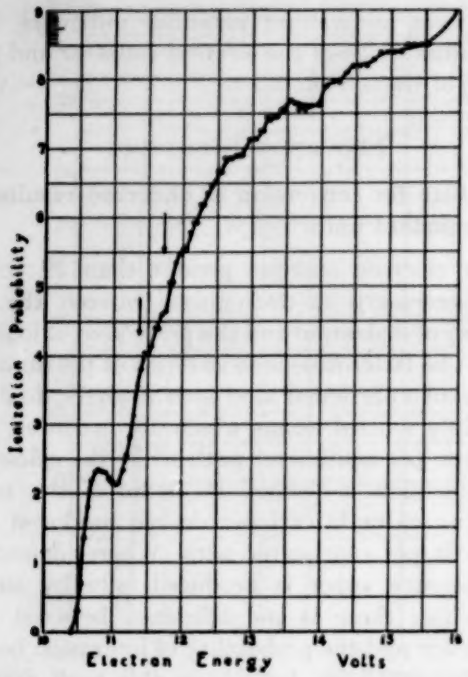

FIG. 13. Probability of ionization in mercury vapor as a function of electron energy in volts. Arrows show location of "negative energy" states.

gas at a pressure of 1.0 mm of mercury and at the temperature of 0°C or T_0°K. (If T_0 is taken at some other value than 273°K, then n_0 will be numerically different.) If T_1 is the absolute temperature of the mercury reservoir and p_1 the vapor pressure of mercury at the temperature T_1, and T is the temperature in the ionization chamber, then assuming ideal gas laws, we have the following expression for n.

$$n=n_0p_1T_0(T_1T)^{-\frac{1}{2}}. \tag{7}$$

Combining these three equations and assuming that experimental conditions are such that $\epsilon_i nL$ is very small, we obtain

$$E_i=(i_+/\alpha i_-)(T_1T)^{\frac{1}{2}}/p_1T_0L. \tag{8}$$

From the discussion so far each of these quantities is directly observable except α and this requires some further explanation. As mentioned above, the ion current was measured as a function of the electron energy with *"neutral field"* conditions along the path of ionization. Over the range for which the ionization efficiency changes rapidly with electron energy it was impossible to determine the value of α by direct measurement since the application of electric fields within the ion chamber to sweep all of the ions to the collector would have destroyed the homogeneity of the electron energies and invalidated the results. Even though the value of α depended to a certain extent on the potentials applied to the ion collector P and the outer grid G_1 to create the "neutral field" condition, it was still possible to put together a sufficient number of overlapping curves to obtain a single complete curve giving the *relative* efficiency of ionization over the entire range of observation from the ionization potential up to 100 volts. As will be shown below, there was a broad maximum in this curve as is well known from the results of previous investigators. Clearly observations made near this maximum did not depend to any great extent on the homogeneity of the electron beam and therefore in this region sweeping-out fields were applied to collect all of the ions at a collector without appreciably vitiating the results and thus allowed the determination of α.

Vapor pressure of mercury

Two sources were used for data on the vapor pressure of mercury. These were the Landolt-Börnstein tables[14] and Kelley's[15] compilation of vapor pressure data. From these two sources the following two equations were obtained:

$$\text{(Kelley)}\quad \log_{10}p=-3283/T-0.827\log_{10}T+10.37, \tag{9}$$

$$\text{(L. and B.)}\quad \log_{10}p=-3342.26/T-0.847\log_{10}T+10.5724. \tag{10}$$

The range of application of the latter formula is given as $-10°$ to $+200$°C. The two formulae above agree very well over the range needed for the present study and can be represented to the required accuracy by the equation

$$\log_{10}p=8.12-3220/T, \tag{11}$$

or

$$p=132\times10^8e^{-7415/T}. \tag{12}$$

In all of the above equations the pressure is given

[14] M. Knudsen, Ann. d. Phys. **29**, 179 (1909); Landolt-Börnstein, Vol. II (1923), p. 1334.
[15] K. K. Kelley, Bureau of Mines Bulletin 383.

in millimeters of mercury and the temperature is in °K.

Ionization near the ionization potential

The final results obtained for the ionization probability in the immediate neighborhood of the ionization potential are presented in Figs. 13 and 14. The general similarity between the curve of Fig. 13 and that obtained by Lawrence[2] is at once obvious. In Fig. 14 the ionization probability has been plotted on a logarithmic scale in order to make available the data obtained within the first few tenths of a volt of the ionization potential. The circles shown give the results as observed without making corrections for the slit width and a small photoelectric current of electrons released from the ion collector by the radiation in the ion chamber. Since the details as to the distribution of electron energies could not be known exactly, it was impossible to apply a rigorous method for reducing the observed results to an accurate ionization probability curve. Approximate methods were used with the result that the solid line shown is thought to be as accurate a representation of the actual probability curve as can be drawn.

The maximum observed at 10.8 volts and the minimum at 11.05 volts are in some ways the most interesting details of the curve. It is quite possible that the cathode fall in a mercury arc discharge is stabilized to a considerable extent because of the fact that 10.8-volt electrons have a higher probability of producing ions than other electrons with energies up to 11.15 volts. The other structural features shown in Fig. 13, are no doubt of less practical significance but may be important to the detailed understanding of the collision process in mercury vapor.

It hardly seems necessary to attribute these irregularities to "ultra-ionization" potentials as is usually done.[2–6] The interpretation which seems most natural is closely related to the proposals made by von Hippel.[16] As will be shown below, the excitation of the $2^3P_1^0$ state of the mercury atom from the 1^1S_0 state, by electron bombardment has zero probability at 4.87 volts (the minimum energy for excitation) but at 5.6 volts the electron has its maximum probability of producing this transition. Although this experiment can not be said to be absolutely conclusive for reasons which will be given, the indications were that no such clear maximum exists for the transition to the 2^1P_1 state. The possibility that the excitation function for intercombination transitions generally has a maximum within a few tenths of a volt of the minimum energy required for excitation and that terms within the singlet system may not have this maximum so near to the minimum excitation potential has been recognized for some time. Since the series limits of both the triplet series and the singlet series are at 10.38 volts it seems reasonable to suppose that the probability of ionization would have a twofold character and that the peak at 10.8 volts might be ionization according to the mode of the principal triplet series while the general background and broad maximum at about 32 volts is to be associated with ionization without change in spin momentum which characterizes the singlet system. Other details, which may be seen between 11.5 and

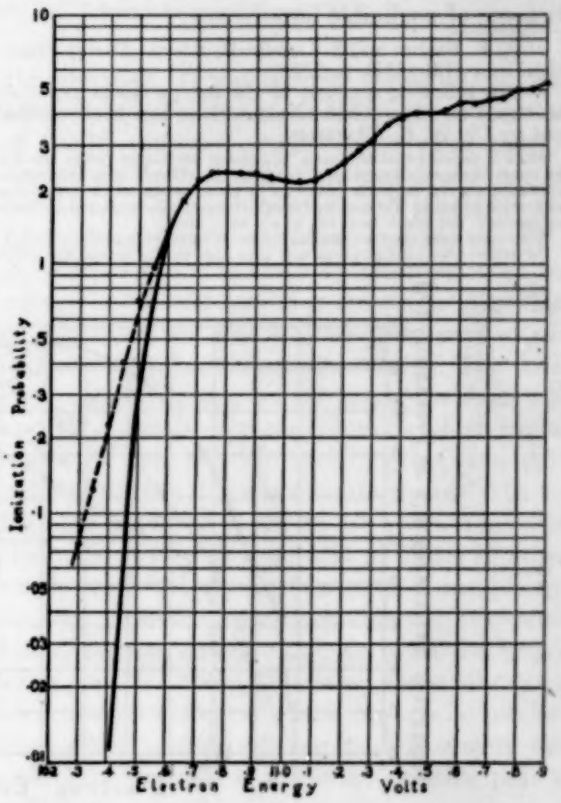

FIG. 14. Probability of ionization showing details within first volt from ionization potential.

[16] A. von Hippel, Ann. d. Physik **87**, 1035 (1928).

15.5 volts, may be due to the influence of the "negative energy" states which involve the initial absorption of energy by both of the valence electrons with the ultimate expulsion of one of these electrons with considerable kinetic energy and the return of the atom to the unexcited ionized state. The location of two of the known "negative energy" states[17] are indicated on Fig. 13 by arrows. The fact that "kinks" occur near these points may be without significance since the probability curve for a particular mode of excitation cannot be expected to have a high value when the electron energy barely exceeds the minimum required for its excitation. In some ways it seems that the more complicated the process of excitation is the nearer the maximum of the probability curve comes to the minimum energy value. Above 15.5 volts no detailed structure could be clearly demonstrated. This suggests that within the first two or three volts of the ionization potential the probability curve is dominated by the superposition of a number of modes of ionization while above 15.5 volts these become of negligible importance.[18]

[17] R. F. Bacher and S. Goudsmit, *Atomic Energy States*, (McGraw-Hill 1932), p. 227.

[18] The following analysis of the energy states expected as based on theoretical considerations has been worked out by Dr. W. E. Albertson.

Since it appears that the most prominent excitation peaks are due to intersystem combinations of the type $^1S_0 - {}^3P_1^0$ it is of interest to speculate on the probable positions of those peaks which arise from excitation to other $^3P_1^0$ and $^3D_1^0$ levels theoretically expected to occur in mercury, but which have not as yet been found.

There are three electron configurations of interest, namely:

$5d^{10}6s^26p$—this configuration will give rise to the levels $^3P_1^0$, $^1P_1^0$, and $^3D_1^0$, all of which have J values of one. Consideration of the relative bindings of the $5d$ and $6s$ electrons indicates that the terms of this configuration occupy the region 8.1 to 11.0 volts above the ground state. $^3P_1$ and $^3D_1$ will probably be below the I.P. (10.38 volts), whereas $^1P_1$ may be close to, but above the I.P.

$5d^{10}6p7s$ and $5d^{10}6p6d$—the former will give rise to the combining levels $^3P_1^0$ and $^1P_1^0$, the latter to $^3P_1^0$, $^1P_1^0$ and $^3D_1^0$. Since the excitation to these states involves a two-electron jump from $5d^{10}6s^2$, it is quite possible that the resulting peaks will be comparatively insignificant.

A rough evaluation of the energies of these configurations may be made by considering the difference in energies between the $6s$ electron and the $7s$ and $6d$ electrons and adding those energies to that of the $5d^{10}6p6s$ configuration.

The difference in energy between $6s^2$ and $6s7s$ is 7.8 volts, hence the excitation potential of $5d^{10}6p7s$ will be, to a first approximation, 4.6 plus 7.8 or 12.4 volts. The levels from this configuration should spread over a region of about two volts, hence the excitation potentials should be near 12.4 volts and on up to 14.4 volts.

In like manner it can be estimated that the excitation potentials for levels from $5d^{10}6p6d$ should be near 13.4 volts and on up to 15.4 volts.

While these estimates are not necessarily accurate to within a volt, they do fall in the range necessary to afford a plausible explanation of several of the minor excitation peaks between 12.5 and 14.5 volts.

(For notation see Chap. XII of H. E. White, *Introduction to Atomic Spectra*, (McGraw-Hill, 1934).)

Ionization by high energy electrons

When mercury vapor is bombarded by electrons with energies exceeding 29 volts, both singly and doubly charged ions are produced with the result that the *efficiency* of ionization is observed instead of the *probability*. The solid curve of Fig. 15 shows the result obtained. Bleakney[12] observed in a mass spectrograph the relative proportions of singly ionized and doubly ionized atoms as a function of the electron energy. His curves were used to reduce the observed efficiency curve to the probability curve, as shown by the dashed line of Fig. 15.

The dotted curves of this figure present the results obtained by Smith[5] and by Compton and

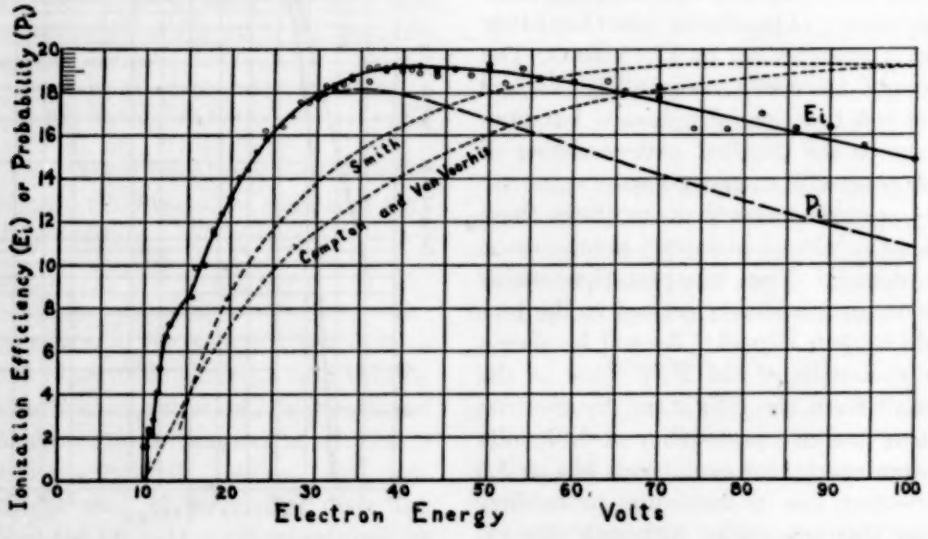

FIG. 15. Efficiency of ionization as a function of electron energy. Dashed curve P_i is probability of ionization with the loss of only one electron. Correction depending on Bleakney's curves.[12]

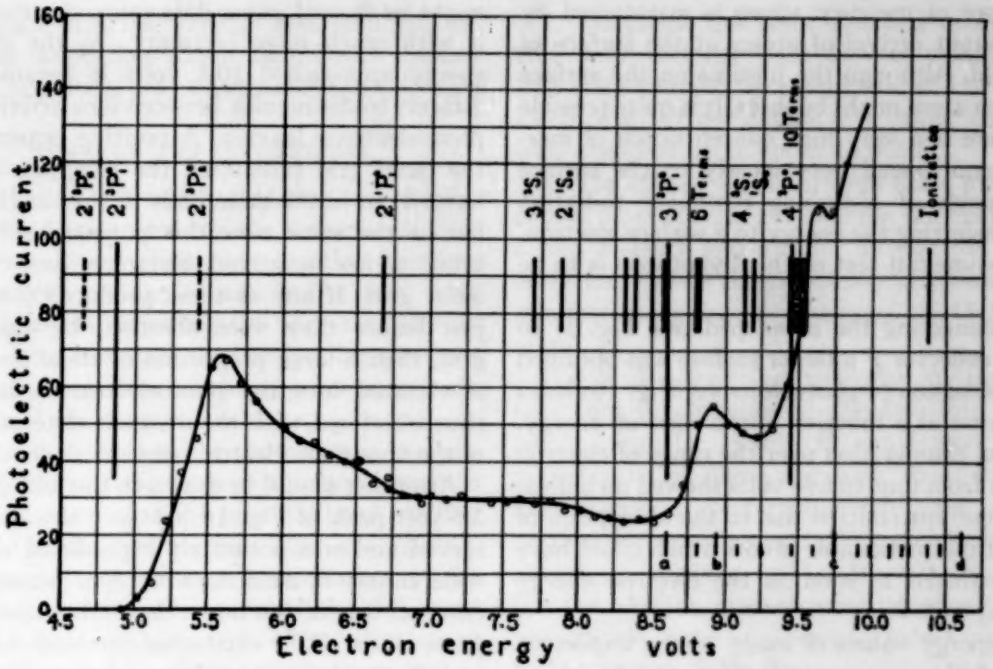

FIG. 16. Photoelectric current from inner grid and electrode P as a function of electron energy. Energy levels of mercury shown above and Smith's[5] critical potentials displaced downward 1.8 volts, shown at lower right. Onset at "a," larger deviations at "b" and "c," hump between "d" and "e."

Van Voorhis.[1] Comparison of these different efficiency curves shows that reasonable agreement exists but the differences greatly exceed the estimated errors in each case. Although certain difficulties experienced by the previous investigators can be pointed out, it cannot be said that the differences are explained in that way. In the present case every test that could be devised to test the validity of the final results was used. Under all circumstances the fact that the ion current was accurately proportional to the electron current indicated that ionization by multiple collisions could be neglected. The ion current was observed to be directly proportional to the mercury density in the ion chamber. This served to show that very few electrons produced ionization at more than one collision. The data for the probability curves shown were taken with the mercury reservoir at 0°C.

EXCITATION OF OPTICAL LEVELS

Excitation of $\lambda = 2537$A radiation

Because of the small area of the ion collector P only one quantum in 1500 was intercepted by this electrode. It was thought therefore that the photoelectric current produced by the absorption of 2537A radiation would be so weak that it could not be detected. This was found not to be the case for experiment showed that $\beta P_e = 0.4$ where P_e is the probability of exciting the $2^3P_1^0$ state from the 1^1S_0 state by electrons with an energy of 5.6 volts and β is the probability that a light quantum which strikes any part of the collector P will emit a photoelectron. The collision probability as given by Brode[19] is about 120 and the fraction of these collisions which excite atoms to this state is probably between 0.01 and 0.1. Seiler's[20] determination gives 0.04 at his maximum and 0.025 at 5.7 volts. This sets the range of β to be from 0.33 to 0.033. In other words, with the smaller value of β one photoelectron is produced for every thirty light quanta falling on the surface of P, or, with the larger value, one in three. This is an unusually large yield and probably calls for some special mechanism which is more efficient than is usually the case. For example, it might be possible that a

[19] R. B. Brode, Proc. Roy. Soc. **A125**, 134 (1929).
[20] R. Seiler, Zeits. f. Physik **83**, 789 (1933).

monolayer of mercury atoms is maintained by the constant arrival of atoms at the surface of the metal. Although the lifetime on the surface of a given atom might be short, it is quite possible that there is a very high concentration of mercury atoms bound very loosely to the surface and capable of absorbing resonance radiation and transferring the energy to a surface electron. An experimental test of this hypothesis is to be made.

By connecting the inner grid (see Fig. 1) to the ion collector P a larger surface was obtained for the emission of photoelectrons. Fig. 16 shows the current as a function of the electron energy. A careful examination over the range of electron energies from four to five volts showed no indication of current emitted due to the absorption of energy from metastable atoms which could have been produced as soon as the electron energy exceeded 4.65 volts.

The energy values of many of the important terms of the mercury spectrum are shown on Fig. 16. A comparison between the observed current and the indicated energy levels shows that the 5.6-volt peak with its onset at 4.9 volts must be associated with the $2^3P_1^0$ transition. There may be two explanations for the fact that there was no important variation in the photoelectric current as the electron energy exceeded that required to excite the $2^1P_1^0$ level. These are, first, the surface might not have been as sensitive photoelectrically to the $\lambda = 1849$A radiation as it was to the 2537A radiation for which it seemed to be abnormally sensitive, and secondly, it is possible that the probability function associated with this transition may start rising very slowly and reach important values at ten or more volts. The sharp rise in photoelectric current beginning at 8.6 volts and reaching a maximum at 8.9 volts seems to be definitely related to the $3^3P_1^0$ term located at 8.60 volts. The next peak located at 9.62 volts is probably associated with the excitation of the $4^3P_1^0$ level which requires a minimum energy of 9.44 volts. The onset in this case is less distinct because of the rapid rise in general background of photoelectric current which becomes so important for energies greater than 9.0 volts. Although the set of data presented in Fig. 16 does not establish the existence of the 9.6 volt peak as convincingly as might be desired, other data taken demonstrated it with much more certainty. As the electron energy approached 10.4 volts it became very difficult to distinguish between ions arriving and photoelectrons leaving. A positive potential on the outer grid prohibited the reception of ions formed out in the main body of the ion chamber but at the same time this potential served to bring a few scattered electrons over to the outer grid. If any of these produced ionization just before they were absorbed by the outer grid, then a large proportion of these ions were accelerated into the photoelectric surface and thus interfered with the accurate determination of the true photoelectric current.

Attention should be drawn to the fact that the 5.6-volt peak of Fig. 16 has been drawn as observed and was accurately reproduced under a wide variety of conditions of vapor pressure and current. One of the latest determinations of the form of the $2^3P_1^0$ excitation function was that of Seiler[20] whose observations were much more indirect in character and led him to conclude that the maximum of the probability function occurred at 6.9 volts. A redetermination of this function using experimental techniques so as to measure the absolute values of the probability function, would no doubt be of great value.

A critical examination of Smith's[5] experimental results leads to the interpretation that some of his "ultra-ionization" potentials were due to photoelectric effects. In his Fig. 7 there is a very noticeable "hump" in the curve near 12.6 volts according to his scale. If it is assumed that this is the 10.8 volt maximum of Fig. 13 then a displacement of his set of critical potentials by 1.8 volts would be demanded. With the intervals maintained as published by Smith, these critical potentials have been recorded, as shown in Fig. 16. It is obvious at once that this displacement brings his first value (a) to 8.6 volts, which marks the beginning of the big rise in the photoelectric current. Critical potentials at (b) and (c) corresponded to larger deviations from a smooth curve than some of the others and might be related to the maxima at 8.9 and 9.6 volts. The "hump" mentioned above lies between (d) and (e). There are many term levels between 9 and 11 volts which are not shown in the figure and since some of these no doubt have excitation

functions which rise rapidly and then fall off, it seems altogether likely that Smith's many critical potentials may be explained in this way.

Summary and Conclusions

1. It has been demonstrated that it is possible to build an apparatus for the determination of the electronic excitation and ionization functions of mercury, which is sufficiently free from spurious effects to permit the accurate determination of the energy of the bombarding electrons from the dimensions of the apparatus and the strength of the magnetic field.

2. Measurements of the photoelectric current, emitted from an electrode within the region of excitation, show that the probability of exciting the $2^3P_1^0$ level of the mercury atom rises rapidly from zero at 4.9 volts to a maximum at 5.6 volts and that the excitation of the $3^3P_1^0$ and the $4^3P_1^0$ levels are characterized by similar curves with maxima at 8.9 and 9.6 volts, respectively.

3. Ionization has been observed to set in at 10.4 volts and rise to a distinct maximum at 10.8 volts followed by a minimum at 11.05 volts. Definite structural details of a minor character were observed up to about 16 volts.

4. The *efficiency* of ionization has a maximum of 19.2 ionic charges per electron per cm path at 1 mm pressure and 0°C for an electron energy of 42 volts while the *probability* of ionization to the first stage has a maximum of 18.2 at 32 volts.

It is a pleasure to acknowledge my indebtedness to my colleagues at the Institute and in particular to Dr. Arthur R. von Hippel for the opportunity of discussing with them many of the interesting problems which arose in connection with this research. For technical assistance I am indebted to Mr. Allyn B. White and for the skillful glass-blowing required in the preparation of the experimental tube I owe much to Mr. Lawrence W. Ryan.

JANUARY 15, 1939 PHYSICAL REVIEW VOLUME 55

Spark Breakdown Potentials as a Function of the Product of the Pressure by the Plate Separation in A, N_2 and H_2 for Pt and Na Cathodes

Florence Ehrenkranz
University of California, Berkeley, California

(Received September 22, 1938)

Measurements were made on the sparking potentials between fixed plane parallel electrodes in purified, *mercury-free* A, N_2 and H_2 for Pt and Na cathodes for extended pressure ranges. The effect on the sparking potentials in H_2 produced by heated Pt and Na cathodes was investigated. In all of the gases studied, the values of the sparking potential are lower for a Na-coated Pt cathode than for a clean Pt cathode throughout the pressure ranges investigated. The percentage lowering, which is especially pronounced near the minimum sparking potential, decreases with increasing $p\delta$. In A, the sparking potentials for a Pt cathode agree very closely with the Fe cathode values of Penning except in the vicinity of the minimum sparking potential; the discrepancy at low values of $p\delta$ is caused by the difference in cathode surface. For a Na-coated surface, the sparking potentials are 50 percent lower in the vicinity of the minimum and 7.5 percent lower at $p\delta$ equal to 240 mm×cm. The predischarge currents within a few volts of breakdown were less than 10^{-9} amp. for both Na and Pt surfaces. The effect of a Na cathode on the breakdown potentials in A is in satisfactory agreement with the quantitative predictions of classical Townsend theory given by Loeb. In N_2, the lowering produced by Na is 28 percent near the minimum and 20 percent at $p\delta$ equal to 340 mm×cm. The N_2 results are not applicable to the theory discussed by Loeb because of the heavy predischarge currents, 360 microamperes at $p\delta$ equal to 356, which occur in the presence of Na. The lowered sparking potentials and the heavy predischarge currents, as well as the increase in the values of the Townsend coefficient α in the presence of a Na-covered cathode which was observed by Bowls, indicate that there occurs in the presence of Na a volatile substance, Na or something else, of vapor pressure greater than 10^{-4} mm and ionization potential less than that of N_2 which acts independently of cathode phenomena. H_2 is intermediate between N_2 and A both with respect to the approach of the Na and Pt curves at high $p\delta$ and the magnitudes of the predischarge currents. In the H_2—Na case, the marked predischarge currents and the lowered sparking potentials are probably caused

by a volatile impurity, Na or something else. The sparking potentials in H_2 with heated Pt and Na cathodes are identical within the limits of experimental error. The coincidence at both low and high values of $p\delta$ may be explained by the formation of NaH and the distilling off from the heated surface of the Na and/or NaH. At low values of $p\delta$, the sparking potentials are governed considerably more by cathode phenomena than by the primary process of ionization by collision. The *heated* Na cathode has no Na nor NaH deposited on it; the cathode emission properties are the same therefore as those of the heated Pt surface. Hence, the sparking potentials are the same. At high values of $p\delta$, α is predominant in determining the sparking potentials, and α is very sensitive to the presence of Na. The formation of NaH, which occurs because of the presence of the heated cathode, probably removes most of the Na vapor and destroys all of the volatile substance which causes the lowering in the case of the cold Na cathodes.

Introduction

NUMEROUS investigations,[1–3] of which those of Paschen[4] in 1889 were among the earliest, on sparking potentials as a function of the product of the pressure by the plate separation $p\delta$ have established the general form of curve which obtains for all gases. This well-known curve has a minimum at some value of $p\delta$, between 0.5 and 4 mm Hg·cm for most gases. Recently, Penning[5–7] and his associates have shown that very small traces of mercury vapor, for example 10^{-4} percent, greatly lower the values of the sparking potential as a function of $p\delta$ in the inert gases, neon and argon. No measurements of sparking potentials in a mercury-free *molecular* gas have been reported. Further, no investigation with modern technique on the effect of *cathode material* on the breakdown potentials *over an extended pressure range* has been made. Loeb[8] has shown that classical Townsend theory predicts a marked cathode effect at low pressures and a small cathode effect at high pressures.

It was the purpose of this investigation to determine the sparking potentials between fixed, plane parallel electrodes, with Pt and Na-coated Pt cathodes, in purified, mercury-free N_2, H_2, and A for extended pressure ranges. Measurements were made for $p\delta$ equal to and greater than the $p\delta$ which corresponds to the minimum sparking potential. Pt and Na-coated Pt surfaces were used because it was anticipated that a cathode effect would be especially marked for these metals because of the large difference in work functions. N_2 was used for the molecular gas because it was hoped that a correlation could be made between the sparking potential data and Bowls'[9] data on the Townsend coefficients in mercury-free N_2. The unexpected results of Bowls on the Townsend coefficients and the

[1] J. J. Thomson, *Conduction of Electricity through Gases* (1903), p. 352.
[2] W. O. Schumann, *Elektrische Durbruchfeldstärke von Gasen* (1923), pp. 94, 95, 96.
[3] Engel and Steenbeck, *Elektrische Gasentladungen*, Vol. 2 (1934), p. 335.
[4] J. S. Townsend, *Electricity in Gases* (1916), p. 351.
[5] F. M. Penning, Naturwiss. **15**, 818 (1927).
[6] F. M. Penning, Zeits. f. Physik **46**, 341 (1928); **57**, 723 (1929); **72**, 338 (1931).
[7] Penning and Addink, Physica **1**, 1007 (1934).
[8] L. B. Loeb, Rev. Mod. Phys. **8**, 267 (1936).
[9] W. E. Bowls, Phys. Rev. **53**, 293 (1938); Thesis (University of California Pub.) 1938.

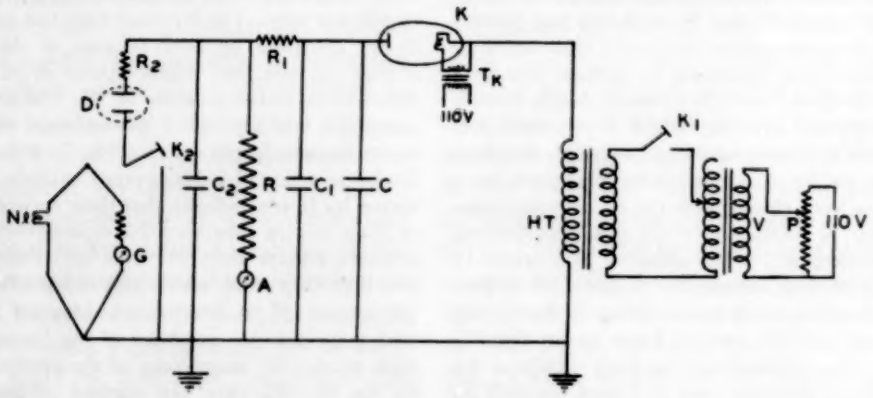

FIG. 1. Diagram of electrical circuit.

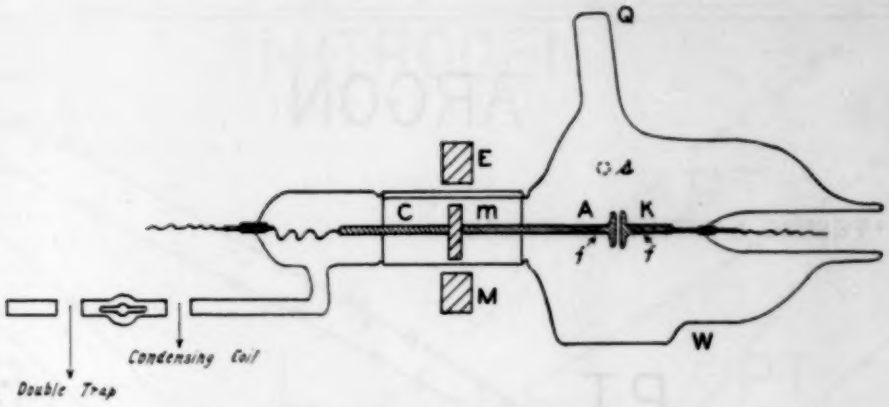

FIG. 2. Horizontal cross section of the discharge tube.

author on the sparking potentials for N_2 in the presence of a Na surface indicated that it would be very desirable to investigate a mercury-free molecular gas which is not characterized by metastable and active states. The second molecular gas chosen, therefore, was H_2. Argon was investigated because data obtained by Neuman,[10] several years ago, indicated that the sparking potentials in A for cold Ni and Na surfaces were identical for pressures greater than 20 mm; for lower pressures, the breakdown potentials were the same for a *heated* Na surface and a cold Ni cathode. It was of interest to see whether these results could be confirmed.

Apparatus and Experimental Procedure

The electrical circuit is shown in Fig. 1. Filtered, half-wave rectified voltage is impressed on the plane-parallel electrodes of the discharge tube, D, by the various devices indicated. Sparking potential measurements were made by throwing the switch K_2 to the right and observing the deflection in the current-reading instrument, A, as the voltage across the gap was increased slowly by manipulating the hand-operated variac, V. At breakdown the needle of A dips abruptly and the sparking potential is calculated from the current just before the breakdown and the resistance, R. Voltages above 750 volts are accurate to within 1.5 percent; voltages below 750 are accurate to within 2.5 percent except for voltages below 250, where the accuracy may be somewhat less.

Predischarge currents within a few volts of breakdown were measured by closing K_2 to the left and observing the reading of the galvanometer, G, just before the spark breaks.

A horizontal cross section of the discharge tube is shown in Fig. 2. The cathode, K, was 36 mm in diameter; the anode was slightly smaller. Both electrodes had curved edges; the curvature was such that flat portions were opposite. The cathode, which was fixed, consisted of 0.008-inch Pt sheet spun over a Ni plate; the anode was made of 0.118-inch Ni. The anode could be moved to any desired plate separation by the action of a double-pole electromagnet, EM. Various plate separations between 0.55 and 0.80 cm were used. For any one series of measurements, the plates were separated by a fixed distance and the pressure varied. The separation was measured by a comparator through the Pyrex window, W. The accuracy of this measurement is of the order of 1 percent.

Light could be focused on K through the quartz window, Q. A quartz mercury arc was used with the Pt cathode and a Mazda lamp with the Na surface. The side arm, s, contained a Na capsule. The capsule could be broken in vacuum. The Na in the capsule was purified by repeated vacuum distillation. The electrodes and the bulb itself were cleaned with acid, grain alcohol and distilled water.

The discharge tube was connected to the pressure gauges, the gas supply and the pumping system through a stopcock on each side of which was a liquid-air trap. The trap between the stopcock and the tube was a helical Pyrex coil

[10] L. J. Neuman, Proc. Nat. Acad. Sci. **15**, 259 (1929).

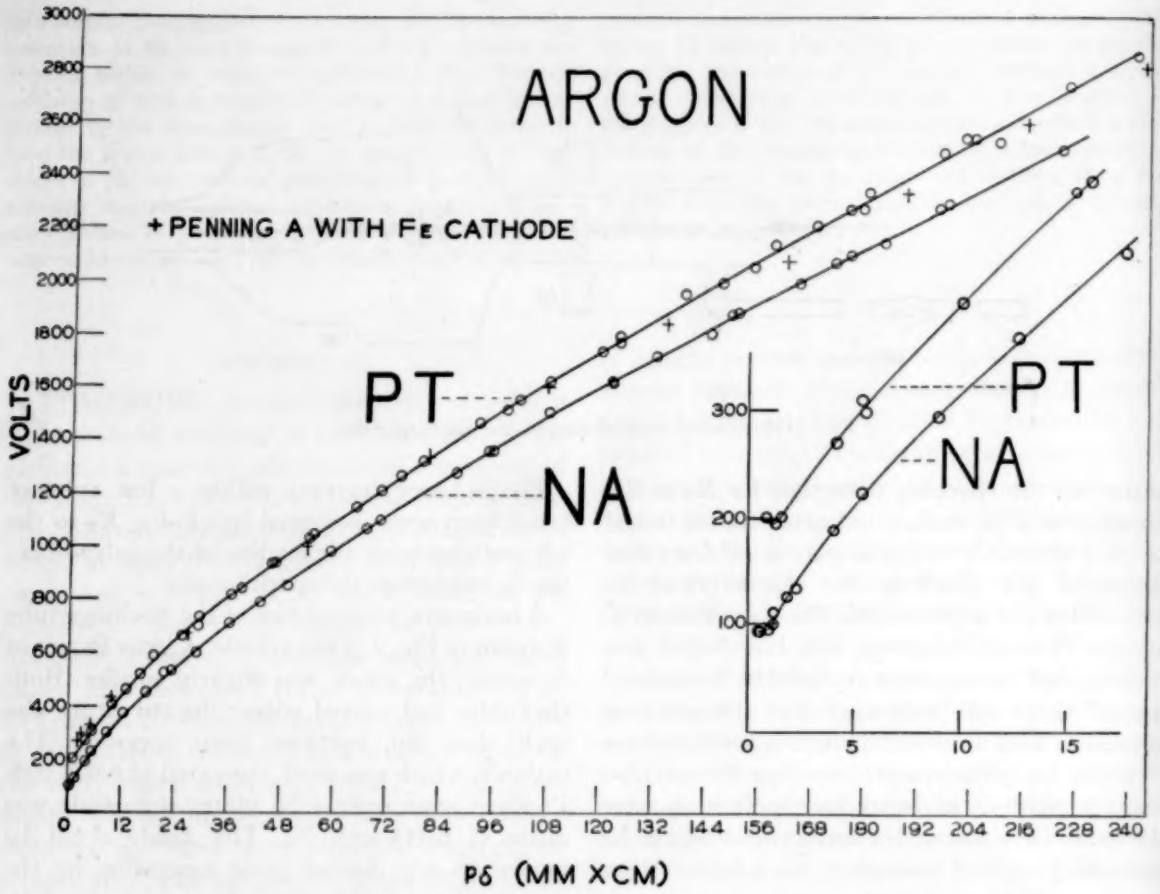

FIG. 3. The sparking potential as a function of pressure × plate separation for Pt and Na cathodes.

with an effective length of 43 cm. For each run made with the Pt cathode, the tube was outgassed at 490°C for one hour. All of the glass tubing between the gas reservoir and the tube was heated with a Bunsen flame during the outgassing of the tube. The stopcock was open only when the double liquid-air trap on the far side of the tube from the stopcock was immersed in liquid air. Before starting a run, a glow discharge was maintained between the plates for about one hour in a few millimeters of purified gas; this gas was pumped out and the tube flushed again with purified gas. Then gas was admitted to the tube at the beginning of the run to the highest pressure to be used in that series of measurements. Thus the usual procedure was to take a measurement at the highest pressure, pump gas from the tube, take another measurement and repeat until the minimum sparking potential was reached.

The procedure for the Na cathode experiments was as follows: The tube was outgassed at 490°C and allowed to cool. With the pumps still working, the Na capsule was broken and the Na distilled on the electrodes. After the Na had cooled, the tube was flushed with purified gas. For the next run, the Na was redistilled by heating the tube with a Bunsen flame. Liquid air was kept on the condensing coil continuously from the time the tube was outgassed until the last Na run for that tube was made. After taking two or three sets of measurements with a given Na surface, the tube and all its elements were dismantled and cleaned; then the tube was reassembled and a side arm containing a fresh Na capsule added.

Pressures were measured by a closed mercury manometer and a McLeod gauge. The accuracy of the pressure measurements was 1 percent or better except for the lowest pressures. For

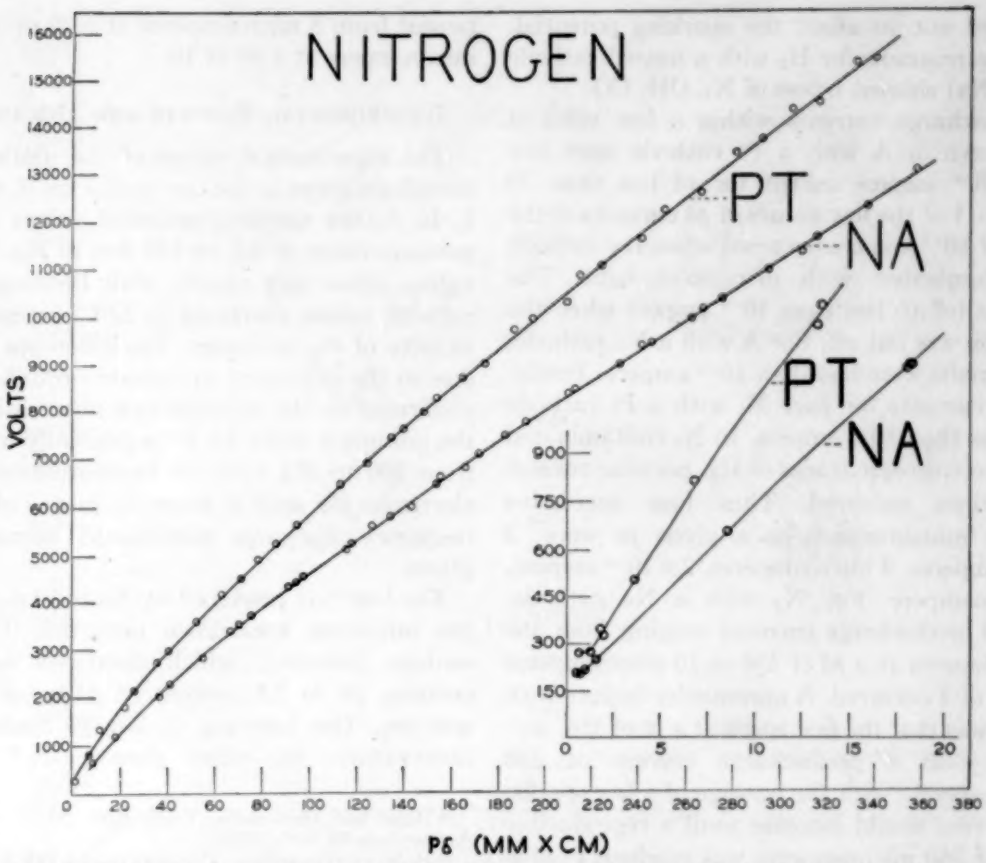

FIG. 4. The sparking potential as a function of pressure×plate separation for Pt and Na cathodes.

pressures less than 3 mm, the error may be greater than 1 percent. The pressures are given as read at the room temperature of 22°C.

PURIFICATION OF THE GASES, TESTS FOR PURITY, PREDISCHARGE CURRENTS

Commercial A was passed over a drying train and then was purified at a pressure of 55 cm in a Ca arc run on 220 d.c. at about 11 amperes for 110 hours. Commercial N_2 was purified by admitting gas very slowly over liquid air to a tube containing heated Cu and CuO filings. The gas then passed through a drying train and circulated in a tube containing a glowing tungsten filament. Electrolytic H_2 was used for most of the H_2 runs; for a few series of measurements, a palladium tube was employed.

The purity of the gases was investigated spectroscopically. Spectrograms in the ultraviolet region of a glow discharge maintained between the discharge plates were obtained by focusing a Hilger quartz spectrograph on the cathode. The sparking potential values given in Fig. 3 for A correspond to runs for which the spectroscopic tests showed no Hg and no bands. The values for N_2 for a Pt cathode given in Fig. 4 correspond to runs for which the spectrograms in the ultraviolet region showed N_2 bands only. *Series for which the spectrograms showed the resonance* Hg *line 2536*A *and/or* NO *bands, however weak, gave sparking potential values between 7 percent and 13 percent lower than those for pure* N_2. The ultraviolet spectrograms for H_2 with a cold Pt cathode always showed a weak OH band as an impurity. This is almost certainly formed from hydrogen and oxygen released from the electrode surface under the discharge conditions. The effect of spectroscopic traces of N_2 was to raise the sparking potential values by a small percentage above the values given. Spectroscopic traces of CO which occurred in one series of measurements

appeared not to affect the sparking potential. The spectrograms for H_2 with a heated cathode (Pt or Na) showed traces of N_2, OH, CO.

Predischarge currents within a few volts of breakdown in A with a Pt cathode were less than 10^{-9} ampere except for $p\delta$ less than 30 mm·cm. For the low values of $p\delta$ currents of the order of 10^{-7} ampere occurred when the cathode was illuminated with ultraviolet light. The currents fell to less than 10^{-9} ampere when the radiation was cut off. For A with a Na cathode, the currents were less than 10^{-9} ampere. Predischarge currents for *pure* N_2 with a Pt cathode were less than 10^{-9} ampere. In N_2 contaminated with spectroscopic traces of Hg, peculiar current fluctuations occurred. Thus four successive current measurements at a given $p\delta$ were: 2 microamperes, 3 microamperes, 2×10^{-9} ampere, 1 microampere. For N_2 with a Na cathode, marked predischarge currents ranging from 360 microamperes at a $p\delta$ of 356 to 10 microamperes at a $p\delta$ of 2 occurred. A noteworthy feature with N_2-Na was that the first spark at a $p\delta$ of 356, say, would yield a predischarge current of 230 microamperes; with the passage of a few sparks, the current would increase until a reproducible value of 360 microamperes was reached. Predischarge currents for H_2 with a Pt cathode were less than 10^{-9} ampere. For H_2-Na, the currents ranged from 8 microamperes at a $p\delta$ of 350 to 1 microampere at a $p\delta$ of 10.

Experimental Results and Discussion

The experimental values of the sparking potential are given in the curves of Figs. 3, 4, 6 and 7. In A, the sparking potential values cover a pressure range of 0.5 to 400 mm of Hg. The Pt values agree very closely with Penning's[7] iron cathode values, corrected to 22°C, except in the vicinity of the minimum. The difference there is due to the difference in *cathode surface*. This is confirmed by the experimental observation that the minimum value for Pt is gradually increased from 200 to 275 volts on bombardment of the electrodes for several hours by means of a high frequency discharge maintained between the plates.

The lowering produced by Na is 50 percent at the minimum breakdown potential. The percentage lowering, which decreases with increasing $p\delta$, is 7.5 percent at $p\delta$ equal to 240 mm·cm. The lowering at low $p\delta$ conforms to observations on other pure gases.[11–14] The

[11] Holst and Oosterhuis, Versl. Kon. Akad. van Wet. Amsterdam **29**, 849 (1920).
[12] Holst and Oosterhuis, Comptes rendus **175**, 577 (1922).
[13] James Taylor, Proc. Roy. Soc. **A114**, 73 (1927); **A117**, 508 (1928).
[14] Engel and Steenbeck, reference 1, p. 46.

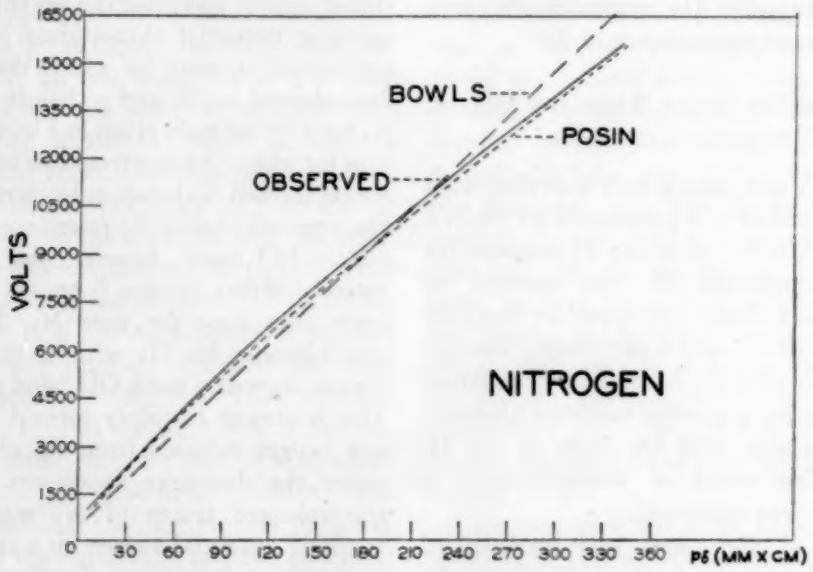

Fig. 5. Calculated sparking potential curves *vs.* the experimental curve for $10<p\delta<360$.

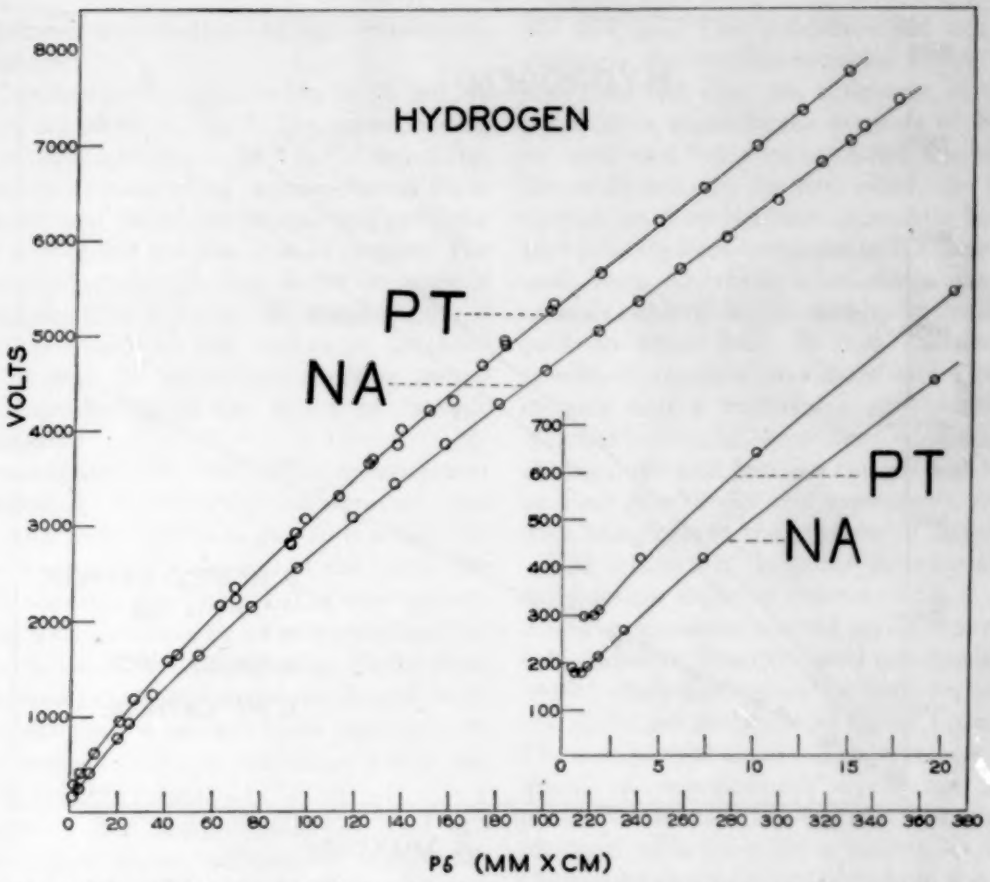

FIG. 6. The sparking potential as a function of pressure×plate separation for Pt and Na cathodes.

sparking potential values at high $p\delta$ do not become as nearly equal for the two cathodes as the simple hypotheses given in Loeb's[8] paper anticipate; nevertheless, the agreement between theory and experiment is satisfactory.

In N_2, the sparking potential values correspond to a pressure range of about 0.5 to 600 mm of Hg. The lowering produced by Na near the minimum is 28 percent and at $p\delta$ equal to 240 mm·cm, it is 20 percent. Thus, the results in N_2 appear to be highly anomalous with respect to theory since the 20 percent lowering produced in the presence of a Na cathode at high $p\delta$ is beyond its predictions. The discrepancy is probably to be associated with the heavy predischarge currents, since the theory does not consider the effect of such currents.

The inferences which may be drawn from the N_2-Na experiments are as follows.

(1) The lowering of the sparking potentials is in qualitative agreement with the increase in the Townsend coefficient, α, in the presence of Na observed by Bowls.[9]

(2) Both Bowls' results on an increased α and the author's results on high predischarge currents and lowered sparking potentials suggest that there occurs in the presence of Na a volatile substance which has a vapor pressure greater than 10^{-4} mm, an ionization potential less than that of N_2, and that it acts independently of cathode phenomena. That this vapor was not hydrogen, as suggested by Bradbury,[9] was proved by the deliberate introduction of various concentrations of hydrogen between 0.03 percent and 11 percent; the sparking potentials for the admixtures with a Pt cathode differed from those for pure N_2 by less than 2 percent. That the very low vapor pressure of Na at room temperature, 10^{-10} mm of Hg, cannot of itself account for his increase in α was shown by Bowls.

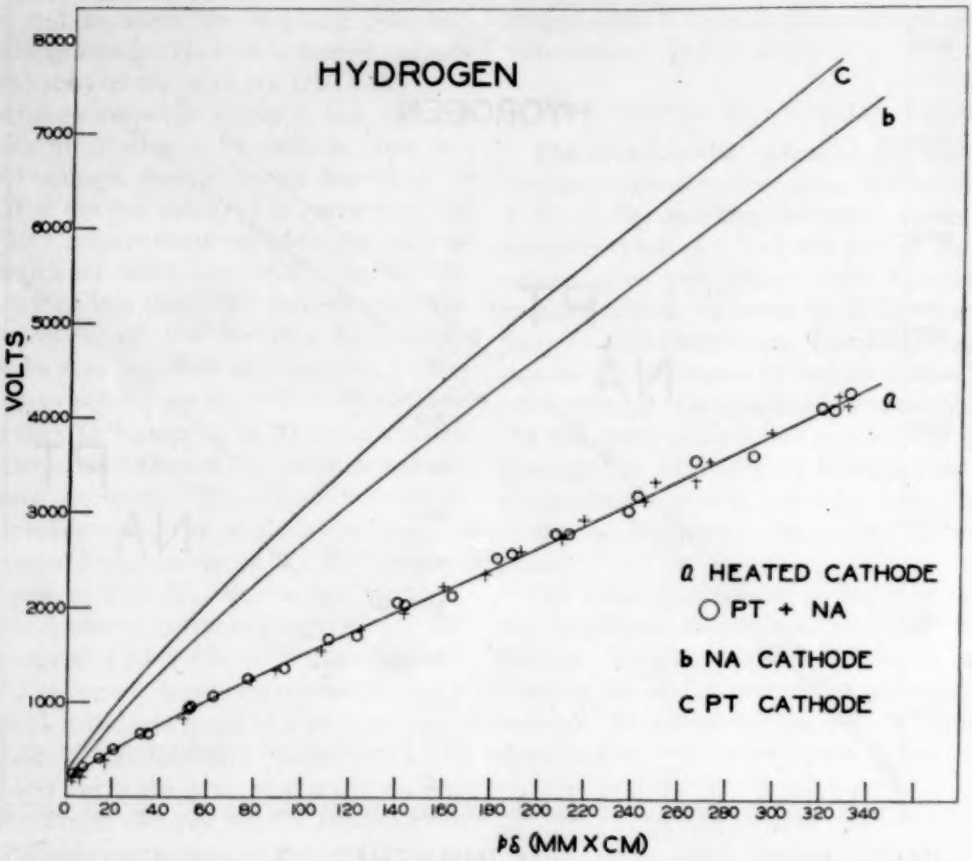

FIG. 7. The sparking potential as a function of pressure×plate separation for heated Pt and Na cathodes.

(3) Under the conditions of discharge in the present work, the Na vapor pressure may have been much greater than 10^{-10} mm of Hg; consequently, it is possible that the lowered sparking potentials are caused by ionization of Na atoms in the gap by metastable N_2 molecules of 8.2 volts energy and by electrons. At present, there is no definite evidence as to the character of the volatile substance. If it is Na, there is no completely satisfactory explanation of its exaggerated vapor pressure in Bowls' experimental chamber since he did not have discharge conditions and his gas-intensified photoelectric currents were very small, about 10^{-13} ampere.

An attempt was made to correlate the author's data for Pt with Bowls' data on the Townsend coefficients in mercury-free N_2.[15] The results of these calculations for a Pt cathode for $p\delta$ greater than 15 mm·cm are shown in Fig. 5. In the broken curve, values of V for $p\delta$ greater than 60 are extrapolated values from Bowls' data. It is seen that although Bowls' data are applicable, to these results, satisfactory agreement does not obtain between the Townsend coefficient data and the sparking potential data. This may, in part, be attributed to the lack of adequate data in Bowls' experiments at low X/p.

The dotted curve of Fig. 5 represents Posin's[16] values for the sparking potentials in N_2 computed from Townsend coefficients for *mercury-contaminated* N_2. In view of the observed lowering of the sparking potentials in the presence of mercury, it appears very probably that the agree-

[15] For the procedure used in making these calculations, see Loeb's paper, reference 8, pp. 276–7. In the present case, the empirical relation used was $\alpha/p=0.6 \ln X/p-2.32$; X/p is the ratio of the field strength in volts per cm to the pressure in mm of Hg. This relation fits Bowls' data for an X/p range between 94 and 59; the corresponding $p\delta$ range is between 15 and 100.

[16] D. Q. Posin, Phys. Rev. 50, 650 (1936).

ment between Posin's data and the author's data is fortuitous.

The breakdown potentials in H_2, for Pt and Na surfaces, are given in Fig. 6. The corresponding pressure range is from about 0.5 to 570 mm of Hg. The lowering produced by the presence of Na is 30 percent near the minimum sparking potential and at a $p\delta$ of 320 mm·cm, it is 11 percent. The marked predischarge currents in the presence of Na suggest that even in H_2 there occurs a volatile substance of low ionization potential which at high $p\delta$ lowers the sparking potentials independently of the action of cathode mechanisms.*

In connection with the H_2-Na measurement the following experimental observation was made. As a result of one or two runs with a Na surface a considerable amount of the Na on the cathode was changed to NaH. The new cathode material is recognizable by its grey color and the heating required for its distillation. Under these circumstances the sparking potentials with NaH present were only 4 percent lower than for a Pt surface except near the minimum where the lowering was 25 percent.

It appears as if the production of NaH had removed some of the volatile Na compound. Finally breakdown voltages in H_2 in the presence of heated cathodes were studied. The procedure in the heated cathode experiments was to heat the cathode to about 600°C. This distilled Na off the cathode and into the gap, and presumably gave Na vapor but a Pt cathode.

It was hoped that such a procedure might indicate whether the lowering of the sparking potential in H_2 in the presence of Na was caused by Na vapor in the gap or to Na actually deposited on the cathode. A definite answer would be given by this experiment only if no chemical reaction occurred between the heated Na and gas. This procedure did not exactly duplicate the conditions under which Neuman had observed that the difference in sparking potential in argon in the presence of Na vapor for cold and hot wire cathodes was the same above 20 mm. In the first place, the hot wire cathode used by Neuman apparently heated the *gas* relatively little compared to the large cathode used here. In these experiments the heated cathode reduced the gas density in the discharge path to about half. It was, therefore, only possible to compare runs made with a heated Pt cathode and a heated Na surface. Secondly, Neuman's results were not complicated by chemical reaction between the gas and Na, since he used A while in this experiment, one dealt with heated H_2 in the presence of heated Na.

The results for H_2 in the presence of heated cathodes are shown in curve *a* of Fig. 7. (Curves *b* and *c* represent control measurements with cold cathodes. The decreased gas density in the heated spark gap lowers the sparking potentials and shifts the minimum to higher values of $p\delta$.) The data plotted in curve *a* show that, within the limits of experimental error, the sparking potential values for a heated Pt cathode are identical with those for a heated Na cathode. One cannot, however, conclude from this that the Na in the gap did not change the sparking potential for it is probable that the formation of NaH removed most of the Na and destroyed all of the volatile substance which causes the lowering in the case of the cold Na cathode. The correctness of this explanation is confirmed by the fact that the operating temperature of the cathode, 600°C with an average gap temperature of 300° was sufficiently high to permit the formation of NaH, which occurs at 350°C, and to evaporate it off the cathode.[17, 18]

The author wishes to express her thanks and appreciation to Professor L. B. Loeb at whose suggestion the problem was undertaken and under whose direction it was carried out. In addition, the author wishes to acknowledge her indebtedness to Mr. William R. Stamper and Mr. E. H. Guyon for their assistance in the frequent dismantling and assemblage of the tube.

* *Note added in proof:* It has been possible to compare these data in H_2 with direct measurements in H_2 and with curves computed from Hale's values of α and γ in H_2 for Pt and for Pt coated with NaH between $p\delta = 1$ and $p\delta = 30$. In pure H_2 with Pt cathodes Hale's computed and observed values except at the minimum lie about 4 percent *above* the curves of Ehrenkranz. This was possibly due to small traces of impurity in Ehrenkranz's gas as a result of repeated sparking. In Hale's work only single values of the potential were taken for each filling. In the case of the NaH cathode the three curves coincide within the limits of experimental error except near the minimum.

[17] *Handbuch der Anorganische Chemie 11.* Vol. 1 (1908), p. 219.

[18] F. G. Keyes, J. Am. Chem. Soc. **34**, 779 (1912).

LETTERS TO THE EDITOR

Prompt publication of brief reports of important discoveries in physics may be secured by addressing them to this department. Closing dates for this department are, for the first issue of the month, the eighteenth of the preceding month, for the second issue, the third of the month. Because of the late closing dates for the section no proof can be shown to authors. The Board of Editors does not hold itself responsible for the opinions expressed by the correspondents.

Communications should not in general exceed 600 words in length.

A New Form of Band Igniter for Mercury-Pool Tubes

The band-igniter principle was discovered by Peter Cooper Hewitt and is used today for the starting of Cooper Hewitt lamps. For a number of years band-igniter tubes have been as stroboscopic light sources and as controls for stroboscopic light sources.[1]

Experimental work has indicated that by the use of thin dielectric layers between the starter and the mercury cathode the ignition voltage can be considerably reduced, and that by using proper electrode configurations the tubes can be made to have a long, useful life. Other workers in the field have been experimenting along similar lines and have had encouraging results.[2]

Glass layers 0.003 to 0.010 inch thick are used as the dielectric. To secure adequate mechanical strength, the glass is bonded to a metallic support, the metal acting as the conducting portion of the igniter. A typical igniter consists of a tungsten wire 0.040 inch in diameter coated with a Nonex layer 0.005 inch thick and mounted in the tube as shown in Fig. 1. It is not practical to use layers much thinner than this because of the difficulty of securing a layer free from flaws that might lower its breakdown strength.

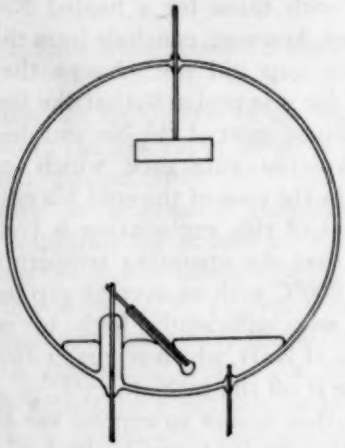

FIG. 1. Typical igniter in tube.

The ignition voltage is proportional to the thickness of the dielectric and depends markedly on the shape of the mercury meniscus. Slanting the igniter at 45 degrees with respect to the mercury surface reduces the starting voltage to half. Groups of two or more igniters placed close together also help to reduce the starting voltage. Carborundum particles embedded in the glass will further reduce the starting voltage, but with thin layers the carborundum is likely to puncture the insulating layer.

One serious difficulty with band igniters has been that with repeated ignitions such as in rectifier service, the mercury begins to wet the glass after a few hours of service. The sticking of the mercury to the glass destroys the meniscus and greatly increases the starting voltage. It has been found that by restricting the size of the igniter the heat supplied by the arc stream is sufficient to keep the insulating surface clean and to prevent the mercury from wetting the glass. The above effect is further enhanced by placing the igniter near the center of the mercury cathode where it is insulated from the cooling effects of the medium surrounding the tube. The materials which cause wetting tend to travel away from the igniter and to the cooler outside walls.

A tube with an igniter consisting of a wire 0.040 inch in diameter, with a glass layer 0.005 inch thick, the wire being slanted at 45 degrees with respect to the mercury surface, will have an ignition voltage of about 1500 volts peak. The ignition voltage will vary greatly from one ignition to the next, because of the motion of the mercury about the starter, and it may be as low as 500 volts in some cases, or as high as 1500 volts. Since the starter is completely insulated from the mercury, it is possible to use alternating current for ignition. Starting occurs when the igniter is positive with respect to the cathode. When the starter is negative there is no cathode spot formed.

The current required for ignition is small, on the order of $\frac{1}{2}$ milliampere. With 1500 volts a.c. it is usual to employ a 2-megohm resistor in series with the igniter.

Starting is affected by the temperature of the condensed mercury and becomes increasingly difficult below 20°C. At 0°C the starting voltage is increased by about 50 percent.

Tubes of the above type have been in service as rectifiers for about 1500 hours and show no signs of deterioration. While it is too early to predict actual life, our experiments indicate that capacity ignited tubes should have a life of 10,000 hours or more.

KENNETH J. GERMESHAUSEN

Department of Electrical Engineering,
Massachusetts Institute of Technology,
Cambridge, Massachusetts,
December 19, 1938.

[1] H. E. Edgerton, "The Mercury Arc as a Source of Intermittent Light," J. Soc. Mot. Pict. Eng., June (1931). H. E. Edgerton, and K. J. Germeshausen, "Stroboscopic Photography," Electronics, July (1932).
[2] H. Rokkaku and S. Katoh, "A Type Sendytron Using a New Method of Starting an Arc," E. T. J., August (1938).

Silver Films on a Mica Crystal Face

We are submitting here microphotographs (Figs. 1 and 2) which may be of interest to some of your readers, particularly those working in the field of thin metal films. The microphotographs (by transmitted light) are of an agglomerated silver film on a mica crystal face. The film was prepared as follows: The mica sheet, approximately thirty microns in thickness, was split from the interior of a heavier sheet and handled only on the margin with forceps, particular care being taken to avoid contamination. There was no preliminary cleaning of the mica slip prior to application of the silver film other than a two-hour bake in vacuum at 450°C. After cooling to room temperature the film was applied by evaporation from a silver bead located about one centimeter from the mica surface, so as to produce a range in film thickness over the sample of approximately 0.01–10.0 microns. Agglomeration was then effected by heating at 400°C for several hours. A vacuum of the order of 10^{-6} mm Hg was maintained during the whole process.

FIG. 1. Microphotograph by transmitted light. Mag. 81.5×.

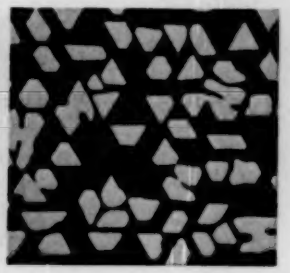

FIG. 2. Small section of Fig. 1. Mag. 531×.

Ordinarily, in a film prepared in this manner, the openings or windows which appear during heat treatment show little evidence of regularity in shape or arrangement. However, in this particular film, the windows are essentially all bounded by straight lines parallel to one of three common hexagonal axes. The orientation of the silver crystals by atomic migration and a building onto the substrate crystal structure is most evident here and is exceptionally uniform over a relatively large area. The phenomenon is naturally most evident in a thickness range of approximately 0.1–0.2 micron. Regarding the crystalline nature of this particular piece of mica, we have no data. It is of the Indian variety of muscovite.

SANFORD ESSIG

1951 Sterling Street,
Philadelphia, Pennsylvania,
December 18, 1938.

The Binding Energy of $4n$-Nuclei on the α-Particle Model

In various recent papers[1] the $4n$-nuclei are regarded as consisting of α-particles which form a crystal lattice; this model is taken as a first approximation in contrast to the Hartree model. One argument in support of the α-particle model is thought to come from the fact that the binding energy of the $4n$-nucleus (n times the mass of the α-particle minus the mass of the nucleus) can in a certain approximation be written as a constant times the number of bonds between pairs of α-particles.[2] The outstanding exception to this rule is ${}_4Be^8$ which has almost zero binding energy instead of the predicted 2.5 Mev. Hafstad and Teller show that this discrepancy can not be explained by taking account of the zero-point vibrations of the α-particles.

It seems that the above difficulty with the α-particle model can be understood in another way. We set up a perturbation calculation by use of a Hartree method, which is fairly good for one α-particle,[3] in that we consider the two protons and two neutrons comprising the α-particles as executing independent harmonic oscillations about the hypothetical lattice-points occupied by the α-particles. The nonorthogonality of the resulting system of antisymmetrical wave functions (constructed from Hermitian functions) can be approximately compensated for in the perturbation calculation. The first-order contribution gives a repulsion of the form $\Sigma E_m{}^I$ where m is to be summed over neighboring pairs of α-particles. The second-order calculation shows that it is not sufficient to consider only processes in which two α-particles participate but one must also include (e.g. in ${}_6C^{12}$), such a transition as the following: a proton from one α-particle and a neutron from another α-particle jump, under the influence of their nuclear force, into an excited state of the third. We write the perturbing potential as $H'=V-V_0$, where V is the nuclear interaction (taken as equal to $-a\exp[-b^2(r-r')^2]T_{ik}$ with $a>0$ and T_{ik} an operator giving the spin and charge dependence) and V_0 is the fictitious zero-order potential. When antisymmetric combinations of oscillator functions are employed, the V^2 contribution to the energy can be evaluated exactly up to a final integral. Thus the above transition gives as its V^2 contribution to the binding energy:

$$-\frac{Ma^2(1-2\gamma)^2}{\hbar^2\alpha(1-e^{-\rho^2/\pi})^3}\int_0^1\frac{dk}{k}\left\{\frac{\exp\left[-\rho^2((1+k)(1+4\gamma^2k^2)/4(1+2\gamma k))+\frac{3}{4}-\frac{3}{4}k\right]}{(1-4\gamma^2k^2)^{\frac{1}{2}}}-\exp\left[-\rho^2\right]\right\}$$

$Ma^2/\hbar^2\alpha$ is of the order of a nuclear binding energy, $1/\alpha^{\frac{1}{2}}$ is the average distance between two single particles in the same α-particle, $\gamma=b^2/(\alpha+2b^2)$, $(1-e^{-\rho^2/\pi})$ comes from normalization, $\rho=\alpha^{\frac{1}{2}}R$ where R is the "lattice spacing," and the integral is equivalent to a summation over intermediate states. This is to be compared with the V^2 contribution to the energy of a pure pair (as occurs in ${}_4Be^8$); one of the characteristic transitions of this type leads to the result:

$$-\frac{Ma^2(1-2\gamma)^2}{\hbar^2\alpha(1-e^{-\rho^2/\pi})^3}\int_0^1\frac{dk}{k}\times\left\{\frac{\exp\left[-\rho^2\{1-k/(1+2\gamma k)\}\right]}{(1-4\gamma^2k^2)^{\frac{1}{2}}}-e^{-\rho^2}\right\}$$

The two integrals are of the same order of magnitude as

can be seen from their series expansions. As a further check, a numerical integration was performed, by using[3] $\gamma=\frac{1}{4}$ and $\rho=1.7$, and the first integral is found to be eight-ninths of the second. Other V^2 terms are of the same order, and the V_0^2, VV_0 contributions to the energy behave similarly. Consequently a more precise knowledge of the interaction between *two* α-particles will not provide an explanation of the binding energies of $4n$-nuclei, in particular the difference between the binding of ${}_4Be^8$ and ${}_6C^{12}$.

Moreover, the perturbation energy of the second order can be written in the form $\Sigma E_m{}^{II}$ where m is to be summed over all configurations involving jumps between neighboring α-particles. Those terms which bring into play only pairs of α-particles just about cancel the corresponding terms in the first-order energy. Hence the other configurations are responsible for the binding energies; in ${}_6C^{12}$ a triangle, in ${}_8O^{16}$ four triangles and one tetrahedron, and so on (in the second-order matrix elements referring to more than four lattice-points cannot appear). Since the binding of ${}_8O^{16}$ is only twice that of ${}_6C^{12}$, the third-order perturbation energy must give an appreciable contribution (and presumably a repulsive one). This must be *à fortiori* true of heavier $4n$-nuclei, to whose binding energy higher approximations must contribute. Taken together with the fact that even in second-order matrix elements between more than two α-particles are essential, this means that the model of an α-particle lattice is a very poor approximation. Instead of near-neighbor interaction between α-particles, one has essentially an interaction among all the constituents of the nucleus, i.e. the liquid-drop model.

B. O. Grönblom
R. E. Marshak

Cornell University,
Ithaca, New York,
December 23, 1938.

[1] W. Wefelmeier, Zeits. f. Physik **107**, 332 (1937); C. F. von Weizsacker, Naturwiss. **26**, 209, 225 (1938).
[2] L. H. Hafstad and E. Teller, Phys. Rev. **54**, 684 (1938).
[3] B. O. Grönblom, Zeits. f. Physik **110**, 37 (1938).

The Viscosity of Air

Within the past few years various authors have reported new determinations of the viscosity of air which point to a value somewhat higher than that published by me[1] in 1916, and on which Millikan placed great reliance when arriving at his value of e. While one or two very recent determinations are as yet unpublished the summary during the past year by Millikan[2] and by Robinson[3] and direct correspondence to me may warrant at this time the following comments.

Although unable to recall any oversight or source of error of sufficient import to account for my result being as much too low as now assumed, I have continued to be much interested in this problem and ready to cooperate in the efforts made to secure an even higher precision in this most important constant. The inherent difficulties in obtaining an accurate value of this constant become obvious to anyone who studies the literature or works experimentally in this field. Even Houston's[4] recently published value (probably the best available) differs from that of Kellström[5] by nearly the same amount that it differs from mine (0.36 percent) though all three determinations are by the same method.

The recent determinations appear to have been carried out with the utmost care, have had the advantage of instruments constructed with the high precision now possible, and refinements in theory and in method have received much attention. Hence it is reasonable to consider the values obtained very reliable. For reasons given in my report I still greatly prefer the cylinder method, and disapprove the use of suspensions in ribbon form or made of phosphor bronze (used by a recent observer). The cylinder used by Kellström was much smaller than that used by me or the one employed by Houston, a disadvantage, possibly. Houston's contribution of certain correction factors would seem to give added weight to his value of η. The uncertainties as to the end corrections, one of the objections to the capillary tube method, have been doubled by Rigden[6] through his use of a pair of tubes for each run. The temperature control is always both critical and uncertain in this method. His result differs by 0.24 percent from that of his immediate predecessor in the work though it would appear to be close to the value now accepted.

Kellström's observation that any eccentricity of the inner cylinder lowers the apparent value of η might account in part for a low value since a defect in the clamping system required in the assembling of the apparatus might escape detection as it is impossible to check the alignment after the outer cylinder is in place. It seems unlikely that any large error of this sort could have entered into my results since the apparatus was so many times taken down and reassembled during the course of the experiments, and the value obtained closely checked that of Gilchrist who previously used the apparatus, and was checked later by Van Dyke, each using his own technique. Houston's corrections would hardly explain in full the discrepancy. Bearden has suggested that the main difficulty centers about the determination of the torque constant of the suspension. Assuming my value is too low I would suspect one or more of the factors mentioned in this paragraph to be responsible since the data obtained supported the accuracy claimed at that time.

As pointed out by Robinson, any of the recent values of η (mine included) if combined with the right oil drop data will yield a value of e acceptable to those in the x-ray field, but it would seem that the Houston-Millikan combination merits special confidence. While it would appear that the value of η has been determined with acceptable precision the writer would appreciate receiving information concerning any unpublished determination, whether completed or in progress.

E. L. Harrington

University of Saskatchewan,
Saskatoon, Saskatchewan, Canada,
December 20, 1938.

[1] E. L. Harrington, Phys. Rev. **8**, 738 (1916).
[2] R. Millikan, Ann. de. Physik **32**, 34 (1938).
[3] H. R. Robinson, Nature **142**, 159 (1938).
[4] W. V. Houston, Phys. Rev. **52**, 751 (1937).
[5] G. Kellström, Phil. Mag. **23**, 313 (1937).
[6] P. J. Rigden, Nature **141**, 82 (1938); Phil. Mag. **25**, 961 (1938).

Self-Diffusion in Copper

Experiments have been made on the rate of self-diffusion in copper by using as indicator the radioactive isotope Cu^{64} (half-life 12.8 hours).[1] The experiments were made by bombarding the face of a cylindrical block of copper with 8 Mev deuterons in the cyclotron. In this way an active layer extending to a depth of about one-tenth of a millimeter was obtained. The copper cylinder was heated in a quartz tube in a furnace (usually for about 40 hours) and the penetration of the active copper into the block was then investigated by cutting successive sections from the specimen and measuring their activities. Since a deuteron bombardment of only three microampere-hours is sufficient to give an activity of about one millicurie, the activities could be easily measured with an electroscope at the conclusion of the heating period. The only other appreciable activity produced by the bombardment is that due to Cu^{66} which decays rapidly (six-minute half-life). There is a small uniform activity throughout the specimen due to activation by neutrons produced in other transformations during the bombardment but this is negligible compared with the deuteron activation. This method of activation has the advantage of simplicity and avoids any possibility of the existence of a boundary disturbance between the active layer and the bulk of the copper. In calculating the diffusion coefficient it is necessary to know the initial distribution of activity in the specimen which can be easily determined by experiment. The results for the distribution of activity after heating were found to be in good agreement with the appropriate solution of the diffusion equation:

$$\partial c/\partial t = D(\partial^2 c/\partial x^2).$$

From the preliminary experiments the following values of the diffusion coefficient have been obtained:

At 1030°C	$D = 2.8\ 10^{-9}$ cm²/sec.
At 940°C	$D = 3.5\ 10^{-10}$ cm²/sec.

A rough measurement at 830°C gave: $D = 4.10^{-11}$ cm²/sec.

These results are sufficient to show that the coefficient is smaller than that predicted by Rhines and Mehl[2] from the rates of diffusion in copper of aluminum, beryllium, cadmium, silicon, tin and zinc alloyed with copper. The activation energy Q for the diffusion process ($D = Ae^{-Q/RT}$) seems to be of the order of 60,000 cal./mole. The measurements are being continued and a full account will be published later.

I should like to thank Dr. G. T. Seaborg for his advice and cooperation in these experiments. The research has been aided by grants from the Research Corporation.

B. V. Rollin

Department of Chemistry,
Radiation Laboratory, Department of Physics,
University of California,
Berkeley, California.
December 21, 1938.

[1] S. N. Van Voorhis, Phys. Rev. **49**, 876 (1936).
[2] J. B. Rhines and R. F. Mehl, Metals Technology, **5**, Jan. (1938).

Proceedings of the American Physical Society

Minutes of the Chicago, Illinois Meeting November 25–26, 1938

THE 223rd regular meeting of the American Physical Society was held at Chicago, Illinois on Friday and Saturday, November 25 and 26, 1938 at the University of Chicago. The presiding officers were Dr. Lyman J. Briggs, President, and Dean John T. Tate, Vice President of the Society. The attendance at the meeting was about three hundred.

On Friday evening the Society held a joint dinner in the International House with the Chicago Physics Club. Professor B. J. Spence, President of the Physics Club, presided at the dinner. After the dinner Dean Henry G. Gale introduced the speaker of the evening, Lord Russell of England, now lecturing at the University of Chicago. His subject was "Determinism in Physics."

Meeting of the Council. At the meeting of the Council held on Friday, November 25, 1938 the deaths of six fellows (Edwin H. Hall, Thomas C. Hebb, G. M. J. Mackay, A. Stanley Mackenzie, John C. Shedd, and E. R. von Nardroff) and two members (John W. Davis and John O. Hamilton) were reported. One hundred and twelve candidates were elected to membership. *Elected to membership:* E. P. Aikman, J. E. Armstrong, H. Dean Baker, Charles A. Barton, Donald L. Benedict, William E. Bennett, H. J. Bhabha, Ronald H. Bingham, Avis Borden, Jean H. Brattin, Sister Ignace Bresch, William C. Bright, Thomas A. Chalmers, John W. Clark, Richard K. Cook, Eugene P. Cooper, Dirk Coster, Neal D. Crane, Craig M. Crenshaw, Philip W. Crist, Charles J. Critchfield, George Dean, J. M. DelFosse, Joseph R. Dillinger, Cerda L. Donovan, John E. Edwards, Leonard Eisenbud, Josef B. Engl, Ralph W. Engstrom, A. Alfred Erickson, Cyril Feldstein, Peter Fireman, Lewis Fussell, Jr., F. Malcolm Gager, Louis A. Gebhard, Charles W. Gilbert, H. C. Gilbertson, Leo G. Glasser, Daniel L. Goldberg, Roy W. Goranson, Rudolph N. Griesheimer, Bernhard Gross, Donald R. Hamilton, Alfred O. Hanson, George E. Hansche, Lawton M. Hartman, III, Gregory K. Hartmann, John H. Hett, William A. Higinbotham, R. D. Hill, James P. Hocker, J. G. Hoffman, Norman J. Holter, John I. Hopkins, Everett H. Hurlburt, John W. Irvine, Jr., Martin W. Johns, Harry Jones, Edmund L. Jossem, Motoharu Kimura, Minoru Kobayasi, R. L. Latham, Harold B. Law, James L. Lawson, W. Bennett Lewis, Russell H. Lyddane, Kenneth R. MacKenzie, Martin S. Maier, L. Marton, Lewis S. Maxfield, Carroll D. McClure, Edward E. Miller, Franklin Miller, Jr., Friedrich Möglich, Julius P. Molnar, Robert L. Mooney, Warren W. Nicholas, Maria del C. Nunez Berro, Herbert A. Nye, Norman L. Oleson, Leonard T. Pockman, Martin A. Pomerantz, J. Harris Purks, George L. Ragan, Charles A. Randall, Hans Reinheimmer, Charles F. Robinson, J. H. Rohrbaugh, Robert W. Rompe, Avrahm B. Rotenberg, Frederick H. Sanders, Jason L. Saunderson, Lawrence R. Schmieder, Michael Schön, F. A. Schwertz, Clifford G. Shull, C. Skarstrom, Elmer G. Smith, Francis J. Steinmetz, Richard R. Syrdal, Yosiro Tasiro, Russell H. Varian, Robert E. Warren, P. R. Weiss, M. W. Welch, Bertine A. Whiting, Lawrence A. Wills, John G. Wilson, Volney C. Wilson, Dean E. Wooldridge, Rufus W. Wright, and Robert C. Wycoff.

The regular scientific program of the Society consisted of forty-eight contributed papers of which one, number twenty-seven, was read by title. The abstracts of these papers are given in the following pages. An Author Index will be found at the end.

W. L. Severinghaus, *Secretary*

ABSTRACTS

1. Cloud-Chamber Analysis of Barytron Secondaries.* J. I. HOPKINS, *West Georgia College;* W. M. NIELSEN AND L. W. NORDHEIM, *Duke University.*—A study has been made of the secondary particles produced by the penetrating radiation (barytrons) filtered by 274 g/cm² of iron in (a) a 0.82 cm lead plate and (b) three spaced 0.31 cm plates in a G. M. controlled cloud chamber. The results are as follows:

(a) Number of secondary particles per traversal	0	1	2	3	4
Number of events	565	49	2	3	1
Relative numbers per plate	100	8.7	0.35	0.53	0.17
(b) Number of events	324	80	8	3	1
Relative numbers per plate	100	8.2	0.8	0.3	0.1

The two series of observations are in very good agreement and show that the number of single secondaries is not increased significantly by increasing the plate thickness from 0.31 cm to 0.82 cm. This result is consistent with the small number (5) of secondaries which also penetrate the plate below. Practically all of the observed secondaries can be explained by assuming that they are produced by direct collisions between barytrons and atomic electrons with no further processes (radiative or unknown) involved.

* To be read by title.

2. On World-Wide Changes in Cosmic-Ray Intensity. S. E. FORBUSH, *Department of Terrestrial Magnetism, Carnegie Institution of Washington. (Introduced by J. A. Fleming.)*—Results of continuous cosmic-ray records from Compton-Bennett meters at Cheltenham (United States), Teoloyucan (Mexico), Christchurch (New Zealand), and Huancayo (Peru), are reduced to a constant barometric pressure. After deducting a 12-month wave at each station except at Huancayo, where none is found, the high correlation ($r \doteq 0.90$) between the means of cosmic-ray intensity for each one-third month at any two of these four stations, definitely indicates the major changes in cosmic-ray intensity are world-wide. By using also published data from the Hafelekar, Austria, the world-wide changes, expressed in percent of the absolute intensity at each station, are found to increase rapidly with altitude for stations at the same latitude and, for stations at high altitude, to increase rapidly between the equator and geomagnetic latitude 30° north, without much further increase to 47° north. The mechanism responsible for the world-wide effect is probably connected with that causing the world-wide decrease in intensity observed during some magnetic storms. The observed 12-month wave is not explained on the basis of a solar magnetic moment.

3. Significance of Sidereal Time Variations of Cosmic Rays. A. H. COMPTON AND P. S. GILL, *University of Chicago.*—A comparison has been made of all of the data available to us of sidereal time variations of cosmic rays. The data include those published by Illing, Schonland and his collaborators, and Forbush, in addition to those which we have immediately available from Mexico, and from the Pacific Ocean. Where sufficient data have been available, the analysis has been carried through both by Fourier analysis and by use of the harmonic dial. A weighted mean of all of the data so far collected indicates an amplitude of the sidereal time variation which is only a small fraction of that predicted by the galactic rotation theory of Compton and Getting. For the data from Mexico and from the Pacific Ocean, where the detailed information required is available, application by Julian Thompson and ourselves of a harmonic dial method suggested to us by S. E. Forbush indicates the probable insignificance of the first harmonic which is present in the Fourier analysis. There is some indication of the existence of a real second harmonic, that is, a twelve-hour sidereal period. These results constitute evidence that the earth is not moving appreciably with respect to the source of the cosmic rays, and hence that the rays are not coming directly from outside our galaxy.

4. Diurnal Variations of Cosmic Rays on the Pacific Ocean. JULIAN L. THOMPSON, *University of Chicago and Emmanuel Missionary College.*—The cosmic-ray data collected by Compton and Turner on the Pacific Ocean from March 1936 to January 1937 have been analyzed for periodic daily variations following solar and sidereal time. The variation following solar time has been studied by the usual harmonic analysis method. A new geomagnetic latitude curve in which the effect of periodic fluctuations is removed is used as the basis of this analysis. Solar diurnal variation curves for latitudes ranging from 55°N to 40°S (geomagnetic) show no substantial variation in either amplitude or phase. The mean amplitude of the first harmonic is found to be 0.24 percent with its maximum at about 14 hours. The problem of distinguishing a true sidereal diurnal variation in cosmic-ray intensity from a seasonal change in the amplitude of the solar diurnal variation is approached from the standpoint of the harmonic dial type of analysis. It is shown that the regular cyclic arrangement of the datum points taken in chronological order serves as a criterion for the presence of a sidereal time variation. The Pacific Ocean data are shown to contain no sidereal diurnal component larger than the experimental error of about ±0.06 percent. There is an indication of an annual variation in the amplitude of the solar diurnal component.

5. Production of Penetrating Cosmic-Ray Particles by Photons. MARCEL SCHEIN AND VOLNEY C. WILSON, *University of Chicago.*—With Geiger-Müller tubes arranged for fourfold vertical coincidence, a Hsiung type of experiment was performed in an aeroplane up to an altitude of 25,000 feet. 8.1 cm of lead were placed between the counter tubes and another lead plate of 2.2 cm thickness was alternately changed from the position above all the tubes to a position between the second and third tubes. From the difference in the two cases, it was found that at an altitude of 25,000 feet an average of 2 ionizing penetrating particles (barytrons?) per minute were ejected in the forward direction from a lead plate (38 cm×5.2 cm×2.2 cm) by the action of non-ionizing rays (photons?). From the direct measurement of (1) the penetrating and (2) the total

vertical radiation at different altitudes, it was found that the electron and hence the photon intensity (soft component) at 25,000 feet altitude is 37 times greater than at sea level. This value gives a cross section for the production of barytrons by photons in lead which is in at least rough agreement with Heitler's calculations. The penetrating component at 25,000 feet is only 2.9 times greater than at sea level.

6. New Evidence for the Existence of Penetrating Neutral Particles. FRANCIS R. SHONKA, *University of Chicago and De Paul University.* (*Introduced by A. H. Compton.*)—An experiment of the Rossi-Hsiung type was performed at an altitude of 14,200 feet with a fourfold coincidence array of Geiger-Müller tubes in a vertical position. Thicknesses of 12.7 to 17.3 cm of lead served as absorber between the counters. Additional varying thicknesses were placed alternately above and between the counters, i.e., in positions A and B. For small thicknesses the ratio of the counting rates with the lead in position A to that for position B is not appreciably greater than unity. For greater thicknesses (19 to 23 cm), however, the ratio A/B becomes 1.06 ± 0.02. Working at sea level, and having the bottom tube shielded with 25 mm of lead, Hsiung obtained the same result. Maass, using no shield for the tubes, found the ratio A/B equal to 1.2. In view of the great thickness of lead required to give the maximum effect, these non-ionizing particles producing secondary barytrons must be much more penetrating than photons. This high penetrating power suggests their identification with the neutrettos (neutral particles having mass and other properties similar to the barytron) postulated by Heitler.

7. On the Nature of the Penetrating Cosmic Rays. V. C. WILSON, *University of Chicago.* (*Introduced by Arthur H. Compton.*)—The following experiments were performed in a coal mine at a depth of 300 meters water equivalent. Coincidences obtained with a fivefold Geiger-Müller tube telescope tipped at 33° from the vertical were 13 times more frequent than coincidences with the three inside tubes moved out of line. This indicates that the large majority of the coincidences are due to single ionizing particles. Placing various thicknesses of lead over a triangular arrangement of the five tubes only decreased the number of recorded showers. When lead was placed between the tubes in the shower arrangement, the counts fell off rapidly, reaching zero with 4.5 inches of lead. With the five tubes in a vertical line, various thicknesses of lead, up to one meter, were placed between the second and third tubes from the top. Within the probable error (about 5 percent) the mass absorption in lead is the same as that obtained with rock above all the tubes. It is concluded that at a depth of 300 meters water equivalent the majority of the rays are penetrating ionizing rays—probably barytrons produced in the upper atmosphere. There are also present some soft showers which are relatively more abundant than at 30 meters depth.

8. The β-Ray Spectrum of N^{13} and the Mass of the Neutrino. ERNEST M. LYMAN,* *University of California.*—The positron spectrum of N^{13} has been investigated by means of a magnetic spectrometer of high resolution. The N^{13} was produced by bombarding Acheson graphite plates with 5.3 Mev deuterons from the cyclotron. The observed spectrum was corrected for the distortion arising from the geometry of the apparatus and from the scattering and absorption of the 1.5μ collodion window in front of the Geiger counter detector. The distortion of the spectrum introduced by the thickness of the source of radioactive material was also considered. The results indicate that the endpoint energy of the N^{13} spectrum is 1.198 ± 0.006 Mev. From nuclear disintegration and mass-spectrograph data, one obtains

$$N^{13}\rightarrow C^{13}+\epsilon^{+}+(\epsilon^{-})+\nu+1.21\pm0.09 \text{ Mev}.$$

Thus the fastest β-particles have the total available energy, which shows that the observed endpoint of the N^{13} spectrum is the true endpoint. Furthermore, the mass of the neutrino is $0\pm0.2m_{\epsilon}$. The shape of the spectrum has been compared to that predicted by the Konopinski-Uhlenbeck theory for allowed β-transitions. It was found that a K-U curve consistent with the data over the major portion of the spectrum predicted far too many high energy positrons and an endpoint energy 25 percent greater than the observed one.

* Now at the University of Illinois.

9. Continuous Spectra of H_2 and D_2. HUBERT M. JAMES AND ALBERT SPRAGUE COOLIDGE, *Purdue University and Harvard University.*—A complete theoretical calculation has been made of the continuous spectra of H_2 and D_2 arising from transitions from the lower vibrational levels of the $1s\sigma 2s\sigma\,{}^3\Sigma_g$ state to the unstable $1s\sigma 2p\sigma\,{}^3\Sigma_u$ state. Use of the Franck-Condon approximation has been avoided by a direct computation of the electric moment of the electronic transition, as a function of nuclear separation; this quantity is found to decrease rapidly with increasing nuclear separation. Spectra are computed for transitions from each of the vibrational levels separately, and absolute mean lives are determined for the various levels. Relative probabilities of excitation from the ground state of the molecule by electron impact are estimated, and the intensity in the spectrum due to excitation by electron impact is computed for a range of energies of the electrons. The Franck-Condon approximation is found to be somewhat more satisfactory than was indicated by a previous investigation. There is sharp disagreement of the results with the observations of Smith.[1] This apparently arises from errors in Smith's intensity standard, and emphasizes the need of a more satisfactory intensity standard in the ultraviolet. Agreement with the results of Finkelnberg and Weizel[2] is obtained, but its significance is weakened by uncertainties in the experimental conditions.

[1] N. D. Smith, Phys. Rev. **49**, 345 (1936).
[2] W. Finkelnberg and W. Weizel, Zeits. f. Physik **68**, 577 (1931).

10. Capture of Neutrons by Atoms in a Crystal. WILLIS E. LAMB, JR., *Columbia University.*—The precise determination of the properties of nuclear resonance levels from the capture of slow neutrons is complicated by the fact that most of the substances used for absorbers and detectors

are in the solid state, so that the calculations of Bethe and Placzek for the influence of the Doppler effect are inapplicable, since these were based on the assumption of a perfect gas. Their calculations have here been generalized to include the effect of the binding of the capturing atom in a crystal lattice. Under the assumption that the crystal may be treated as a Debye continuum, it is shown that if the lattice binding is sufficiently weak, the absorption line has the same form as it would have in a gas, not at the temperature of the crystal, however, but at a temperature which corresponds to the average energy per vibrational degree of freedom of the lattice (including zero point energy). In cases of somewhat stronger lattice binding, the line form is found to be more complicated, and may even have a fine structure. Plots of the absorption line in several typical cases will be shown. An approximate formula for the cross section for self-indication is also derived.

11. The State of Liquid Helium below the λ-Point and the Bose-Einstein Condensation. F. LONDON,* *Institut Poincaré, Paris.*—It has recently been shown[1] that, contrary to current views, an ideal Bose-Einstein gas shows a discontinuity in the course of its specific heat curve. This anomaly is connected with a kind of condensation process already mentioned by Einstein. Some evidence has been given[2] to support the idea that the peculiar phase transition (λ-point) liquid helium undergoes at 2.19°K might be regarded as the condensation phenomenon of the Bose-Einstein statistics, distorted, of course, owing to the fact that it manifests itself in the liquid and not in the gaseous state. Further evidence in favor of this interpretation is furnished by an elementary discussion of the transport properties of the condensed phase. It is shown[1] that the theory accounts for the sudden increase of fluidity and of heat conductivity when going below the λ-point. The latter phenomenon comes out,[3] not as an ordinary heat conductivity, but rather as a reversible phenomenon, similar to the heat transport in a thermoelement, namely as a reversible transformation of heat into mechanical work. This thermomechanical effect also furnishes the explanation of the so-called "fountain phenomenon" discovered by Allen and Jones.

* At present at Duke University.
[1] Phys. Rev., in print.
[2] Nature **141**, 643 (1938).
[3] H. London, Nature **142**, 612 (1938).

12. Resonance Scattering of Neutrons in Helium. W. E. STEPHENS[1] AND H. STAUB,[2] *California Institute of Technology.*—We have measured (in a cloud chamber filled first with ethane, then with helium) the numbers of forward recoil particles from the neutrons produced when beryllium is bombarded with 0.6 Mev and 0.9 Mev deuterons.[3] The number of helium recoils divided by the number of hydrogen recoils in each of the four neutron groups gives the relative probability of backward neutron scattering for these different neutron energies. For neutrons of about 1 Mev, there was found a relatively large probability of backward scattering in helium. This is in good agreement with what would be expected if the *n*-He combination had a *p* state at about 0.8 Mev unstable. Hence this supports the evidence of Williams, Shepherd, and Haxby[4] and Staub and Stephens[5] that He^5 has an 0.8 Mev unstable state.

[1] At present a Westinghouse Research Fellow, Westinghouse Research Laboratories, East Pittsburgh, Pa.
[2] International Exchange Fellow, now at Physics Department, Stanford University, California.
[3] Bonner and Brubaker, Phys. Rev. **50**, 308 (1936).
[4] Williams, Shepherd, and Haxby, Phys. Rev. **51**, 888 (1937) and **52**, 340 (1937).
[5] Staub and Stephens, Phys. Rev. **54**, 236 (1938).
Stephens and Staub, Phys. Rev. **54**, 237 (1938).

13. On the Neutron-Proton Interaction. JULIAN SCHWINGER, *Columbia University.*—Recent experiments have shown that current theory provides an inadequate representation of phenomena involving the neutron-proton interaction. In an attempt to isolate the cause of these difficulties, we have examined the consequences of the most general interaction not explicitly involving the momenta of the interacting particles. This involves, essentially, the addition of interaction terms of the type

$$\left(3\frac{\sigma_1\cdot\mathbf{r}\sigma_2\cdot\mathbf{r}}{\mathbf{r}^2}-\sigma_1\cdot\sigma_2\right)J(\mathbf{r})$$

to those already in vogue. Among the principal results deduced from this novel interaction are a decrease in the neutron-proton scattering cross section for fast neutrons, a decrease in the neutron magnetic moment as deduced from the proton and deuteron moments, and the existence of an electric quadripole moment of the deuteron. The bearing of experimental data on these predictions and on modifications introduced into the theory of the radiative capture of slow neutrons and the photodisintegration of the deuteron will be discussed.

14. On the Excitation Functions of Intermediate Elements. E. J. KONOPINSKI, *Indiana University.*—An attempt has been made to apply the Breit-Wigner "dispersion" formula for nuclear reactions, together with the Gamow-Condon-Gurney theory of barrier penetration, to the excitation functions of reactions involving elements having mass numbers between about 10 and 30, for which the data are most abundant. Here most of the simplifications used for very light or very heavy nuclei are not possible.[1] It is found that, in general, the uncertainties about the number and weight of the possible residual states overshadow all other analyzable effects. However, for certain specific reactions, in particular endoergic ones, arguments can be given to reduce the effect of the uncertainties considerably. Such a case, given special attention, is the $C^{12}(d,n)N^{13}$ reaction for which measurements have been made by Newson. This has special interest because of the decrease of the yield caused by competition from the $C^{12}(d,\alpha)B^{10}$ reaction. The influence of the residual states of B^{10} is largely eliminated by the smallness of the penetration probability of the outgoing alpha-particle. It is found then that the experimental yield curve allows for surprisingly small weights of the highly excited states of N^{13}.

[1] Konopinski and Bethe, Phys. Rev. **54**, 130 (1938).

15. Scattering of Fast Electrons. J. H. BARTLETT AND R. E. WATSON, *University of Illinois.*—Mott[1] has developed exact formulae for the scattering of Dirac electrons

by a Coulomb field. With these as a basis, we have calculated the angular distribution of the scattering for very fast electrons (i.e. energies greater than 2 Mev). In this region, both the total cross section and the angular distribution take on asymptotic values. The angular distribution is of Rutherford type for very small angles, but the scattering at 60° is about twice as large as Rutherford scattering. The calculations are being extended to lower energies.

[1] Mott, Proc. Roy. Soc. **135**, 429 (1932).

16. *K*-Electron Capture in Ag^{106}. J. REGINALD RICHARDSON,[1] *University of Michigan.*[2]—The distribution of the electrons emitted by the 8-day isomer[3] Ag^{106} has been investigated. A thin sheet of silver was activated by fast neutrons from the cyclotron, and seven days later was placed across the center of a twelve-inch hydrogen filled cloud chamber. The striking feature of the distribution is that forty-five percent of the 524 tracks are in a small band of energies below 17 kv, the remainder ranging up to 800 kv. The conclusion seems inevitable that the low energy group consists of Auger electrons and photoelectrons associated with the *K*-electron capture process in Ag^{106}. From the thickness of the source one can determine the ratio of the number of *K* quanta to the number of electrons in the main part of the spectrum to be 50 to 1. In view of this ratio it seems possible that the electrons above 20 kv are entirely due to the internal conversion process. A preliminary investigation has been made of the photoelectrons ejected by the gamma-radiation from a thin Pb lamina. The resulting distribution is very similar in shape to the part of the electron spectrum above 20 kv.

[1] National Research Fellow.
[2] Now at the University of Illinois.
[3] Pool, Phys. Rev. **53**, 116 (1938).

17. The Secondary Emission of Electrons Due to Protons. J. S. ALLEN, *University of Minnesota.*—The secondary emission of electrons from various metals due to protons has been studied. For targets of Al, Cu, Ni and Pt at an angle of 90° to the incident proton beam the ratio of the secondary electron to the proton current for surfaces that have not been outgassed was approximately 3 for protons of 120 kv energy. As the angle between the incident proton beam and the surface of the target was varied this ratio followed the relation $\delta = \delta_{90} \operatorname{cosec} \theta$ where θ is the angle between the proton beam and the surface of the target and δ_{90} is the secondary electron-proton ratio at 90°. The measurements were continued with targets outgassed by heating to a dull red during the readings. The results for targets set at 90° to the proton beam are given in the table below.

Secondary Electron-Proton Ratio.

Proton Energy	Be	C	Cu	Ni	Pt
72 kv	7.3	2.3		1.9	
120 kv	7.5	2.3	2.0	1.8	2.4
166 kv	7.4	2.2	1.9	1.9	2.2
212 kv		2.0	2.0	2.1	2.1

18. Ionization and Dissociation of $CHBrF_2$ by Electron Impact. RICHARD F. BAKER AND JOHN T. TATE, *University of Minnesota.*—The ions formed in $CHBrF_2$ by electron impact have been studied with a mass spectrograph of the 180° focussing type. The molecular ion $CHBrF_2^+$ first appears at 12.0±0.2 volts electron energy, with an abundance (at 100 volts electron energy) of six percent that of the most abundant ion CHF_2^+. The small probability of formation of the molecular ion, coupled with a large probability of dissociation under electron impact, is a feature shared by the other halogen derivatives of methane which have been studied with the mass spectrograph.[1] Negative bromine ions were abundant, and were formed in four processes. Three of the processes were of the resonance type corresponding to dissociation, with capture of the incident electron, and had low energy thresholds. These processes are: $CHBrF_2 \rightarrow CHF + F + Br^-$; $CHBrF_2 \rightarrow CH + 2F + Br^-$; $CHBrF_2 \rightarrow C + H + 2F + Br^-$. In the remaining process the negative ions were formed simultaneously with a positive ion: $CHBrF_2 \rightarrow C^+ + Br^- + H + F_2$. Negative fluorine ions were observed with an abundance ~1/10 that of negative bromine. The appearance potential of F^- indicates that it is formed simultaneously with the ion CBr^+. No capture processes were observed for F^-.

[1] Baker and Tate, Phys. Rev. **53**, 683 (1938).

19. The Diffraction of X-Rays by Liquid Sulphur at Different Temperatures. NEWELL S. GINGRICH, *University of Missouri.*—X-ray diffraction patterns of liquid sulphur at 128°C, 166°C, 190°C, 210°C, 225°C, and 300°C have been obtained photographically using monochromatic Mo $K\alpha$-radiation and a cylindrical camera of 8.85 cm radius. Relative intensities were obtained with the aid of a microphotometer, and each pattern shows one peak and a "shelf." The variation in the position of the peak with temperature agrees roughly with that reported by Blatchford. The diffraction pattern for plastic sulphur at room temperature has been obtained by changing the sample frequently. In this case, a weak secondary maximum was observed in addition to the main peak. The intensity curves in each case were corrected for absorption in the sample, for polarization, and for incoherent radiation and they were then placed on an absolute basis in the usual manner. The atomic distribution curves obtained from these curves will be presented and discussed. In the case of liquid sulphur at 128°C, the first concentration of atoms occurs at about 2.05A, and the number of nearest neighbors is given as approximately two.

20. Experiments on the $F+H^1$ Gamma-Radiation and the Klein-Nishina Absorption Coefficient at 5.7 Mev. J. HALPERN AND H. R. CRANE, *University of Michigan.*—The recoil electrons ejected from a 1.5 mm carbon scatterer by the gamma-radiation from $F+H^1$ have been further investigated by the cloud-chamber method. The carbon sheet was placed across the center of the cloud chamber, and gamma-radiation, collimated by a lead channel, was allowed to fall on the center of the carbon. The distribution

of negative electrons originating in the carbon shows the radiation to be monochromatic at about 5.7 Mev. A similar measurement was made with the CaF_2 target inside the cloud chamber and surrounded by 1½ mm of carbon. The group of electrons at about 4 Mev reported by Gaerttner and Crane[1] was observed, but further tests indicated that this group was due to the negative members of internal conversion pairs, and not to a second gamma-ray line. The Klein-Nishina absorption of this radiation in 10 cm of Al was then measured by observing the recoil electron distribution from the carbon sheet with the Al inserted between source and collimator on alternate expansions of the cloud chamber. The results are in good agreement with theory.

[1] Phys. Rev. **52**, 582 (1937).

21. Diffuse Scattering of Cu $K\alpha$ X-Rays from Single Zinc Crystals. O. J. Baltzer and E. M. McNatt, *Washington University.* (*Introduced by A. L. Hughes.*)—Formerly all experiments on the diffuse scattering of x-rays from zinc crystals have been made with the continuous spectrum from an x-ray tube. We have now been able to obtain the diffuse scattering of Cu $K\alpha$ x-rays from single crystals of zinc. The Cu $K\alpha$-rays from an all-metal tube with a copper target operated at 20 kv and 100 ma were reflected from a crystal of rocksalt set at the proper angle. The diffuse scattering of these reflected rays from various zinc crystals was studied. X-rays of half the wave-length of the Cu $K\alpha$-rays are also reflected from the rocksalt crystal and these produce fluorescent rays in the zinc crystal. Correction for these fluorescent rays was made by placing thin aluminum foil between the rocksalt and the zinc crystals.

22. Atomic Structure Factors for Zinc Crystals at Large Scattering Angles. E. M. McNatt and G. E. M. Jauncey, *Washington University.*—The diffuse scattering of x-rays of average wave-length 0.48A from single zinc crystals of orientation angles 0° and 90° has been measured at temperatures of 100°K and 295°K out to $(\sin\phi/2)/\lambda = 1.5$ (average value). At this value of $(\sin\phi/2)/\lambda$ the diffuse scattering curves for all orientations and temperatures tend to come together. From these curves the atomic structure factors for zinc may be determined for values of $(\sin\phi/2)/\lambda$ approaching 2. A semi-empirical formula for the structure factors in this region has been obtained. It seems possible to relate this formula to the critical absorption wave-lengths of x-rays in zinc.

23. The Possibility of the Internal Scattering of the Beta-Rays from RaE. G. E. M. Jauncey, *Washington University.*—Gray and Hinds[1] have recently reported a γ-ray spectrum from RaE containing lines whose energies are 5.8, 9.700, 15.8, 21.6 and 63 kv. Since the energies of the K–L_{II}, L_{II}–N_V, M_I–N_{III} x-ray spectrum lines of Bi are 78, 14.8 and 3.2 kv, it may be that ordinary x-rays of Bi were being observed. The discrepancies then would be due to the absorption method of resolving the spectrum. This spectrum can be explained if a beta-ray in passing through the rest of the atom occasionally makes a close collision with an orbital electron. If a K electron is knocked out, then the K spectrum of Bi should be produced. We call this "internal scattering" in analogy to "internal conversion" of γ-rays. Rutherford has suggested that in scattering problems the magnetic as well as the electric force between two electrons must be considered. Both magnetic and electric collision parameters are recognized. Using the accepted magnetic moment of the electron, we find that about 0.02 of the β-rays are internally and inelastically scattered, thus giving rise to 0.02 photon per beta-ray. This agrees with Gray and Hinds' value of 0.015 photon per beta-ray.

[1] Can. J. Res. **16**, 75 (1938).

24. Effect of Molecular Shape on Molecular Attraction in Monolayers. Robert T. Florence and William D. Harkins, *University of Chicago.*—The shapes of otherwise identical molecules affect very greatly intermolecular attraction in monolayers. Molecules of the following substances contain 18 carbon atoms: stearyl alcohol, stearic acid, and stearyl amine, with straight chains; elaidic acid, a *trans* compound, with a slight bend at its central double bond, and oleic acid with an identical molecule except that it is a *cis* form with a much greater bend. On an acidic subsolution stearic acid gives a condensed, oleic acid an expanded film, and the equimolecular mixture also is expanded. While oleic is as strongly attracted as stearic acid by the water, nevertheless oleic acid is seen to be bound much less tightly in the film, since it may be quantitatively separated from the mixed film by increase of pressure. The effects are most remarkable on a basic subsolution, since the addition of elaidic acid, which by itself gives an expanded film, to a condensed film of stearyl amine, condenses the latter even more, while the addition of stearyl amine, which gives a condensed film, to an expanded film of oleic acid, expands it even more. These differences are explained by the differences in bending of the hydrocarbon chain, which has a great effect upon the van der Waals interaction.

25. The Molecular Aspect of the Energies of Adhesion Between Various Liquids and Solids: Adsorption as the Result of Electrostatic Forces. George Boyd and William D. Harkins, *University of Chicago.*—By the use of a calorimeter with a sensitivity of 0.00003C the energy of immersion of dry inorganic powders in various pure liquids was determined. This gives the adhesional energy between the liquid and the powder provided the area of surface of the powder is known. The relative energies of adhesion for titanium dioxide (anatase) are: water 1.00, ethyl alcohol 0.90, butyric acid 0.83, ethyl acetate 0.67, butyl alcohol 0.64, nitrobenzene 0.57, carbon tetrachloride 0.37, benzene 0.37, iso-octane (0.18 in one experiment). Such relative values as have been determined are approximately the same with SnO_2, SiO_2, $ZrSiO_4$, and $BaSO_4$, while with carbon tetrachloride NaCl gives 0.35. It is apparent that on solids of this class (hydrophilic) the

values are higher for liquids whose molecules exhibit a dipole moment, but it is obvious that the magnitude of this moment is not the only factor involved. Graphite, a hydrophobic solid, gave much higher relative values with nonpolar liquids. The values given above are practically independent of the area of the powder. The apparent area was determined by the adsorption of higher fatty acids from dry, nonpolar solvents. The adhesional energy for titanium dioxide is 1050 ergs per cm² with water and 390 with benzene. With NaCl the values are half, and with zirconium dioxide or silicate more than twice, as large.

26. Packing Fraction Differences Among the Heavy Elements. ALVIN C. GRAVES, *University of Chicago.*—Values of the differences between packing fractions of heavy elements are given and compared with the work of other investigators by means of a packing fraction curve. Results were obtained by bracketing an isotope of one element between two isotopes of a second differently charged element and measuring the separations of the lines. The following cases were studied: Cr(53)–Gd(158), Gd(160); Cr(52)–Gd(155), Gd(157); Gd(160)–Cr(53), Cr(54); Sr(86)–Yb(171), Yb(173); Sr(87)–Yb(173), Lu(175); Lu(175)–Yb(173), Yb(174); Pt(194)–Ru(96), Ru(99); Pt(175)–Ru(96), Ru(99); Pt(196)–Ru(96), Ru(99); U(238)–Sn(118), Sn(120); Au(197)–Mo(98), Mo(100); Ta(181)–Zr(90), Zr(91); Pt(195)–Mo(96), Mo(98). Doublets were measured as follows: Os(192), Ru(96); Pt(198), Ru(99); Pt(196), Ru(98); U(238), Sn(119); Th(232), Sn(116); Gd(156), Cr(52); Yb(172), Sr(86); Yb(174), Sr(87). Measurements on the lines were in most cases reproducible to better than a thousandth of a millimeter. The plates were taken on the double focusing mass spectrograph of Professor A. J. Dempster, and measured visually on a Gaertner comparator.

27. Internuclear Distances in the Gas Molecules Se_2, HgCl, Cu_2Cl_2, Cu_2Br_2 and Cu_2I_2 by Electron Diffraction. LOUIS R. MAXWELL AND VERNON M. MOSLEY, *Bureau of Chemistry and Soils, U. S. Department of Agriculture.*—Electron diffraction photographs have been obtained from selenium vapor at 900°C under conditions suitable for a high concentration of diatomic molecules. Five interference maxima were obtained at the relative positions expected for a diatomic structure which led to a nuclear separation of 2.21±0.03A. At lower temperatures the diffraction pattern became more complex due to the presence of higher polymers, and gave maxima in approximate agreement with results obtained by previous workers.[1] A diatomic interference pattern was obtained from mercurous chloride vapor by heating the salt to about 450°C. This gave an internuclear separation of 2.21±0.04A. Chemical analysis of the material condensed after photographing showed that only a small amount of decomposition had occurred, leaving at least 95 percent HgCl. Electron diffraction data from Cu_2Cl_2, Cu_2Br_2, and Cu_2I_2 indicated the existence of two prominent distances l and $2l$ in each molecule where l = 2.13A, 2.25A and 2.40A, respectively. A satisfactory structure for these molecules has not been determined; however, many possible forms have been excluded. A linear model does not fit in all details. For Cu_2Cl_2 the 2.13A distance agrees closely with recent band spectrum data for the nuclear separation in the normal state of CuCl.

[1] J. D. Howe and K. Lark-Horovitz, Phys. Rev. 51, 380 (1937).

28. A Precision Current Control Device. J. L. LAWSON AND A. W. TYLER, *University of Michigan.* (*Introduced by H. R. Crane.*)—A vacuum tube circuit is described in which a current can be controlled and maintained very accurately. The current control for the Michigan cyclotron is described in detail. This unit controls the magnet current of up to 250 amperes, furnished from a generator excited by commercial 220 volts direct current, to one part in five thousand over a prolonged length of time. Variations in power supply voltages of twenty percent are properly handled. Tests over an eight month period have shown this control to be quite satisfactory. Applications have also been made to the magnet current control for a magnetic beta-ray spectrograph, and high voltage control for a Geiger-Müller tube. Further applications are suggested.

29. The Energy of the β-Rays from Potassium. W. J. HENDERSON, *Purdue University.*—The β-ray spectrum of potassium has been investigated by the absorption method using a cylindrical counter and concentric absorbers. Because of the low intensity of the β-radiation from potassium the range from such an experiment is too small. This apparent range of 0.375 g/cm² is corrected by comparison with the ranges of RaE and UrX_2 β-rays measured under the same conditions of geometry and intensity. The corrected range is found to be 0.55 g/cm² which gives a value of 1.3 million volts for the upper limit of the β-ray spectrum of potassium. This is considerably higher than the values found by other methods. Also, the measurements give no evidence for two groups of β-rays in the spectrum.

30. Fluorescence and Absorption of Diacetyl. G. M. ALMY, H. Q. FULLER, G. D. KINZER, *University of Illinois.*—The well-known fluorescence of acetone vapor excited by λ3130 is identical with the fluorescence of diacetyl vapor when excited by λ3130[1] or with Hg λλ3650, 4047, 4358. The spectrum of the fluorescence is independent of the exciting frequency, and of the pressure of diacetyl over a range of 0.1 mm to 50 mm Hg. With water solution the fluorescence has the same general appearance though the fine structure is diffused. The intensity of the fluorescence measured with photo-cell and electrometer tube amplifier increases linearly with diacetyl pressure and linearly with the intensity of the exciting light. It decreases with increasing temperature. The fluorescence is strongly quenched by oxygen falling to one-half intensity at an oxygen pressure of 0.01 mm Hg. The drop is more rapid than expected on a simple picture of one excited state attacked by oxygen (Stern-Volmer law). With continued illumination the fluorescence recovers, the oxygen being

consumed in the process of quenching. Further evidence that the process without oxygen is not simple fluorescence is obtained by examining the absorption of irradiated diacetyl. If the diacetyl is radiated for a few minutes, then allowed to stand in the dark for a time (1 to 1000 min.), then radiated a second time, a new strong continuous absorption appears extending to longer wave-lengths than the diacetyl absorption. The intensity of this absorption, appearing only upon second radiation after a dark period, varies with the elapsed time of the second radiation and passes through at least three maxima (at about 7 sec., 2 min., and 6 min. with our illuminating apparatus). This phenomenon is destroyed by the addition of oxygen to the diacetyl.

[1] Matheson and Noyes, J. Am. Chem. Soc. **60**, 1857 (1938).

31. The Correction of Experimental Curves for the Resolving Power of the Apparatus. ROY C. SPENCER, *University of Nebraska.*—The apparatus transforms the original function $G_0(x)$ into $G_1(x)$. The resolving power function, $F(x)$, is the response of the apparatus to a unit impulse. The weight function, $W(x)=F(-x)$, has moments μ_n' (unprimed if about its c.g.). Types of apparatus: (1) *Static*, e.g. a spectrometer. The integral equation may be expanded into a series, if μ_n' is finite.[1]

$$G_1(x)=\int_{-\infty}^{\infty}G_0(x+\beta)W(\beta)d\beta=(\Sigma_0 M_n'D^n)G_0(x),$$

where $M_n'=\mu_n'/n!$. (2) *Dynamic*, e.g. a galvanometer. $F(x)$ is a particular solution of the differential equation,

$$G_0(x)=(\Sigma_0 a_n'D^n)G_1(x).$$

Either series (1) for the prediction of errors, or series (2) for the correction of errors, may be used for the same apparatus, since the two operators are reciprocals of each other. The area of $W(x)$ is $M_0'=1/a_0'$. Henceforth, unit area is assumed. $M_1'=-a_1'$, $M_1=a_1=0$, $M_2=-a_2$, and $M_3=-a_3$. (Note that $M_n=\mu_n/n!$.) Several successive operations are indicated by the product of their operators. The resultant coefficients M_1', M_2, M_3 or a_1', a_2, a_3 are each the sum of their respective coefficients. These three coefficients are proportional to the changes in c.g., curvature and asymmetry of $G(x)$.

[1] R. C. Spencer, Phys. Rev. **38**, 618 (1931), Eq. (21).

32. Oscillation of Close-Coupled Circuits. R. R. RAMSEY, W. L. CHENAULT AND L. E. LONG, *Physics Department, Indiana University.*—During the early days of radio when all sending stations were spark or damped wave stations, "resonance" curves often turned out to be double-humped curves. It was found that these curves were produced by close-coupled circuits. A theoretical explanation of this effect is given by A. Oberbeck.[1] A somewhat detailed discussion is given by J. A. Fleming.[2] The general conclusion seems to be that close-coupled circuits or apparatus always produce or manufacture two frequencies. If one uses modern tube oscillators it is practically impossible to obtain the double-humped curve. In a detailed study, it is found possible for close-coupled oscillators to oscillate at two frequencies while the circuit constants remain the same. However, the circuit does not oscillate at both frequencies at the same time. The metastable mode is obtained by shifting gradually from the stable to the metastable mode. Close-coupled circuits are tuned for two frequencies, but do not oscillate at these frequencies unless they are generated in some neighboring oscillator. Further experiments indicate that damped oscillators give a band of frequencies. The close-coupled circuit selects the two frequencies to which it is tuned.

[1] A. Oberbeck, Wied. Ann. d. Physik **55**, 623 (1895).
[2] J. A. Fleming, *Principles of Electric Wave Telegraphy*, 190t, pp. 220–.

33. Absolute Intensities in Halide Spectra, ROBERT S. MULLIKEN, *University of Chicago.*—Quantum-mechanical calculations have been made of the over-all absolute intensities of certain $^1\Sigma^+\rightarrow{}^3\Pi_1$ and $^1\Pi$ electronic transitions in the spectra of the halogen, hydrogen halide, and methyl halide molecules. These transitions give rise to a large part of the well-known ultraviolet continuous spectra of these molecules, and to a part of the banded visible spectra of some of them. In spite of the very roughly approximate character of the wave functions used, there is for the most part a close parallelism, and even a very roughly quantitative agreement, between the calculated and observed over-all absolute intensities of the transitions. This result confirms the interpretation of the electronic levels of these molecules, and also indicates that similar calculations for other spectra should be significant. Calculations already made for a number of other spectra have given a variety of interesting results.

34. A New Ultraviolet Band System of Silver Iodide. NICHOLAS METROPOLIS, *University of Chicago. (Introduced by R. S. Mulliken.)*—A new ultraviolet band system of AgI has been photographed in absorption at temperatures 750°–900°C. At higher temperatures the system is overlapped by strong continuous absorption, which advances gradually from shorter wave-lengths. The new system lies at shorter wave-lengths than the known system, and its lower electronic state agrees with the ground state given by Brice. The rotational structure and the very small isotope effect are not resolved. The equation for the band heads may be written

$$\nu_h=44722+152.8(v'+\tfrac{1}{2})-1.1(v'+\tfrac{1}{2})^2 -206.2(v''+\tfrac{1}{2})+0.43(v''+\tfrac{1}{2})^2.$$

This formula is based upon progressions to $v'=4$ and to $v''=10$. The results are in harmony with the predictions of Mulliken.

35. Townsend Ionization Coefficients and Glow Potentials in an Argon-Barium Phototube. R. W. ENGSTROM, *Northwestern University. (Introduced by W. S. Huxford.)*—The Townsend ionization coefficients and glow potentials for argon were measured in a tube with parallel plate arrangement. Electrode separations were controlled magnetically by a method designed to avoid extra metal parts in the vacuum system. Highly purified argon was admitted at a pressure of 1.51 mm and exposed to a barium mirror to remove traces of impurities. Light was admitted through

a wire mesh at the center of the nickel anode. The cathode was covered with barium by evaporation in vacuum. α, the number of ionizing collisions for an electron per cm of path, was measured in the usual manner by varying the plate separation and was found to be in close agreement with the values of Kruithoff and Penning[1] throughout the measured range from $X/p=30$ to 300 volts cm^{-1} mm^{-1}. Values for γ, the number of electrons released by each argon ion at the barium cathode, were calculated from the ionization curves and also from the measured starting potentials for a glow discharge. The values obtained by the two methods are in good agreement. γ increased from 0.065 at $X/p=50$ to 0.10 at $X/p=300$.

[1] Kruithoff and Penning, Physica **3**, 515 (1936).

36. Sparking Potentials at Low Pressures. ROBERT B. QUINN, *University of Chicago.* (*Introduced by A. J. Dempster.*)—At gas pressures less than the Paschen critical value the sparking potential rises rapidly with decrease in pressure. Measurements are difficult because of undesired discharges over longer paths than the main sparking distance. A successful sparking tube has been designed with which measurements have been made on air, carbon dioxide, hydrogen, and helium up to 24 kv with nickel electrodes, and on air with a stainless steel cathode. The results are compared with those of Cerwin, of Carr, and of Penning. The equations of the straight portions of the sparking potential curves are of the form $V=a+b \log pd$.

37. Apparent Ionic Volumes in Aqueous Solutions of Strong Electrolytes. G. W. STEWART, *State University of Iowa.*—In continuation of experiments described in former abstracts[1] the change in minor peak height of the x-ray diffraction curve has been used as an arbitrary measure of the alteration of the four-coordinated structure of the solute, water. Fifteen strong electrolytes have now been tested and, using this arbitrary measure, their results have been compared with the apparent ionic volumes as dependent upon concentration. The conclusion is quite clear that the apparent ionic volumes are more dependent upon the altered density of the solute than upon the electrostatic effects of free ions in the solution.

[1] G. W. Stewart, Phys. Rev. **53**, 202 (1938), and **53**, 323 (1938).

38. The Joule-Thomson Effect in Carbon Dioxide. J. R. ROEBUCK AND T. A. MURRELL, *University of Wisconsin.*—This is the worst material to handle yet measured, due largely to its liquefaction in the compressor cooling coils. Heat required to revaporize is large and live steam was required. Also with bath below 50°C the cold fluid leaving the plug forms snow and blocks the passages, requiring a high pressure steam heater. Air impurity was reduced to 0.01 percent by freezing a large cylinder of liquid with dry ice and snifting the vapor liberally. The curves cover 300°C to −56°C and 1–200 atmos. The general picture is extremely like other gases.[1] Special experiments around T_c show that isenthalps in air-free liquid run without bend directly into saturation curve. Air impurity leads to steeper slope and near saturation isenthalp breaks to line downwards and toward saturation. The break point moves toward saturation with decreasing air impurity. A low temperature liquid isenthalp of positive slope keeps positive right to saturation. Thus the inversion curve does not turn down in liquid. In the unsaturated vapor one curve is tangent to and bends slightly toward saturation curve, suggesting association in the vapor.

[1] Phys. Rev. **46**, 785 (1934).

39. Nerve Conduction with Distributed Capacitance. ALVIN M. WEINBERG, *University of Chicago.* (*Introduced by N. Rashevsky.*)—Rashevsky's theory of nerve conduction[1] has been extended to include the effects of distributed capacitance along the nerve fiber. The simple theory of Rashevsky, based on the idea of local re-excitation by bioelectric currents according to Blair's law of excitation,[2] leads to a formula for the initial velocity of the nerve impulse:

$$v=\frac{ak}{\log\left[I/(I-R)\right]},$$

where a is the distance between Ranvier nodes, k measures the excitability of the nerve, I is the local exciting current, and R is the threshold current for excitation. This result does not depend explicitly on G, the node leakance. The present analysis gives for the initial velocity, in case $G/C \gg k$,

$$v=\frac{ak}{\log\left[I/(I-(R+\phi))\right]},$$

where ϕ is a complicated function of C and vanishes when $C=0$. In case G/C is not $\gg k$, the velocity is given as the root of a transcendental equation which may be solved numerically. Formulae for the asymptotic velocity of propagation are similarly related in the two cases. Empirical data necessary to check the validity of these results are as yet unavailable; the types of experiments needed to obtain these data are suggested.

[1] N. Rashevsky, *Mathematical Biophysics* (University of Chicago Press, 1938), Chapter 20.
[2] Ibid., Chapter 16.

40. The Excitation Functions of Lithium and Boron. RALPH B. BOWERSOX, *University of Chicago.*—The excitation functions for the reactions:

$$Li^6+H^1 \rightarrow He^3+He^4$$
$$B^{11}+H^1 \rightarrow Be^8+He^4$$

have been determined by using proton energies up to 400 kv. Measurements were made on thick targets of LiOH and LiF and the observed yields were multiplied by a factor of 4 to make them correspond to the yields from pure lithium. The cross section of lithium for this process, based on a thin target curve derived from these yields, was found to follow an exponential curve. A thick target of compressed amorphous boron was used in the investigation of the second reaction. The alpha-particle resonance was observed at a potential of 172 kv; and the excitation function was extended up to 400 kv proton energy.

41. On the Penetration Probability of Fast Protons into Nuclei. V. F. WEISSKOPF AND D. H. EWING, *University of Rochester.*—The influence of the repulsive Coulomb field on the penetration of a proton into a nucleus can be calculated if the radius of the nucleus is known, at least for energy values not too close to the top of the potential barrier of the Coulomb field.[1] The total cross section can then be split up into a factor effected by the shielding Coulomb field and a factor which is suitably called the sticking probability of the proton. A quantitative investigation of the cross sections of the nuclei Ni^{61}, Ni^{62}, Ni^{64}, Cu^{63}, Se^{78}, Se^{80}, Se^{82}, Pd^{106}, Pd^{108}, Sn^{120}, Sn^{122} for disintegration by protons up to 6.7 Mev has been carried out by using the results obtained by the Rochester Group. It is found that the sticking probabilities depend on the energy of the bombarding particle and are of the order of 1/10 if one assumes a nuclear radius of $1.50 \cdot 10^{-13} \cdot A^{\frac{1}{3}}$. A radius $1.00 \cdot 10^{-13} \cdot A^{\frac{1}{3}}$ would give rise to a larger value of the sticking probabilities by a factor of about ten, but can be excluded by other evidences. The small value of the sticking probabilities indicates a special mechanism for the penetration of a particle into the nucleus, since according to our present knowledge the sticking probability of a heavy particle should approach unity for energies of several million electron volts.

[1] See H. Bethe and E. Konopinski, Phys. Rev. **54**, 130 (1938).

42. Proton Reactions of $_{48}$Cd and $_{49}$In. S. W. BARNES, *University of Rochester.*—Indium bombarded by 6.7 Mev protons exhibits decay periods of 20 min.+, 50 days−, (50 min.+) and 4 hr.−. The first two are obtained from the Sn precipitate, the second two from the In precipitate. The 20 min.+ activity is assigned to Sn^{113} formed by a p-n reaction from In^{113}. The 50-day activity is as yet unassigned. The 50-min.+ activity appears only weakly in the In precipitate and may be an impurity. The 4 hr. period is assigned to a metastable excited state of In^{115} called In^{*115}. In^{*115} is formed either by an inelastic collision in analogy to the neutron excitation of In^{116} already found by Goldhaber and Szilard or by the action of the electric field of the proton as it passes nearby. The second process seems to be the more probable for protons. The observed cross section for this reaction is about 5×10^{-30} cm^2. All of the activities induced by protons on cadmium appear in the In precipitate. They are 18 min., 55 min., 2 hr., 4 days and 48 days. The 48-day is to be ascribed to In^{114}, the 58-min. activity which shows strong γ-rays of about 1 Mev may be the known 54-min. activity of In^{116}. The 2 hour-activity may be the 2.3-hr. period of In^{117} formed by proton capture from Cd^{116}. The assignment of the other activities is discussed.

43. The Technique of High Intensity Bombardment with Fast Particles. FRANZ N. D. KURIE, *Indiana University.*—Recent improvements in cyclotron technique have led, in the case of the 37″ cyclotron at the University of California, to the utilization of beams of such intensity that nearly a kilowatt of power must be dissipated in the target. To maintain high operating efficiency it is desirable that targets should be bombarded in elementary form rather than as compounds and that the cyclotron vacuum chamber should be protected from the debris of bombardment at all times. The former requirement puts a severe limitation on the designer because many elements are neither refractory nor are they good heat conductors. The second requirement necessitates that a thin metal window be used to isolate the target from the vacuum chamber, because most elements sublime or spatter in one way or another no matter how well cooled they may be. To meet this situation a window has been developed (a "bell-jar" window). It consists of a rectangular copper box with one end closed by a water-cooled copper plate carrying the target and the other by a thin metal window. The window end is bolted to the cyclotron's target orifice and the interior of the box is filled with hydrogen or helium at a pressure of a few centimeters. The presence of the gas serves to keep the window cool, to keep the target from being damaged by the beam and finally to protect the cyclotron in the event of a sudden failure of the window. The metal windows are supported on a grid of elongated holes which has a geometrical aperture of about 93 percent. The target plate is heavily knurled and the element being bombarded may either be fused on it or pressed into the knurlings with a spatula. The surface of the target can further be protected by covering it with thin gold foil. With this arrangement it has been found possible to bombard red phosphorus, sodium metal, lithium metal and many other difficult targets with the full intensity of the cyclotron.

44. On the Dynamical Theory of X-Ray Diffraction in Crystals. W. H. ZACHARIASEN, *University of Chicago.*—It has been customary to deal with two theories of x-ray diffraction in single crystals, the kinematical theory of von Laue and the dynamical theory of Ewald-Darwin. The kinematical theory has been applied to small crystals or to large crystals of the mosaic type, while the dynamical theory is used for large perfect crystals. General solutions are given for the intensity of diffraction from a plane parallel plate of arbitrary thickness using the dynamical theory. It is shown that as the thickness goes towards zero, the results become identical with those predicted from the kinematical theory. The area under the diffraction peak (integrated power), if plotted as function of the thickness, is for very thin crystals linear. In the Laue case (diffracted beam transmitted) the integrated power reaches a maximum value and approaches for greater thickness asymptotically an exponentially declining curve. In the Bragg case the integrated power approaches a constant value (dependent upon the absorption coefficient) as the thickness increases. The effect of absorption on the symmetry of the diffraction peak will be discussed. In the particular case where the x-rays are reflected from a sequence of lattice planes normal to the crystal plate (symmetrical Laue case) the diffraction peak is always symmetrical. If the reflecting lattice planes are parallel to the crystal plate (symmetrical Bragg case), the peak is symmetrical when the absorption index is considered a constant, but unsymmetrical if the absorption index is treated as a function of position in the lattice. It is suggested that the coefficient of incoherent

absorption should be treated as constant, that of coherent absorption as a function of position. Accordingly the diffraction peak is unsymmetrical only for critical absorption.

45. Proton Diffraction by Vapors. H. J. YEARIAN,* *Purdue University.*—The methods of electron diffraction in molecular structure analysis are inapplicable to molecules of low molecular weight because of the low scattering power of such molecules. Since protons should be scattered much more strongly than electrons, extensive experiments have been made to investigate their diffraction by molecular vapors. It was found possible to obtain diffraction patterns of CCl_4 but not of lighter molecules. The apparatus used, difficulties encountered, and principal results will be discussed.

* This research was carried on while the author was holding a National Research Fellowship at the California Institute of Technology.

46. Application of Trigonometric Interpolation to X-Ray Analysis. C. LANCZOS AND G. C. DANIELSON, *Purdue University.*—The integral representing the intensity distribution of x-ray diffraction in liquids can be evaluated by the method of trigonometric interpolation instead of approximating the integral by the sum of a large number of terms. This reduces considerably the number of ordinates required in the calculation without decreasing the accuracy. As an example, the diffraction patterns of vitreous selenium and liquid KCl and LiCl, obtained and analyzed by K. Lark-Horovitz and E. P. Miller, have been interpreted. For the curves so far analyzed, 36 ordinates were found to be sufficient. Owing to symmetry properties the Fourier coefficients can be found with a minimum of calculation. This yields directly the value of the distribution function in discrete equidistant points. The value of the function for any intermediate point may then be determined in a simple manner by pure calculation. The resulting curves agree very closely with those obtained by Lark-Horovitz and Miller.

47. Fluorescence, Absorption, and Discharge in a Mercury-Thallium Mixture. J. GIBSON WINANS, FRANCIS J. DAVIS AND VICTOR A. LEITZKE, *University of Wisconsin.*—The sensitized fluorescence of Tl was observed with apparatus like that used for tin.* All Tl lines reported by Cario and Franck except 6550 were observed. Excitation by λ1854 from an Al spark with the mercury at low pressure gave the higher series Tl lines with greater intensity with respect to the lower series lines than when excitation was with λ2537. At higher pressures of mercury the Tl lines 3775 and 5350 were the most intense for either 1854 or 2537 excitation. Both excitations produced fluorescence bands with maxima at 6558, 5225, 4585, and 3810. 2536 excitation gave one also at 4296. A Tesla discharge gave these bands with good intensity. They appeared only when both mercury and thallium were present.† All but 3810 showed resolvable fine structure. The absorption spectrum of the mixture using a hydrogen discharge tube as source showed the line absorption of Tl and the one band 3810. The spectra showed fourteen absorption lines of the diffuse series and a band beginning at the series limit (2034). Beyond the series limit was a strong absorption band with long wave edge at 2008A. Additional absorption lines which did not fit the usual energy levels of Tl were found at approximately 2210, 2277′, 2299′, 2337′, 2373, 2575, 2816′. Lines marked ′ may be due to impurities.

* J. G. Winans and R. M. Williams, Phys. Rev. **52**, 930 (1937).
† J. G. Winans and Francis J. Davis, Phys. Rev. **53**, 930 (1938).

48. An X-Ray Study of the Changes Produced in Metals by Fatiguing. RAYMOND G. SPENCER, *Albion College.*—Carefully prepared specimens of several different metals have been fatigued, x-ray diffraction patterns being taken as fatiguing progressed. This report will be confined largely to the results obtained with malleable iron. When malleable iron is stressed in the safe range, x-ray diffraction patterns reveal no appreciable change in grain size or strain. This result is in agreement with Gough and Wood's[1] conclusions but in disagreement with Barrett's[2] conclusions. When malleable iron is fatigued with a stress beyond the safe range, very marked changes are revealed by the diffraction patterns. Early stages of fatiguing often produce rotation of individual grains and some grain fragmentation. As fatiguing progresses, very marked lattice distortion of the crystallites becomes evident. Gough and Wood concluded that grain fragmentation down to a limiting size of 10^{-4} to 10^{-5} centimeter preceded failure of their specimens. The author finds that the grains are severely strained just prior to failure but it does not appear to him that fragmentation to the extent suggested by Gough and Wood occurs. However, it is evident that grains adjacent to the fracture are finely fragmented after failure. The author concludes that much of this fragmentation is caused by the process of rupture.

[1] H. J. Gough and W. A. Wood, Proc. Roy. Soc. **165A**, 358–371 (1938)
[2] Charles S. Barrett, Metals and Alloys **8**, 13–21 (1937).

Author Index to Abstracts of Chicago Meeting

Allen, J. S.—No. 17
Almy, G. M., H. Q. Fuller and G. D. Kinzer—No. 30

Baker, Richard F. and John T. Tate—No. 18
Baltzer, O. J. and E. M. McNatt—No. 21
Barnes, S. W.—No. 42
Bartlett, J. H. and R. E. Watson—No. 15
Bowersox, Ralph B.—No. 40
Boyd, George and William D. Harkins—No. 25

Chenault, W. L.—see Ramsey, R. R.
Compton, A. H. and P. S. Gill—No. 3
Coolidge, Albert S.—see James, Hubert M.
Crane, H. R.—see Halpern, J.

Danielson, G. C.—see Lanczos, C.
Davis, F. J.—see Winans, J. G.

Engstrom, R. W.—No. 35
Ewing, D. H.—see Weisskopf, V. F.

Florence, Robert T. and William D. Harkins—No. 24
Forbush, S. E.—No. 2
Fuller, H. Q.—see Almy, G. M.

Gill, P. S.—see Compton, A. H.
Gingrich, Newell S.—No. 19
Graves, Alvin C.—No. 26

Halpern, J. and H. R. Crane—No. 20
Harkins, William D.—see Boyd, George
——see Florence, Robert T.
Henderson, W. J.—No. 29
Hopkins, J. I., W. M. Nielsen and L. W. Nordheim—No. 1

James, Hubert M. and Albert S. Coolidge—No. 9
Jauncey, G. E. M.—see McNatt, E. M.
——No. 23

Kinzer, G. D.—see Almy, G. M.
Konopinski, E. J.—No. 14
Kurie, Franz N. D.—No. 43

Lamb, Willis E.—No. 10
Lanczos, C. and G. C. Danielson—No. 46
Lawson, J. L. and A. W. Tyler—No. 28
Leitzke, V. A.—see Winans, J. G.
London, F.—No. 11
Long, L. E.—see Ramsey, R. R.
Lyman, Ernest M.—No. 8

McNatt, E. M.—see Baltzer, O. J.
—— **and G. E. M. Jauncey**—No. 22
Maxwell, Louis R. and Vernon M. Mosley—No. 27
Metropolis, Nicholas—No. 34
Mosley, Vernon M.—see Maxwell, Louis R.
Mulliken, Robert S.—No. 33
Murrell, T. A.—see Roebuck, J. R.

Nielsen, W. M.—see Hopkins, J. I
Nordheim, L. W.—see Hopkins, J. I.

Quinn, Robert B.—No. 36

Ramsey, R. R., W. L. Chenault and L. E. Long—No. 32
Richardson, J. Reginald—No. 16
Roebuck, J. R. and T. A. Murrell—No. 38

Schein, Marcel and Volney C. Wilson—No. 5
Schwinger, Julian—No. 13
Shonka, Francis R.—No. 6
Spencer, Raymond G.—No. 48
Spencer, Roy C.—No. 31
Staub, H.—see Stephens, W. E.
Stephens, W. E. and H. Staub—No. 12
Stewart, G. W.—No. 37

Tate, John T.—see Baker, Richard F.
Thompson, Julian L.—No. 4
Tyler, A. W.—see Lawson, J. L.

Watson, R. E.—see Bartlett, J. H.
Weinberg, Alvin M.—No. 39
Weisskopf, V. F. and D. H. Ewing—No. 41
Wilson, Volney C.—see Schein, Marcel
——No. 7
Winans, J. G., F. J. Davis and V. A. Leitzke—No. 47

Yearian, H. J.—No. 45

Zachariasen, W. H.—No. 44